2013-01-24

Identification and Analysis of the Domain Required for Trans-Acceleration Kinetics in the Human Glucose Transporter GLUT1: A Dissertation

Sabrina S. Vollers
University of Massachusetts Medical School

IDENTIFICATION AND ANALYSIS OF THE DOMAIN REQUIRED FOR TRANS-ACCELERATION KINETICS IN THE HUMAN GLUCOSE TRANSPORTER GLUT1

A Dissertation Presented

By

Sabrina S. Vollers

Submitted to the Faculty of the
University of Massachusetts Graduate School of Biomedical Sciences, Worcester
In partial fulfillment of the requirements for the degree of

DOCTOR OF PHILOSOPHY

January 24, 2013

Biochemistry and Molecular Pharmacology

IDENTIFICATION AND ANALYSIS OF THE DOMAIN REQUIRED FOR TRANS-ACCELERATION KINETICS IN THE HUMAN GLUCOSE TRANSPORTER GLUT1

A Dissertation Presented

By

Sabrina S. Vollers

The signatures of the Dissertation Defense Committee signify completion and approval as to style and content of the Dissertation

Dr. Anthony Carruthers, Thesis Advisor

Dr. Silvia Corvera, Member of Committee

Dr. Daniel Bolon, Member of Committee

Dr. Christopher Cheeseman, Member of Committee

The signature of the Chair of the Committee signifies that the written dissertation meets the requirements of the Dissertation Committee

Dr. Reid Gilmore, Chair of Committee

The signature of the Dean of the Graduate School of Biomedical Sciences signifies that the student has met all graduation requirements of the school.

Anthony Carruthers, Ph.D.,
Dean of the Graduate School of Biomedical Sciences

Biochemistry and Molecular Pharmacology

January 24, 2013

This work is dedicated to my parents, Annette Meiners and Joseph Vollers. For over three decades and counting, through every difficulty, you support me; every doubt, you believe in me; every triumph, you celebrate with me; and every day, you always love me.

And in loving memory of Dr. Robert M. Simms, who stoked those intellectual fires that my parents first lit.

ACKNOWLEDGEMENTS

I would like to express my sincerest appreciation to my mentor, Dr. Anthony Carruthers, who has provided the perfect combination of support, wisdom, and trust. Dr. Carruthers took a chance on me when others would not, helped me to carve out and direct a successful project from start to finish, gave me the freedom to work very independently, and then the opportunity and support to embark on the next exciting step in my career as a scientist. For all these things, I am eternally grateful.

I would like to thank my thesis committee, Dr. Reid Gilmore, Dr. Silvia Corvera, and Dr. Dan Bolon, for their extremely helpful guidance and advice through the past years. I would also like to thank Dr. Christopher Cheeseman for taking his valuable time to join my committee in evaluating this thesis and traveling so far for my defense.

Though my present academic mentors are directly responsible for this work, I am forever indebted to those mentors who paved the way for me to undertake this journey.
Dr. William Meehan has been an incredible resource and support throughout graduate school. Monica Lane, Dr. Shekar Ganesa, Dr. Anders Lund, Dr. Rebecca Sendak, and Dr. Blaine Stine were instrumental in my decision to pursue my doctorate, as were Dr. Gal Bitan and Dr. David Teplow, who are directly responsible for my interest in biochemistry. My early pursuit of science is thanks to Dr. Craig Woodard, Dr. Rachel Fink, Dr. Sarah Bacon, Dr. Sheila Cancella, and Dr. Ed Coher. Though I must attribute my passion for study to the dedicated guidance of Dr. Robert Simms. It was his mentorship that started it all, and the memory of his enthusiasm is still with me each day.

There are many friends without whom I could not have completed this work. In particular, these are Dr. Anthony Cura and Dr. Jay Sage. Through many hours of assay training, troubleshooting, editing, and practice talks, I have always valued their opinions and support. I would also like to thank Dr. Siobhan O’Brien for her scientific input and assistance. I am very

grateful to Dr. Zu Ting Shen and Dr. Walter Kim for some of the best advice I have ever taken. I would have had no roof over my head for the past 3 years were it not for the true friendship of Matthew Norgren. I will also never forget the support of Andrew Hobgood and his family; nor the bright cheeriness and kindness of Lisa McCoig, nor the extremely straightforward advice of Dr. Jennifer Songer; may you both rest in peace.

But, as with all things, I am most thankful to my family. This includes Fabien Nisol, whose love, patience and support over the last 3 years, and over the last 105,000 miles, have been nothing short of amazing. I also want to thank my loving, fierce and inspiring brothers, Kendrick Meiners-Vollers and Cormac Meiners; and my grandmother, Ruth Meiners-Eggers, for being the role model of an independent, strong woman. Last but not least, my mom and dad, Annette Meiners and Joseph Vollers. My dad, who made my education top priority - for him, and for me. Who would ask me if it was my best, who showed me how to work hard and play hard, the value of getting it done, and the never-fail maxim of ‘don’t complain, don’t explain.’ My mom, whose many hours on the phone with me are unparalleled. Dr. Simms once called her an academic stage-mother, and she took it as the true compliment it was. She’s been there behind the scenes for every bit of everything, always with understanding and sage advice, and always with an eye to the future. With both my parents on my side, which is where they always are, they’ve always made me feel like I could do pretty much anything.

ABSTRACT

Since the initial characterization of the human glucose transporter GLUT1, it has been observed that the presence of intracellular sugar stimulates the unidirectional rate of sugar uptake by a kinetic phenomenon known as trans-acceleration. Both GLUTs 1 and 3 catalyze trans-acceleration, while both GLUTs 2 and 4 do not. Although the basis for trans-acceleration is unknown, potential explanations include the requirement of a modulating cofactor, cellular context, or that the behavior is an artifact of imperfect transport measurements. This thesis examines whether trans-acceleration is a sequence-specific property intrinsic to the transporter. A method for detecting trans-acceleration in mammalian cells at physiologic temperature was developed through transport of two different glucose analogs. Homology-scanning mutagenesis was employed to exchange transmembrane domains (TMs) of GLUTs 1 and 4, and thereby test for accelerated-exchange loss- or gain-of-function. This approach was extended to GLUTs 2 and 3. The catalytic rates of these chimeric proteins were determined through transport measurements and expression measured by cell-surface biotinylation. These studies show that the sequence of putative scaffolding domain TM6 is both necessary and sufficient for trans-acceleration in scaffolds of GLUT1, GLUT2, and GLUT4. The substitution of TM6 sequence between these transporters has no effect on the turnover under exchange conditions, yet profoundly modifies turnover in the absence of intracellular sugar. We propose that the sequence-specific interaction of TM6 with other TMs structurally restrains relaxation of the empty carrier in GLUTs which catalyze trans-acceleration, and that binding of intracellular sugar affects these interactions to reduce the overall duration of the transport cycle. In addition, our model suggests that the substrate binding constant and rate of carrier relaxation are inter-dependent. In this model, the dissociation constant determined by substrate binding and dissociation rates at the endofacial sugar binding site must be larger than the equivalent constant at the exofacial site in order for trans-acceleration to occur.

TABLE OF CONTENTS

LIST OF TABLES

LIST OF FIGURES

PREFACE

Parts of this dissertation have appeared in the following:

Vollers, S.S. and Carruthers, A. (2012) Sequence Determinants of GLUT1-mediated Accelerated-exchange Transport: Analysis by Homology-scanning Mutagenesis. J Biol Chem, 287 (51), 42533-44.

All work presented was performed by the author, with the exception of the simulations in Figure 1.6 and Figure 2.7, which were performed by Dr. Anthony Carruthers. In addition, the model and simulations presented in Figure 5.1 and Tables 5.1, 5.2, and 5.3 represent a collaborative effort between Dr. Anthony Carruthers and Sabrina Vollers.

LIST OF ABBREVIATIONS

2-DG	2-deoxy-D-glucose
2-DG-6-P	2-deoxy-D-glucose-6-phosphate
3-MG	3-O-methyl-D-glucose
3T3-L1	murine embryonic fibroblast-derived cell line
Ab	antibody
ABC	ATP-Binding Cassette transporter
ADP	adenosine-5'-diphosphate
Akt	protein kinase B
AMP	adenosine-5'-monophosphate
AMPK	adenosine-5'-monophosphate-dependent kinase
ATP	adenosine-5'-triphosphate
Bis-Tris	2-[Bis(2-hydroxyethyl)amino]-2-(hydroxymethyl)-1,3-propanediol
BSA	bovine serum albumin
CCB	cytochalasin B
CD	circular dichroism spectroscopy
CNS	central nervous system
DHA	dehydroascorbic acid
DIC	differential interference microscopy
DMEM	Dulbecco's modified Eagle medium
DPBS; DPBS-Mg	Dulbecco's phosphate buffered saline; with $MgCl_2$
DTT	dithiothreitol
e(), e(S)	occluded carrier; bound to substrate
e_1; $e.S_1$	exofacial facing-carrier; bound to substrate
e_2; $e.S_2$	endofacial facing-carrier; bound to substrate
EDTA	ethylenediaminetetraacetic acid
EE	equilibrium exchange
EM	electron microscopy
E_{max}	V_{max} with saturating intracellular sugar
EmrD	multi-drug transporter
FTIR	fourier transform infared spectroscopy
FucP	fucose transporter
G1DS	GLUT1 deficiency syndrome
G-6-P	glucose-6-phosphate
GAPDH	glyceraldehyde 3-phosphate dehydrogenase
GlpT	glycerol-3-phosphate transporter
GAP	GTPase-activating protein
GLUT	facilitative glucose transporter

GTP	guanosine triphosphate
HE	hetero-exchange
HEK	human embryonic kidney-derived cell line
HEPES	(N–[2–Hydroxyethyl]piperazine–N'–[2–ethanesulfonic acid])
HIV	human immunodeficiency virus
HK	hexokinase
HMIT	human myoinositol transporter
IBMX	3-isobutyl-1-methylxanthine
IT	infinite-trans
k_{cat}	carrier turnover; catalytic rate
$K_{0.5}$	half-maximal concentration
K_E	intracellular sugar concentration which elicits 50% E_{max}
K_m, K_{mapp}	affinity constant, apparent affinity constant
K_i, K_{iapp}	inhibition constant, apparent inhibition constant
LacY	lactose permease transporter
LB	luria broth medium
MCT	monocarboxylate transporter
MES	2-(N-morpholino)ethanesulfonic acid
MFS	Major Facilitator Superfamily
$MgCl_2$	magnesium chloride
MsbA	multi-drug transporter
NaCl	sodium chloride
NHS	N-Hydroxysuccinimide
OxIT	oxalate transporter
PCR	polymerase chain reaction
PI3K	phosphatidyl-inositol-3-kinase
PKC	protein kinase C
PNGase F	N-linked glycosidase F
PVDF	polyvinylidene difluoride
RT-PCR	reverse transcriptase polymerase chain reaction
Rab	Ras-related GTPase protein
qPCR	quantitative reverse-transcriptase polymerase chain reaction
S_1	interstitial (side or substrate)
S_2	intracellular (side or substrate)
SDS-PAGE	sodium dodecyl sulfate-polyacrylamide gel electrophoresis
SGLT	sodium-linked glucose transporter
SOC	super optimal broth with catabolite repression
SP	sugar porter transporter
$T_{0.5}$	half-time

TAE	tris base, acetic acid and EDTA buffer
TBS	tris-buffered saline
TM	GLUT transmembrane domain
TBS-T	tris buffered saline containing 0.2% Tween 20
Tris; Tris-Hcl	2-Amino-2-hydroxymethyl-propane-1,3-diol; hydrochloride
v	uptake
V_{max}	maximum velocity rate constant
ZT	zero-trans

CHAPTER I

Introduction and Literature Review

Metabolism and Homeostasis

One of the most basic needs of all life forms is energy in the form of ATP. This energy is required for nearly all life-sustaining functions including growth, movement, and catabolic and anabolic processes. The generation of ATP is the result of a breakdown of nutrients derived from a variety of sources, particularly from dietary intake. At the cellular level, some of the simplest inputs for processes to generate ATP are monosaccharides, or sugars. Fructose and glucose are the predominant dietary sugars in mammals. Overall carbohydrate homeostasis reflects a balance between sugar import, utilization, synthesis, secretion and excretion.

Glucose is rapidly converted into ATP by both aerobic and anaerobic pathways. This energy may be consumed immediately or stored for later use, in the form of glycogen or triglycerides. When external sugar is unavailable, these complex carbohydrate and lipid stores can be used to generate glucose through gluconeogenesis. A host of environmental factors, including the supply and demand of glucose, impact the utilization of aerobic or anaerobic metabolic pathways in the cells and tissues within the body. Therefore, glucose homeostasis is an essential cellular and organismal function and involves a complex interplay of metabolic, hormonal, and neural pathways.

Just as there must be a balance between the consumption, metabolism, and supply of nutrients in the body, there must also be a balance between the uptake, reabsorption, and output of glucose and other metabolites in the blood, brain, and various organs. This is achieved by a diverse set of transporters, mainly the facilitative glucose transporters (GLUTs), sodium-linked glucose transporters (SGLTs), and monocarboxylate transporters (MCTs), of which the GLUTs and MCTs are part of the Major Facilitator Superfamily (MFS).

Integral Membrane Transporters

While small, non-polar solutes may enter the cell by simple diffusion across the plasma membrane, larger or charged molecules require membrane-spanning proteins, such as pores, ion channels, or transporters, to gain entry into the cell. This may be achieved through passive transport, also known as facilitated diffusion, whereby molecules flow down their concentration gradient across the plasma membrane. In contrast, molecules may be moved against their concentration gradient through active transport. Primary active transport requires the input of ATP, while secondary active transport requires the presence of an electrochemical gradient. This allows a molecule to be transported against its concentration gradient when it is coupled to the transport of another molecule down its concentration gradient. This can occur with both molecules moving in the same direction (co-transport or symport) or in opposite directions (exchange or antiport).

Transporters appear to differ fundamentally from ion channels or pores in that they must undergo a conformational change in order to translocate substrate across the plasma membrane. This occurs after substrate binding at a specific site, which is often accessible when the carrier is in either of two conformations: endofacial (cytoplasmic; e_1 conformation) or exofacial (extracellular; e_2 conformation). The carrier (whether empty or substrate-bound) is in the transitional occluded state (e()) while it undergoes this conformational change, as neither substrate binding site is accessible. Although these characteristics distinguish membrane transporters from channels and pores, a wide variety of active and passive transporters with a multitude of substrates exist. These are grouped under two superfamilies: the Major Facilitator Superfamily (MFS) and the ATP-Binding Cassette (ABC) superfamily, each of which comprises thousands of transporters expressed across all organisms (1).

As the larger of the two groups, the ABC superfamily is composed of transmembrane proteins that transport a diverse set of substrates, including macromolecules. Transport by ABC proteins is coupled to the binding of ATP in an active-transport mechanism (1). Unlike the ABC transporters, the MFS transporters are passive transporters whose substrates are only small molecules. As facilitative carriers, they are able to transport a single molecule down its concentration gradient (uniport), or couple transport to the concentration gradient of another molecule through symport or antiport. There are a variety of MFS transporters, many of which are H^+-coupled symporters; some function as antiporters of metabolic intermediates and substrates,

including nucleosides, phosphates, oxalates, and sugars (2). The largest MFS group is that of the sugar porters (SP), comprising over 130 transporters, which transport hexoses in a variety of organisms (3).

Although all members of the SP family are similar in that they contain either 12 or 14 membrane spanning domains (TMs) and cytoplasmic N- and C-termini, they vary in size, tissue-specific distribution, and specificity for substrate(s). For example, expression of the monocarboxylate transporters (MCTs; (4)) in mammalian erythrocytes, neurons, and cells of the muscle, liver, and kidney is essential for the export and uptake of the critical metabolites pyruvate and lactate. An integral component of blood glucose homeostasis includes the reabsorption of glucose from plasma in the small intestine and kidney, where a family of sodium-glucose linked transporters (SGLTs; (5)) uses the intracellularly-directed Na^+ gradient to catalyze the net uphill flow of glucose from the lumen to the cytoplasm. However, export of epithelial cell glucose to the interstitium is mediated by the solute-linked carrier 2A gene family (SLC2A) of facilitative glucose transporters (GLUTs (6)), which accelerate the net downhill flow of glucose across cell membranes.

The GLUTs are classified as uniporters because they are able to transport sugar through uptake or export without requiring the presence of sugar at the opposite *trans* side of the membrane. They are also capable of coupling import of one sugar molecule to the export of a second sugar molecule (antiport), but unlike some other MFS transporters, GLUTs are not obligate antiporters. Only one of the GLUTs (GLUT13 or HMIT, the H+/

myoinositol symporter) displays symport, where the movement of one molecule (myoinositol) against its concentration gradient is driven by co-transport of another molecule down its concentration gradient (in this case, H+).

GLUT Classes I-III

To date, fourteen members of the human GLUT family have been identified (7), GLUTs 1-14. With the exception of GLUT1, which is known as the basal glucose transporter due to its ubiquitous expression, the GLUTs are expressed in a highly tissue-specific manner (Table 1.1). The numbering of the GLUTs is mostly based on the advent of their discovery and cloning, beginning with the identification of GLUT1 more than 30 years ago (8), (9). The transporters have been grouped into 3 classes based on sequence similarity (10), and to a lesser extent, substrate specificity.

The Class I transporters, comprising GLUTs 1-4, show 48-63% sequence identity with one another. This class of GLUTs has been the most extensively studied and characterized, particularly GLUT1, which was first cloned in 1985 (11). While GLUT1 is found in all tissues, it is most highly expressed in red blood cells (erythrocytes, (12)), in the vascular endothelia at blood-tissue barriers such as the brain, retina, and placenta (13), (14), and in CNS astrocytes (15). GLUT2 (16) is critical for glucose transport in hepatic metabolic processes, although its detection has been extended to the pancreas and small intestine (17). More recently, a role has emerged for GLUT2 in glucose sensing

Table 1.1 Tissue Specific Expression of Class I-III Human Glucose Transporters (GLUTs)

TRANSPORTER	CLASS	TISSUE-SPECIFIC EXPRESSION
GLUT 1	I	Ubiquitous; particularly erythrocytes and endothelia, astrocytes
GLUT 2	I	Liver, pancreas, kidney and small intestine
GLUT 3	I	Neurons, leukocytes, sperm, and embryo
GLUT 4	I	Adipocytes and skeletal/cardiac muscle
GLUT 5	II	Intestine, testis, kidney, skeletal muscle, adipose, and brain.
GLUT 6	III	Brain and spleen
GLUT 7	II	Small intestine and colon
GLUT 8	III	Testis, brain, adipose, liver, and spleen
GLUT 9	II	Kidney, liver, placenta, lung, and small intestine
GLUT 10	III	Heart, lung, brain, liver, skeletal muscle, pancreas, placenta and kidney
GLUT 11	II	Heart, skeletal muscle, kidney, adipose, placenta and pancreas
GLUT 12	III	Heart, skeletal muscle, adipose, and prostate
GLUT13 (HMIT)	III	Brain
GLUT 14 (duplicon of GLUT3)	I	Testes

mechanisms and feeding response (18), (19). The expression of GLUT3 (20) is high in neurons (21), where it plays an important role in delivery of glucose to these metabolically active brain cells. GLUT14, which is nearly identical (~96%) in sequence to GLUT3 and is thought to be a gene duplication, has only been found to be expressed in the testis (22). GLUT4 (23), in contrast, is expressed mostly in adipose tissue and skeletal muscle, where the majority of the transporter resides in intracellular pools until its presence at the cell surface is stimulated by muscle contraction or insulin.

The class I transporters transport glucose and galactose, and with the exception of GLUT2, also transport dehydroascorbic acid (DHA), the oxidized form of vitamin C (23), (24), (25), (26). GLUT2, the only low-affinity Class I glucose transporter (27), transports glucosamine with high-affinity and also transports fructose. All Class I transporters are also sensitive to the compound cytochalasin B (CCB), which can non-competitively inhibit transport (28), (29).

Unlike Class I, the members of Class II are primarily fructose transporters, and mostly are insensitive to inhibition by CCB. Class II transporters comprise GLUTs 5, 7, 9, and 11, which show 36-40% sequence identity with one another. GLUT5 (30), (31) is primarily responsible for reabsorption of fructose in the small intestine, where it may be aided by GLUT7 (32), (33), which is also highly expressed in the testis and prostate. Both GLUT9 (34) and GLUT11 (35) have several splice variants that affect their expression. Of the two splice variants of GLUT9, GLUT9a is localized to the basolateral membrane of kidney proximal tubules, while GLUT9b is localized to the apical membrane (36),

(37), (38). Recently, GLUT9 has been shown to transport urate in high capacity, with the ability to exchange urate for glucose or fructose (39). Of the three isoforms of GLUT11, the first (GLUT11A) is expressed in the kidney and cardiac/skeletal muscle; GLUT11B is found in hepatic, adipose, and placental tissue; and GLUT11C is expressed in cardiac/ skeletal muscle and adipocytes (40), (41), (42). Currently, the role of GLUT11 in metabolic homeostasis is not well understood.

The least-characterized GLUTs are also the least similar to one another in sequence, with 19-41% sequence conservation. These are the Class III transporters, comprising GLUTs 6, 8, 10, 12, and HMIT. The members of Class III are more similar to Class I in that they are primarily glucose transporters, although there is recent evidence of GLUT8-mediated fructose transport in enterocytes (43). GLUT8 has also been shown to transport glucose with high affinity (17), as has GLUT10 for glucose and galactose (44). While not all Class III GLUTs have been investigated, GLUT8 has shown sensitivity to CCB (45). Some Class III transporters, particularly GLUT6 (46), GLUT8 (45), (17), and GLUT12 (47) also contain targeting sequences that keep them sequestered in different compartments within the cell, where they may have specific functions. For example, GLUT8 has been shown to mediate glucose exit from the endoplasmic reticulum into the cytoplasm in neurons (48). Although GLUTs 6 and 8 do not appear to translocate to the plasma membrane in response to hormonal stimuli (49), GLUT12 may be another insulin-responsive transporter (50). GLUT13 (HMIT) has been shown to be expressed primarily in the brain (51), where it transports myoinositol, a critical second messenger

molecule and phospholipid precursor. At this point in time, the precise roles of some of the class III transporters remain unclear (52).

GLUT-based Mutations and Disease

Because one or more of the GLUTs is expressed in every cell in the body, mutations to GLUT-encoding genes or factors affecting transporter localization can have major consequences for metabolism of certain sugars or proper function and homeostasis of different organ systems.

For example, mutations to the basal transporter GLUT1 can have severe effects on development and brain function. GLUT1-haploinsufficiency, or G1DS (53), is a rare autosomal dominant genetic disorder with approximately 100 known cases (54), some of which are familial (55), (56). Different mutations in the GLUT1 gene have varying effects on the ability of the protein to transport glucose, which is particularly detrimental to cerebral glucose supply. Phenotypes of the disorder include high levels of lactic acid, causing seizures and delays in development. Some of these effects can be offset by lifelong adherence to a ketogenic diet (57), if detected early enough.

Similarly, Fanconi-Bickel syndrome is present in a small number of individuals with autosomal recessive mutations to the GLUT2 gene (58), (59), some of which completely abrogate the transport capability of GLUT2. This results in the inability of these individuals to ingest simple sugars. Fanconi-Bickel syndrome is characterized by

slowed growth, hypoglycemia, enlarged liver, and kidney damage, which may result from impaired ability to reabsorb sugar from urine (60).

More globally, a role for GLUTs as markers for cancer has been under investigation for many years, as upregulation of certain GLUTs (61) is necessary for the increased metabolism and rapid cell growth characteristic of many cancers (62). GLUT1 and/or GLUT3 are highly upregulated in several tumor types, including breast, skin, ovarian, cervical, kidney, brain, lung, and colorectal cancers (63), (64), (65), (66), (67), (68), (69), (70). There is a potential role in cancer metabolism for GLUT12, which was identified in mammary and prostate cancer cells (71), (72), and is upregulated in cancer lines in response to hormonal stimulation (73).

Hormonal control of glucose transport is also central to metabolic disorders. For example, diabetes is a chronic metabolic disorder that affects over 300 million people worldwide. In type 1 diabetes, a loss of pancreatic β cell mass or function results in cessation of insulin production, while in type 2 diabetes, cells become resistant to secreted insulin. The effect of either disease state is hyperglycemia, with long-term complications such as damage to the cardiovascular tissues, kidneys, and nervous system. A role for GLUT4 regulation in type 2 diabetes is still under active investigation, as the vast majority of glucose uptake in response to insulin is due to an increase in GLUT4 at the plasma membrane in muscle cells (74), (75), (76). Loss of this insulin-stimulated GLUT4 translocation is a hallmark of insulin resistance, an early pathology in the development of type 2 diabetes (77). Studies in transgenic mice have shown that

alterations to GLUT4 (78) or the pathways signaling its trafficking result in higher plasma levels of insulin and glucose (79). Knockouts of muscle or adipose cell type-specific GLUT4 result in defective endocrine signaling, which perturbs the normal physiological responses to feeding – namely increased glycogen synthesis and inhibition of liver gluconeogenesis – further contributing to insulin resistance and elevated blood glucose (80), (81). Such chronic hyperglycemia is damaging to organs and further impairs the ability of tissues to maintain glucose homeostasis through normal sensing and counter-regulatory responses (72).

Manipulation of GLUT4-mediated glucose transport is further linked to metabolic disorders through side effects observed with medications. Some of the protease inhibitors commonly prescribed to HIV-patients, such as indinavir, have been shown to directly interact with GLUT4 (82), (83). Over time, this results in development of metabolic syndrome in many of these patients, which is characterized by increased blood glucose levels, triglycerides, and cholesterol; abdominal adiposity, hypertension, and risk of type 2 diabetes and cardiovascular disease (84), (85), (86), (87). There is also an increased prevalence for patients with these types of metabolic disorders to show hyperuricemia, the condition of elevated levels of uric acid in the blood leading to gout (88). Linking plasma urate levels to allelic variance led to the discovery of GLUT9 (89), which was recently functionally characterized as a urate transporter (39), (90), expanding the importance of GLUT-mediated urate homeostasis in disease (91).

Clearly, there are numerous established and potential roles for GLUTs in the pathologies of a broad spectrum of metabolic diseases and syndromes. As the gatekeepers for cellular hexose entry and exit throughout the body, GLUTs are an integral part of metabolic processes, both normal and disordered. As such, GLUTs remain potential therapeutic targets, particularly in diabetes and cancer. If manipulation of GLUT expression, function, and regulation are to be viable strategies, these processes first must be clearly understood through rigorous study.

Common Topology and Motifs

In order to characterize differences in functional properties of the glucose transporters, it is helpful to compare their sequence and structural attributes. Like many of the MFS transporters, while they do not share a high degree of sequence conservation (25-68%), all of the 14 mammalian GLUTs share similar topology. Hydropathy analysis predicts a total of 12 trans-membrane spanning α-helices (TMs) (11), (92), which was confirmed by scanning glycosylation mutagenesis (93), FTIR (94) and CD (95) spectroscopy analysis. Within the 12 TMs, there is symmetry between TMs 1-6 and TMs 7-12, which may be the result of gene duplication early in GLUT evolution (96). The first 6 TMs are connected to the last 6 by a long intracellular loop known as loop 6 (see Figure 1.1). The length of each GLUT is variable, with an average sequence length of approximately 500 amino acids. GLUT1 is 492 residues with a molecular weight of ~55kDa, while GLUT8 is the smallest (477 residues) and HMIT is the largest, at 648

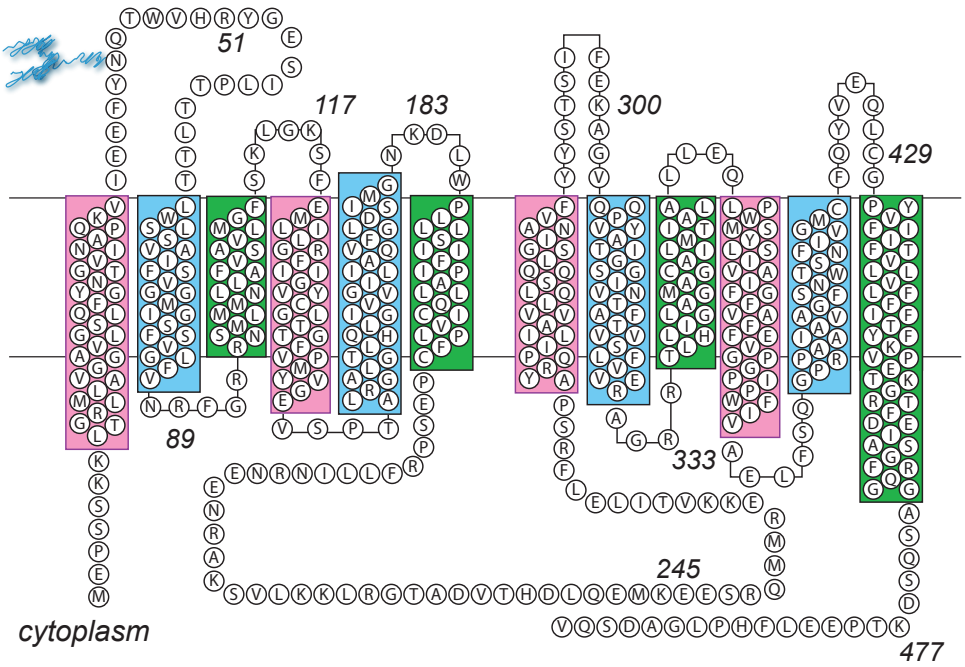

Figure 1.1 Putative topology of human GLUT1

The 12 transmembrane TM domains of the transporter are shown as a cross-section through the membrane, with the same coloring scheme as the TMs in Figure 1.2. Both the N- and C-termini are cytoplasmic, as is the large loop (loop 6) connecting TMs 6 and 7. The single glycosylation site on loop 1 (asn 45) is indicated.

amino acids. Differences in length tend to result from variations in the length of the N- and C-termini and the loops connecting the TMs, while the length of each TM is more similar across the GLUT family members. Indeed, the 12 TMs are the regions of the protein that have the highest sequence conservation among the GLUTs (10).

The regions with the highest degree of sequence divergence among the GLUTs are thus the N- and C-termini and loops connecting the TMs, in particular loops 1 and 9 (10). A single N-linked glycolsylaton site is present in one of these two loops; in Class I and II, loop 1 is glycosylated (GLUT1, asn 45; (97)), while Class III transporters are glycosylated on loop 9. Although the other GLUTs have not been as extensively characterized as GLUT1, the heterogeneous glycosylation of GLUT1 has been linked to its transport ability (98). There are several conserved sequence motifs among the GLUTs, including PMY (TM4), PESPRY/FLL (loop 6), GRR (loop 8), VPETKG (C-terminus), and QQLSGIN (TM7). Transporter selectivity for fructose appears to be due to critical hydrophobic residues in TM7, as has been shown in GLUTs 2, 5, 7 (99), 9, and 11 (100).

Although GPGPIP/TW (TM10) is also conserved, the class II GLUTs lack the Trp residue, which has been shown to be critical for sensitivity to the compounds CCB and forskolin, both transport inhibitors of the class I GLUTs (101). Presence of the Trp in TM10 may have a direct role in CCB inhibition, as both this motif and sensitivity to CCB are absent in the Class II transporters (102). While Class III GLUTs contain the TM10 Trp, investigation of their inhibitor profiles is incomplete. A different Trp in TM11, which is conserved in all GLUTs, is critical for the proper localization and function of GLUT1

(103). Several studies investigating the importance of conserved residues GLUT1 and GLUT4 have shown loss of glucose transport ability with point mutations in loop 2 (R92), loop 4 (R153), loop 7 (Y293), loop 8 (RR 333-334; E329), TM10 (P385), and loop 10 (E393; R400) (104), (105), (106), (107).

Although many of the studies referenced above draw from comparative sequence analysis across all of the 14 GLUTs, the vast majority of functional characterization has focused on the Class I glucose transporters, particularly GLUT1 and GLUT4. This is due in part to the earlier discovery and cloning of the Class I members. The abundance and ability to purify relatively large amounts of GLUT1 protein from erythrocytes has also aided in its characterization. Many efforts have focused on analysis of the surface expression and trafficking of GLUT4 in response to insulin, due to its importance in diabetic metabolism. More recently, the importance of GLUT3 in brain metabolism has emerged, prompting analysis of the cooperative roles of GLUT3 with other transporters, such as GLUT1 at the blood-brain barrier and MCTs in lactate transport among astrocytes and neurons (108), (109). Although initially characterized as a hepatic glucose transporter, GLUT2 has an emerging additional role as a critical glucose sensor in counter-regulation, poised to mediate metabolic signaling at the neuronal/endocrine axis (110), (111). Though the importance of the Class II and Class III glucose transporters is undisputed, their individual functions are less well characterized and are the subject of current investigation. Because most of our structural and functional knowledge of glucose transporters relies upon analysis of the Class I GLUTs, they are the focus of this work.

Class I GLUT Tertiary Structure

Although common putative topology and sequence motifs exist among the glucose transporters, a crystal structure for a member of this family has yet to be solved. In the absence of such data, it is difficult to predict the spatial arrangement of TMs and their interactions during various conformational states of the transport cycle. However, structures displaying similar architecture have been solved for several homologous MFS bacterial transporters (96), including a cryo-EM structure of the oxalate transporter (OxIT (112)), and crystal structures of the lactose permease symporter (LacY (113)) and the glycerol-3-phosphate antiporter (GlpT (114)). Through homology-modeling the sequences of GLUTs 1, 3, and 4 on these bacterial transporter crystal structures, studies have proposed putative models of GLUT tertiary interactions.

Analysis of GLUT1 structure has been performed based on both LacY (115) and GlpT (116), with the GlpT-based model achieving better statistical scores. These studies juxtapose TMs 1, 2, 4, 5, 7, 8, 10, and 11 in a symmetrical arrangement, forming a central, water-filled sugar translocation channel coordinated by the scaffolding TMs 3, 6, 9, and 12 (see Figure 1.2; (116)). The proposed structure for GLUT3 (117) is based on the crystal structure of the channel protein MscL (118) and, more loosely, on the low-resolution structure of the pore aquaporin (119). While this model proposes a similar overall architecture in that several TMs are arranged to form a central transport cavity, the putative translocation pore is formed by only TMs 5, 7, 9, and 11.

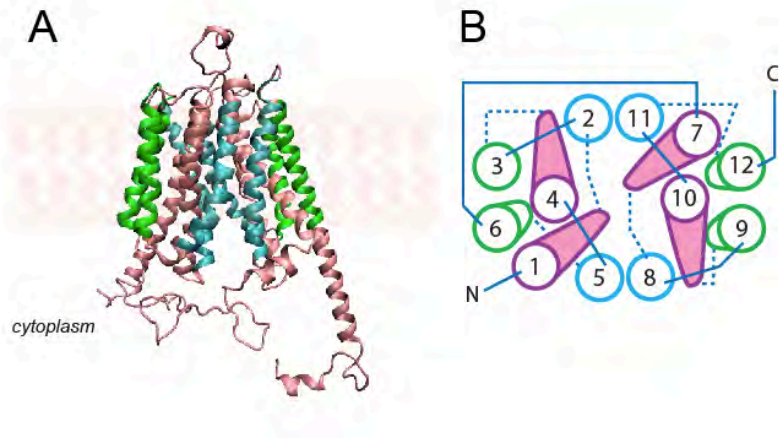

Figure 1.2 Threaded model of human GLUT1 based on homology-modeling with the GlpT crystal structure

A, Cross-sectional view of the 12 transmembrane (TM) spanning α-helices in the plasma membrane, colored corresponding to the color scheme in *B*, based on the homology modeling of GLUT1 on GlpT (Salas-Burgos et al., 2004). *B*, Cartoon diagram of the 12 TMs arranged spatially, looking up through the transporter from inside the cell, where the cytoplasmic loop 6 (connecting TMs 6 and 7), N- and C-termini are indicated by blue lines. The translocation pore is formed by TMs 1, 4, 7, and 10 (magenta) with TMs 2, 11, 5, and 8 (blue). The remaining TMs 3, 6, 9, and 12 (green) are positioned as scaffolding domains coordinating the arrangement of the TMs involved in sugar binding and translocation.

While the general TM arrangement is somewhat similar to the GLUT1 modeling, there are a disparate number of TMs between GLUT3 (12 TMs) and the scaffold proteins (MscL has 10 TMs; aquaporin has 6 TMs), neither of which is an MFS transporter. The docking studies of GLUT4 (120), (121), however, were also performed based upon the GlpT crystal structure. The proposed GLUT4 structure agrees with the spatial arrangement of the other GLUT homology models, showing interactions between glucose and putative translocation-channel TMs 1, 5, and 11, with helical interactions between TMs 1-5 and 2-4, respectively. However, one caveat of the GLUT3 and GLUT4 models is that both are partially based on biochemical data obtained for GLUT1, despite sequence agreement among the transporters of 63% or less. However, the GLUT4 model was extended with molecular dynamics simulations of not only substrates and inhibitors common to the Class I GLUTs, but also of GLUT4-specific inhibitors (121).

While both the LacY and GlpT structures were crystallized in the endofacial conformation, other MFS homologs have been crystallized in the exofacial conformation (fucose transporter, FucP; (122)) and an intermediate conformation (multi-drug transporter, EmrD; (123)). Further modeling of GLUT1 based on these scaffolds may provide insight on helix-packing and TM arrangements in these orientations, with implications for modeling the substrate-bound or occluded empty carrier during conformational transitions.

While the putative topology of GLUT1 has been refined and tested by further studies probing the accessibility of regions of the protein by various methods, these data

must also be used to assess the homology-threaded structure presented above. Several point mutations in GLUT1 shown to be critical to glucose transport based on investigation of residues involved G1DS (124), (125) or mutagenic structural studies (103), (126), (127), (128), (129) are indeed positioned within the sugar translocation pore in the GlpT-based model (116). Exposure of the TM-TM connecting loops has been analyzed by scanning glycosylation mutagenesis (93). Exposed lysine residues were analyzed by accessibility to proteolytic cleavage and modification by various probes (130), revealing that TMs 1 and 8 readily dissociate from the membrane upon being released from the rest of the scaffold. Extensive cysteine-scanning mutagenesis studies support the putative arrangement of the TMs in the model presented above, particularly that TMs 3, 6, 9, and 12 are outer (scaffolding) helices (131), (132), (133), (134), and that TM8 is part of the sugar translocation pore (135). However, some of these studies also show accessibility in regions that are not predicted to be accessible by the model (136).

A study aimed at testing the accuracy of MFS homology modeling compared the modeling of GlpT on the crystal structure of LacY to the actual crystal structure of GlpT as a proof of concept (137). The results suggest that while the GlpT-based GLUT1 model is consistent with overall TM arrangement and topology, it is insufficient to predict positioning of individual residues and side chains, and hence interactions among specific residues within the TMs and loops. This is not surprising, as GLUT1 sequence identity with these bacterial homologs is less than 20%. However, the sequence conservation among crystallized MFS proteins (LacY, GlpT, FucP, EmrD) is also only ~30%, yet all

solved structures show a similar architecture. In addition, the modeling of GlpT on LacY deliberately excluded any experimental evidence to avoid bias (137), whereas the modeling of all three GLUT structures attempted to validate and even constrain proposed interactions with the available experimental data. In general, these results are in good agreement with the homology-modeled structures, with the exception of the putative endofacial binding site of the inhibitor CCB in the GLUT1 model (116).

While the accuracy and utility of homology-modeled structures can be debated from either viewpoint, the reality exists that without a GLUT crystal structure, homology modeling and refinement based on additional experimental evidence is the only avenue currently available to explore the structure-function relationships in glucose transporters. As definitive characterization of GLUT tertiary structure has eluded the field, so too has an understanding of interactions between multiple GLUT subunits, and thus the potential role of oligomerization in catalytic function.

Class I GLUT Quaternary Structure

To date, the oligomeric state(s) of GLUT1 have been the most studied. While GLUT1 dissociates to a molecular weight consistent with a monomer when resolved on a denaturing gel (8), a variety of other studies suggest it exists in a higher order oligomeric state. Based on whether or not the samples were exposed to reducing conditions, particle sizes consistent with dimers and tetramers have been shown by freeze-fracture electron microscopy (138), (139), dynamic light scattering (138), size-exclusion chromatography

(140), (141), (142), and co-immunoprecipitation of heterologously-expressed GLUT1-GLUT4 fusion proteins (143). Based on the observation that GLUT3 appears to exist as a functional monomer or dimer ((144), Levine K, DeZutter J, and Carruthers A, in preparation), efforts to identify the domain(s) required for GLUT1 oligomerization by domain-swapping mutagenesis with GLUT3 implicate GLUT1 TM9 as a tetramerization motif (Levine et al., in preparation). The oligomeric state of GLUT1 may complicate analysis of its kinetic behavior; for example, studies aimed at defining CCB-binding stoichiometry support two fundamentally different oligomerization states, depending on whether the transporter is purified in the presence (145), (12) or absence (146), (140), (141) of reductant.

While studies employing size-exclusion chromatography analysis of the other Class I transporters, GLUTs 2 and 4, are ongoing (J. DeZutter and A. Carruthers, unpublished), their oligomerization state(s) is not yet known. Aside from the potential catalytic advantages of multimeric organization, the relative activity of glucose transporters may be affected by either direct regulation or by control of GLUT expression at the plasma membrane.

Regulation of Class I GLUT-mediated Transport

GLUT1 sequence contains several nucleotide-binding motifs ($GFSKLGKS_{111-118}$, a Walker A nucleotide binding motif; $KSVLK_{225-229}$; and $GRRTLHL_{332-338}$, a Walker B nucleotide binding motif). While depletion of intracellular ATP through metabolic stress

stimulates net sugar uptake, presence of ATP has been shown to decrease both capacity and affinity for sugar uptake in red cells (147), (148), an effect that can be competitively reversed by AMP and ADP (149). The binding of ATP to GLUT1 displays cooperativity (150), where the binding of one molecule of ATP has an effect on the affinity of binding a second. As this evidence argues for a direct interaction between ATP and GLUT1, many studies have aimed to elucidate the region(s) of the protein involved. Utilizing analysis of protection by covalent modification (151) and protease accessibility (152) in the presence and absence of ATP, studies have determined that cytoplasmic regions in the N- and C-termini, loop 6, and the loop connecting TMs 8 and 9 (loop 8) are implicated in ATP modulation of the transporter. Further investigation by alanine-scanning mutagenesis confirms that two residues within loop 8 are critical for ATP interaction with GLUT1 (153).

This nucleotide-binding motif in loop 8 is conserved within the other Class I GLUTs, as well. While the specific regulation by ATP has not been investigated for these transporters, ATP has been shown to reduce glucose uptake in insulin-stimulated adipocytes, implying regulation of GLUT4-mediated transport (154). GLUT4 has shown sensitivity to tyrosine kinase inhibitors (155) and flavonoids (156), such as genistein and quercitin, which also block GLUT1 uptake by interacting with the loop 8 ATP-binding motif (157). An interaction between ATP and this motif in GLUT4 was modeled in a ligand-docking study (158), implying that direct modulation is possible for GLUT4 as well. While this phenomenon has not been investigated as thoroughly in GLUTs 2 and 3,

intestinal cells expressing GLUT2 also show inhibition of uptake by flavonoids (159). These studies raise the possibility that several of the glucose transporters can be regulated at putative nucleotide-binding domains by multiple ligands.

Aside from direct interaction with other molecules or cofactors, the activity of GLUTs can be modulated through changes in how much transporter is present at the surface. For example, while GLUT3 is expressed at the plasma membrane in the brain, it is intracellular in both platelets and white blood cells. In platelets, GLUT3 is sequestered in α-granules until it is translocated to the surface upon stimulation by thrombin (160). In monocytes and β-lymphocytes, GLUT3 surface expression is triggered by insulin (161), (162), (163), which has also been shown to increase GLUT1 at the surface in insulin-responsive cells (164), (165).

GLUT4 has long been known as the ‘insulin-sensitive transporter’ due to its rapid release from intracellular pools to the plasma membrane upon insulin stimulation (166). Under basal conditions, GLUT4 is sequestered in intracellular pools by N-terminal FQQI (167), C-terminal dileucine (168), (169), (170), (171) and endosomal targeting (TELEYLGP, (172)) motifs. The hormonally-activated, reversible translocation of GLUT4 has been extensively studied (173), and it has been shown that insulin acts upon the rate of GLUT4 exocytosis through the trafficking pathways mediated by Akt/PI3K (phosphatidylinositide-3 kinase) (174) and Rab/GAP (GTPase Activating protein) (175). This results in an 8- to 20-fold increase in insulin-stimulated glucose uptake over basal conditions (176), (177).

Stimulation of other major signaling cascades, such as the protein kinase C (PKC) pathway, also contributes to plasma membrane localization of GLUTs. This has been shown with a variety of growth factors, which are able to increase surface levels of GLUT1 (178), (179). In addition, metabolic stress (i.e. hypoxia, exercise) also has been shown to cause an increase in GLUT4 surface expression through the AMP-activated protein kinase (AMPK) pathway (180), (181). More recently, this has been extended to show that acute metabolic stress increases GLUT1 cell-surface expression in endothelial cells (182) in an AMPK-dependent manner (183). Stimulation of transporter recruitment to the cell surface by both metabolic stress and insulin are capable of stimulating sugar transport up to 50-fold over basal rates (184).

While the activity of glucose transporters may be modulated by the extent of their expression or binding of external factors, the GLUTs possess intrinsically different substrate affinities and transport capabilities as well. These characteristics have been studied most extensively in GLUT1, particularly in red cells. Many of the classical kinetic assays were first established in erythrocyte experimental systems, but have since been extended to analyze differences in substrate transport by other GLUTs in a variety of cell types.

Kinetics of GLUT-mediated Glucose Transport

Several common experimental methods have been established to perform kinetic analysis of GLUT-mediated sugar transport (185), (186), (187); in all three, V_{max} and K_m

can be obtained for both sugar entry and exit under different conditions. The first, zero-trans (ZT), describes the measurement of unidirectional uptake or efflux of a varied concentration of labeled sugar on one side (*cis*) of the cell, to another side (*trans*), where no sugar is present. For example, zero-trans uptake measures the rate of sugar import from the interstitium into a cell that does not contain sugar. In the second type of experiment, equilibrium exchange, the total concentration of sugar may be varied, but it is kept equal on the *cis* and *trans* sides; in this way, the rate of exchange may be measured while the system is at equilibrium. The third method, infinite-cis, measures sugar moving from a saturating concentration on one side (*cis*) to the other side where sugar is varied to saturating (*trans*). More commonly, in an infinite-trans experiment, the cell is pre-loaded with a saturating amount of sugar inside (*trans*), and uptake of a varying amount of sugar from the outside (*cis*) is measured.

The majority of sugar transport studies have focused on the class I GLUTs, and GLUT1 has been the most extensively characterized (188), (189), (190) due to the experimental advantage presented by the high expression levels of GLUT1 in erythrocytes and the ability to isolate and purify the transporter from these cells. Although transport measurements of metabolized sugars are simplified by the slower metabolic processes in erythrocytes compared to conventional cell lines, the kinetics of red blood cell transport have proven to be complex as well (184). Many systems for heterologous expression have been used to add to the characterization of GLUT1-

mediated sugar transport, such as *Xenopus* oocytes (191), (192), (134), mammalian cell lines (164), (142), (24), (193), and yeast (194), (196).

Many studies employ both radiolabeled analogs of glucose and specific inhibitors in order to measure and stop transport. Two widely used sugar analogs are 2-deoxy-D-glucose (2-DG) and 3-O-methyl-D-glucose (3-MG) (29). Measurements of unidirectional sugar uptake are simplified by use of 2-DG, because it is phosphorylated inside the cell by hexokinase into 2-deoxy-D-glucose-6-phosphate (2-DG-6-P) (195), which is no longer a substrate for the cell. All Class I GLUTs have been shown to transport 2-DG. In contrast, 3-MG is not metabolized, and thus can be transported into and out of the cell (196). As previously referenced, the compound CCB is a potent endofacial inhibitor of Class I GLUT-mediated transport ($K_{i(app)}$ ~0.2 μM; (28), (29)), and is often used in experimental studies to quench transport measurements. Other commonly used inhibitors include phloretin, which is thought to act at both endo- and exofacial sites ($K_{i(app)}$ ~0.2 μM; (28)); and maltose, a lower-affinity competitive exofacial inhibitor ($K_{i(app)}$ ~6 mM; (28)). Studies employing these inhibitors and sugar analogs have aimed to characterize the transport capacity and affinity among the glucose transporters.

While physiologic affinity (K_m) for substrate varies with both transporter and substrate, the affinities for glucose and 2-DG are similar between GLUT1 and GLUT4 ($K_{m(app)}$ 2-6 mM (197), (198), (199), (144) or 10-14 mM (200)). While the reported affinities of GLUT1 and GLUT4 for 3-MG differ in some reports ($K_{m(app)}$ ~20 mM for

GLUT1 and ~2-5 mM for GLUT4 (191), (201), (202)), other studies have shown that they are similar ($K_{m(app)}$ ~6 mM for both (203); ~4 mM for GLUT1 (204), (205)).

One of the hallmarks of human erythrocyte GLUT1-mediated transport is asymmetry between the rates of sugar uptake and efflux. Both the rate and affinity of D-glucose and 3-MG exit are ~5- to 10-fold greater than the V_{max} and K_m for entry under zero-trans conditions (206), (207). While the magnitude of asymmetry is larger at lower temperatures, it can be measured over the range of 4 to 37°C (207). Despite the presence of asymmetry in human GLUT1, the ratio of V_{max} : K_m is the same under zero-trans exit, entry, and equilibrium exchange uptake conditions. Unlike GLUT1, both GLUT2 and GLUT4 display symmetrical uptake and exit of 3-MG when endogenously expressed in rat hepatocytes (208) or in basal and insulin-stimulated adipocytes (209). Because the absolute affinities may vary based on the system in which the transporters are tested, the experimental parameters, and the temperature at which the measurements are taken, it is important that direct comparisons be performed.

While it has been observed that common methods of measuring sugar transport may underestimate rates in erythrocytes (210), particularly those of 2-DG transport, there exists a complex interplay of variables including the cell system employed, surface expression of the transporter, choice and concentration of sugar analog(s), time point of measurements, and temperature at which the measurements are performed. Some of the complex kinetic characteristics of GLUT1-mediated transport become more or less pronounced depending on these variables.

While the initial kinetic studies in sheep placenta were the basis for the differentiation between transporters and simple channels (211), emerging data of complex kinetic behavior in erythrocytes have been incompatible with the most basic models for GLUT-mediated substrate transport. Over time, a growing body of experimental evidence has led to the development and refinement of several transport models to explain these observations.

The Simple Carrier Model

The most straightforward and oldest model for GLUT-mediated transport is the simple carrier (211), (212), (213), (214), which assumes that the basic catalytic unit comprises a single GLUT molecule. The simple carrier is capable of presenting a single substrate-binding cavity, which exists in either the endofacial (e_1) or exofacial (e_2) conformation (see Figure 1.3). When a single molecule of substrate is bound by the carrier in either conformation, the carrier undergoes a transformational change through an intermediate, occluded stage (e(S)). The substrate-binding cavity then reorients to face the opposite side from which the substrate was bound, and the substrate dissociates from the transporter, generating an empty carrier in the opposing conformation. One cycle of this unidirectional movement of substrate is known as translocation. In the instance of translocation of a sugar molecule into the cell, the empty carrier is now in an endofacial

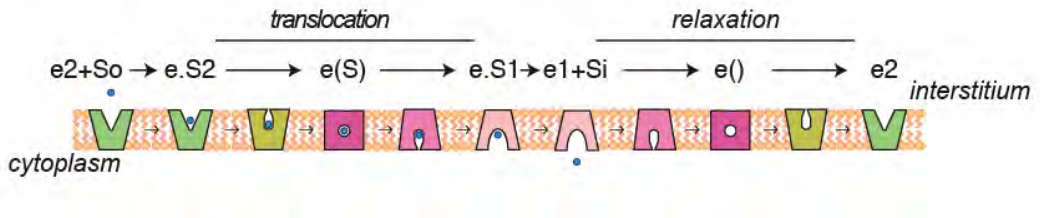

Figure 1.3 The Simple Carrier model for transport

The simple carrier may present 1 of 3 conformations at any instant: e_2, exposing an exofacial sugar binding site; e(), an intermediate state in which neither surface of the carrier exposes a sugar binding site and where a central cavity is occluded from extra- and intracellular water; and e_1, exposing an endofacial sugar binding site. These 3 states reversibly inter-convert as $e_2 \rightleftharpoons e() \rightleftharpoons e_1$. When extracellular sugar (S_o) or intracellular sugar (S_i) is complexed to e_2, e(), or e_1 (denoted as $e.S_2$, e(S), or $e.S_1$, respectively), the inter-conversions are termed “translocation.” When no sugar is bound, the inter-conversions are termed “relaxation.”

(e_1) conformation. In order to bind a second molecule of sugar on the outside of the cell, the substrate-binding cavity must first reorient to the exofacial (e_2) state. This can occur through one of two pathways. If the carrier remains empty, it must undergo "relaxation," in which it isomerizes from the e_1 to the e_2 conformation via e(). Alternately, if intracellular sugar is present, the e_1 conformer can become complexed with another molecule of sugar (to form $e.S_1$), undergo reorientation via e(S) to form $e.S_2$, and release the bound sugar at the exterior of the cell to regenerate e_2. Because this second pathway involves translocation of a substrate, it is called "translocation," not relaxation. However, the simple carrier is not compatible with all experimentally observed transport, particularly in erythrocytes. Studies have shown that the endofacial inhibitor CCB is able to inhibit transport at the same time as the extracellular inhibitor maltose (215). The simple carrier model is incompatible with the apparent binding of both endo- and exofacial ligands simultaneously.

The Fixed-Site Carrier Model

An alternate model of the single subunit-based carrier is the fixed-site carrier (see Figure 1.4; (262)). This model posits a higher-affinity exofacial binding site and a lower-affinity endofacial binding site, allowing for the greater V_{max} and K_m observed for sugar exit than entry under saturating extracellular sugar concentrations (206), (216), (217). The fixed-site carrier model differs in that the carrier presents both endo- and exofacial (e_1 and e_2) binding sites simultaneously.

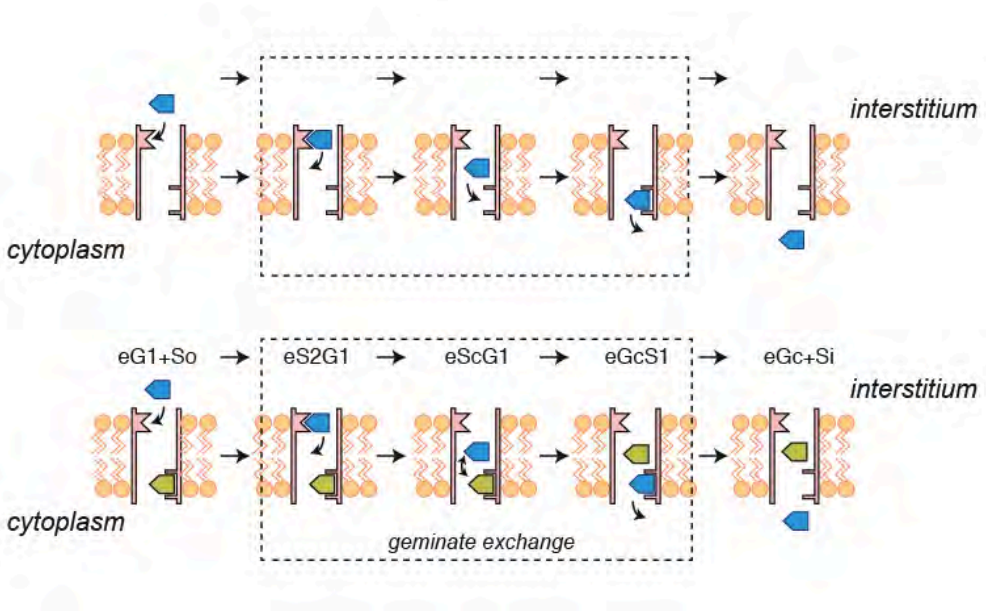

Figure 1.4 The Fixed-Site Carrier model for transport

The fixed site carrier simultaneously presents two sugar binding sites, endofacial (e_1) and exofacial (e_2), and a central cavity. The central cavity is large enough to permit 2 sugar molecules to pass in opposite directions. Dissociation of sugar from e_2 to the cavity and subsequent association with e_1 is called exchange (top cycle). When e_1 and e_2 are occupied by sugar, exchange of bound sugar with cavity sugar is called “geminate exchange” (bottom cycle).

This would allow sugar or inhibitors to bind the transporter on both sides at the same time and be taken up into a central cavity, where the molecules could exchange past one another to *cis*- and *trans*- binding sites within the cavity, upon which they would dissociate from the carrier and be released to the opposite side of the membrane.

The fixed-site carrier explains how the V_{max} for exchange can be equal for two substrates with disparate translocation rates (218). This model is also compatible with the observed differences in substrate stereospecificity (219). Despite the partial overlap in common substrates (glucose, fructose, and 2-DG) among GLUTs of all three classes, there is evidence which suggests that the stereospecificity of the substrate plays an important role in its recognition by the transporter. For example, the hexose C1 hydroxyl position appears to be most important for glucose-exofacial transporter interactions in Class I GLUTs (204), while the C3 and C4 hydroxyl positions may also play a role in fructose transport by GLUTs 2 and 5 (220), (221). Evidence suggests differences in the endofacial binding site, where the C6 position of the hexose may become increasingly important for interactions (222). It has been proposed that the differences in substrate specificity indicate the presence of a selectivity filter that is distinct from the sugar translocation pore (223).

The fixed-site carrier model is also consistent with the multiphasic nature of transport. Uptake at millisecond time points determined by quench-flow analysis indicates that GLUT1-mediated transport in erythrocytes is multiphasic (224). This study describes rapid, fast and slow phases of glucose translocation, which are complicated by

potential re-binding of substrate at the e_1 site, or slow release of substrate into a water-based compartment formed by the cytosolic domains of the transporter.

While both the simple carrier and the fixed site carrier models are consistent with the asymmetry observed in GLUT1-mediated transport, neither can explain the low K_m observed in infinite-cis entry or infinite-trans exit (206), (225), (226). In addition, the fixed site carrier model fails to explain data suggesting allosteric or cooperative binding of modulators or inhibitors, such as ATP and CCB (227), (228), (229), (150). Although ATP has been shown to modulate GLUT1-mediated transport, the precise mechanism is unknown. Binding of ATP is thought to affect transport rate and substrate affinity by allosteric modulation of intracellular sugar binding sites (230). Interestingly, GLUT1 binding of endofacial inhibitors (CCB, forskolin) or exofacial inhibitors (maltose) at low concentrations has been shown to increase affinity for sugar at the exofacial site (228), (229). This cooperativity indicates the presence of non-catalytic sites for allosteric modulation of the transporter, leading to the necessary refinement of the fixed-site carrier model.

The Modified-Fixed Site Carrier Model

To address the complex behaviors of allostery and cooperativity observed in red cell transport, a hybrid model of the simple and fixed-site carriers has been proposed (see Figure 1.5; (228)). In this model, two (or more) functional simple carrier subunits are coupled in a functionally anti-parallel fashion. Each subunit may still only present a

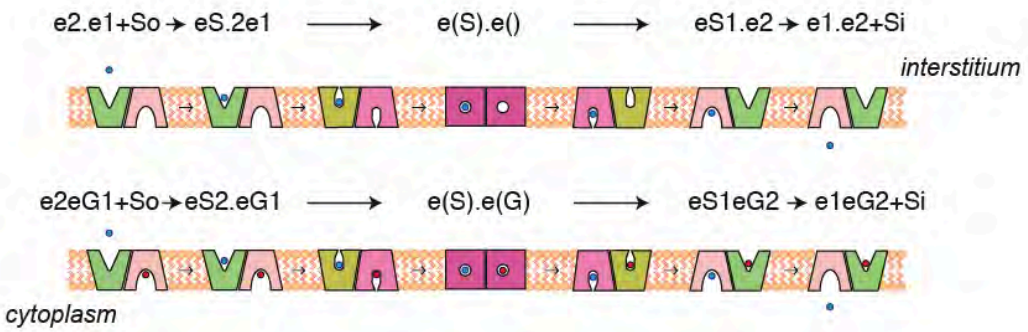

Figure 1.5 The Modified Fixed-Site Carrier model for transport

A two-site variant of the simple carrier in which the carrier comprises 2 (or more) subunits, which are functionally coupled in an anti-parallel fashion. If one subunit presents an e_2 site, the adjacent subunit must present an e_1 site and *vice versa*, even if only one subunit translocates a sugar molecule (top cycle). If only one subunit contains a bound sugar, the unoccupied subunit impedes translocation via the occupied subunit because the unoccupied subunit undergoes relaxation, which is slower than translocation (as with the simple carrier, Figure 1.3).

single substrate binding site at opposite sides of the membrane (e_1 or e_2, as in the simple carrier). However, conformational change of one subunit forces the adjacent subunit to undergo the opposite isomerization to the opposite confirmation, regardless of whether it is empty or complexed with substrate. Sugar could be translocated in both directions at the same time, or unidirectional sugar uptake or efflux could occur with one carrier occupied and the other, vacant.

As additional experimental data is gathered in a variety of systems, further refinement of these transport models is expected. However, lack of a crystal structure for any of the GLUTs precludes a definitive understanding of the physical mechanism of transport. The current models have been developed based on decades of experimental evidence, and some have been refined based on the topology and threaded structure discussed above. Several models exist due in part to the complex transport behavior exhibited by erythrocyte GLUT1, which cannot always be explained by the more simplistic models of carrier-mediated sugar transport. However, there are other observed kinetic behaviors that are consistent with all three models for transport, yet the basis of which are not understood. One such behavior is that of accelerated-exchange transport, or trans-acceleration.

Trans-acceleration in Class I GLUTs

Since the early experimental characterizations of GLUT1-mediated sugar transport, it has been reported that a 2- to 10-fold stimulation of unidirectional sugar

uptake is observed in the presence of intracellular sugar (188), (206), (207). This stimulation, or acceleration, of uptake when there is sugar in *trans* has been observed with a variety of substrates (glucose, 2-DG, 3-MG) in a variety of cellular environments, such as human, avian, dolphin, and rat erythrocytes (231), (148), (232), (233), mouse endothelial cells (182), and heterologously expressed GLUT1 in HEK cells (234) and *Xenopus* oocytes (235). Trans-acceleration is also observed for other carrier-mediated transport systems such as nucleoside and amino acid transporters, and is one of several important functional behaviors that distinguish carriers from channels (186). However, it has not been established whether this phenomenon is sequence-based and thus intrinsic to GLUT1, whether it is an allosteric modulation of the transporter that requires co-factors, whether it is dependent on cellular context, or whether it is simply an artifact of experimental conditions used to measure transport.

Like asymmetry, trans-acceleration in GLUT1-based systems has been shown to be temperature-dependent (207); trans-acceleration is more pronounced at 4°C than at physiological temperature. It has been suggested that this is due to the higher prevalence of inward-facing carrier (e_1) at lower temperatures (207), but this cannot explain trans-acceleration in the absence of transport asymmetry (e.g. in ATP-free human red cell ghosts (236) or in rat erythrocytes (230)).

The ability to catalyze trans-acceleration has been tested in all the class I GLUTs. Human GLUT3 expressed in *Xenopus* oocytes displays trans-acceleration (237), (24). Interestingly, the other Class I transporters, GLUTs 2 and 4, do not display trans-

acceleration. For example, GLUT2-expressing rat hepatocytes do not show accelerated exchange (208). In rat adipocytes stimulated with insulin, where GLUT4 expression is very high, trans-acceleration is not observed (203), (177).

Trans-acceleration in the Context of Transport Models

While many of the complex behaviors of GLUT-mediated transport are supported by one of the prevailing models for transport, trans-acceleration is compatible with all three models. In the context of the simple carrier, trans-acceleration is explained by assuming that relaxation of the empty carrier is slower than translocation by the substrate-complexed carrier. Indeed, relaxation in human erythrocyte GLUT1 proceeds 50- to 100-fold more slowly than translocation at 4°C (207), (238). In such a case, intracellular sugar would permit the carrier to bypass the slower step of relaxation, thereby undergoing many more rounds of translocation until equilibrium is reached. At ice temperature, a greater proportion of the transporters exist in the e_1 conformation, assuming the simple carrier hypothesis is correct (207). While this might lead to the conclusion that a greater number of opportunities would exist to drive e_1 back to e_2 via translocation in the presence of intracellular sugar, any such affect would be offset by the 10-fold lower affinity that e_1 has for substrate (207). Therefore, the major determinant of trans-acceleration via the simple carrier derives from the relative rates of translocation and relaxation.

For transporters that do not display trans-acceleration (i.e. GLUT4), this would be explained by equal rates of relaxation and translocation. In this case, there would be no advantage to the presence of intracellular sugar, as the rates of carrier conformational change would be equal in the presence or absence of substrate.

In the context of the fixed-site carrier, trans-acceleration occurs if the presence of a sugar in either the *cis*- or *trans*- binding site accelerates the binding and thus exchange of another molecule of sugar at the opposite binding site, a process termed geminate exchange (239). This model assumes that occupancy of one binding site would affect the affinity or binding constant of sugar in the opposite binding site for carriers that display trans-acceleration. However, these affinities or binding constants would have to be equal in both sugar-binding sites in carriers that do not catalyze trans-acceleration.

The basis of trans-acceleration can be understood in the context of the modified fixed-site carrier by assuming that, as in the simple carrier, relaxation is the rate-limiting step in the transport cycle. In this case, the translocation of one molecule of sugar into the cell ($e.S_2$ to $e.S_1$) would be as slow as the coupled relaxation of the neighboring empty carrier (e_1 to e_2) in the absence of intracellular sugar. However, sugar inside the cell would allow the second subunit to also translocate a molecule of sugar, thereby accelerating uptake by the first subunit. Thus the conformational change in one subunit is constrained (inhibited or accelerated) by those of the adjacent subunit. Here, the assumption would be the same as that of the simple carrier: in transporters that show trans-acceleration, the conformational relaxation step would be slower than translocation,

whereas the two rates would be equal in carriers which do not display accelerated exchange.

Trans-Acceleration in Homeostasis

In order to understand why some transporters might display this kinetic phenomenon and others may not, it is helpful to consider the possible advantage of trans-acceleration. In simulations where the V_{max} of sugar uptake and time to equilibration are modeled in the presence and absence of trans-acceleration (see Figure 1.6; (240) and A. Carruthers, unpublished), it is apparent that the half-time to equilibration is much shorter when trans-acceleration is extant. This could be a physiological advantage in situations where the amount of sugar is under tight control and a rapid equilibration would be desirable, e.g. at blood-tissue barriers such as the brain, placenta, retina, and lactating mammary gland. Indeed, such barriers show high expression of either GLUT1 (241), (242), (243), (244) and/or GLUT3 (245), (246), both of which are capable of catalyzing trans-acceleration. In contrast, in tissues where hormonal control can tune the amount of cell-surface transporter in order to affect sugar uptake rates, trans-acceleration would not present the same advantage. The liver, pancreas, skeletal muscle, and adipose tissue, which are the common sites of GLUT2 and GLUT4 expression (17), (247), are responsive to hormonal control.

Expression of a combination of transporters that can and cannot catalyze trans-acceleration could be advantageous for tissues to adapt to sudden metabolic changes. For

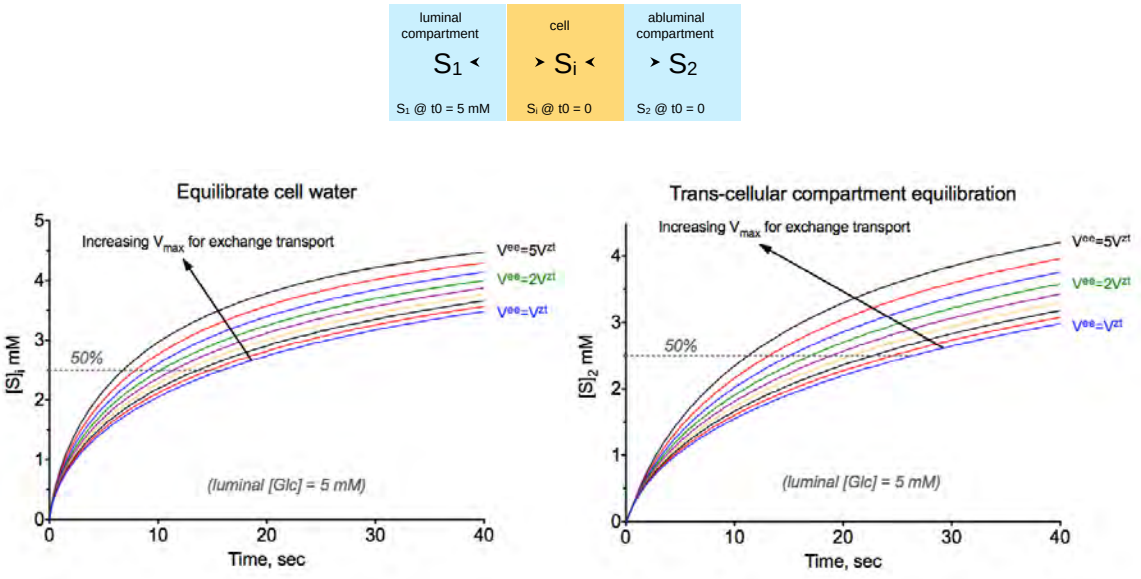

Figure 1.6 Simulation of the effect of trans-acceleration on half-time to compartmental equilibration

The simulated data for 5 mM sugar (Glc) on the outside, or luminal compartment (cyan; S_1), taken up in zero-trans into a cell with no intracellular sugar (orange; S_i), and no sugar present in the abluminal compartment (cyan; S_2). As sugar is taken up into the cell (left graph) from the luminal compartment (*ordinate*) over time (*abscissa*), the half-time to equilibration decreases as the V_{max} for exchange increases. This is observed when trans-acceleration is set to increase 2- to 5-fold (V^{ee}=2V^{zt} to V^{ee} =5V^{zt}; V^{ee}, V_{max} for equilibrium exchange; V^{zt}, V_{max} for zero-trans transport) over when no trans-acceleration is set (V^{ee} = V^{zt}). In the second transport step (right graph), the sugar from inside the cell (S_i) is exported in zero-trans into the abluminal compartment (S_2), which is devoid of sugar. As sugar equilibrates to S_2 (*ordinate*) over time (*abscissa*), the half-time to equilibration from S_1 through the cell to S_2 is reduced. When a 5-fold stimulation by trans-acceleration is set, the half-time to equilibration is reduced by ~70% (10 sec versus 30 sec).

example, adipocytes and cardiomyocytes express both GLUT1 and GLUT4 (248), (76). Although total protein expression levels of GLUT4 are often much higher than that of GLUT1 (79), GLUT1 is the predominant glucose transporter at the cell surface during basal metabolic states. However, signaling by insulin or exercise induces rapid translocation of intracellular GLUT4 (173), (249), where it becomes the primary glucose transporter. This would quickly increase the ability to take up more glucose, with less emphasis on equilibration; in adipose tissue, for conversion and storage, and in cardiomyocytes, to respond to the increased metabolic demands of exercise.

While other transporter characteristics such as affinity, capacity, and specificity for different substrates are critical in the tissue-specific and temporal changes in GLUT expression, it is possible that ability to catalyze trans-acceleration is a previously unknown factor.

Remaining Questions

In the absence of a structure to clarify the mechanism of GLUT-mediated glucose uptake, evaluating the existing models for GLUT1 structure and transport mechanism based on experimental observation is the only way to expand our understanding. The proposed models must explain the observed data, and the experimental evidence can be used to refine the models further. Through iterative refinement of data interpretation and defining the next questions to ask experimentally, we may further elucidate the structure and function of glucose transporters. If or when these proteins are crystallized, the solved

structures will also be evaluated based on their agreement with the substantial body of evidence that has been collected about glucose transport over the last 60 years. The dangers of not reconciling transporter structure with the existing body of data on transporter biochemistry and behavior are vividly illustrated in the case of the ABC transporter MsbA, where an inverted structure was published and later retracted (250), (251).

While the modified fixed-site carrier is consistent with much of the data available for GLUT-mediated transport, certain complexities, particularly those of erythrocyte transport, are not explained by any of the current models (225), (226), (234). This highlights the intrinsic difficulties in modeling the transport cycle based on kinetic data alone; the field awaits more detailed knowledge relating transporter structure and function.

Although the kinetic phenomenon of trans-acceleration has been observed since the beginning of glucose transporter characterization, its mechanism is unknown. While a multitude of GLUT variants and point mutants have been tested for activity, expression, substrate and inhibitor specificity or affinity, localization, and structural dynamics, none of these has evaluated whether or not trans-acceleration is intrinsic to the carrier. If it is not, does trans-acceleration occur based on cellular environment, i.e. in response to a modulating co-factor? If trans-acceleration is sequence-based, are the required elements related to those determining substrate or inhibitor binding, or oligomerization of carrier

subunits? Can the identity of the necessary domain(s) be explained by the putative models of GLUT1 structure, or refine the current available models for glucose transport?

This thesis attempts to address these questions by evaluating systems and methodologies for measuring trans-acceleration, defining the domain(s) that are necessary and sufficient for trans-acceleration in Class I glucose transporters, and evaluating their potential role in the transport cycle within the current models for GLUT structure and transport.

CHAPTER II

Detecting Changes in Trans-Acceleration of Transport Mediated by Endogenous GLUT1 and GLUT4 in 3T3-L1 Fibroblasts and Adipocytes

Abstract

The human facilitative glucose transporter GLUT1 displays accelerated-exchange transport in the presence of intracellular sugar, while the related transporter GLUT4 does not. Comparison of these proteins may assist in understanding the basis for this phenomenon, known as trans-acceleration. Because the factor(s) governing the ability of a glucose transporter to catalyze trans-acceleration may be determined by cellular context, a system with endogenous expression of these GLUTs is ideal for comparison. Characterization of the 3T3-L1 fibroblast/adipocyte cell line confirmed that while GLUT1 is the basal transporter in fibroblasts, GLUT4 expression is significantly increased in adipocytes. In order to determine whether catalysis of trans-acceleration is intrinsic to GLUT sequence, it is necessary to first establish experimental conditions under which trans-acceleration can be measured. Analysis of transport 3T3-L1 cells confirmed that fibroblasts show GLUT1-mediated trans-acceleration of sugar uptake. However, upon differentiation, trans-acceleration persists in both basal and insulin-stimulated adipocytes, a characteristic which is not displayed by GLUT4. This implies

the presence of a heterogenous population of cell-surface transporters and/or cells in various differentiation states. In addition, temporal mapping of the counterflow transient, a signature of carrier-mediated transport, was indicative of extremely rapid kinetics. Sugar uptake proved to be so rapid ($t_{0.5}$ ~1-2 seconds) as to preclude accurate, reproducible comparisons of GLUT1- and GLUT4-mediated transport in 3T3-L1 cells. This study revealed that alternate approaches to transporter expression and methodologies to measure trans-acceleration are necessary to analyze sequence-based kinetic differences in GLUTs 1 and 4.

Introduction

Since the very first kinetic characterizations of the ubiquitously expressed human GLUT1 glucose transporter in the 1950's, it has been observed that the presence of sugar in *trans* results in an acceleration of unidirectional sugar uptake or efflux, termed trans-acceleration (188), (206), (207). This phenomenon results in a 2- to 10-fold stimulation in the V_{max} for the rate of exchange compared to the V_{max} for the rate of zero-trans sugar uptake. The ability to catalyze trans-acceleration may present an advantage in certain physiological contexts in that it allows the equilibration of sugar on either side of the cell membrane to be reached more rapidly (Figure 1.6; (240) and A. Carruthers, unpublished).

In contrast, the related human isoform GLUT4 does not show trans-acceleration in the presence of intracellular sugar. This has been observed experimentally in rat

adipocytes (209), (177). Unlike GLUT1, GLUT4 is mainly expressed in adipocytes and skeletal muscle. Despite differences in expression patterns, GLUT1 and GLUT4 are similar in length (492 and 508 amino acids, respectively) and are both Class I glucose transporters. While these transporters show a greater sequence conservation than most of the other 12 GLUT isoforms, they still only exhibit 68% sequence identity. Variations in sequence are primarily in the N-terminal half of the protein, the intracellular loop 6, and the cytoplasmic C-terminus. These disparities between GLUT1 and GLUT4 prompt the hypothesis that accelerated-exchange may be sequence-based.

While a multitude of studies has employed mutations in GLUT1 TM domains, loops, and both termini, none has been used specifically to analyze whether trans-acceleration is intrinsic to GLUT1 sequence. As such, many of these mutations are not conservative. Alanine- and cysteine-scanning mutagenesis have been used extensively to characterize which region(s) of GLUT1 are exposed to proteolysis or are critical for substrate/inhibitor binding (129), (135), (136), (153), (130). Some of these mutations are not possible to test because they prevent proper folding, expression, or function of the protein. Due to these complexities, an approach using more conservative sequence substitutions is desirable. Despite the variations in sequence between GLUTs 1 and 4, the TM-domain regions are the most highly conserved in both length and sequence (10). Thus the substitution of TM regions among these transporters would increase the likelihood of proper folding, TM insertion into the membrane, and functional transport.

As the glucose transporter which was first identified and cloned, more is known about the kinetic characteristics of GLUT1 (8), (252) than the other human glucose transporters. Due to its potential role in diabetes as an insulin-sensitive transporter, GLUT4 kinetics and expression also have been studied thoroughly. The affinities for 2-DG transport by GLUT1 and GLUT4 in skeletal muscle have been shown to be indistinguishable (K_m ~10 mM; (200)). While some studies report that GLUT4 has a ~4-fold higher affinity for 3-MG than GLUT1 (191), (201), (202), other comparisons of K_m for 3-MG have shown a similar range for both transporters (~4-6 mM; (209), (204), (205)). In addition, the ability to induce large amounts of GLUT4 expression at the plasma membrane by insulin stimulation provides a tunable expression system that could aid in transport measurements.

Despite the sequence disparity between GLUTs 1 and 4, it is possible that trans-acceleration is governed by a phenomenon external to the protein. For example, interaction with modulating co-factors, perhaps even in specific cellular contexts, may play a role. Thus it would be ideal to establish methodologies for measuring the presence and absence of trans-acceleration in cells with endogenously expressed transporters.

The obvious choice for comparing GLUT1 and GLUT4 kinetics in a system where both are expressed would be skeletal muscle or adipose tissue (249), (76). Because GLUT1 is the basal transporter used in the majority of tissues, its ability to catalyze trans-acceleration should be evident in the basal metabolic state, provided it is the dominant GLUT isoform expressed. GLUT4 contains targeting sequences that keep the transporter

sequestered in intracellular storage compartments under basal conditions (167), (168), (169), (170), (171). However, stimulation by insulin and/or exercise affects trafficking pathways within the cell. This results in the rapid translocation of GLUT4-containing vesicles to the plasma membrane, where GLUT4 becomes the primary transporter (166). This would provide a unique opportunity to compare the presence and absence of trans-acceleration in transport mediated by GLUT1 and GLUT4, respectively, in the same system where both are endogenously expressed.

Because expression of GLUT1 or GLUT4 can be theoretically controlled by cellular differentiation, adipose tissue offers an experimental advantage over skeletal muscle for this purpose. Although insulin stimulates both cell types, the greatest amount of GLUT4 translocation in muscle cells is observed with a combination of insulin and contraction (200), (253). In contrast, high levels of GLUT4 translocation to the cell surface in adipocytes only requires the addition of insulin. The murine fibroblast cultured cell line 3T3-L1 has been used for decades to study GLUT4 trafficking and insulin responsiveness, and is thus well characterized (254), (255), (256), (257).

While it is the ultimate goal of the study to compare human glucose transporters, alignments of murine and human isoforms show high sequence conservation. Mouse GLUT1 sequence is 97% homologous to human GLUT1, with a difference of only 17 amino acids; while mouse GLUT4 is 95% identical to the human isoforms, with 24 disparate residues.

Here we characterize expression levels of GLUT1 and GLUT4 mRNA in 3T3-L1 fibroblasts and adipocytes using reverse transcriptase (RT) and quantitative PCR (qPCR), and protein expression by Western blot. We then establish parameters for kinetic measurements of 3-MG transport by performing time courses and dose-responses. These experiments produce transport data that deviate from Michaelis-Menten behavior, suggesting that we did not measure initial rates of transport. Changing the inhibitor we used to quench transport and shifting our measurements to earlier time points indicated that we could measure counterflow, which we mapped over several time points to confirm. The slope of the counterflow measured in fibroblasts indicated the presence of GLUT1-mediated trans-acceleration. However, trans-acceleration persisted in insulin-stimulated adipocytes, indicating that either background GLUT1 expression levels were too high or a mixed population of fibroblasts and adipocytes precluded the detection of GLUT4-mediated loss of trans acceleration. In addition, a time course of 3-MG uptake in stimulated adipocytes was even more rapid than transport observed in fibroblasts. These data suggest that 3-MG transport in 3T3-L1 cells is too rapid to compare kinetics of stimulated adipocytes and basal fibroblasts experimentally, even at ice temperature.

Experimental Procedures

Materials

Frozen 3T3-L1 cells of passage 3 were obtained from the laboratory of Dr. Michael Czech, Program in Molecular Medicine, University of Massachusetts Medical

School, Worcester. DMEM, DPBS, penicillin/streptomycin, trypsin, Bis-Tris gels and MES buffer were obtained from Invitrogen. FBS was obtained from HyClone. All primers were purchased from Integrated DNA Technologies. RNeasy, Qiashredder and One-Step RT-PCR kits were from Qiagen. iScript One-Step PCR kit with SYBR green was purchased from BioRad. PVDF membranes were obtained from ThermoFisher. 10% bovine serum albumin was from American Bioanalytical. Super Signal Pico West and micro-BCA kits were from Pierce. Protease inhibitor cocktail tablets were from Roche. [^{3}H]-3-O-methyl-D-glucose was purchased from MP Biomedical. Insulin, SDS, 3-MG, maltose, CCB, phloretin, methyl-3-isobutyl xanthine (IBMX), dexamethasone (DMT) and all other chemicals were purchased from Sigma.

Solutions

Growth medium was DMEM containing 10% FBS, 1% penicillin/streptomycin. Freezing medium was growth medium containing 5% DMSO. Cell lysis buffer consisted of DPBS, 1% SDS plus protease inhibitiors with EDTA. TBS contained 20 mM Tris base, 135 mM NaCl, pH 7.6. Sample buffer consisted of 0.5 M Tris-Cl, pH 6.8, 40% (v/v) glycerol, 8% SDS, bromophenol blue, and 150 mM DTT. Stop solution consisted of either 10 µM CCB and 100 µM phloretin or 80 mM maltose, as indicated.

Antibodies

A custom-made (New England Peptide) affinity-purified rabbit polyclonal antibody raised against a peptide corresponding to GLUT1 C-terminal residues 480-492 was used at 1:10,000 dilution as described previously (152). A goat polyclonal anti-

GLUT4 C-terminal antibody (Santa Cruz sc-1608) was used at 1:1,000 dilution. Horseradish peroxidase-conjugated goat anti-rabbit and donkey anti-goat secondary antibodies (Jackson ImmunoResearch) were used at 1:50,000 and 1:30,000 dilution, respectively.

Tissue Culture

3T3-L1 fibroblasts were prepared by thawing the original vial of P3 cells into 2x150mm^2 plates with growth medium. After 48 hours, these were split at a ratio of 1:4. Cells were dissociated from the dish for passage or storage by incubating with 0.5% trypsin for 5 min at 37°C, centrifuging for 5 min at 950 rpm, and resuspension in medium for growth.

A fresh vial of 3T3-L1 fibroblasts was thawed each week. These were grown in 150 mm^2 dishes at 37°C, 5% CO_2 and fed every 48 hours with growth medium. When confluent, fibroblasts were dissociated from the plate by incubation with 0.5% trypsin-EDTA for 5 minutes and split at 1:4 and/or used for experiments after 4 days of growth and feeding. Differentiation into adipocytes was performed as described previously (258). Briefly, 0.5 µg/ml insulin, 0.5 mM IBMX and 0.25 µM DMT were added to fibroblasts on day 7. Differentiating cells were fed with normal growth medium on day 10 and day 12. Adipocytes were used for experiments on or after day 14, and the change in cell morphology was verified by phase-contrast microscopy prior to all experiments.

For transport experiments, all cells were transferred to 12-well plates at least 24 hours prior to transport measurements. When indicated, adipocytes were stimulated with

100 nM insulin during the final 20 minutes of the 2-hour serum starve at 37°C prior to performing transport measurements.

Endpoint RT-PCR

Total RNA was isolated from 3T3-L1 fibroblasts or adipocytes using the RNeasy kit and Qiashredder. End point RT-PCR was performed as per the One-Step RT PCR kit instructions using mouse GLUT1- and GLUT4-specific primers (see Appendix, Table A2; primers were obtained from Dr. Anthony Cura). RT-PCR products were resolved on a 1.5% agarose gel in TAE buffer. Bands were visualized by ethidium bromide staining under UV light on a FujiFilm LAS 3000 and analyzed using FujiFilm MultiGauge software.

Quantitative RT-PCR

Expression levels of GLUTs 1 and 4 were measured by qPCR using the iScript One-Step PCR kit with SYBR green. Reactions were performed according to the kit protocol using 100 ng total RNA isolated using the RNeasy kit and Qiashredder, and using mouse GLUT1- and GLUT4-specific qPCR primers (see Appendix, Table A2; primers were obtained from Dr. Anthony Cura). Samples were run in duplicate on an MJ Research PTC-200 Peltier Thermal Cycler with a Chromo4 real time PCR detector running Opticon Monitor 3 software (Bio-Rad). Results were analyzed by using the delta-delta Ct method (259) and normalized to an EIF-1α control.

Western Blotting

Cells were trypsinized, pelleted, washed with DPBS, lysed in cell lysis buffer, and protein concentration was assessed using a micro-BCA kit. Lysates were normalized for total protein concentration and resolved by SDS-PAGE on a 10% Bis-Tris gel in MES buffer. Gels were transferred onto PVDF membranes, blocked with 10% bovine serum albumin in TBS-T, probed with primary antibody overnight at 4°C, probed with secondary antibody for 1 hour at room temperature, and developed using Super Signal Pico West Chemiluminescent substrate. Blots were imaged on a FujiFilm LAS-3000 and relative band densities were quantitated using ImageJ software.

3-MG Transport and Time Course

3-MG transport was performed as described previously (234). Briefly, 12-well plates of confluent 3T3-L1 cells were serum- and glucose-starved for 2 hours at 37°C in FBS- and penicillin/streptomycin-free DMEM lacking glucose. Cells were washed with 0.5 mL DPBS at 4°C, then exposed to 0.4 mL of uptake solution containing the indicated concentration of cold 3-MG plus 2.5 µCi/ml [^{3}H]-3-MG for the indicated time point at 4°C. Uptake was stopped by addition of 1 mL ice-cold stop solution. Cells were washed twice with ice-cold stop solution and extracted with SDS extraction buffer. Total protein concentration was analyzed in duplicate using a micro-BCA kit. Each sample was counted in duplicate by liquid scintillation spectrometry. Each condition was performed in triplicate.

Zero-Trans, Equilibrium Exchange and Infinite-Trans 3-MG Uptake Measurements

Zero-trans sugar uptake describes uptake of sugar into cells lacking intracellular sugar. This was achieved by using no glucose or sugar analogs during the 2 hour serum-starve and PBS washes described above. Equilibrium exchange uptake describes equal amounts of sugar inside and outside of the cell. This was achieved by pre-loading cells with the same amount of 3-MG (5-40 mM) contained in the uptake medium for that condition, a concentration which was kept constant throughout the 2 hour serum starve and PBS washes prior to uptake. Infinite-trans uptake describes uptake into cells that have been pre-loaded with a saturating amount of sugar. This was achieved by pre-loading the cells with either 40 or 80 mM 3-MG, as indicated, during the 2 hour serum starve and PBS washes.

Transport Data Analysis

All data analysis was performed using GraphPad Prism (La Jolla, CA, v 5.0). For sugar uptake experiments, background counts were subtracted from all samples and uptake, *v*, was normalized to [total protein]/well. [^{3}H]-3-MG uptake (DPM/µg) was then converted to mol/µg protein/min by using the measured specific activity of the uptake solution. For dose-response experiments, sugar uptake was fitted to the Michaelis Menten equation (Equation 2.1):

$$v = \frac{V_{\max}[S]}{K_m + [S]}$$

by non-linear regression analysis, which yielded the values for V_{max} and K_m.

For experiments studying the inhibition of uptake by maltose, sugar uptake was fitted to the inhibition equation (Equation 2.2):

$$y = y_0 - \frac{span[maltose]}{K_{i(app)} + [maltose]}$$

by non-linear regression analysis, where y_o is the y-intercept ([maltose] = 0) and span is the distance between the maximal and minimal values for sugar uptake. The inhibition constant (K_{iapp}) for transport inhibition by maltose was extracted from the fit.

Results

Differentiation and GLUT1/GLUT4 expression in 3T3-L1 fibroblasts and adipocytes

In order to assess whether the 3T3-L1 cell line could be used to measure GLUT1- and GLUT4-mediated transport, we first had to characterize the changes in expression of these transporters during differentiation of fibroblasts into adipocytes. Differential interference contrast (DIC) microscopy was used to compare the morphology of live, unmodified pre- and post-differentiation cells (Figure 2.1A and B). While undifferentiated 3T3-L1 cells have a typical fibroblast morphology, this changes when the same cells are examined 1 week after culturing in the presence of IBMX, DMT and insulin. The adipocyte morphology (260) is characterized by accumulation of fat droplets

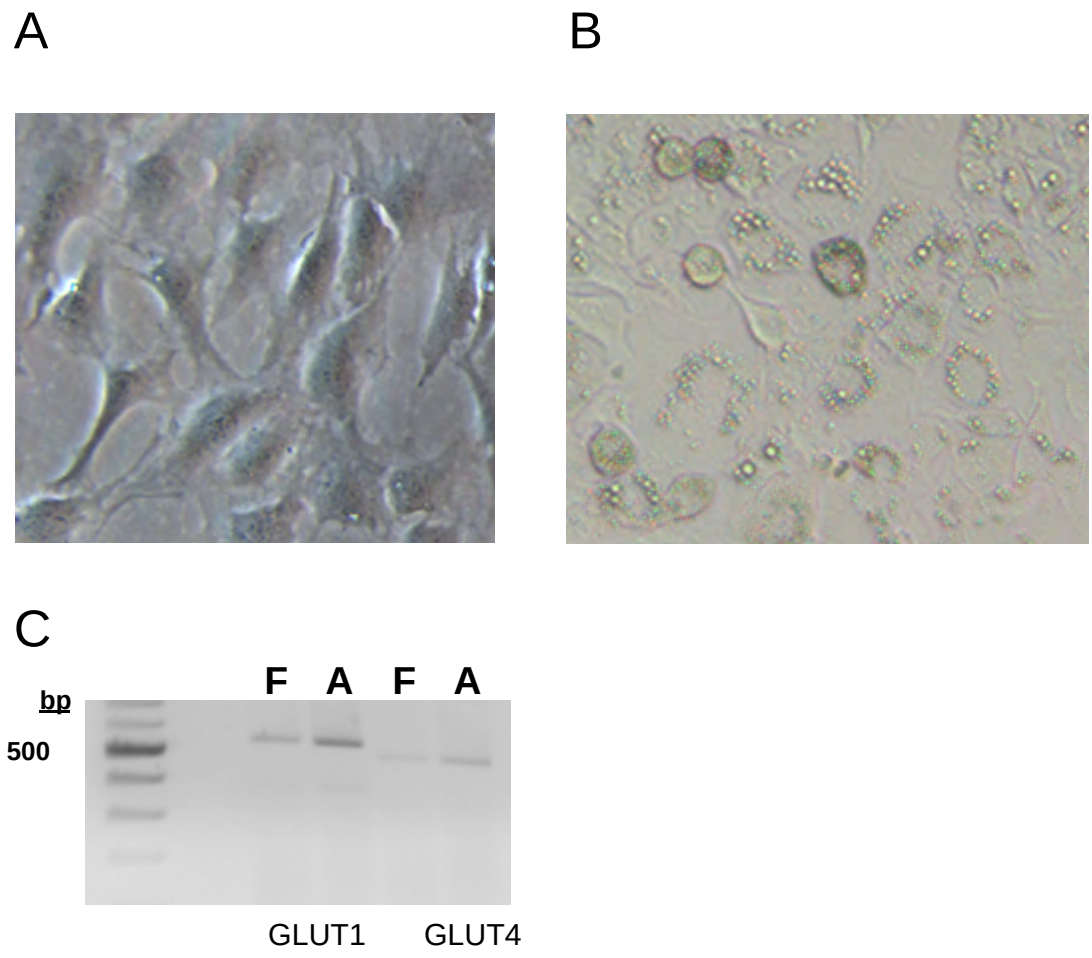

Figure 2.1 Morphology and expression of GLUT1 and GLUT4 mRNA in 3T3-L1 fibroblasts and differentiated adipocytes

A, Live fibroblasts were imaged by DIC microscopy at 10x. *B*, Live adipocytes on day 7 post-differentiation were visualized using DIC microscopy at 10x. *C*, Total RNA extracts from fibroblasts (F) and adipocytes (A) were used as a template for RT-PCR using primers specific to mouse GLUT1 (product size: 515 bp) and GLUT4 (product size: 444 bp). The products were resolved on a 1.5% agarose gel and visualized using ethidium bromide.

in the cytoplasm, which results from increased triglyceride synthesis after differentiation (261).

Total RNA was extracted from both fibroblasts and differentiated adipocytes and screened for GLUT1 and GLUT4 mRNA by RT-PCR (Figure 2.1C). As expected, both fibroblasts and adipocytes show expression of GLUT1 and GLUT4 mRNA. The relative amount of message was examined using qPCR (Figure 2.2A). Analysis by qPCR revealed that GLUT4 mRNA expression was only 40% of GLUT1 mRNA expression in fibroblasts. However, upon differentiation into adipocytes, the expression of GLUT4 message was increased to 4000% when compared to GLUT1 message.

In order to verify that similar changes occurred in protein levels, whole cell lysates of both fibroblasts and adipocytes were analyzed by Western blot. When probed with a C-terminal anti-GLUT1 antibody (Figure 2.2B), a ~55 kDa band of GLUT1 is detected in both fibroblasts and adipocytes, although its expression is more abundant in fibroblasts. However, when probed with a C-terminal anti-GLUT4 antibody (Figure 2.2C), a ~55 kDa GLUT4 band is detected in adipocytes, but not in fibroblasts. The combination of morphological changes and increase in GLUT4 mRNA and protein expression over GLUT1 confirmed the successful differentiation of 3T3-L1 fibroblasts into adipocytes.

A

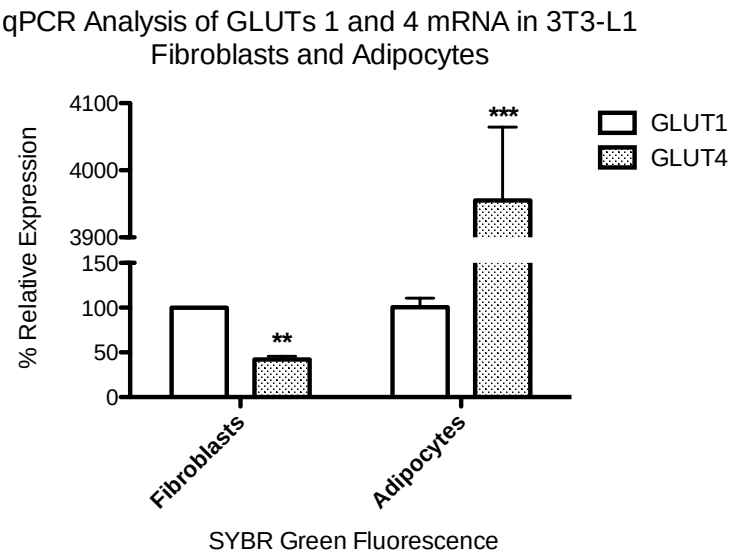
qPCR Analysis of GLUTs 1 and 4 mRNA in 3T3-L1 Fibroblasts and Adipocytes
% Relative Expression
4100
4000
3900
150
100
50
0
**
***
GLUT1
GLUT4
Fibroblasts
Adipocytes
SYBR Green Fluorescence

B

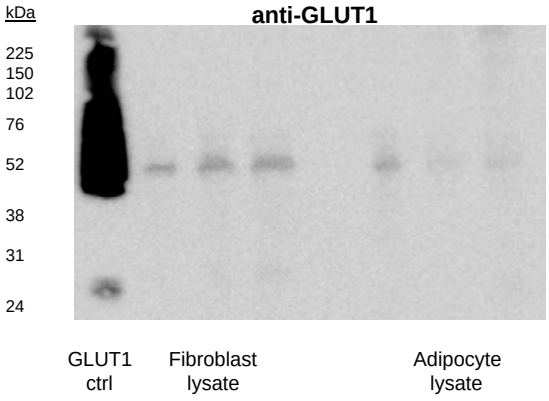
kDa
anti-GLUT1
225
150
102
76
52
38
31
24
GLUT1 ctrl
Fibroblast lysate
Adipocyte lysate

C

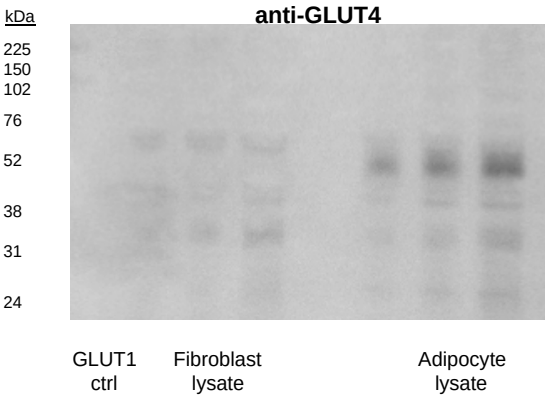
kDa
anti-GLUT4
225
150
102
76
52
38
31
24
GLUT1 ctrl
Fibroblast lysate
Adipocyte lysate

Figure 2.2 Comparative expression of GLUT1 and GLUT4 in 3T3-L1 fibroblasts and adipocytes

A, Quantitative RT-PCR analysis of fibroblast and adipocyte total RNA cell extracts using qPCR primers specific to mouse GLUT1 and GLUT4. Results are normalized to GLUT1 message expression and plotted as relative expression (*ordinate*) for each cell extract (*abscissa*). Samples were run in duplicate on 2 separate occasions. The significance of the difference between GLUT4 (shaded bars) and GLUT1 (empty bars) mRNA relative expression was computed using an unpaired, 2-tailed Student's t-test yielding ** $P \leq 0.01$; *** $P \leq 0.001$. *B*, Western blot analysis of GLUT1 protein expression in whole cell lysates fibroblasts and adipocytes using a GLUT1 C-terminal antibody (~55 kDa). *C*, Western blot analysis of GLUT4 protein expression in whole cell lysates from fibroblasts and adipocytes using a GLUT4 C-terminal antibody (~55 kDa). 5-20 μg of lysate was loaded beside a control of GLUT1 purified from human erythrocytes.

Initial characterization of 3-MG uptake in fibroblasts

In order to establish an appropriate time point during the linear phase of uptake for future transport experiments, we performed a time course over 10 minutes of 5 mM 3-MG uptake in fibroblasts at 4°C (Figure 2.3A). Previous experiments in our laboratory have indicated that 3-MG transport in other murine cell lines is rapid, even at ice temperature (182). In 3T3-L1 fibroblasts, the cells were equilibrated by 2 minutes. To make an initial comparison of whether transport rates were stimulated by intracellular sugar, we chose a time point of 1 minute and performed dose-responses in cells that were either pre-loaded or devoid of intracellular sugar (Figure 2.3B).

To examine uptake in the absence of intracellular sugar (zero-trans), fibroblasts were depleted of sugar for the 2 hours prior to uptake. To examine transport in the presence of intracellular sugar (infinite-trans), cells were pre-loaded with a saturating concentration of sugar (80 mM 3-MG). While comparison of 5-40 mM 3-MG uptake under zero- and infinite-trans conditions did show a stimulation (trans-acceleration) of sugar uptake rates at the 20 mM and 40 mM doses of extracellular 3-MG, the dose-response of pre-loaded cells was linear. This indicates that either 3MG transport is an extremely low affinity process or initial rates were not measured, and the resulting transport does not provide accurate values for V_{max} or K_m. Indeed, when the zero-trans uptake data are fitted with the Michaelis-Menten equation (Equation 2.1), the calculated V_{max} is 219 ± 183 pmol/μg/min and the K_m is 133 ± 137 mM. This is much higher than the

K_m for 3-MG reported in other systems, which is 4-20 mM (204), (205), (192), (201), (202). While the calculated V_{max} for the infinite-trans dose-response is higher than under zero-trans conditions (6960 ± 3420 pmol/μg/min), the K_m (2958 ± 14682 mM) is not reasonable.

These results indicated that an earlier time point was necessary to perform accurate dose-responses of 3-MG uptake. While the disparity between intra- and extracellular sugar in infinite-trans experiments (80 mM vs 5-40 mM 3-MG) can cause changes in cell volume (262), we sought to avoid these complications by ensuring that all uptake solutions were osmotically balanced with sucrose, which is not a substrate for GLUT-mediated transport. However, the control condition in the time course (Figure 2.3A) showed increasingly negative counts with time of incubation with cytochalasin B (CCB), a commonly used GLUT-specific inhibitor. This implied that the choice of CCB for quenching uptake could be causing increased cell permeability and could contribute to difficulty with data analysis. This led us to consider whether a different inhibitor, maltose, would be a better transport inhibitor to use for these assays.

Comparison of maltose and CCB inhibition of transport

Maltose is a competitive inhibitor of GLUT-mediated uptake, as it binds at the exofacial site (28). When used at high concentrations, it can rapidly inhibit uptake of sugar or sugar analogs. We chose to compare inhibition of 3-MG uptake by 80 mM maltose or 10 μM CCB (Figure 2.4A). In order to test whether either inhibitor caused

leaking of cellular contents over time, we pre-incubated fibroblasts with each inhibitor for 0 to 120 seconds prior to adding 5 mM 3-MG uptake, and then processed the cells after 1 minute. The 0 second time point indicates that both inhibitor and uptake solution were added at the same time. For comparison, uptake was measured in control wells with no inhibitor until uptake had proceeded for 1 minute. While this assay was performed at 4°C, we also included a pre-incubation point at 37°C for comparison. Whereas CCB inhibition of 3-MG transport showed a higher background and was variable over the pre-incubation times tested, maltose showed low background and a very reproducible inhibition of 3-MG transport. These data could partially be explained by the comparatively higher off-rate of CCB compared to maltose (28).

In order to ensure we were using an appropriately high concentration of maltose for inhibition in future experiments, we performed a dose-response of maltose inhibition of 3-MG transport (Figure 2.4B). We examined the amount of 10 mM 3-MG uptake at 5 seconds in fibroblasts when simultaneously exposed to 0 to 100 mM maltose. These results showed a $K_{i(app)}$ of ~6 mM for maltose, which is in agreement with what has been reported previously ($K_{i(app)}$ ~6 mM (28)). This confirmed that the use of 80 mM maltose was sufficient for transport inhibition.

A

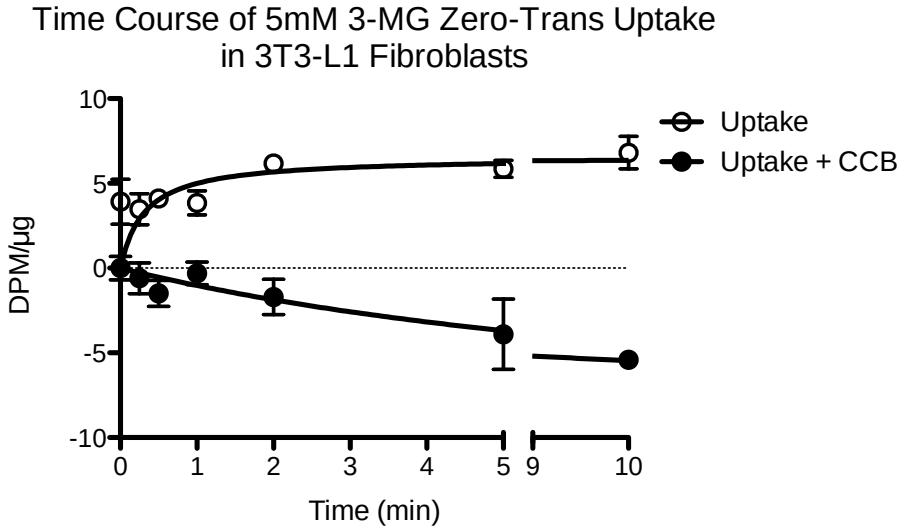
Time Course of 5mM 3-MG Zero-Trans Uptake
in 3T3-L1 Fibroblasts
Uptake
Uptake + CCB
DPM/µg
10
5
0
-5
-10
0
1
2
3
4
5
9
10
Time (min)

B

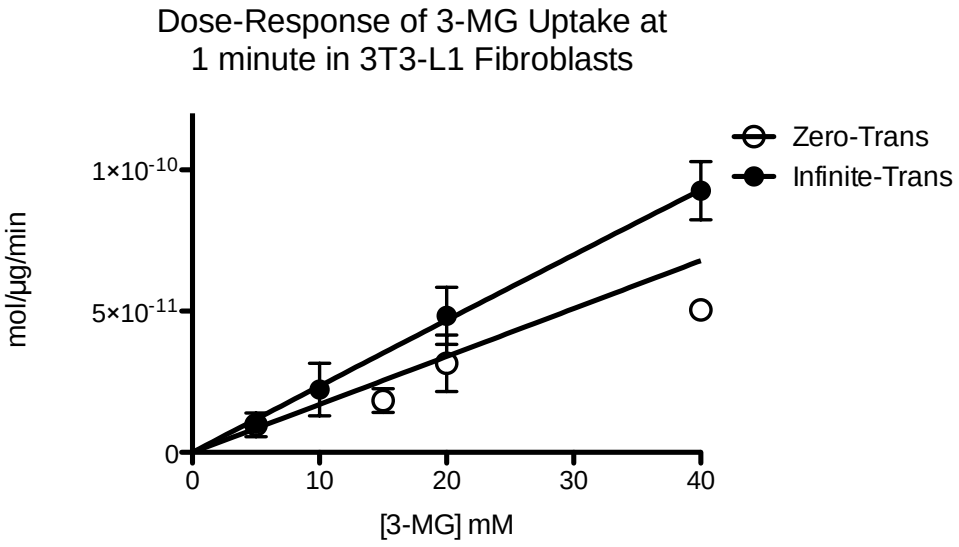
Dose-Response of 3-MG Uptake at
1 minute in 3T3-L1 Fibroblasts
Zero-Trans
Infinite-Trans
mol/µg/min
1×10-10
5×10-11
0
0
10
20
30
40
[3-MG] mM

Figure 2.3 Initial characterization of 3-MG transport in 3T3-L1 fibroblasts

A, Time course of 5 mM 3-MG zero-trans uptake in fibroblasts at 4°C. Amount of uptake of ^{3}[H]-3-MG was normalized to total protein concentration (*ordinate*) and plotted for the length of time of uptake (*abscissa*). Samples were either incubated with 10 μM CCB from the start of the time course (●) or stopped with 10 μM CCB at the indicated time point (○). Data are plotted as mean ± SEM for n=2 assays. Curves drawn through the data were computed by nonlinear regression assuming that uptake is described by Equation 2.1. *B*, Dose response of 3-MG uptake at 1 minute in fibroblasts at 4°C. The rate of uptake (*ordinate*) was plotted for uptake of 5-40 mM 3-MG (*abscissa*) in cells depleted of intracellular sugar (zero-trans; (○)) or cells pre-loaded with 80 mM 3-MG (infinite-trans; (●)). For infinite-trans, 5-40 mM 3-MG uptake solutions were balanced with sucrose to 80 mM. Uptake was stopped with 10 μM CCB and 100 μM phloretin. Data are plotted as mean ± SEM for n=3 assays. Curves drawn through the data were computed by nonlinear regression assuming that uptake is described by Equation 2.1.

A

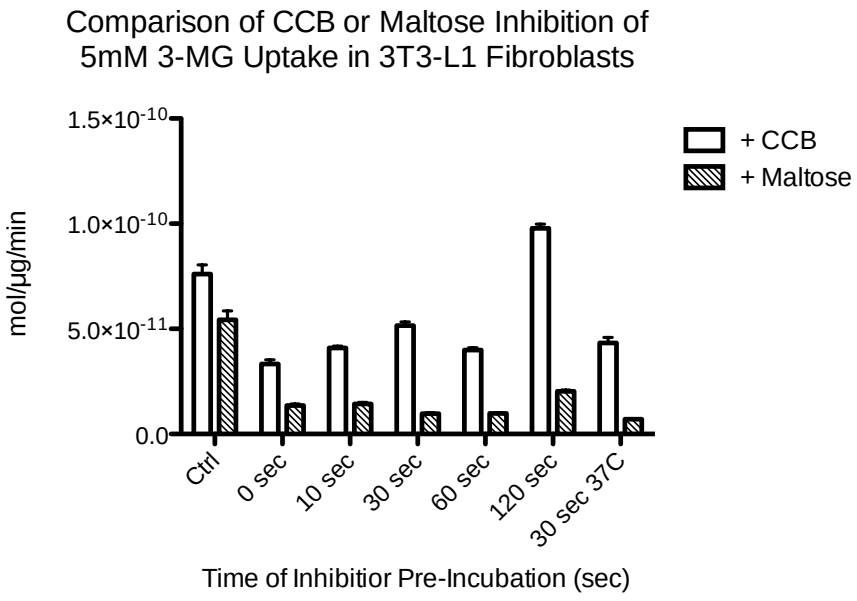
Comparison of CCB or Maltose Inhibition of
5mM 3-MG Uptake in 3T3-L1 Fibroblasts
1.5×10-10
1.0×10-10
5.0×10-11
0.0
mol/µg/min
+ CCB
+ Maltose
Ctrl
0 sec
10 sec
30 sec
60 sec
120 sec
30 sec 37C
Time of Inhibitior Pre-Incubation (sec)

B

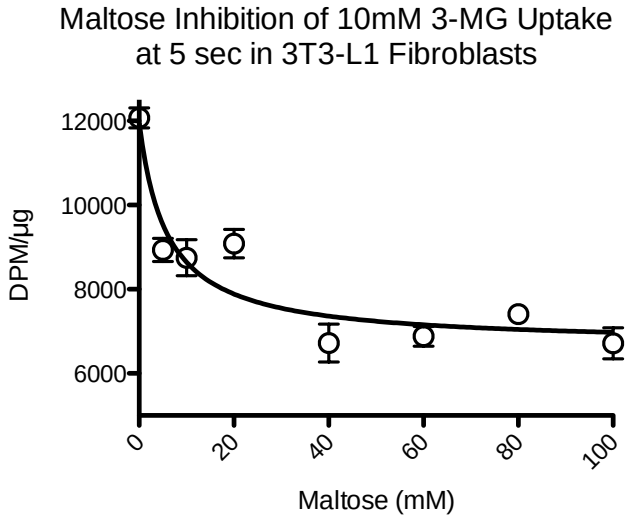
Maltose Inhibition of 10mM 3-MG Uptake
at 5 sec in 3T3-L1 Fibroblasts
12000
10000
8000
6000
DPM/µg
0
20
40
60
80
100
Maltose (mM)

Figure 2.4 Characterization of maltose vs CCB inhibition of 3-MG uptake in fibroblasts

A, The rate of uptake of 5 mM 3-MG (*ordinate*) is plotted against the time of pre-incubation (*abscissa*) with either 10 μM CCB or 80 mM maltose to inhibit transport, at 4°C unless otherwise noted. The non-inhibited uptake of 5 mM 3-MG, stopped with either CCB or maltose after 1 minute, is shown (Ctrl). All following samples had inhibitor added for the time indicated, then 5 mM 3-MG, and samples were aspirated and processed after 1 minute. *B*, The inhibition of 10 mM 3-MG uptake (*ordinate*) at 5 seconds in fibroblasts at 4°C is shown for 0-100 mM maltose (*abscissa*). The curve drawn through the data was computed by nonlinear regression assuming that inhibition is described by Equation 2.2. The resulting analysis yields parameters of K_i= 5.9 ± 3.4 mM with an R^2 = 0.8916.

Characterization of 3-MG transport in fibroblasts using maltose

Because our previous time course with CCB and the linear infinite-trans results had indicated a rapid equilibration, we chose to revisit the time course of 5 mM 3-MG zero-trans uptake at shorter time points and using maltose to stop transport (Figure 2.5A). When uptake of 3-MG is analyzed over the course of 1 minute, it is apparent that equilibration is nearly complete by 10 seconds, which is far faster than our previous dose-this set of experiments, we chose to compare equilibrium exchange (pre-loading the cells with 5-20 mM 3-MG, such that intra- and extra-cellular [sugar] were equal) to zero-trans, so that the higher concentrations of sugar (40-80 mM) employed in the previous experiments could be avoided. While dose-responses under these conditions were no longer linear and provided more reasonable values for K_m (~26-52 mM), there was no stimulation of V_{max} with the presence of intracellular sugar. We reasoned that perhaps the the time point was still too long and that rapid equilibration was preventing the detection of trans-acceleration.

Evaluation of 3-MG transport in fibroblasts at a 2 second time point

As a proof-of-principle, we chose to compare infinite-trans and zero-trans uptake of 10 mM 3-MG at 2 and 5 seconds, respectively (Figure 2.6A). While there is no stimulation of uptake with intracellular sugar (40 mM pre-loaded 3-MG) at 5 seconds, there is an approximate 2-fold stimulation of uptake observed at 2 seconds when intracellular sugar is present. This confirmed that our previous time points were too long to measure trans-acceleration.

A

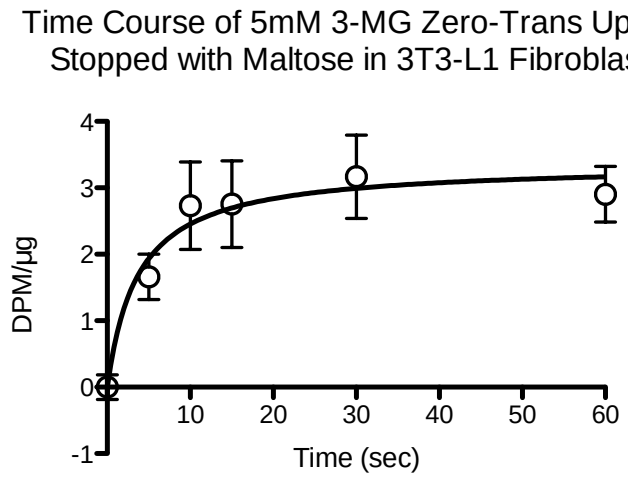
Time Course of 5mM 3-MG Zero-Trans Uptake
Stopped with Maltose in 3T3-L1 Fibroblasts
DPM/µg
4
3
2
1
0
-1
10
20
30
40
50
60
Time (sec)

B

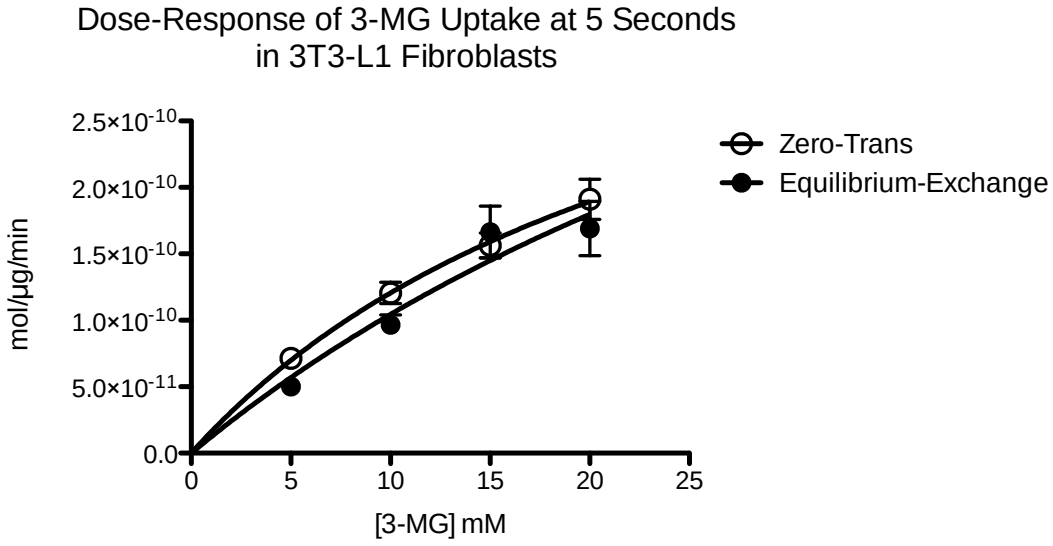
Dose-Response of 3-MG Uptake at 5 Seconds
in 3T3-L1 Fibroblasts
mol/µg/min
2.5×10-10
2.0×10-10
1.5×10-10
1.0×10-10
5.0×10-11
0.0
0
5
10
15
20
25
[3-MG] mM
Zero-Trans
Equilibrium-Exchange

Figure 2.5 Characterization of 3-MG uptake in fibroblasts using modified stop conditions

A, Time course of 5 mM 3-MG zero-trans uptake in fibroblasts at 4°C. Amount of uptake of ^{3}[H]-3-MG was normalized to total protein concentration (*ordinate*) and plotted for the length of time of uptake (*abscissa*). Samples were stopped with 80 mM maltose at the time points indicated. The curve drawn through the data was computed by nonlinear regression assuming that uptake is described by Equation 2.1, with $R^2 = 0.9643$. *B*, Dose response of 3-MG uptake at 5 seconds in fibroblasts at 4°C. The rate of uptake (*ordinate*) was plotted for uptake of 5-20 mM 3-MG (*abscissa*) in cells depleted of intracellular sugar (zero-trans; (○)) or cells pre-loaded with 5-20 mM 3-MG (equilibrium-exchange, (●)). Uptake was stopped with 80 mM maltose. Data are plotted as mean ± SEM for n=2 assays. Curves drawn through the data were computed by nonlinear regression assuming that uptake is described by Equation 2.1. The resulting analysis yields parameters of V_{max} = 440.4 ± 32.9 pmol/µg/min, K_m = 26.5 ± 3.1 mM, with $R^2 = 0.9983$ for zero-trans 3-MG uptake; V_{max} = 643.3 ± 654.7 pmol/µg/min, K_m = 51.6 ± 68.4 mM, with $R^2 = 0.9321$ for equilibrium exchange 3-MG uptake.

A

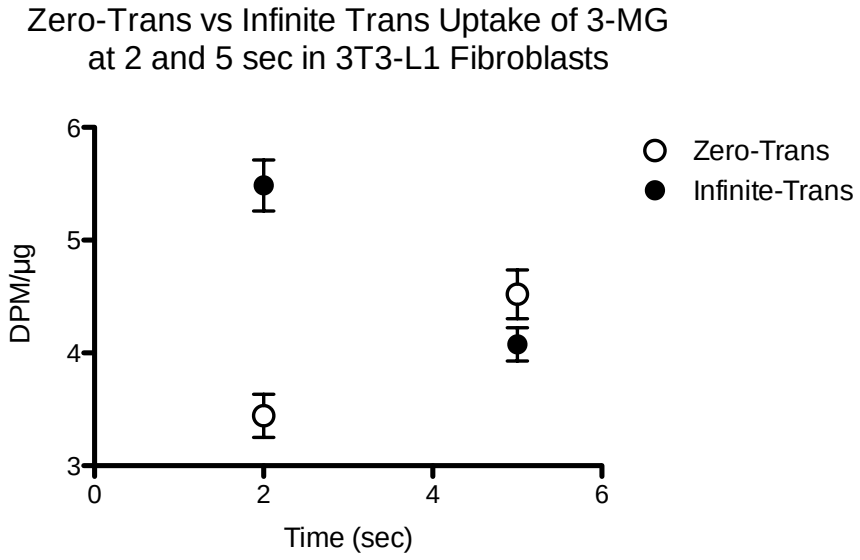
Zero-Trans vs Infinite Trans Uptake of 3-MG
at 2 and 5 sec in 3T3-L1 Fibroblasts
DPM/µg
6
5
4
3
0
2
4
6
Time (sec)
Zero-Trans
Infinite-Trans

B

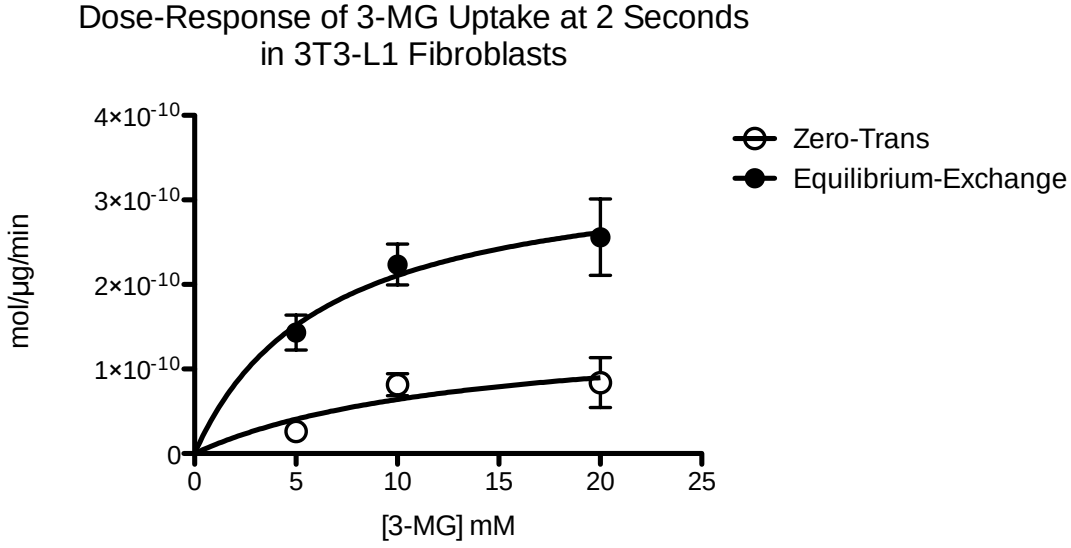
Dose-Response of 3-MG Uptake at 2 Seconds
in 3T3-L1 Fibroblasts
mol/µg/min
4×10-10
3×10-10
2×10-10
1×10-10
0
0
5
10
15
20
25
[3-MG] mM
Zero-Trans
Equilibrium-Exchange

Figure 2.6 Analysis of the effect of intracellular sugar on 3-MG uptake in fibroblasts at 2 second uptake measurements

A, The uptake of 10 mM 3-MG (*ordinate*) at 2 or 5 seconds (*abscissa*) in fibroblasts with no intracellular sugar (zero-trans; (○)) or pre-loaded with 40 mM 3-MG (infinite-trans; (●)). Data are plotted as mean ± SEM for n=2 assays. *B*, Dose-response of the rate of uptake (*ordinate*) of 5-20 mM 3-MG (*abscissa*) in fibroblasts with 0 intracellular sugar (zero-trans; (○)) or pre-loaded with 5-20 mM 3-MG (equilibrium exchange, (●)). All uptake was performed at 4°C and stopped with 80 mM maltose. Curves drawn through the data were computed by nonlinear regression assuming that uptake is described by Equation 2.1. The resulting analysis yields parameters of V_{max} = 150.5 ± 130.8 pmol/μg/min, K_m = 13.5 ± 23.2 mM, with R^2 = 0.7431 for zero-trans 3-MG uptake; V_{max} = 345.0 ± 47.5 pmol/μg/min, K_m = 6.4 ± 2.4 mM, with R^2 = 0.9599 for equilibrium exchange 3-MG uptake.

We then repeated the dose-response of 5-20 mM 3-MG uptake under zero-trans (ZT) and equilibrium-exchange (EE) conditions at 2 seconds (Figure 2.6B). This experiment showed trans-acceleration at each dose of 3-MG uptake measured, with a 2.3-fold increase in V_{max} (ZT V_{max} = 150.5 ± 130.8 pmol/μg/min; EE V_{max} = 345.0 ± 47.5 pmol/μg/min). In addition, the calculated K_m for each experiment was within the range of reported values (ZT K_m = 13.5 ± 23.2 mM; EE K_m = 6.4 ± 2.4 mM). These results confirmed that we were able to measure GLUT1-mediated trans-acceleration in fibroblasts. However, these rapid uptake measurements proved to be difficult to reproduce, and prompted us to ask whether we were still underestimating trans-acceleration at 2 seconds. The ability to detect trans-acceleration at 2 seconds, yet not at 5 seconds, indicated that we might have been measuring the counterflow transient at 2 seconds, which would disappear due to equilibration by 5 seconds.

Mapping the counterflow transient in fibroblasts

While counterflow can occur when trans-acceleration does not, in such a case the initial velocity of uptake will be the same as that of zero-trans uptake (Figure 2.7A). However, when counterflow is measured in a system where trans-acceleration occurs, this will be reflected by an increase in the slope of the initial rate of transport over the slope of zero-trans uptake. When we performed uptake of 10 mM 3-MG at 1-second intervals between 1 and 5 seconds under infinite-trans and zero-trans conditions (Figure 2.7B), this

A

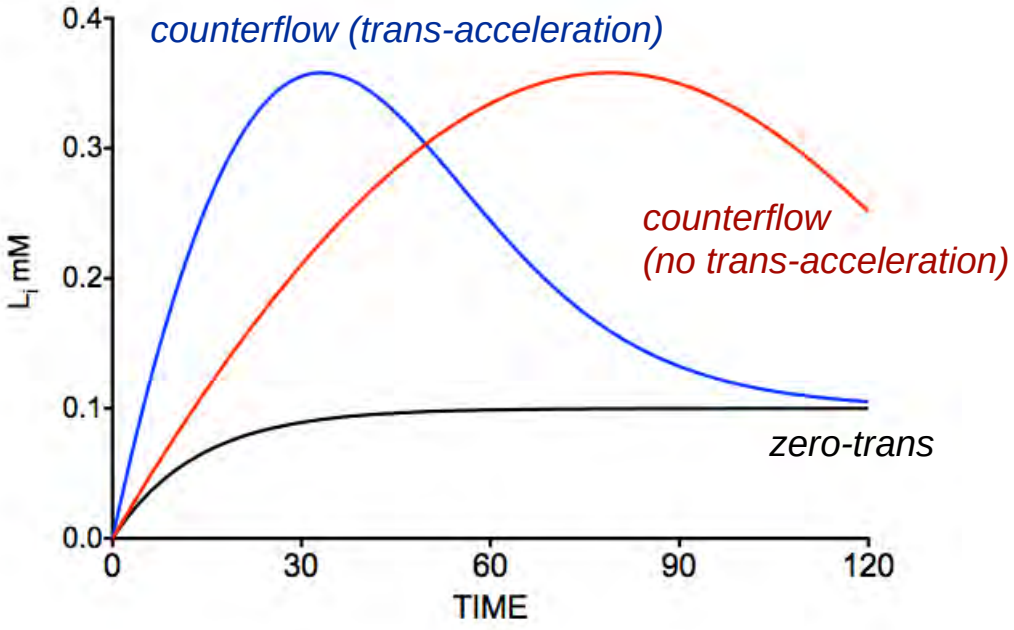
counterflow (trans-acceleration)
counterflow
(no trans-acceleration)
zero-trans
L_i mM
0.4
0.3
0.2
0.1
0.0
0
30
60
90
120
TIME

B

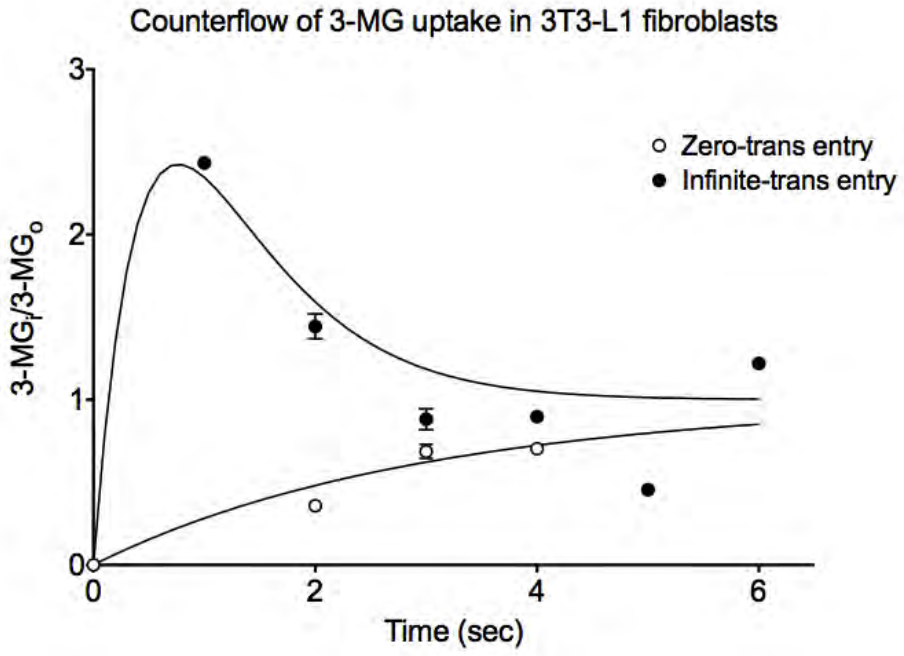
Counterflow of 3-MG uptake in 3T3-L1 fibroblasts
Zero-trans entry
Infinite-trans entry
$3\text{-MG}_i/3\text{-MG}_o$
3
2
1
0
0
2
4
6
Time (sec)

Figure 2.7 Measuring counterflow of 3-MG uptake in 3T3-L1 fibroblasts and adipocytes

A, Example simulations of counterflow by carriers which do and do not catalyze trans-acceleration. The amount of uptake represented by accumulated intracellular label (L_i; *ordinate*) is graphed over time (*abscissa*) under zero-trans (*black line*) and pre-loaded conditions where trans-acceleration is allowed (*blue line*) or is not allowed (*red line*). *B*, The ratio of intracellular sugar over extracellular sugar (*ordinate*) is plotted for the first 6 seconds of 10 mM 3-MG uptake (*abscissa*) in fibroblasts depleted of intracellular sugar (zero-trans; (○)) or pre-loaded with 40 mM 3-MG (infinite-trans; (●)). All uptake was performed at 4°C and stopped with 80 mM maltose.

is exactly what we observed. While the initial time points (1 and 2 seconds) show the stimulation of uptake we observe with intracellular sugar, equilibration is reached rapidly and the stimulation over zero-trans is undetectable by 3 seconds. In addition, we can see from the slope of the fit between 0 and 2 seconds that the initial velocity is much greater under infinite-trans conditions, indicative of trans-acceleration.

Indeed, the fit of the infinite-trans data indicates that trans-acceleration is even underestimated at a 1-second measurement. Because these 1 to 5 second measurements were so rapid, we sought to confirm that counterflow was actually occurring and not an artifact of the experimental conditions, particularly variations in temperature. To test this, we compared uptake of 10 mM 3-MG at 1 and 5 seconds for fibroblasts that had been pre-incubated on ice for 5-20 minutes prior to performing uptake (Figure 2.8). This experiment showed the presence of counterflow at 1 second with no dependence on the amount of time at 4°C. In addition, we varied the order in which 1-5 second uptakes were performed over several assays, with no change in results. This confirmed that we were able to measure the counterflow transient at 1 second of uptake.

Characterization of 3-MG uptake in basal and insulin-stimulated adipocytes

In order to assess whether we would be able to make comparative measurements in adipocytes, we performed a time course of 10 mM 3-MG uptake (Figure 2.9A). This was done in both basal (2 hour serum starve) and insulin-stimulated (2 hour serum starve with 100 nM insulin in the final 20 minutes) adipocytes to test whether stimulation would

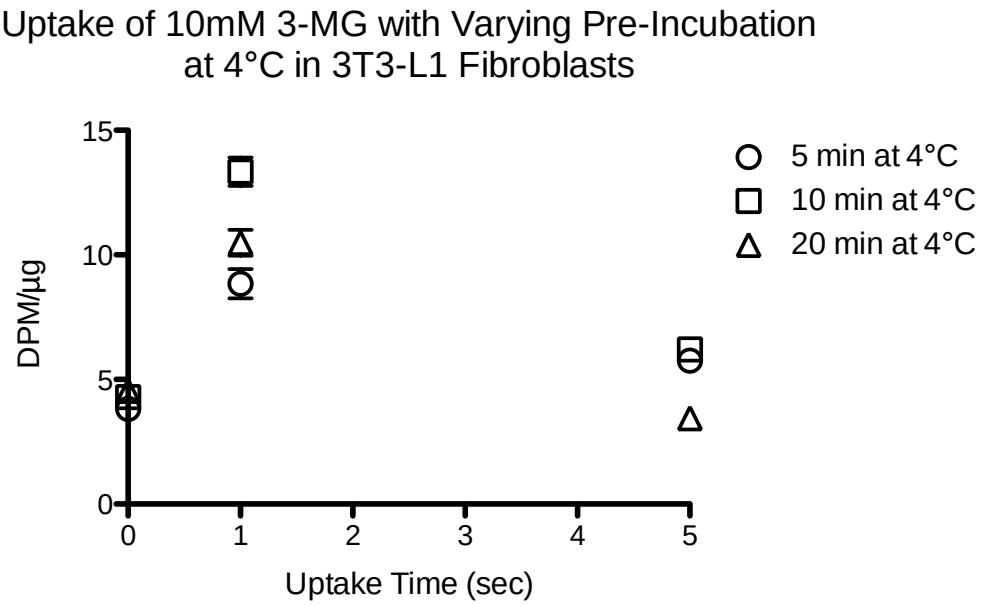

Figure 2.8 Analysis of duration at ice temperature and effect on counterflow measurements

The amount of uptake (*ordinate*) is plotted at 1 and 5 seconds (*abscissa*) for 10 mM 3-MG uptake in fibroblasts pre-loaded with 40 mM 3-MG, which were pre-incubated for 5-20 min at 4°C prior to performing uptake. All uptake was stopped with 80 mM maltose.

A

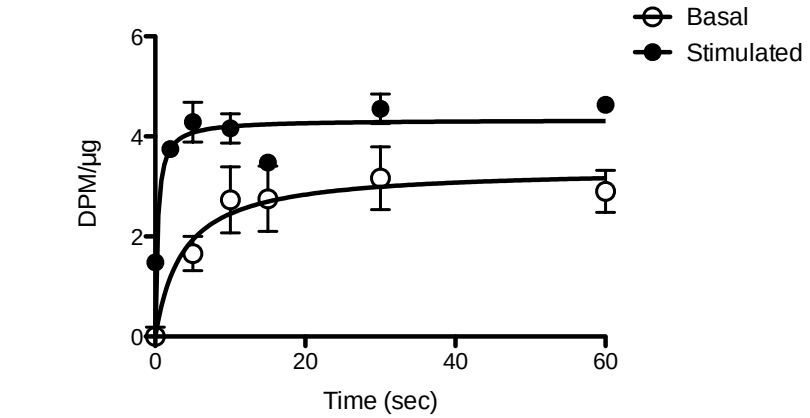
Time Course of 10mM 3-MG
Uptake in 3T3-L1 Adipocytes
Basal
Stimulated
DPM/µg
0
2
4
6
0
20
40
60
Time (sec)

B

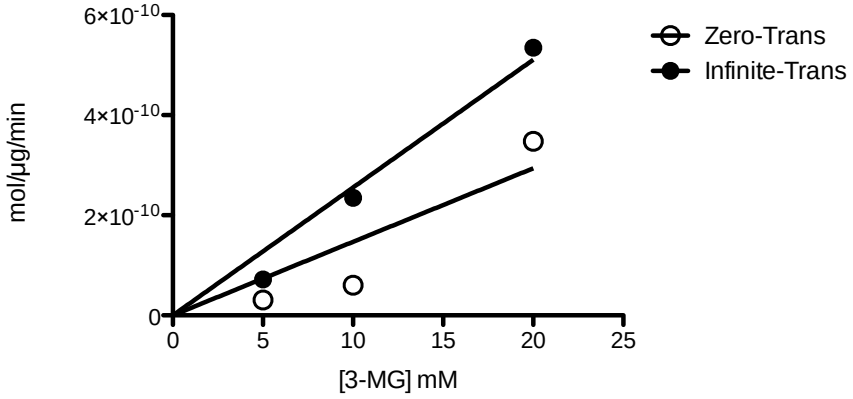
Dose-Response of 3-MG Uptake at
2 seconds in 3T3-L1 Basal Adipocytes
Zero-Trans
Infinite-Trans
mol/µg/min
0
2×10-10
4×10-10
6×10-10
0
5
10
15
20
25
[3-MG] mM

C

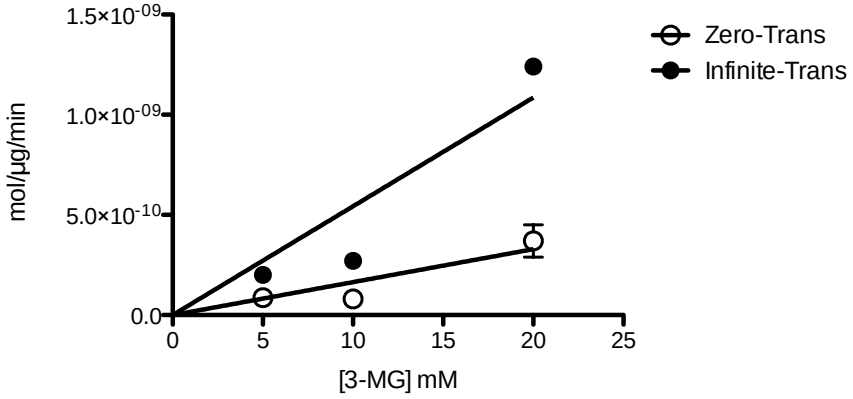
Dose-Response of 3-MG Uptake at
2 seconds in 3T3-L1 Stimulated Adipocyte
Zero-Trans
Infinite-Trans
mol/µg/min
0.0
5.0×10-10
1.0×10-09
1.5×10-09
0
5
10
15
20
25
[3-MG] mM

Figure 2.9 Characterization of 3-MG transport in basal and insulin-stimulated 3T3-L1 adipocytes

A, Time course of 10 mM 3-MG uptake in basal or insulin-stimulated adipocytes. Amount of uptake of 3[H]-3-MG was normalized to total protein concentration (*ordinate*) and plotted for the length of time of uptake (*abscissa*) for basal (○) or insulin-stimulated (●) adipocytes. Data are plotted as mean ± SEM for n=2 assays. Curves drawn through the data were computed by nonlinear regression assuming that uptake is described by Equation 2.1, with $R^2 = 0.9643$ for the fit of uptake under basal conditions and $R^2 = 0.5748$ for the fit of uptake under insulin-stimulated conditions. *B*, Dose response of 3-MG uptake at 2 seconds in basal adipocytes. The rate of uptake (*ordinate*) was plotted for uptake of 5-20 mM 3-MG (*abscissa*) in adipocytes depleted of intracellular sugar (zero-trans; (○)) and adipocytes pre-loaded with 40 mM 3-MG (infinite-trans; (●)). *C*, Dose response of 3-MG uptake at 2 seconds in insulin-stimulated adipocytes. The rate of uptake (*ordinate*) was plotted for uptake of 5-20 mM 3-MG (*abscissa*) in adipocytes depleted of intracellular sugar (zero-trans; (○)) and adipocytes pre-loaded with 40 mM 3-MG (infinite-trans; (●)). All uptake was performed at 4°C and stopped with 80 mM maltose. The lines drawn through data in *B* and *C* were computed by nonlinear regression analysis assuming that uptake is described by Equation 2.1.

increase the rate of transport, as expected. Indeed, we observed that over 60 seconds, both the amount of uptake and the initial rate at which it occurred was faster in stimulated adipocytes. The overall V_{max} for uptake is higher in stimulated adipocytes, and the entire time course curve is shifted to the left, indicating faster equilibration.

While this implied that transport would again be too rapid to measure accurately in adipocytes, we performed a dose-response of 3-MG uptake at 2 seconds and compared this in basal and stimulated adipocytes (Figure 2.9B-C). Indeed, both sets of dose-responses are linear, indicating that transport at 2 seconds is even more rapid than in fibroblasts. Despite an inability to extract meaningful K_m and V_{max} values from these data, the results in both basal and insulin-stimulated adipocytes show that trans-acceleration is still present under infinite-trans versus zero-trans conditions.

To confirm this observation, we wanted to test whether we could measure counterflow in adipocytes. When we mapped uptake under infinite-trans conditions over 1-5 seconds (Figure 2.10), we did indeed observe counterflow in both basal and insulin-stimulated adipocytes. As we found in the dose-response experiments, the amount of uptake in stimulated adipocytes was greater than in basal adipocytes over the first 2 seconds of uptake. The sharp peak of the counterflow transient and its rapid equilibration by 3 seconds is similar to the counterflow observed in fibroblasts, supporting that GLUT1-mediated trans-acceleration is operant in these cells.

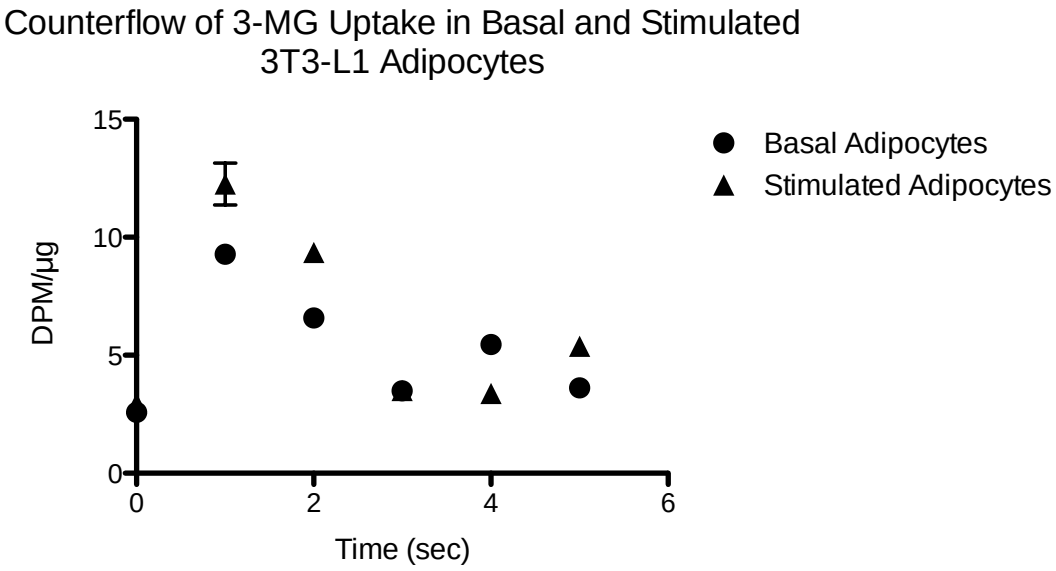

Figure 2.10 Counterflow of 3-MG uptake in basal and insulin-stimulated adipocytes

Amount of uptake of ^{3}[H]-3-MG was normalized to total protein concentration (*ordinate*) over the first 5 seconds of 10 mM 3-MG uptake (*abscissa*), which is plotted for adipocytes pre-loaded with 40 mM intracellular 3-MG under basal (●) and insulin-stimulated (▲) conditions. All uptake was performed at 4°C and stopped with 80 mM maltose.

Discussion

After initial characterization, the 3T3-L1 system appeared ideal for our proof-of-concept studies. Not only did we see successful differentiation of fibroblasts into adipocytes, but the relative expression changes from predominantly GLUT1 to predominantly GLUT4 seemed promising for investigating changes in trans-acceleration. However, this proved to be more complicated than anticipated.

Although we successfully measured GLUT1-mediated trans-acceleration in fibroblasts, the extremely rapid time points necessary to detect this stimulation were difficult to reproduce. This raised the possibility that we would not be able to accurately measure transport in insulin-stimulated adipocytes, where we expected to see more rapid transport. This assumption was based on experimental evidence in 3T3-L1 adipocytes showing that insulin stimulation resulted in both an increase in total membrane protein and a 2- to 20-fold stimulation of transport over basal conditions (164), (263). We confirmed this in our time course experiment, which showed that 3-MG uptake was approximately twice as rapid in stimulated over basal adipocytes.

We also were able to measure and map counterflow in fibroblasts. Counterflow refers to the transient increase in intracellular accumulation of labeled sugar prior to equilibration. This phenomenon is based upon the presence of cold intracellular sugar acting as a competitive inhibitor to exit of the initially accumulating labeled sugar, which then equilibrates over time. While the presence of counterflow is merely indicative of

carrier-mediated transport (29), (186), the slope of the counterflow can be used to determine the presence of trans-acceleration. However, the fit of the experimental counterflow data indicated that even at 1 second measurements, we were likely underestimating the magnitude of the counterflow transient peak. This further supported our concerns that transport in 3T3-L1 cells was extremely rapid and difficult to measure.

Despite this technical issue, we were able to use our map of counterflow to show GLUT1-mediated trans-acceleration in fibroblasts. By comparing the initial rate of influx in zero-trans uptake versus pre-loaded conditions, we observed that the rate of counterflow is faster than the rate of zero-trans uptake, showing stimulation of transport. The same characteristics were retained in counterflow measurements in both basal and insulin-stimulated adipocytes, indicating that trans-acceleration persisted. Indeed, when we sought to test for trans-acceleration in adipocytes, we observed accelerated exchange uptake under both basal and insulin-stimulated conditions.

There could be several reasons for this result. First, performing uptake at sub-5 second time points introduces higher variability, and less reproducibility. In addition, it is possible that stimulation with insulin could increase the amount of GLUT4 at the cell surface of the adipocytes, some GLUT1 would still be present in both basal and stimulated adipocytes. Although the amount of GLUT1 at the surface of CHO and 3T3-L1 cells has been shown to increase in response to insulin in some studies (264), (265), others show contradictory results (164), (258). In one study, the insulin-induced increase in plasma membrane expression of GLUT1 (~6-fold) was accompanied by a greater

increase of surface GLUT4 (~17-fold; (263)); another study reported a 90% decrease in GLUT1 activity in differentiated adipocytes (266). For our purposes, the critical aspect was whether the amount of total GLUT1 at the surface would be significant enough to result in a positive read-out for trans-acceleration, which appears to be the case.

A third possible explanation would be the presence of a heterogeneous population of adipocytes and some undifferentiated fibroblasts. This would likely preclude accurate and reproducible measurements of “loss” of trans-acceleration, as a variable number of cells would still be utilizing GLUT1 as the primary transporter. Regardless of the explanation for the results observed in adipocytes, the 3T3-L1 system proved to exhibit transport properties too rapid to be useful as a proof-of-principle model for our study.

Therefore, we concluded that in order to measure trans-acceleration experimentally, we require an experimental system where transport is slowed sufficiently to provide reliable, reproducible measurements. This would allow us to ensure the ability to measure both gain and loss of trans-acceleration ability above background. In addition, in order to compare the effect of sequence differences between GLUT1 and GLUT4, we require a cell system where neither is expressed endogenously, such that both transporters and mutation(s) to either could be transiently over-expressed. Future studies will focus on establishing these parameters and comparing domains of GLUT1 and GLUT4 as they pertain to ability to catalyze trans-acceleration.

CHAPTER III

Sequence Determinants of GLUT1-Mediated Trans-Acceleration: Analysis by Homology-Scanning Mutagenesis

Abstract

The class 1 equilibrative glucose transporters GLUT1 and GLUT4 are structurally similar but catalyze distinct modes of transport. GLUT1 exhibits trans-acceleration in which the presence of intracellular sugar stimulates the rate of unidirectional sugar uptake. GLUT4-mediated uptake is unaffected by intracellular sugar. We devised an approach to measure trans-acceleration in transfected HEK cells at physiologic temperature by analyzing hetero-exchange uptake of two sugar analogs. Using homology-scanning mutagenesis in which domains of GLUT1 are substituted with equivalent domains from GLUT4 and *vice versa*, we show that GLUT1 transmembrane domain 6 is both necessary and sufficient for trans-acceleration. In addition, substitution of this sequence in GLUTs 1 and 4 alters the catalytic activity of each transporter under zero-trans conditions. Transmembrane domain 6 is not directly involved in GLUT1 binding of substrate or inhibitors. Rather, this region is part of two putative scaffold domains, which coordinate membrane-spanning amphipathic helices that form the sugar

translocation pore. We propose that GLUT1 transmembrane domain 6 restrains import when intracellular sugar is absent.

Introduction

The GLUT family of glucose transporters catalyzes tissue-specific facilitative monosaccharide transport in mammalian cells (7). GLUT1 mediates sugar uptake in red blood cells, smooth muscle and across blood-tissue barriers (12), (267), (268). GLUT4 is expressed in adipose tissue, skeletal, and cardiac muscle (269), where it is responsible for insulin-stimulated sugar uptake (270), (271).

While GLUTs 1 and 4 exhibit similar affinities for substrates and antagonists (202), (272), their catalytic behaviors are very different. GLUT4 displays kinetic symmetry (V_{max} and K_m for net sugar uptake are indistinguishable from the corresponding parameters for net exit (203), while GLUT1 kinetics are asymmetric (V_{max} and K_m for net sugar uptake are significantly lower than the corresponding parameters for net exit (185)). In addition, GLUT1 displays a behavior termed trans-acceleration, whereas GLUT4 does not (177), (188), (189), (203), (206).

Trans-acceleration (also called accelerated-exchange transport) occurs when unidirectional uptake of sugar is stimulated by the presence of intracellular sugar or, conversely, when unidirectional exit of sugar is stimulated by the presence of extracellular sugar (186). Trans-acceleration may provide a metabolic advantage to the

cell because it results in a more rapid equilibration of the cytoplasm with extracellular sugar. Trans-acceleration is one of several behaviors that distinguishes carrier-mediated- from channel-mediated facilitative diffusion systems (273), but the physical basis of accelerated exchange transport is unknown. Comparative analysis of GLUTs 1 and 4 may, therefore, permit definition of the sequence-determinants and thereby the physical basis of trans-acceleration.

GLUTs 1 and 4 are structurally similar, containing cytoplasmic N- and C-termini, 12 transmembrane spanning α-helices (TMs), and a large intracellular loop connecting TMs 6 and 7 (252), (10), (184). In the absence of GLUT crystal structures, our understanding of GLUT1 tertiary structure derives largely from scanning cysteine mutagenesis (129), (136), (134), (135) and modeling studies (116), (115), which align and thread GLUT1 sequence through the crystal structures of Major Facilitator Superfamily bacterial transporter homologs GlpT (274) and LacY (113). While these homology-based threaded structures provide quite accurate descriptions of transporter topography and helix-packing arrangements, they fail to accurately predict helix and amino acid side chain orientation within the active sites (137).

Some functional domains of GLUT1 have been mapped at low resolution. These include components of the GLUT1 nucleotide binding domain (151), (193), (152), substrate binding sites (275), (134), inhibitor binding sites (276), (277), allosteric modulation sites (213), (230), (229) and oligomerization domains ((142), Levine et al., in preparation). However, detailed structures of these domains and the conformational

changes associated with transport are not yet available. In addition, analogous modeling studies have yet to be extended to GLUT4. Thus, the available data do not yet provide an explanation for substrate binding and translocation by GLUTs 1 and 4, or why GLUT1 catalyzes trans-acceleration but GLUT4 does not.

This study attempts to investigate the determinants of transporter function using homology-scanning mutagenesis of structurally related but functionally different members of a transporter family. We engineered GLUT1 and GLUT4 chimeras in which we substituted progressively smaller domains of one transporter by the corresponding domains of the other transporter. These chimeras exhibit sequence-dependent trans-acceleration gain- or loss-of-function.

We observe trans-acceleration in GLUT1-transfected HEK cells but not in cells transfected with human GLUT4. Homology-scanning mutagenesis reveals that TM6 of GLUT1 is both necessary and sufficient to confer trans-acceleration to the GLUT4 scaffold. Similarly, the replacement of GLUT1 TM6 with the corresponding region in GLUT4 ablates trans-acceleration in the GLUT1 scaffold. These results confirm that trans-acceleration is sequence-dependent, requiring a motif within the putative scaffold region of GLUT1, rather than in the translocation pore-forming region of the protein. The implications of our findings are discussed in the context of the prevailing models for GLUT-mediated sugar transport.

Experimental Procedures

Materials

[^{3}H]-2-deoxy-D-glucose was purchased from MP Biomedical. HEK-293 cells were purchased from ATCC. DMEM, DPBS, penicillin/streptomycin, Lipofectamine 2000, DH5α-Subcloning cells, pcDNA 3.1 (+) mammalian expression vector, Bis-Tris gels and MES buffer were obtained from Invitrogen. All restriction enzymes and associated buffers were obtained from New England Biolabs. All primers were purchased from Integrated DNA Technologies. Herculase polymerase, XL1-Blue Competent cells and QuikChange Multi Site-Directed Mutagenesis kits were obtained from Stratagene. RNeasy, Qiashredder, One-Step RT-PCR, MinElute Gel Purification, PCR Purification, and HiSpeed Maxi kits were from Qiagen. iScript One-Step PCR kit with SYBR green was purchased from BioRad. PVDF membranes were obtained from ThermoFisher. 10% bovine serum albumin was from American Bioanalytical. Super Signal Pico West, NeutrAvidin Gel, micro-BCA kits, spin columns and EZ-Link Sulfo-NHS-SS-Biotin were from Pierce. Protease inhibitor cocktail tablets were from Roche. Other reagents were purchased from Sigma Chemicals.

Solutions

Cell lysis buffer consisted of DPBS, 0.5% Triton X-100 plus protease inhibitiors with EDTA. TBS contained 20 mM Tris base, 135 mM NaCl, pH 7.6. Biotin lysis and column wash buffer comprised TBS, 0.5% Triton X-100 and protease inhibitors with

EDTA. Sample buffer consisted of 0.5 M Tris-Cl, pH 6.8, 40% (v/v) glycerol, 8% SDS, bromophenol blue, and 150 mM DTT; biotinylation sample buffer did not contain bromophenol blue. DPBS-Mg contained 5 mM $MgCl_2$. 2-DG uptake solution contained 100 µM 2-DG with 2.5 µCi/ml [^{3}H]-2DG in DPBS-Mg. Stop solution consisted of 10 µM cytochalasin B and 100 µM phloretin in DPBS-Mg. Triton extraction buffer contained 0.5% Triton X-100 and 50 µM EDTA in DPBS-Mg. 2-DG/3-MG uptake solution consisted of 100 µM 2-DG with 2.5 µCi/ml [^{3}H]-2DG in DPBS-Mg with 40 mM 3-MG.

Antibodies

A custom-made (New England Peptide) affinity-purified rabbit polyclonal antibody raised against a peptide corresponding to GLUT1 C-terminal residues 480-492 was used at 1:10,000 dilution as described previously (152). A rabbit polyclonal anti-GLUT4 C-terminal antibody (Sigma G4048) was used at 1:3,000 dilution. A rabbit polyclonal anti-myc antibody (AbCam ab9106) was used at 1:5,000 dilution. Horseradish peroxidase-conjugated goat anti-rabbit secondary antibody (Jackson ImmunoResearch) was used at 1:50,000 dilution. A rabbit polyclonal anti-Na^+,K^+-ATPase antibody (Cell Signaling Technologies 3010) was used at 1:500 dilution.

Tissue Culture

HEK-293 cell culture was as previously described previously (195). All experiments were performed with confluent cells. Plates were subcultured into 12 well plates at a ratio of 1:2-1:4 2-4 days prior to transfection. Passages 4-19 were used for all experiments.

Mutagenesis

GLUT1- or GLUT4-encoding cDNA was inserted into the EcoRV-Not1 restriction sites of pcDNA 3.1 (+). Myc-tagged constructs were made using overlapping primers to insert the myc tag in exofacial loop 1, between GLUT1 residues 55-56 or GLUT4 residues 72-73. All TM-domain chimeras were engineered by designing overlapping primers for each region of interest, amplifying each fragment via PCR using Herculase polymerase, purifying each fragment with the MinElute Gel Purification kit, joining fragments by PCR, and repeating until a full-length insert was obtained. The insert was purified by the PCR Purification kit, digested with restriction enzymes, purified by the MinElute Gel Purification kit, and inserted into pcDNA 3.1 (+) with the same restriction sites. All final constructs were subcloned into either XL1-Blue Competent cells or DH5α-Subcloning cells, purified using a HiSpeed Maxi kit, and verified by sequencing analysis (Davis Sequencing, Davis, CA). All point mutations and amino acid substitutions were engineered using QuikChange Multi Site-Directed Mutagenesis kits and were verified by sequencing. For a complete list of primers used, see Appendix (Table A1).

Quantitative and End Point Reverse-Transcriptase PCR

Total RNA was isolated from HEK cells using the RNeasy kit and Qiashredder. End point RT-PCR was performed as per the One-Step RT PCR kit instructions using GLUT-specific primers. RT-PCR products were resolved on a 1.5% agarose gel and visualized by ethidium bromide staining. Expression levels of detected GLUTs were measured by quantitative RT-PCR using the iScript One-Step PCR kit with SYBR green.

Samples were run in duplicate on an MJ Research PTC-200 Peltier Thermal Cycler with a Chromo4 real time PCR detector running Opticon Monitor 3 software (Bio-Rad). Results were analyzed by using the delta-delta Ct method (259) and normalized to a GAPDH control. For a complete list of primers used, see Appendix (Table A2).

Transient Transfection

Cells (70-90% confluency) were transfected with 2 µg DNA per well (12 well plates) or 5 µg DNA per well (6 well plates), unless otherwise specified. Transfections were performed 36-48 hours prior to analysis of sugar uptake or protein expression.

Western Blotting

Cells were pelleted, washed with DPBS, lysed in cell lysis buffer, and protein concentration was assessed using a micro-BCA kit. Lysates were normalized for total protein concentration and resolved by SDS-PAGE on a 10% Bis-Tris gel in MES buffer. Gels were transferred onto PVDF membranes, blocked with 10% bovine serum albumin in TBS-T, probed with primary antibody overnight at 4°C, probed with secondary antibody for 1 hour at room temperature, and developed using Super Signal Pico West Chemiluminescent substrate. Blots were imaged on a FujiFilm LAS-3000 and relative band densities were quantitated using ImageJ software.

Biotinylation

6-well plates of HEK cells were washed twice with ice-cold DPBS and incubated on ice with ice-cold DPBS containing 5 mM EZ-Link Sulfo-NHS-SS-Biotin for 30 min with gentle rocking. Reactions were quenched by adjusting each well to 12.5 mM Trizma

base. Cells were harvested, re-suspended in biotin lysis buffer and lysates were bound to Neutravidin Gel in spin columns according to kit instructions. Protein concentration was determined spectrophotometrically, and normalized loads were analyzed by Western blot as described above.

2-deoxy-D-glucose Sugar Uptake

2-deoxy-D-glucose (2-DG) is an analog of the natural GLUT1 substrate, D-glucose. At physiologic temperature, cytoplasmic 2-DG is phosphorylated by hexokinase to form 2-deoxy-D-glucose-6-phosphate (2-DG-6-P), which is neither metabolized further nor is a GLUT1 substrate (195), (278). Imported [^{3}H]-2-DG is therefore trapped within the cell as [^{3}H]-2-DG-6-P.

2-DG uptake was measured as described previously (234). Briefly, 36-48 hours post-transfection, 12-well plates of confluent HEK-293 cells were serum- and glucose-starved for 2 hours at 37°C in FBS- and penicillin/streptomycin-free DMEM lacking glucose. Cells were washed with 0.5 mL DPBS-Mg at 37°C, then exposed to 0.5 mL of [^{3}H]-2-DG uptake solution for 0 to 30 min at 37°C. Uptake was stopped by addition of 1 mL ice-cold stop solution. Cells were washed twice with ice-cold stop solution and extracted with Triton extraction buffer. Total protein concentration was analyzed in duplicate. Each sample was counted in duplicate by liquid scintillation spectrometry. Each condition was performed in triplicate on at least 3 separate assay occasions.

Zero-Trans and Hetero-Exchange Transport Measurements

Zero-trans sugar uptake describes uptake of sugar into cells lacking intracellular sugar. Hetero-exchange sugar uptake describes uptake of sugar into cells preloaded with a different, but transportable sugar (226). Zero-trans uptake of [^{3}H]-2-DG by sugar-depleted cells was measured as described above with one modification - the transported sugar 3-O-methyl-D-glucose (3-MG; 40 mM) was included in the uptake medium. Extracellular 3-MG competitively inhibits [^{3}H]-2-DG uptake and thus permits more accurate measurement of transport over a 5 minute interval at physiologic temperature (37°C). Because 3-MG is not a hexokinase substrate (196), any 3-MG that enters the cells during transport or by pre-loading the cells does not compete with intracellular 2-DG for interaction with hexokinase. In hetero-exchange uptake, the concentration of 3-MG inside and outside of the cell is identical (40 mM). This is accomplished by adding 40 mM 3-MG to glucose-free DMEM during serum starvation and to DPBS-Mg used in pre-uptake washes. This method was developed to measure trans-acceleration in transfected HEK cells; analysis of 3T3-L1 fibroblast transport under these conditions did not show trans-acceleration (Appendix Figure A3.1)

Data Analysis

All data analysis was performed using GraphPad Prism (La Jolla, CA, v 5.0). For sugar uptake experiments, background counts were subtracted from all samples and uptake, *v*, was normalized to [total protein]/well. [^{3}H]-2-DG uptake (DPM/µg) was then converted to mol/µg protein/min by using the measured specific activity of the uptake

solution. Average uptake in mock-transfected controls was subtracted from the uptake of the corresponding transfected samples. For experiments where $[3\text{-MG}]_i$ was varied, sugar uptake, v, was fitted to the following approximation (Equation 3.1):

$$v = v_b + \frac{E_{\max}[S]}{K_E + [S]}$$

by non-linear regression analysis, where v_b is sugar uptake in the absence of 3-MG$_i$, E_{max} is the stimulation of sugar uptake produced by saturating 3-MG$_i$, [S] is the concentration of 3-MG$_i$ and K_E is that concentration of 3-MG$_i$ which stimulates sugar uptake by 50%. In experiments evaluating whether trans-acceleration is observed, the ratio of hetero-exchange (HE) uptake:zero-trans uptake (ZT) was computed for each construct. As we shall show, this normalizes for experimental variation in transporter cell surface expression. When this ratio is significantly greater than 1, trans-acceleration is present. The results of paired experiments were analyzed using Student's t-test.

Results

GLUT1 and GLUT4 chimeras

In order to identify GLUT1 domain(s) required for trans-acceleration, we swapped specific transmembrane regions of GLUT1 with equivalent GLUT4 sequence. This allows us to map the involvement of large regions of the transporter in trans-acceleration and thereby narrow our focus to smaller sub-domains (Figure 3.1). Chimera nomenclature divides the GLUTs into 4 sets of three contiguous TMs (1-3, 4-6, 7-9, 10-12). A chimera comprising the first half of GLUT1 plus the second half of GLUT4 is termed 1144 - GLUT1 TMs 1-3 and 4-6 plus GLUT4 TMs 7-9 and 10-12. If loop 6 linking TMs 6 and 7 is the focus, this is indicated in parenthesis. Thus, 44(1)11 is GLUT4 TMs 1-6, GLUT1 loop 6, and GLUT1 TMs 7-12. 1411 is GLUT1 TMs 1-3 plus GLUT4 TMs 4-6 plus GLUT1 loop 6 and TMs 7-12 (Figure 3.1B). Mutations involving only 1 or 2 TMs list the scaffold GLUT with substitutions from the other GLUT in parenthesis, e.g. GLUT4 (5,6 G1) is GLUT4 containing GLUT1 TMs 5-6.

Trans-Acceleration in HEK Cells

HEK-293 cells were selected for heterologous expression of GLUT1, GLUT4 and GLUT1-GLUT4 chimeras because of their very low endogenous expression of human GLUTs 1 and 4, as determined by qPCR (Figure 3.2). Net uptake of 100 μM 2-DG increases linearly with time (0 – 10 min) in GLUT1-transfected cells (Figure 3.3A). The

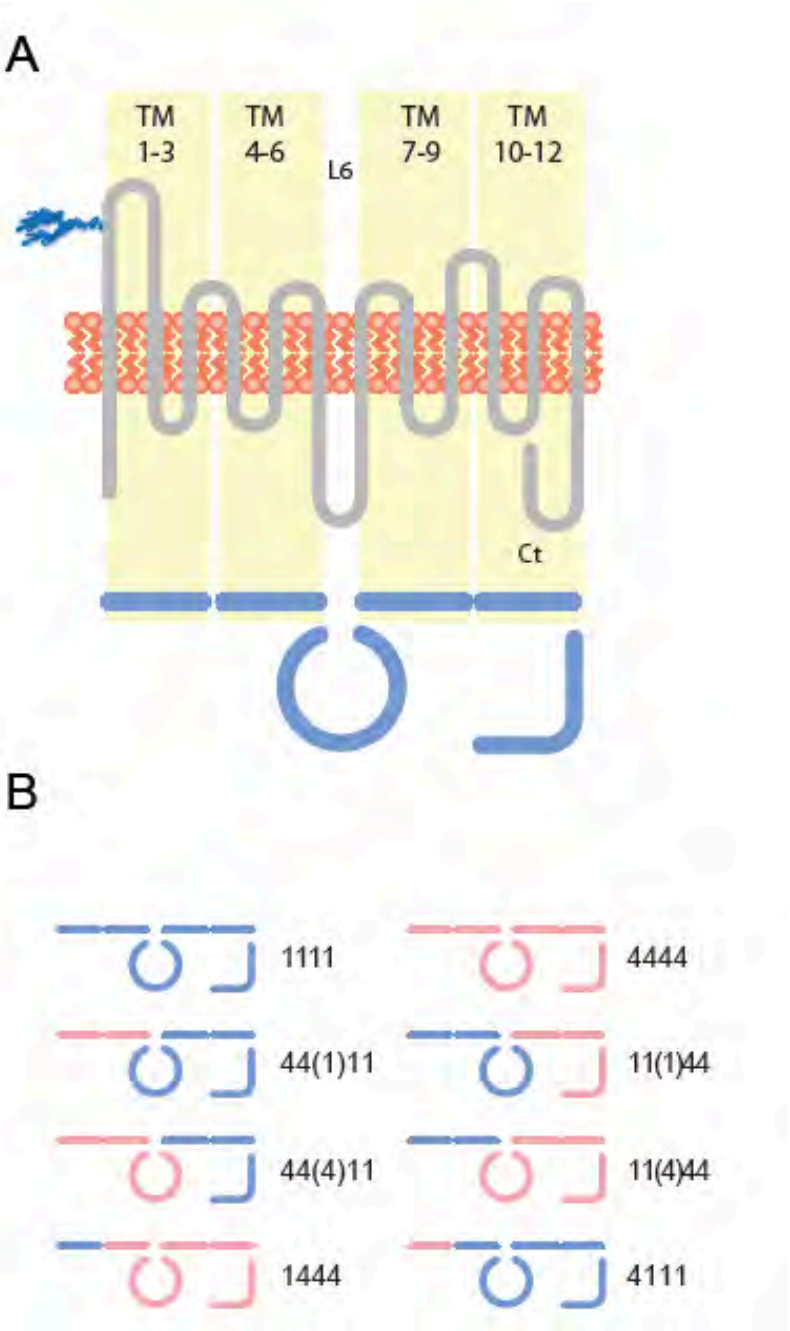
A
TM 1-3
TM 4-6
L6
TM 7-9
TM 10-12
Ct
B
1111
4444
44(1)11
11(1)44
44(4)11
11(4)44
1444
4111

Figure 3.1 GLUT1/GLUT4 chimeras

A, Schematic of GLUT topology; trans-membrane domains (1-12) are numbered in blocks of 3. Intracellular loop 6 (L6) connects TMs 6-7 and the carboxy-terminus (Ct) is cytoplasmic. *B*, Chimera nomenclature derives from the origin of each block of 3 TMs and from the origin of loop 6 (in parentheses). When substitutions smaller than 3 TMs are made, the chimera is named by the scaffold protein (GLUT1 or GLUT4) with the substituted TM domain(s) in parenthesis (i.e. GLUT4 containing TMs 5-6 of GLUT1 is GLUT4 (5,6 G1)).

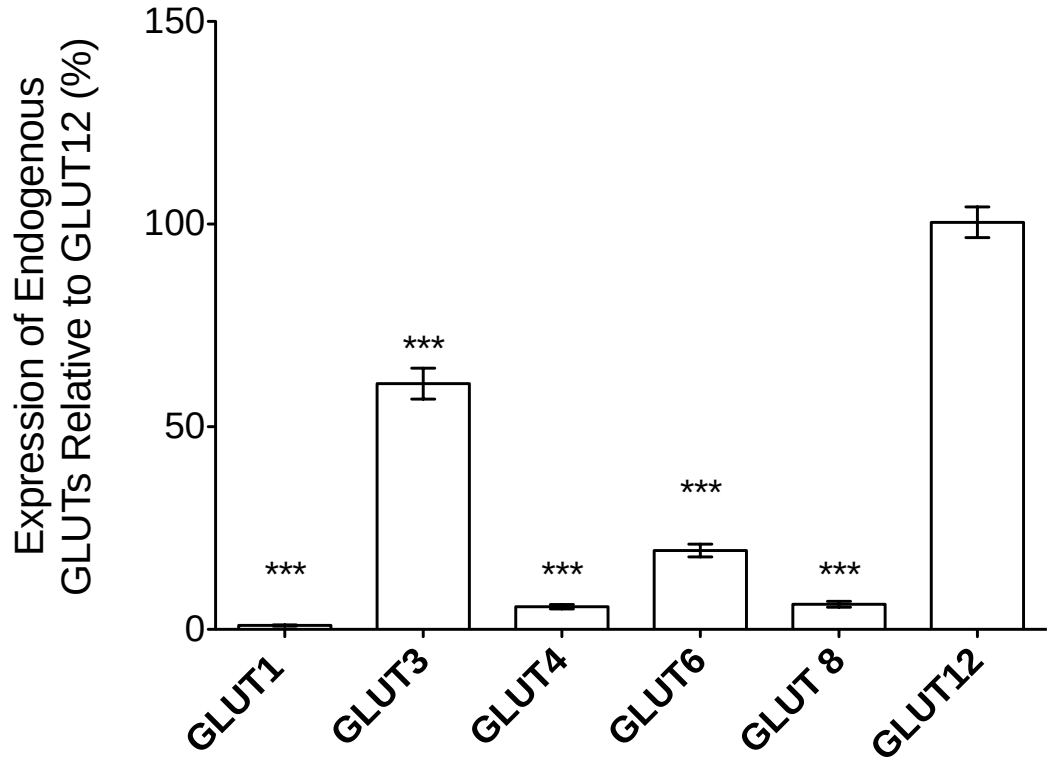

Figure 3.2 Analysis of HEK cell endogenous GLUT mRNA expression by qPCR

HEK cells were screened for the presence of all GLUTs by end-point RT-PCR (Appendix Figure A3.1). Quantitative RT-PCR was then used to compare message expression levels. Expression relative to GLUT12 message (*ordinate*) is plotted versus GLUT identity (*abscissa*). The significance of the difference between GLUT12 and other GLUTs was computed by an unpaired, 2-tailed Student's t-test with the following results:

*** $P \leq 0.005$.

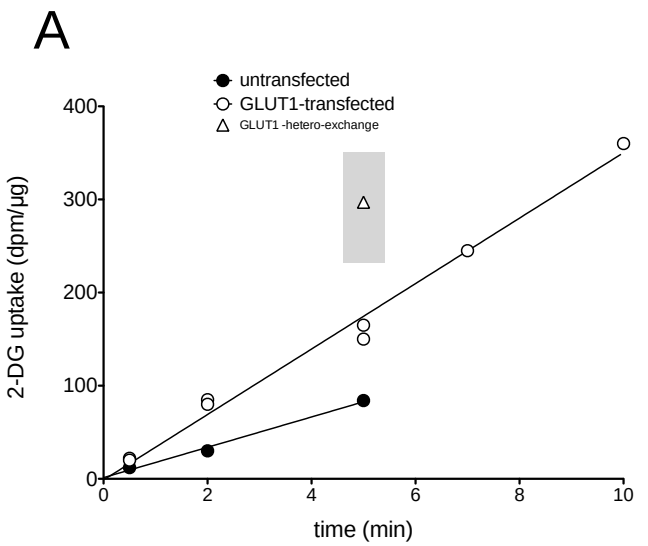
A
untransfected
GLUT1-transfected
GLUT1 -hetero-exchange
2-DG uptake (dpm/µg)
400
300
200
100
0
0
2
4
6
8
10
time (min)

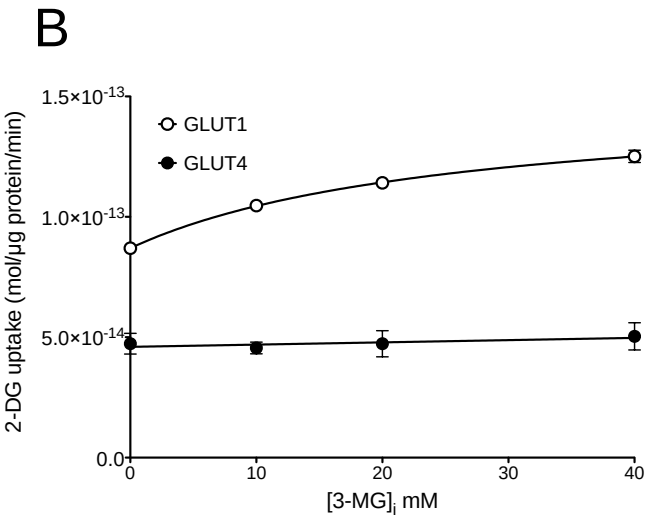
B
1.5×10-13
1.0×10-13
5.0×10-14
0.0
GLUT1
GLUT4
2-DG uptake (mol/µg protein/min)
0
10
20
30
40
[3-MG]i mM

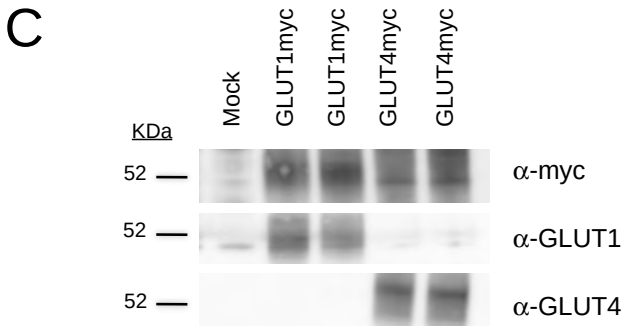
C
Mock
GLUT1myc
GLUT1myc
GLUT4myc
GLUT4myc
KDa
52
52
52
α-myc
α-GLUT1
α-GLUT4

Figure 3.3 Sugar uptake in HEK cells expressing GLUT1, GLUT4, and myc-tagged GLUTs

A, Time course of ^{3}[H]-2-DG uptake in control and GLUT1-transfected cells. *Ordinate*: 2-DG uptake in dpm per μg total cell protein; *abscissa*: time in minutes. 2-DG uptake is shown in mock-transfected (●) and GLUT1-transfected (○) cells. Lines drawn through the points were computed by linear regression. GLUT1-mediated hetero-exchange is indicated by the triangle (Δ) and the gray rectangle indicates the range of transport produced by a 2-3-fold stimulation of transport during hetero-exchange at 5 minutes. *B*, Dose-response of 100 μM 2-DG uptake (*ordinate*) from medium containing 40 mM 3-MG into HEK cells pre-loaded with 0-40 mM 3-MG (*abcissa*) and transfected with GLUT1 (○) or GLUT4 (●). Basal uptake by mock-transfected cells was subtracted at each 3-MG concentration. Data points represent the mean ± SEM for three separate assays. The curve drawn through the GLUT1 data was computed by nonlinear regression assuming that uptake is described by equation 3.1. The resulting analysis yields parameters of v_b = 0.087 ± 0.003 pmol/μg/min; E_{max} = 0.063 ± 0.002 pmol/μg/min; K_E = 25.8 ± 1.5 mM. The line drawn through the GLUT4 data was computed by linear regression. *C*, Western Blot analysis of total protein levels in GLUT1myc- and GLUT4myc-transfected HEK cells. Representative Western blot of whole cell lysates from HEK cells transfected with GLUT1myc or GLUT4myc constructs. Lysates were resolved by SDS-PAGE, transferred to PVDF membranes and probed with α-myc Ab (top), α-GLUT1 C-terminal Ab (middle), or α-GLUT4 C-terminal Ab (bottom).

time course of 2-DG uptake is even slower in the presence of competing 3-MG (Appendix Figure A3.3). The experiments reported in this study employ a 5-minute uptake interval, which provides an ample range of linearity to detect a 2- to 3-fold increase in 2-DG uptake during hetero-exchange transport catalyzed by transfected GLUTs. In order to characterize differences in sugar uptake in response to intracellular sugar, [^{3}H]-2-DG uptake from medium containing 40 mM 3-MG was measured in GLUT1- or GLUT4-transfected HEK cells pre-loaded with 0 to 40 mM 3-MG (Figure 3.3B). GLUT1-transfected HEK cells show a dose-dependent stimulation of 2-DG uptake with increasing intracellular [3-MG], while GLUT4-transfected HEK cells do not. This confirms that human GLUT1 displays trans-acceleration at 37ºC, whereas human GLUT4 does not. GLUT1-mediated 2-DG uptake increases in a saturable manner with $[3\text{-MG}]_i$, showing a maximal stimulation (E_{max}) of 1.72 ± 0.02-fold with 50% stimulation (K_E) at 25.6 ± 1.5 mM 3-MG_i. 40 mM 3-MG_i was used in all further hetero-exchange experiments.

Modification of GLUT4 to increase surface expression

The pre-loading experiment (Figure 3.3B) indicates that zero-trans 2-DG uptake in GLUT4myc-transfected HEK cells is significantly slower than uptake in GLUT1myc-transfected cells. Total protein expression levels appear similar by Western blot (Figure 3.3C), suggesting either that significantly less GLUT4myc is expressed at the cell surface or that GLUT4myc has lower intrinsic activity (k_{cat}) than GLUT1myc. We show below

that cell surface protein biotinylation analysis indicates that GLUT4myc surface expression is less than half that of GLUT1myc. Efforts to increase GLUT4myc surface expression by transfecting greater [GLUT4myc] DNA were ineffective (Appendix Figure A3.4)

GLUT4myc surface expression was improved by engineering 3 GLUT4 mutations known to affect surface expression in a variety of cell types. GLUT4 N- and C-termini contain internalization (168), (171) and surface-targeting (167), (169) motifs. GLUT4myc mutations F5A and LL489-490AA were tested individually and together; their surface localization was verified by biotinylation (Appendix Figure A3.5) and their function was tested in assays of 100 μM 2-DG uptake under zero-trans conditions (Figure 3.4A). In these experiments, 2-DG uptake by GLUT4myc is only one quarter of that catalyzed by GLUT1myc. 2-DG uptake by GLUT4myc F5A and by GLUT4myc LL489-490AA approaches 80% of GLUT1myc-mediated uptake. The triple mutant (GLUT4myc F5A/LL489-490AA) catalyzes a level of 2-DG uptake indistinguishable from that of GLUT1myc. This mutant (GLUT4myc-3x) was used as the GLUT4 scaffold in all further mutational analysis. GLUT1myc typically displays a 1.8 ± 0.15-fold stimulation of sugar uptake under hetero-exchange conditions (Table 3.1). However, both GLUT4myc and GLUT4myc-3x display no trans-acceleration (Figure 3.4B). This confirms that the loop 1 exofacial myc tag and the cell surface-expression mutations introduced into GLUT4 do not significantly perturb wild-type exchange-transport behavior.

A

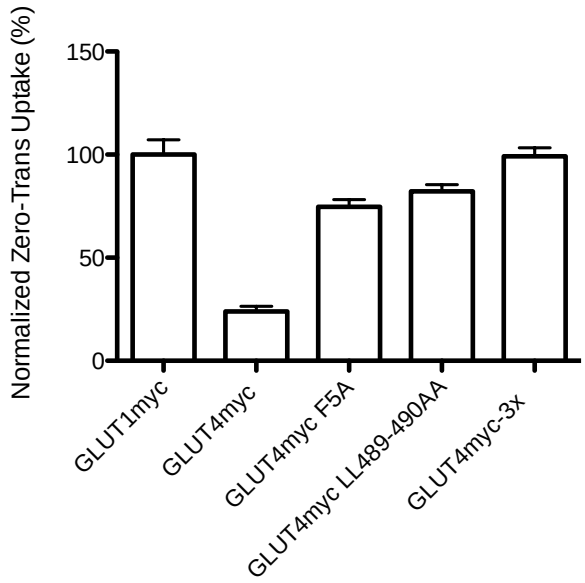
Normalized Zero-Trans Uptake (%)
150
100
50
0
GLUT1myc
GLUT4myc
GLUT4myc F5A
GLUT4myc LL489-490AA
GLUT4myc-3x

B

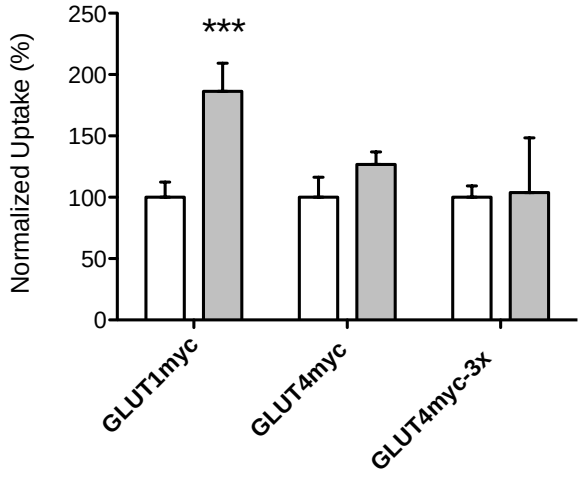
Normalized Uptake (%)
250
200
150
100
50
0
***
GLUT1myc
GLUT4myc
GLUT4myc-3x

Figure 3.4 Sugar transport by GLUT4myc mutants aimed at increasing surface expression

A, Zero-trans uptake measurements of 100 μM 2-DG in HEK cells (*ordinate*) transfected with GLUT1myc, GLUT4myc, and GLUT4myc mutants (*abscissa*) engineered to increase surface expression (GLUT4 F5A, GLUT4 LL489-490AA, and GLUT4-3x (GLUT4 F5A/LL 489-490AA)). Uptake is normalized to zero-trans uptake by GLUT1myc transfected cells. *B,* Uptake measurements (*ordinate*) of 100 μM 2-DG in the presence of 40 mM 3-MG in HEK cells transfected with GLUT1myc, GLUT4myc, or GLUT4myc-3x (*abscissa*) under zero-trans (*empty bars*) or hetero-exchange (*gray bars*) conditions. Results are shown as mean ± SEM for three separate assays. The significance of the difference between control and test conditions was computed by an unpaired, 2-tailed Student's t-test analysis yielding the following P values: *** $P \leq 0.001$.

Transport rates are proportional to cell surface GLUT expression

The absolute rates of GLUT1-mediated zero-trans (ZT) and hetero-exchange (HE) 2-DG uptake are proportional to the amount of transporter at the cell surface. However, transport behavior (GLUT1-mediated trans-acceleration) is unaffected by expression level. To illustrate this, HEK cells were transfected with a range of [GLUT1myc DNA], and the relationship between cell surface GLUT1myc expression and GLUT1myc-mediated zero-trans and hetero-exchange transported was investigated (Figure 3.5).

Surface expression was quantitated by biotinylation of cell surface protein at 4ºC followed by membrane solubilization, streptavidin affinity-purification of labeled proteins and quantitation of their GLUT1myc content by immunoblot analysis using α-myc antibody (Figure 3.5A-B). While the relationship between cell surface expression and GLUT1myc-dependent zero-trans or hetero-exchange 2-DG uptake is linear (Figure 3.5C), the nearly 2-fold increase in hetero-exchange over zero-trans uptake rates remains constant at every level of cell surface GLUT1myc observed. We show below that while GLUT4 and its engineered variants achieve differing cell surface expression levels, their inability to catalyze trans-acceleration is independent of expression level (see Figure 3.4B and Figure 3.8).

Trans-acceleration (or lack thereof) is therefore independent of the amount of transporter expressed at the cell surface and is an intrinsic property of the transport protein. This is not unexpected. Endothelial cell GLUT1-mediated zero-trans and accelerated-exchange 3-MG uptake (the latter being twice as fast as zero-trans uptake)

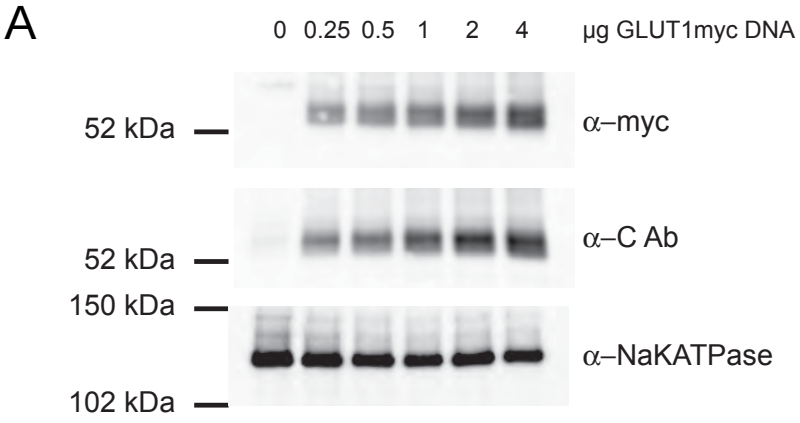
A
0 0.25 0.5 1 2 4
µg GLUT1myc DNA
52 kDa
α–myc
52 kDa
α–C Ab
150 kDa
102 kDa
α–NaKATPase

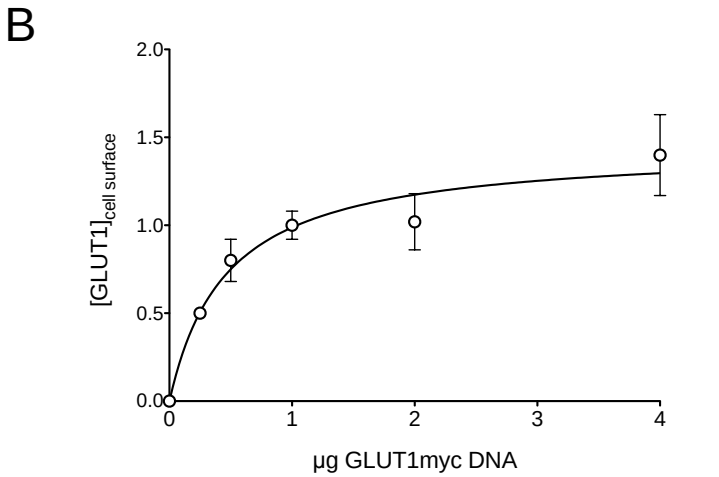
B
[GLUT1]cell surface
2.0
1.5
1.0
0.5
0.0
0
1
2
3
4
µg GLUT1myc DNA

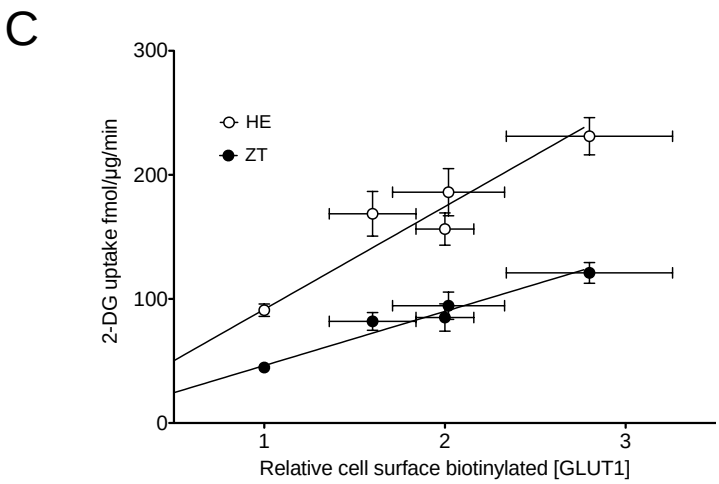
C
2-DG uptake fmol/µg/min
300
200
100
0
HE
ZT
1
2
3
Relative cell surface biotinylated [GLUT1]

Figure 3.5 The effect of GLUT1myc cell surface expression on transport rates and trans-acceleration

A, HEK cells were transfected with varying [GLUT1myc DNA]. Two days later, cell surface proteins were biotinylated, solubilized and affinity purified on streptavidin beads, and GLUT1myc was detected by immunoblot analysis using either α-myc Ab or GLUT1 α-Ct Ab. As a loading control, the α-subunit of the Na^+,K^+-ATPase was detected using α-Na^+,K^+-ATPase Ab. The mobility of molecular weight standards is indicated. The amount of GLUT1myc DNA added at transfection is shown above representative blots from an experiement. ***B,*** Data obtained in the above experiment and from two similar experiments were analyzed by densitometry, background corrected, normalized to loading controls, and averaged. *Ordinate*: relative cell surface [GLUT1]; *abscissa*: μg DNA added at transfection. Results are shown as mean ± SEM for three separate assays. The curve is a section of a single rectangular hyperbola characterized by $K_{0.5}$ = 0.47 ± 0.13 μg DNA; maximum expression = 1.45 ± 0.12 with expression normalized to unity at 1 μg DNA. *C,* Rate of GLUT1myc-catalyzed zero-trans (●) and hetero-exchange (○) 2-DG uptake as a function of cell surface [GLUT1myc] as detected by cell surface biotinylation. Cells were transfected with GLUT1myc DNA as in *A*, and measurements of ZT and HE 2-DG uptake or cell surface [GLUT1myc] were made in triplicate on 3 separate occasions. Uptake measured in mock transfected cells was subtracted. Results are shown as mean ± SEM for three separate assays. The lines drawn through the points were computed by the method of least squares and have the following parameters: ZT, slope = 43.7 ± 2.8 fmol/μg/min/unit biotinylation, y-intercept = 2.6 ± 5.1 fmol/μg/min, R^2 = 0.98; HE, slope = 82.8 ± 8.5 fmol/μg/min/unit biotinylation, y-intercept = 8.8 ± 15.3 fmol/μg/min, R^2 = 0.96.

are both doubled when endothelial cell surface [GLUT1] is doubled by acute metabolic stress (182), (183). Rat erythrocytes express 1,000-fold less GLUT1 than do human erythrocytes, but both cells display accelerated-exchange sugar transport (233), (279). Rat adipocyte GLUT4-mediated zero-trans and equilibrium exchange 3-MG uptake are both increased approximately 12-fold by insulin-induced GLUT4 recruitment to the cell surface, but the characteristic GLUT4 kinetic behavior (lack of trans-acceleration) is unchanged (209). Provided that heterologous expression of the transporter is sufficient to measure its function over background, parental transport, the kinetic behavior of the GLUTs (trans-acceleration or lack of trans-acceleration) is independent of cell surface expression levels. The measurement of some kinetic constants, such as k_{cat}, does require specific knowledge of cell surface expression (see below).

Analysis of half- and quarter-protein domain-chimeras for trans-acceleration

Zero-trans and hetero-exchange 2-DG transport were measured in HEK cells transfected with either GLUT1myc or the half-protein domain chimeras containing GLUT1 loop 6 (11(1)44 and 44(1)11). GLUT1 TMs 7-12 are not important for trans-acceleration (Table 3.1). 2-DG uptake by GLUT1myc and by 11(1)44 is increased under hetero-exchange conditions, while transport catalyzed by 44(1)11 is not (Table 3.1). To ascertain whether loop 6 sequence is critical, we tested an analogous set of half-domain chimeras containing the GLUT4 sequence of loop 6 (Table 3.1). 2-DG uptake by 11(4)44 or by 11(1)44 is significantly increased under HE conditions but transport by

Table 3.1

Zero-Trans and Hetero-Exchange 2-DG Uptake by GLUT1myc-GLUT4myc Chimeras

[a]Chimera	[b]Residues	[c]Zero-Trans Uptake (ZT) fmol/μg/min	[d]Fold-Stimulation During Hetero-Exchange (HE) HE:ZT	[e]Trans-Acceleration (P value)
GLUT1myc	1-492	117.2 ± 14.9	1.80 ± 0.15	Y P ≤ 0.001
GLUT4myc	1-509	42.0 ± 6.8	0.96 ± 0.08	N
GLUT4myc-3x	1-509	77.4 ± 7.4	1.04 ± 0.45	N
44(1)11	G4 1-223 G1 208-492	35.4 ± 4.6	0.94 ± 0.17	N
11(1)44	G1 1-266 G4 283-509	66.4 ± 7.4	1.90 ± 0.21	Y P ≤ 0.001
44(4)11	G4 1-282 G1 267-492	40.3 ± 9.0	0.96 ± 0.18	N
11(4)44	G1 1-207 G4 224-509	35.3 ± 7.3	2.00 ± 0.31	Y P ≤ 0.01
1444	G1 1-119 G4 136-509	103.0 ± 7.0	1.10 ± 0.11	N
4111	G4 1-135 G1 120-492	47.3 ± 5.9	1.70 + 0.21	Y P ≤ 0.01
1411	G1 1-119; 208-492 G4 136-223	146.1 ± 10.2	1.00 ± 0.13	N
4144	G4 1-135; 224-509 G1 120-207	61.6 ± 8.1	1.80 ± 0.09	Y P ≤ 0.00001
GLUT4myc (4,5 G1)	G4 1-135; 203-509 G1 120-186	60.1 ± 4.5	0.65 ± 0.15	N
GLUT4myc (5,6 G1)	G4 1-166; 224-509 G1 151-207	38.1 ± 3.9	1.90 ± 0.14	Y P ≤ 0.00001
GLUT4myc (5, G1)	G4 1-166; 203-509 G1 151-186	53.2 ± 5.7	0.57 ± 0.09	N
GLUT4myc (6, G1)	G4 1-203; 224-509 G1 187-207	25.8 ± 6.2	1.80 ± 0.23	Y P ≤ 0.01
GLUT1myc (6, G4)	G1 1-186; 208-492 G4 203-223	168.3 ± 12.5	1.10 ± 0.11	N
GLUT1myc SIIFI 191-195 GLTVL	G1 1-190; 196-492 G4 208-212	162.4 ± 7.9	1.30 ± 0.05	Y P ≤ 0.001
GLUT1myc CIV 202-204 LVL	G1 1-201; 205-492 G4 218-220	64.1 ± 7.2	2.20 ± 0.18	Y P ≤ 0.00001
GLUT4myc GLTVL 208-212 SIIFI	G4 1-207; 213-509 G1 191-195	55.8 ± 4.9	0.59 ± 0.09	N
GLUT4myc LVL 218-220 CIV	G4 1-217; 221-509 G1 202-204	92.1 ± 5.1	0.97 ± 0.05	N

[a]The chimeras employed in this study were constructed using two backbones: GLUT1myc (wt GLUT1 residues 1-492 with a c-myc epitope (EQKLISEEDL) inserted between residues 55 and 56) and GLUT4myc-3x (wt GLUT4 residues 1-509 in which F5, L489 and L490 is each mutagenized to A, and with a c-myc epitope (EQKLISEEDL) inserted between residues 72 and 73). All residue numbering ignores the inserted c-myc sequence. Chimera nomenclature is described in the Results section and in Figure 1.

[b]The sequence composition of chimeras is described as fusions of GLUT1myc (G1) and GLUT4myc-3x (G4) sequence in which G1 and G4 sequence numbering ignores the inserted c-myc epitope.

[c]Zero-trans uptake (ZT) of 100 μM 2-DG (fmol/μg protein/min) from medium containing 40 mM 3-MG was measured in transfected HEK cells depleted of intracellular sugar. Values are reported as mean ± SEM for a minimum of n = 3 assays and are background-corrected for 2-DG uptake measured in non-transfected cells (41 ± 4 fmol/μg protein/min).

[d]Stimulation of 2-DG uptake observed under hetero-exchange conditions (extra- and intracellular [3-MG] = 40 mM) was determined as the ratio of hetero-exchange (HE) 2-DG uptake to ZT uptake (fmol/μg/min). Values are reported as mean ± SEM for a minimum of n = 3 assays.

ZT and HE uptakes were measured for GLUT1myc in every assay. This table reports the GLUT1myc data as a global mean ± SEM for a minimum of n=30 assays. The range observed in these assays for zero-trans uptake was 39.2 ± 5.36 to 185 ± 18.8 fmol/μg/min. The range observed for HE:ZT was 1.48 ± 0.11 to 2.3 ± 0.31

[e]Trans-acceleration is absent (N) when HE:ZT is not significantly greater than 1. Trans-acceleration is present (Y) when HE:ZT is significantly greater than 1. Significance was determined using an unpaired, 2-tailed student’s t-test.

44(4)11 or 44(1)11 is not. Cytoplasmic loop 6, therefore, does not contain isoform-specific sequence that is essential for trans-acceleration. These results allowed us to focus on GLUT1 TMs 1-6 for further analysis.

2-DG uptake by 4111 shows trans-acceleration while uptake by 1444 does not (Table 3.1). These data show that isoform-specific sequence in TMs 1-3 is not essential for trans-acceleration. In contrast, TMs 4-6 appear essential for trans-acceleration (Table 3.1). GLUT1myc-mediated 2-DG accelerated-exchange is ablated when GLUT4 TMs 4-6 are substituted into GLUT1 (1411). Conversely, swapping TMs 4-6 of GLUT1 into a GLUT4myc-3x scaffold (4144) produces a gain-of-function chimera characterized by robust trans-acceleration (Table 3.1).

Analysis of TMs 4-6

We next examined paired TM substitutions in TMs 4-6. We tested for gain-of-function in GLUT4myc-3x containing either GLUT1 TMs 4-5 (GLUT4 (4,5 G1)) or TMs 5-6 (GLUT4 (5,6 G1); Table 3.1). Our results show that GLUT4 (4,5 G1) does not show exchange stimulation. However, GLUT4 (5,6 G1) displays trans-acceleration gain-of-function. This result indicates that TMs 5-6 are required for trans-acceleration. Because TM5 is also present in the TMs 4-5 chimera, these data suggest either that TM6 alone is required for trans-acceleration, or TM6 in combination with TM5 is required. Indeed, when we substitute GLUT1 TM6 into GLUT4myc-3x (GLUT4 (6, G1)), we observe a trans-acceleration gain-of-function (Table 3.1). Conversely, GLUT1 (6, G4) displays a trans-acceleration loss-of-function, indicating that GLUT4 TM6 cannot substitute for

GLUT1 TM6. GLUT4 (5, G1) does not show trans-acceleration, indicating that GLUT1 TM5 alone is insufficient to produce trans-acceleration in GLUT4 (Table 3.1). Taken together, these data confirm that GLUT1 TM6 is both necessary and sufficient for trans-acceleration. The relative stimulation of HE transport over ZT observed with all the TM-domain chimeras is summarized in Figure 3.6.

Analysis of transmembrane domain 6 amino-acid substitutions

Sequence alignment of GLUT1 and GLUT4 TM6 reveals two regions of sequence disparity (Figure 3.7). Region A comprises GLUT1 $SIIFI_{191\text{-}195}$, corresponding to GLUT4 $GLTVL_{208\text{-}212}$. Region B is GLUT1 $CIV_{202\text{-}204}$, corresponding to GLUT4 $LVL_{218\text{-}220}$. We chose to exchange the amino acids in Regions A or B between GLUT1 and GLUT4. We observe that neither Region A nor B of GLUT1 sequence confers trans-acceleration when individually substituted into GLUT4 (Table 3.1). Similarly, substitution of either Region A or B of GLUT4 into GLUT1 does not produce a loss-of-function (Table 3.1). These results suggest that all or some of the 8 disparate amino acids within TM6 are required for trans-acceleration.

Analysis of k_{cat}/K_m for wild-type and TM6 GLUT1 and GLUT4 mutants

Despite the use of GLUT4myc-3x to increase GLUT4 surface expression, there remained consistently lower levels of 2-DG transport among the GLUT4-based chimeras

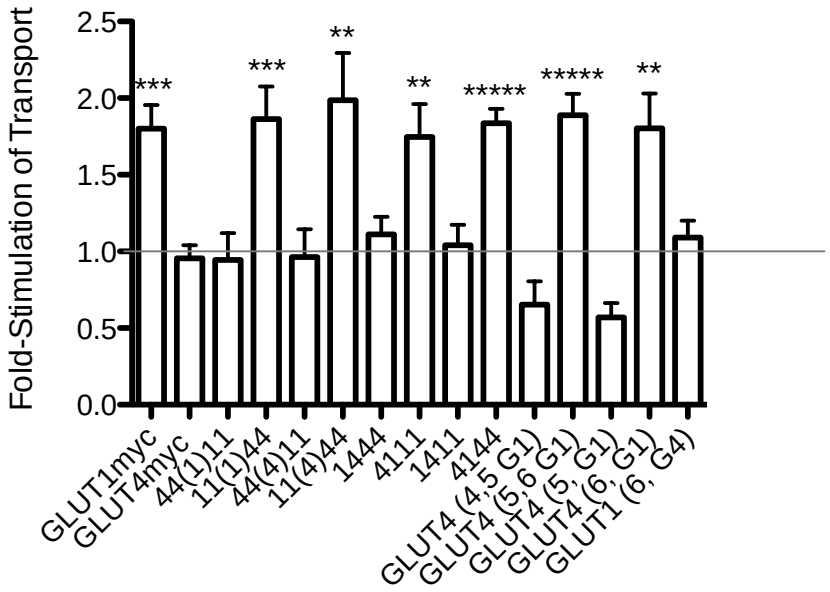

Figure 3.6 Summary of stimulation under hetero-exchange conditions for transmembrane domain chimeras

The amount of stimulation observed under hetero-exchange conditions is expressed as a ratio of HE:ZT (*ordinate*), shown for all of the chimeras with TM domain substitutions in either GLUT1myc or GLUT4myc scaffolds (*abscissa*). The global average of HE:ZT for GLUT1myc (n=30 assays; Table 3.1) was reported for reference. Trans-acceleration is absent when HE:ZT is ≤ 1; a *line* is drawn to show where HE:ZT is 1. Trans-acceleration is present when HE:ZT is significantly above 1. Significance was computed using an unpaired, 2-tailed Student's t-test yielding the following values: ** $P \leq 0.01$; *** $P \leq 0.001$; ***** $P \leq 0.00001$.

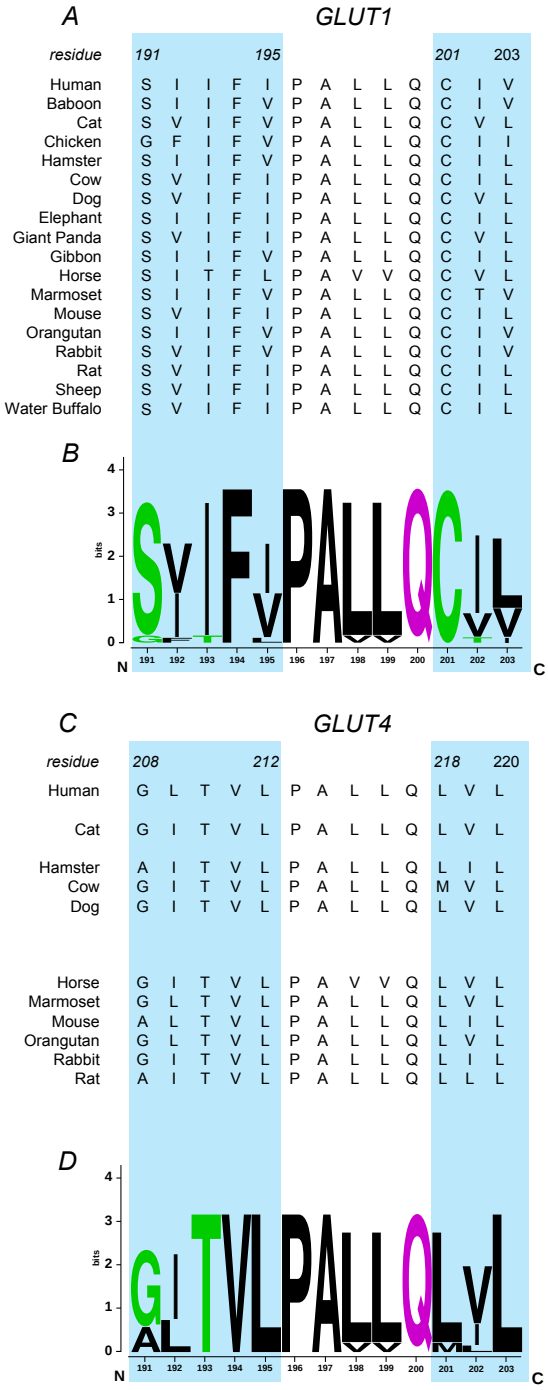
A
GLUT1
residue
191
195
201
203
Human S I I F I P A L L Q C I V
Baboon S I I F V P A L L Q C I V
Cat S V I F V P A L L Q C V L
Chicken G F I F V P A L L Q C I I
Hamster S I I F V P A L L Q C I L
Cow S V I F I P A L L Q C I L
Dog S V I F I P A L L Q C V L
Elephant S I I F I P A L L Q C I L
Giant Panda S V I F I P A L L Q C V L
Gibbon S I I F V P A L L Q C I L
Horse S I T F L P A V V Q C V L
Marmoset S I I F V P A L L Q C T V
Mouse S V I F I P A L L Q C I L
Orangutan S I I F V P A L L Q C I V
Rabbit S V I F V P A L L Q C I V
Rat S V I F I P A L L Q C I L
Sheep S V I F I P A L L Q C I L
Water Buffalo S V I F I P A L L Q C I L
B
bits
4
3
2
1
0
191 192 193 194 195 196 197 198 199 200 201 202 203
N
C
C
GLUT4
residue
208
212
218
220
Human G L T V L P A L L Q L V L
Cat G I T V L P A L L Q L V L
Hamster A I T V L P A L L Q L I L
Cow G I T V L P A L L Q M V L
Dog G I T V L P A L L Q L V L
Horse G I T V L P A V V Q L V L
Marmoset G L T V L P A L L Q L V L
Mouse A L T V L P A L L Q L I L
Orangutan G L T V L P A L L Q L V L
Rabbit G I T V L P A L L Q L I L
Rat A I T V L P A L L Q L L L
D
bits
4
3
2
1
0
191 192 193 194 195 196 197 198 199 200 201 202 203
N
C

Figure 3.7 Sequence alignment and conservation of TM6 in GLUTs 1 and 4

A, Sequence alignment of the trans-acceleration subdomains (cyan background) of GLUT1 transmembrane domain 6 (amino acids spanning 191-195-PALLQ-201-203) in 18 mammals. *B*, WebLogo plot (http://weblogo.berkeley.edu/) for this alignment. Dolphin GLUT1 also displays trans-acceleration (67), but its sequence is not yet known. *C*, Sequence alignment of the trans-acceleration subdomains (cyan background) of GLUT4 transmembrane domain 6 (amino acids spanning 208-212-PALLQ-218-220) in 11 mammals. *D*, WebLogo plot for this alignment.

(Table 3.1). This may be related in part to protein stability, as we observe similar amounts of message for transfected constructs (Appendix Figure A3.6) but different protein expression levels (Appendix Figure A3.7, A3.8). Although we attempted to examine cell surface expression by immunofluorescence microscopy (Appendix Figure A3.9), this was not quantitative. Due to these differences in chimera expression, we measured relative surface GLUT expression by cell-surface biotinylation and used this value to scale zero-trans uptake rates for constructs of interest.

Streptavidin pull-downs of biotinylated cell surface proteins confirm the presence of transfected myc-tagged GLUTs (Figure 3.8A). The identity of each myc-tagged transporter was verified by either anti-GLUT1 or anti-GLUT4 antibodies. Quantitation of α-myc signal reveals that GLUT4myc surface expression is 42% ± 2% relative to GLUT1myc expression, while surface expression of GLUT4myc-3x is only slightly improved (55% ± 18%). GLUT1 (6, G4) shows comparable surface expression to GLUT1myc (94% ± 29%), whereas GLUT4 (6, G1) achieves only 17% ± 3% of the GLUT1myc level. Scaling the measured zero-trans uptake rate by relative surface expression allows us to compare differences in catalytic activity (Figure 3.8B). Adjusted rates of zero-trans uptake by GLUT1myc, GLUT4myc, and GLUT4myc-3x are similar (Figure 3.8B). However, the trans-acceleration loss-of-function GLUT1 chimera GLUT1 (6, G4) has an adjusted rate that is 1.5-fold greater than GLUT1myc. In contrast, the gain-of-function mutant, GLUT4 (6, G1), has an adjusted zero-trans rate that is lower than both wt GLUT4myc and GLUT4myc-3x. However, these differences are not

A

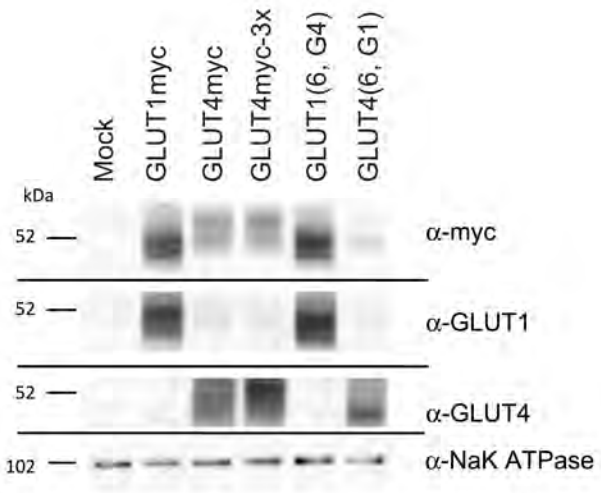
Mock
GLUT1myc
GLUT4myc
GLUT4myc-3x
GLUT1(6, G4)
GLUT4(6, G1)
kDa
52
α-myc
52
α-GLUT1
52
α-GLUT4
102
α-NaK ATPase

B

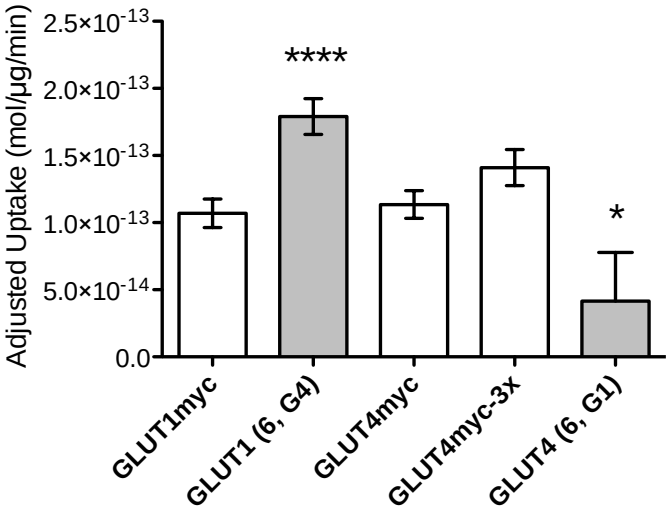
Adjusted Uptake (mol/µg/min)
2.5×10-13
2.0×10-13
1.5×10-13
1.0×10-13
5.0×10-14
0.0
****
*
GLUT1myc
GLUT1 (6, G4)
GLUT4myc
GLUT4myc-3x
GLUT4 (6, G1)

C

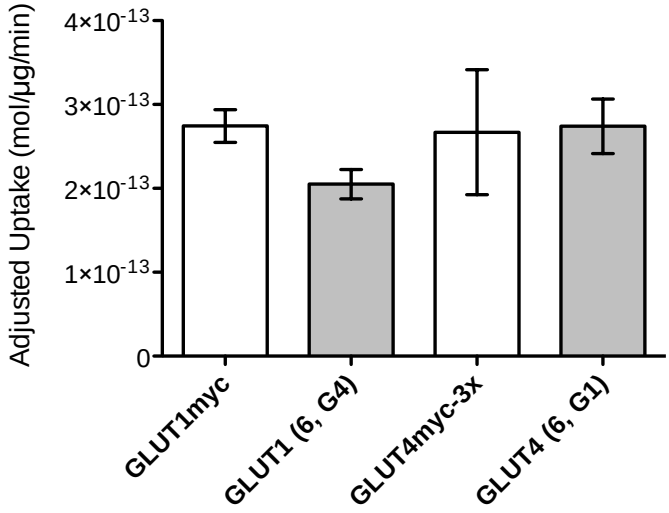
Adjusted Uptake (mol/µg/min)
4×10-13
3×10-13
2×10-13
1×10-13
0
GLUT1myc
GLUT1 (6, G4)
GLUT4myc-3x
GLUT4 (6, G1)

Figure 3.8 Catalytic activity of cell surface GLUT1, GLUT4, and TM6 mutants

A, Cell surface expression of GLUT1myc, GLUT4myc, GLUT4myc-3x, GLUT1 (6, G4), and GLUT4 (6, G1) quantitated by cell surface biotinylation. The streptavidin pull downs were probed using α-myc, α-GLUT1, α-GLUT4 and α-Na^+,K^+-ATPase (α-subunit) antibodies. Average densities of bands detected by α-myc were corrected for density observed in mock-transfected cells, normalized to GLUT1myc density and used to calculate the data in *B* and *C*. *B*, Adjusted zero-trans 100 μM 2-DG uptake (mol/μg/min, *ordinate*) of GLUT1myc, GLUT1 (6, G4), GLUT4myc, GLUT4myc-3x, and GLUT4 (6, G1) (*abscissa*). Adjusted rates were obtained by scaling the average zero-trans rate of each construct by its surface expression relative to GLUT1myc. Results are shown as mean ± SEM for three separate assays. An unpaired, 2-tailed Student's t-test analysis yields the following P values: * $P \leq 0.07$; **** $P \leq 0.0001$. *C*, Adjusted hetero-exchange 100 μM 2-DG uptake (mol/μg/min, *ordinate*) of GLUT1myc, GLUT1 (6, G4), GLUT4myc-3x, and GLUT4 (6, G1) (*abscissa*). Adjusted rates were obtained by scaling the average hetero-exchange rate of each construct by its surface expression relative to GLUT1myc. Results are shown as mean ± SEM for three separate assays.

observed when the hetero-exchange rate of uptake is scaled by relative surface expression (Figure 3.8C). When intracellular sugar is present, the adjusted rates of GLUT1myc, GLUT4myc and both TM6 chimeras are nearly indistinguishable.

Discussion

Using homology-scanning mutagenesis, we demonstrate that GLUT1 TM domain 6 is both necessary and sufficient to confer a trans-acceleration gain-of-function to the GLUT4 scaffold. Conversely, substituting GLUT4 TM6 into the GLUT1 scaffold ablates trans-acceleration. These results establish that trans-acceleration is intrinsic to GLUT1 sequence, and is not due to modulating co-factors or other cellular contexts. Although GLUT1 and GLUT4 TM6 differ by a total of 8 amino acids in two sub-regions, homology substitution of either region alone does not materially affect the trans-acceleration profile of each transporter. This suggests that these sub-domains work in concert to affect GLUT1 trans-acceleration of sugar transport.

The canonical explanation of trans-acceleration centers on two kinetic models for carrier-mediated transport: the simple carrier and the fixed-site carrier. The simple carrier (Figure 1.3) is proposed to alternate between exofacial and endofacial orientations (212), (280), (211), (213). During sugar uptake, an external sugar binds to the exofacial orientation, which then undergoes a conformational change to the endofacial state, from which the sugar dissociates into cytoplasm. For an additional round of sugar uptake to

occur, the endofacial orientation of the carrier must now reorient to the exofacial state. Conformational changes (exofacial to endofacial and *vice versa*) are termed translocation when a sugar is bound, and relaxation when no sugar is bound (186). Trans-acceleration of sugar uptake occurs when translocation (endofacial to exofacial) is faster than relaxation. The absence of trans-acceleration is observed when translocation proceeds at the same rate as relaxation. Trans-inhibition would be observed if translocation were slower than relaxation.

The fixed-site carrier model (Figure 1.4) proposes that the carrier exposes endofacial and exofacial sugar binding sites simultaneously (262), (185), (281), (282). Transport proceeds concurrently in both directions, implying that sugars initially bound at exo- or endofacial sites exchange into a central cavity, whence they associate with the trans-binding site prior to release into the cytoplasm or interstitium, respectively. Simple exchange describes the release of a bound exo- or endofacial sugar into the central cavity when the trans-site is unoccupied by sugar. Geminate exchange describes the release of a bound exo- or endofacial sugar into the central cavity when the opposite site is occupied by sugar (239). Trans-acceleration is observed when geminate exchange is faster than simple exchange (239).

A hybrid model (Figure 1.5) has also been proposed, in which the transporter comprises 4 simple carriers arranged in a coupled, anti-parallel configuration. At any instant, two subunits (carriers) present exofacial orientations and two subunits present endofacial orientations (141). If one exofacial subunit undergoes a reorientation to the

endofacial state, the adjacent endofacial subunit must undergo a reorientation to the exofacial state. If translocation is faster than relaxation, it is easy to see how intracellular sugar could stimulate sugar uptake.

The current study suggests that GLUT4 TM6 sequence allows equal rates of simple carrier relaxation and translocation or equal rates of fixed-site carrier exchange and geminate-exchange. In contrast, GLUT1 TM6 sequence inhibits simple carrier relaxation but not translocation, or inhibits fixed-site carrier exchange but not geminate-exchange, thereby allowing intracellular sugar to stimulate unidirectional sugar uptake. Whichever kinetic model is correct, the following generalization is consistent with experimental evidence. In carriers containing GLUT1 TM6 sequence, an empty endofacial sugar-binding site is inhibitory to the rate of uptake. In carriers containing GLUT4 TM6 sequence, this inhibition is removed and the rate of uptake is unaffected by the presence of intracellular sugar.

This hypothesis is further supported by the observed differences in k_{cat}/K_m ratios for GLUT1, GLUT4, and the TM6 chimeras. V_{max}/K_m for enzyme-catalyzed reactions is normally obtained by measuring the rate constant, k, for the reaction at limiting substrate concentrations, which is converted to k_{cat}/K_m by dividing k by [enzyme]. V_{max}/K_m is obtained from measurements of 2-DG uptake and then normalized to cell surface GLUT expression to give k_{cat}/K_m. While it is possible that TM6 mutants could alter the affinity ($\sim 1/K_m$) of GLUT1 and GLUT4 for substrate, this seems unlikely because TM6 is a putative scaffold TM quite distant to the hypothesized GLUT1 substrate-binding cavity

(116). Moreover, $K_{m(app)}$ for GLUT1- and GLUT4-mediated sugar uptake is similar for both 2-DG (9-10 mM; (200)) and 3-MG (~6 mM; (209)). We therefore hypothesize that the observed changes in k_{cat}/K_m (Figure 3.8B) largely reflect changes in k_{cat}.

If TM6 affects the relative rates of simple carrier relaxation and translocation, or of fixed-site carrier exchange and geminate-exchange, we predict that the inhibitory sequence of GLUT1 TM6 would reduce GLUT4-catalyzed zero-trans uptake. Indeed, we observe that k_{cat}/K_m for GLUT4 (6, G1) is ~70% lower than that for either wt GLUT4myc or the surface-expression mutant GLUT4myc-3x (Figure 3.8B). In contrast, substituting GLUT4 TM6 sequence into GLUT1 should increase zero-trans k_{cat}/K_m relative to that of wt GLUT1, and this is observed. By the same rationale, we would predict that this inhibitory sequence would be without effect in the presence of intracellular sugar, as relaxation is bypassed with translocation. When we compare the adjusted hetero-exchange rates of the TM6 chimeras (Figure 3.8C), this is indeed the case.

GLUT1 TM6 trans-acceleration sub-domains are highly conserved (F194 and C202 are 100% conserved among 18 mammalian species; S191 and I193 are 94% conserved; see Figure 3.7). A homology-modeled GLUT1 three-dimensional structure (116) juxtaposes putative scaffold TMs 6 and 3 with the translocation pore-forming TM1 (Figure 3.9 A-B). A study by Liu et al., aimed at identifying sequences important for ATP-modulation of GLUT1 (235), showed that a point mutation in TM3 (G111A) abolishes trans-acceleration of GLUT1 expressed in *X. laevis* oocytes. We did not observe this effect in the TMs 1-3 chimeras because this glycine is conserved between

GLUT1 and GLUT4, and is therefore present in both chimeras. While our data suggest that G111 alone is not sufficient for trans-acceleration, it does not rule out the possibility that G111 makes critical contacts with TM6. The sequence of the membrane-spanning region of TM1 is invariant between GLUTs 1 and 4, with the exception of GLUT1 T_{30} (Figure 3.9C). This position is conserved in GLUTs 1 and 3 (those carriers showing trans-acceleration), but not in GLUTs 2 and 4 (carriers lacking trans-acceleration). However, a potential role of T_{30} in trans-acceleration is eliminated by the observation that the 4111 chimera contains the substitution T30I, yet still displays trans-acceleration. It is tempting to speculate that GLUT1 TM6 residues 191-195 and 202-204 interact with partners in TM1 and/or TM3 (Figure 3.9C) to stabilize endo- and exofacial orientations of the substrate-deficient-carrier, thereby restraining conformational changes between exo- and endofacial states (e.g. relaxation). We hypothesize that when sugar binds to exofacial or endofacial sites, these interactions are weakened, TM arrangements are destabilized, and conformational change is accelerated.

While the ability to catalyze trans-acceleration has not been studied in all GLUTs, exchange transport has been measured in all four of the class I glucose transporters (GLUTs 1-4). Human GLUT3 catalyzes trans-acceleration in rat cerebellar granule neurons (283) and in transfected HEK cells, while rat liver GLUT2 does not exhibit trans-acceleration (208). TM6 sequence comparisons across GLUTs 1 - 4 (Figure 3.9D) show that the same 2 sub-domains responsible for trans-acceleration in GLUT1 represent the only variable TM6 sequence among all four transporters.

A

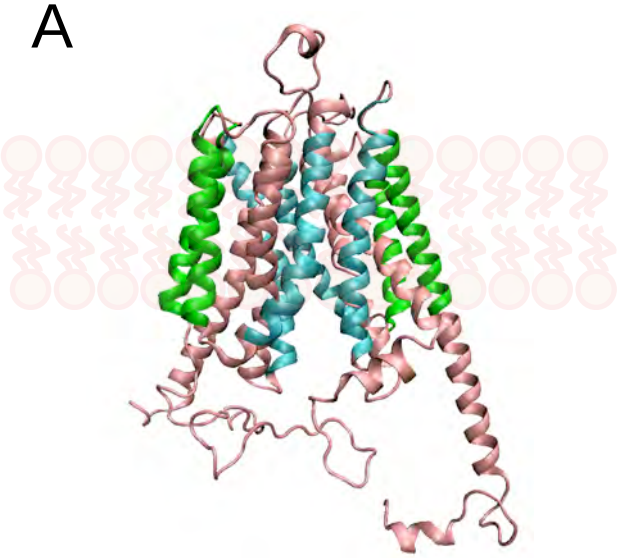

B

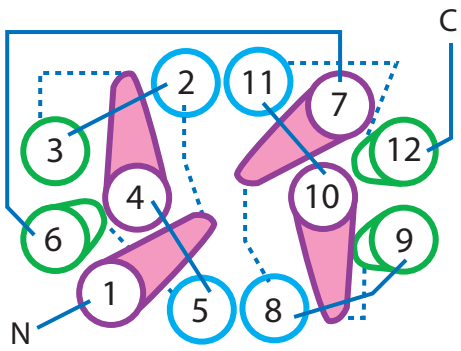

C

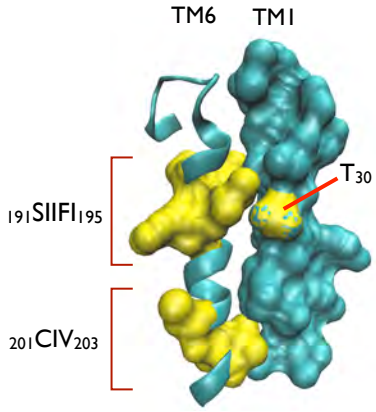

D

							191				195						201		203	
GLUT1	L	W	P	L	L	L	S	I	I	F	I	P	A	L	L	Q	C	I	V	L
GLUT3	L	W	P	L	L	L	G	F	T	I	L	P	A	I	L	Q	S	A	A	L
GLUT2	L	W	H	I	L	L	G	L	S	G	V	R	A	I	L	Q	S	L	L	L
GLUT4	L	W	P	L	L	L	G	L	T	V	L	P	A	L	L	Q	L	V	L	L
consensus	L	W	P	L/I	L	L	G	.	.	.	.	P	A	L/I	L	Q	.	.	.	L

Figure 3.9 Role of TM6 in GLUT1-mediated trans-acceleration.

Putative glucose transport proteins (GLUT1) homology-modeled structure based on the GlpT homology model and visualized using VMD 1.8.5 (© University of Illinois 2006). GLUT1 coordinates were obtained from the RCSB Protein Data Bank (entry No. 1SUK). *A*, GLUT1 viewed along the bilayer plane. The limits of the bilayer are indicated by the cartoon representations of phospholipids. *B*, Putative helix packing arrangement viewed from the cytoplasmic surface. TMs are *numbered* and *colored* as in *A*. Cytoplasmic loops are indicated by *solid* lines and exofacial loops by *dashed* lines. *C*, Putative stacking of TMs 6 and 1. TM6 is shown as a ribbon cartoon (cyan) and residues 191-195 and 201-203 as surface representations (yellow), respectively. TM1 is shown as a surface representation (cyan), with residue T30 highlighted (yellow). *D*, Sequence alignment of TM6 from human GLUTs 1, 3, 2 and 4. GLUTs 1 and 3 catalyze trans-acceleration. GLUTs 2 and 4 do not. Numbering corresponds to GLUT1 sequence. The areas lacking homology are shaded cyan. A putative consensus sequence is indicated.

Further homology scanning mutagenesis studies extending TM6 substitutions into GLUT2 and GLUT3 may reveal whether TM6 plays a central role in trans-acceleration in all glucose uniporters.

CHAPTER IV

Further Characterization of Mutations to TM6 in GLUT1 and the Role of TM6 in Class I GLUT-Mediated Trans-Acceleration

Abstract

The kinetic phenomenon of trans-acceleration has been studied in all four of the Class I glucose transporters. Both GLUTs 1 and 3 display accelerated exchange transport, whereas both GLUTs 2 and 4 do not. Our previous studies have shown that the putative scaffolding domain TM6 is necessary and sufficient for trans-acceleration in GLUTs 1 and 4. This domain differs in a total of 8 amino acids across 2 sub-regions of the sequences, which also represent the most variable regions of TM6 in both GLUTs 2 and 3. Substitution of these 8 residues show that GLUT2 TM6 sequence causes a trans-acceleration loss-of-function in GLUT1, and substitution of GLUT3 TM6 sequence results in a gain-of-function in GLUT4. These changes in ability to catalyze trans-acceleration have been associated with changes in k_{cat}/K_m of the transporter. Here, we show that substitutions to GLUT1 TM6 do not change the intrinsic affinity of the transporter for substrate, supporting the hypothesis that changing TM6 sequence changes catalytic activity. The GLUT2 and GLUT3 TM6 substitutions in GLUTs 1 and 4 are associated with the same patterns of change in zero-trans k_{cat}. In addition, we show that

mutation of the GLUT2 TM6 region to GLUT1 or GLUT3 sequence results in a trans-acceleration gain-of-function. These studies support the hypothesis that the conformational changes which rate-limit transport by Class I GLUTs are controlled by TM6.

Introduction

The mammalian family of glucose transporters (GLUTs) are the primary carriers used by cells to transport the sugars required for metabolic processes. Although the 14 members of this family share a similar putative topology and have overlapping specificities for different substrates, they differ in many aspects, including tissue-specific expression, kinetic characteristics, and protein sequence (102), (184). Of these, the Class I glucose transporters (GLUTs 1-4) have been the most extensively characterized.

The basal glucose transporter, GLUT1, is expressed in all tissues in the body, particularly in red blood cells, the heart, and at blood-tissue barriers (12), (13), (284). GLUT1 is a high-affinity glucose transporter with a K_m for glucose and 2-deoxy-D-glucose (2-DG) of ~ 2-6 mM (237), (197), (194), (199), and a K_m for 3-O-methyl-D-glucose (3-MG) of 4-20 mM, depending on experimental conditions (197), (201), (202), (209), (204), (205). The kinetics of GLUT1-mediated transport have been the most characterized of the GLUTs, as it was the first glucose transporter to be identified and cloned. The high levels of GLUT1 expression in erythrocytes have made the red cell a

classical model system for studying carrier-mediated glucose transport. Such studies have shown that GLUT1-mediated transport is quite complex, displaying rapid, multi-phasic kinetics (210), (224), asymmetry in the V_{max} and K_m for sugar uptake and exit (206), (207), and accelerated-exchange transport (also known as trans-acceleration; (188), (207), (201), (232)).

One other Class I transporter, GLUT3, has also been shown to catalyze trans-acceleration (283). While also present in the testes and in platelets, GLUT3 is highly expressed within the brain, particularly in neurons (21). Like GLUT1, GLUT3 is a high-affinity glucose transporter with an even lower K_m for glucose (237), (285). GLUT3 has also been shown to be ~5-fold more catalytically active than GLUT1 (283). The brain is the organ with the greatest demand for glucose, with brain function in delicate balance with glucose supply and delivery. It seems appropriate that GLUTs 1 and 3, glucose transporters with high affinity, high turnover, and the ability to rapidly equilibrate sugar through trans-acceleration, are the predominant GLUTs expressed at the blood-brain barrier and within the brain itself.

In contrast, the other Class I transporters, GLUTs 2 and 4, do not catalyze trans-acceleration (208), (177), (201). GLUT2 is mainly expressed in the liver, pancreas, and small intestine (16). In addition to its critical role in hormonally regulated sugar homeostasis in these tissues, GLUT2 has emerged as a key mediator of glucose sensing in the counter-regulatory feedback loop (18). While GLUT2 is the only Class I transporter that transports fructose, it is also a low-affinity glucose transpoter (K_m ~ 17

mM (27), (237), (285)). Studies in rat hepatocytes have shown that GLUT2 displays neither asymmetry nor trans-acceleration of glucose (208). Similarly, GLUT4 expression is limited to other hormonally-regulated tissues, mainly skeletal/cardiac muscle and adipocytes (23). In these cells, the majority of GLUT4 resides in intracellular pools until stimulation by insulin (and in muscle cells, contraction) induces a rapid translocation of GLUT4 to the plasma membrane (286), (175), (173). Once at the surface, GLUT4 is also a high-affinity transporter, with a K_m on the order of or lower than that of GLUT1 (200), (202), (287); reported GLUT4 affinity for 3-MG ranges from ~2-6 mM (197), (201), (202), (209). Like GLUT3, GLUT4 has been shown to display a greater turnover than GLUT1 (202), (287), and does not show asymmetry (203).

While all four Class I GLUTs transport glucose with high affinity (with the exception of GLUT2) and show sensitivity to the specific inhibitor cytochalasin B (CCB) (28), (272), (285), their sequence homology is only 48-63% (10). As with sequence conservation among all 14 glucose transporters, the most variant regions are the N- and C-termini, intracellular loop 6, and the other loops connecting the 12 transmembrane (TM) domains. However, our previous studies have shown that 8 disparate amino acids within GLUT1 transmembrane domain 6 are necessary and sufficient for trans-acceleration (288). Because the trans-acceleration profiles of GLUT2 and GLUT3 have been determined experimentally, we asked whether conserved sequence motifs in the TM6 region could dictate ability or inability to catalyze trans-acceleration. A precursory analysis of the TM6 sequences for all four Class 1 transporters (Figure 3.9D) reveals that

the significant sequence variations within GLUT2 and GLUT3 TM6 also occur within the same 2 sub-regions of 8 amino acids that govern trans-acceleration in GLUT1.

In this study, we sought to investigate whether substitution of GLUT1 or GLUT3 TM6 sequence was able to confer trans-acceleration in GLUT2 and GLUT4, and *vice versa*. We also sought to determine whether increases in 2-DG uptake attributed to trans-acceleration were due to changes in K_m, k_{cat}, or both. We report the affinity of GLUT1 for 2-DG (K_m ~1 mM) to be unchanged when TM6 is mutated to GLUT4 sequence. Competition of 2-DG uptake by 3-MG is also similar between wt GLUT1 and its TM6 mutant. When we made further substitutions to the TM6 regions of GLUTs 1 and 4 with the sequences of GLUTs 2 and 3, we show that GLUT2 TM6 causes a loss-of-function in GLUT1, and GLUT3 sequence causes a gain-of-function in GLUT4. These substitutions are associated with a modified zero-trans k_{cat}. We then extended the Class I TM6 sequence substitution analysis to show that mutation of the 8 amino acids to either GLUT1 or GLUT3 sequence shows a trans-acceleration gain-of-function in GLUT2.

Experimental Procedures

All materials and procedures used are the same as those reported in Chapter III Experimental Procedures, with the following exceptions or additions:

Mutagenesis

GLUT1-, GLUT2- or GLUT4-encoding cDNA was inserted into the EcoRV-Not1 restriction sites of pcDNA 3.1 (+). GLUT3-encoding cDNA was inserted into the BamHI-Not1 restriction sites of pcDNA 3.1 (+), unless otherwise noted in the legend of Table 4.1. Myc-tagged constructs were made using overlapping primers to insert the myc tag in exofacial loop 1, between GLUT2 residues 44-45 or GLUT3 residues 49-50. For a complete list of primers used, see Appendix (Table A1).

Transient Transfection

HEK cells (70-90% confluency) were transfected with 2 µg DNA per well (12 well plates) or 5 µg DNA per well (6 well plates), unless otherwise specified. Transfections were performed 36-48 hours prior to analysis of sugar uptake or protein expression.

2-deoxy-D-glucose Sugar Uptake

2-DG uptake was measured as described previously (Chapter III; (234)). Zero-trans or hetero-exchange uptake of [^{3}H]-2-DG by sugar-depleted cells was measured as described previously (Chapter III; (288)).

Data Analysis

For experiments where the uptake of 2-DG in the presence of increasing competing [3-MG], sugar uptake, $K_{i(app)}$, was fitted to the following equation for competitive inhibition (Equation 4.1):

$$K_{i(app)} = y_0 - \frac{span[3 - MG]}{K + [3 - MG]}$$

Where y_o is the amount of 2-DG uptake in the absence of competing 3-MG and is constrained to less than 15 fmol/µg/min, *K* is the [3-MG] at half-maximal competition of 2-DG uptake, and *span* is the difference between the maximum and minimum values for 2-DG uptake.

In experiments evaluating whether trans-acceleration is observed, the ratio of hetero-exchange (HE) uptake:zero-trans uptake (ZT) was computed for each construct. As we have shown previously (288), this normalizes for experimental variation in transporter cell surface expression. When this ratio is significantly greater than 1, trans-acceleration is present. The results of paired experiments were analyzed using Student's t-test.

Results

Comparison of substrate affinity in GLUT1 and its TM6 mutant

In order to compare the relative affinities of GLUT1 and GLUT1 containing the TM6 sequence of GLUT4 (GLUT1 (6, G4)), a zero-trans dose-response to 2-DG uptake was measured (Figure 4.1A). As the experiments testing for changes in trans-acceleration relied upon 2-DG uptake, this was the analog chosen to examine the affinity of the

GLUT1 TM6 mutant. Analysis of the dose-response by fitting the data to Equation 4.1 shows that while the V_{max} of wt GLUT1 is over 2.5-fold greater than the V_{max} for GLUT1 (6, G4), the affinities for 2-DG are within error of one another (K_m ~1 mM). It is not possible to compare the K_m obtained for zero-trans dose responses with a K_m under equilibrium-exchange conditions for 2-DG, due to the activity of hexokinase on the pre-loaded 2-DG. Although the affinities for 2-DG uptake were the most critical comparison, uptake media in the trans-acceleration experimental format contain 40 mM cold 3-MG as a competitive inhibitor of 2-DG uptake. Thus we sought to examine whether the competition of 2-DG uptake by increasing $[3\text{-MG}]_o$ was similar for both transporters. Analysis of 3-MG inhibition of 2-DG uptake (Figure 4.1B) yields values for $K_{i(app)}$ that are within the same magnitude for both transporters (wt GLUT1myc $K_{i(app)}$ = 2.9 ± 9.9 mM; GLUT1 (6, G4) $K_{i(app)}$ = 6.8 ± 1.9 mM).

Alignment of Class I transporter transmembrane domain 6 sequence

TM6 is only 21 amino acids long, according to the most recent putative topology of GLUT1 (130). As the sequence conservation among the GLUTs is highest in the TM-spanning regions, alignment of the putative TM6 sequences across all Class I transporters is straightforward (Figure 3.9D). The first 4 residues are invariant (PLLL), with the exception of the first 2 residues in GLUT2 (HI), showing 87.5% consensus overall. The

A

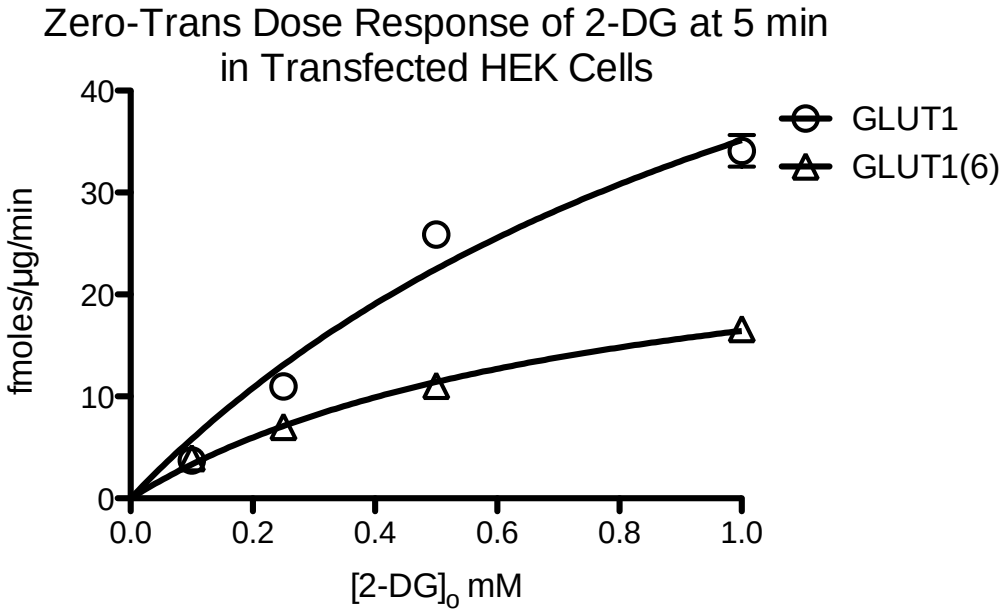
Zero-Trans Dose Response of 2-DG at 5 min
in Transfected HEK Cells
fmoles/µg/min
40
30
20
10
0
0.0
0.2
0.4
0.6
0.8
1.0
[2-DG]o mM
GLUT1
GLUT1(6)

B

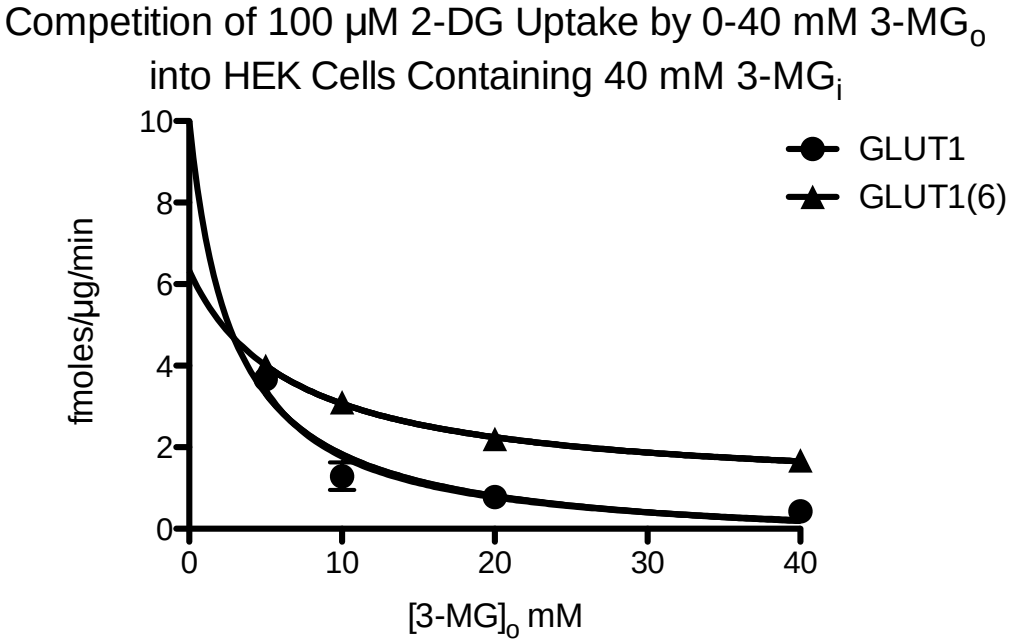
Competition of 100 µM 2-DG Uptake by 0-40 mM 3-MGo
into HEK Cells Containing 40 mM 3-MGi
fmoles/µg/min
10
8
6
4
2
0
0
10
20
30
40
[3-MG]o mM
GLUT1
GLUT1(6)

Figure 4.1 Characterization of 2-DG transport by GLUT1myc and GLUT1 TM6 mutant

A, Dose-response of 2-DG uptake (*ordinate*) from medium containing 0-1 mM 2-DG (*abscissa*) into HEK cells depleted of intracellular sugar and transfected with wtGLUT1myc (○) or GLUT1 (6, G4) (△). Curves are drawn using nonlinear regression assuming that uptake is described by Equation 2.1, with the following results: wt GLUT1myc V_{max} = 80.1 ± 37.3 fmol/μg/min, K_m = 1.3 ± 0.9 mM with R^2 = 0.9630; GLUT1(6, G4) V_{max} = 29.3 ± 3.2 fmol/μg/min, K_m = 0.78 ± 0.2 mM with R^2 = 0.9937. Data are plotted as mean ± SEM for three separate assays. *B*, Competition of 2-DG uptake (*ordinate*) from medium containing 0-40 mM cold 3-MG (*abscissa*) into HEK cells pre-loaded with 40 mM 3-MG and transfected with wt GLUT1myc (●) or GLUT1 (6, G4) (▲). Curves are drawn using nonlinear regression assuming that inhibition is described by Equation 4.1, where y_o was constrained to 15 pmoles/μg/min. The resulting analysis yielded the following values: wt GLUT1myc K_{iapp} = 2.9 ± 9.9 mM with R^2 = 0.9264; GLUT1 (6, G4) K_i = 6.8 ± 1.9 mM with R^2 = 0.9988. Data are plotted as mean ± SEM for two separate assays. In both experiments, uptake was measured at 5 minutes at 37°C, and basal uptake by mock-transfected cells was subtracted from each data point.

A

Human GLUT2 residue	*223*				*227*						*233*		235
Human	G	L	S	G	V	R	A	I	L	Q	S	L	L
Chicken	G	L	S	G	V	A	A	L	L	Q	F	F	L
Cow	G	L	S	A	V	P	A	I	L	Q	C	L	L
Horse	G	L	S	A	V	P	A	V	L	Q	S	L	M
Mouse	G	L	S	A	V	P	A	L	L	Q	C	L	L
Rat	G	L	S	A	V	P	A	L	L	Q	C	L	L
Boar	G	L	S	A	V	P	A	V	L	Q	S	L	M

B

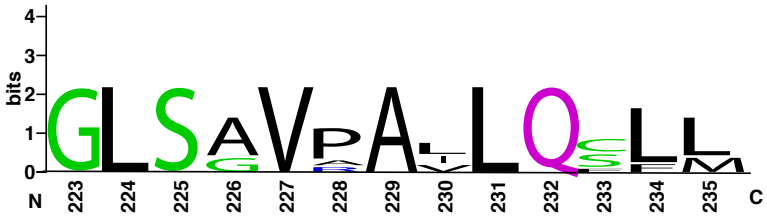

C

Human GLUT3 residue	*189*				*193*						*199*		201
Human	G	F	T	I	L	P	A	I	L	Q	S	A	A
Chicken	G	F	T	I	V	P	A	V	L	Q	C	V	A
Cow	G	F	T	I	L	P	A	I	I	Q	C	A	A
Dog	G	F	T	I	I	P	A	V	L	Q	S	A	A
Mouse	G	L	T	I	I	P	A	I	L	Q	S	A	A
Orangutan	G	F	T	I	L	P	T	I	L	Q	S	A	A
Rat	G	L	T	I	I	P	A	I	L	Q	S	A	A
Sheep	G	F	T	I	L	P	A	I	I	Q	C	A	A

D

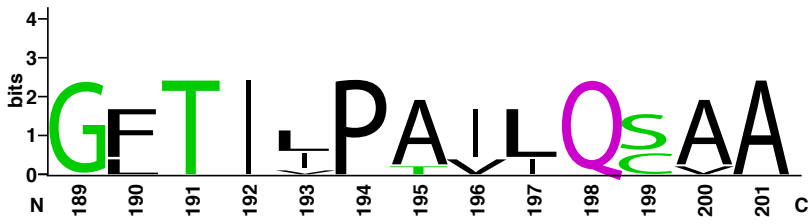

Figure 4.2 Sequence alignment and conservation of the sub-regions of transmembrane domain 6 in GLUTs 2 and 3

A, Sequence alignment of the GLUT2 regions corresponding to the trans-acceleration sub-regions (orange background) of GLUT1 transmembrane domain 6 (human GLUT2 amino acids spanning 223-227-RAILQ-233-235) in 7 mammals. *B*, WebLogo plot (http://weblogo.berkeley.edu/) for this alignment. *C*, Sequence alignment of the GLUT3 regions corresponding to the trans-acceleration sub-regions (orange background) of GLUT1 transmembrane domain 6 (human GLUT3 amino acids spanning 189-193-PAILQ-199-201) in 8 mammals. *D*, WebLogo plot for this alignment.

same 8 amino acids which determine GLUT1-GLUT4 changes in trans-acceleration represent the most variant sequence in all Class I GLUT TM6 sequence. These are distributed across two sub-regions, spanning amino acids 5-9 and 15-17 of the 21 amino acid TM6 sequence, which are referred to as A and B, respectively. In sub-region A, there are no conserved residues among the transporters which display trans-acceleration (GLUTs 1 and 3). There are 3 of 5 residues (60%) conserved between the transporters which do not show trans-acceleration (GLUTs 2 and 4). Similarly, in sub-region B, there is no similarity between GLUTs 1 and 3, and there is 60% conservation of these 3 residues among GLUTs 2 and 4. The remainder of TM6 sequence is more highly conserved; the 5 residues between the sub-regions A and B are 85% conserved, with 1 difference each in GLUT3 and GLUT2. The final 4 amino acids of TM6 are 94% conserved among the class I GLUTs. With these sequence comparisons in mind, we designed Class I TM6 subdomain-swapping chimeras in which only the amino acids of sub-regions A and B were exchanged among the transporters.

For GLUTs 2 and 3, sequences are known across several mammalian species (Figure 4.2). Within TM6, GLUT2 shows 100% conservation of the GLSGV sequence in sub-region A, with the exception of human Gly226, which is Ala in 5 other species. Sub-region B, SLL, is more species-variant, with more than half of the sequences showing Cys rather than Ser233. The remaining Leu residues are more conserved (70-85%). In GLUT3, TM6 sequence is also more conserved in sub-region A, where the Gly, Thr, and Ile of GFTIL are 100% conserved. The Phe190 is Leu in 2 species, while the final Leu is

Ile or Val in half of the species examined. In sub-domain B, SAA, the alanines are nearly 100% conserved (with one exception in chicken GLUT3, which is also the most variant of the GLUT2 TM6 species analyzed). However, as in GLUT2, the Ser199 is also a Cys in a third of the species.

Analysis of Class I transmembrane domain 6 substitutions in GLUTs 1 and 4

As we were able to effect trans-acceleration gain- and loss-of-function by substitution of the 8 amino acids comprised by sub-regions A and B in previous studies (288), we used the same strategy in comparing the effects of other class I transporter sequences (see Table 4.1 for a detailed composition of chimeras). GLUT2 does not catalyze trans-acceleration (208). When GLUT2 $_{223}$GLSGV$_{227}$/$_{233}$SLL$_{235}$ is substituted for GLUT1 $_{191}$SIIFI$_{195}$/$_{202}$CIV$_{204}$ in the mutant GLUT1 (6, G2), we observe a trans-acceleration loss-of-function (Figure 4.3).

Due to previous issues with surface expression of both wtGLUT4 and a triple mutant, GLUT4myc-3x (288), we sought to improve surface expression by substitution of the C-terminal 32 amino acids of GLUT1, in the construct GLUT4myc-cG1. This also simplifies analysis of chimera expression by using the same epitope (GLUT1 C-term) for the same antibody across multiple constructs. The C-terminal substitution improved upon wtGLUT4myc surface expression in both average zero-trans uptake (86.2 ± 8.4 fmol/μg/min (Table 4.1) versus 42.0 ± 6.8 fmol/μg/min (Table 3.1)) and cell-surface expression,

Table 4.1

Zero-Trans and Hetero-Exchange 2-DG Uptake by GLUT1myc, GLUT4myc, GLUT2myc, and GLUT3myc Chimeras

[a]Chimera	[b]Residues	[c]Zero-Trans Uptake (ZT) fmol/μg/min	[d]Fold-Stimulation During Hetero-Exchange (HE) HE:ZT	[e]Trans-Acceleration (P value)
GLUT1myc	1-492	117.2 ± 14.9	1.80 ± 0.15	Y P ≤ 0.001
GLUT4myc-cG1	G4 1-476 G1 460-492	86.2 ± 8.4	1.11 ± 0.10	N
GLUT1 (6, G2)	G1 1-190; 196-200; 204-492 G2 223-227; 233-235	90.8 ± 8.6	1.30 ± 0.17	N
GLUT4 (6, G3)	G4 1-206; 212-216; 220-476 G3 189-193; 199-201	43.4 ± 7.9	1.80 ± 0.10	Y P ≤ 0.00001
GLUT2myc-cG1	G1 460-492 G2 1-491 G1 460-492	80.6 ± 4.4	1.19 ± 0.04	N
GLUT2 (6, G1)	G2 1-222; 228-232; 236-491 G1 191-195; 201-203; 460-492	29.7 ± 7.6	2.40 ± 0.13	Y P ≤ 0.0001
GLUT2 (6, G3)	G2 1-222; 228-232; 236-491 G3 189-193; 199-201	23.8 ± 4.4	2.43 ± 0.22	Y P ≤ 0.001
GLUT3+cG4[f]	G1 460-492 G3 1-497 G4 497-509	91.2 ± 5.3	2.00 ± 0.10	Y P ≤ 0.00001
1311+cG4[f]	G1 1-126; 205-492 G3 125-202 G4 497-509	112.7± 10.1	1.79± 0.10	Y P ≤ 0.00001
GLUT3myc-cG1	G3 1-457 G1 460-492	111.2 ± 12.1	1.11 ± 0.13	N
GLUT3myc	G3 1-497	223.5 ± 7.3 198.7 ± 8.5*	0.81 ± 0.20 0.61 ± 0.10*	N

[a]The chimeras employed in this study were constructed using four backbones: GLUT1myc (wt GLUT1 residues 1-492 with a c-myc epitope (EQKLISEEDL) inserted between residues 55 and 56); GLUT4myc-cG1 (wt GLUT4 residues 1-476, in which F5 is mutagenized to A and the C-terminal 32 amino acids of GLUT1 are substituted for the C-terminus of GLUT4; and where a c-myc epitope (EQKLISEEDL) is inserted between residues 72 and 73); GLUT2myc-cG1 (wt GLUT2 residues 1-491 in which the C-terminal 32 amino acids of GLUT1 are substituted for the C-terminus of GLUT2; and where a c-myc epitope (EQKLISEEDL) is inserted between residues 44 and 45); and GLUT3 (wt GLUT3 residues 1-497 with a c-myc epitope (EQKLISEEDL) inserted between residues 49 and 50). All residue numbering ignores the inserted c-myc sequence. Chimera nomenclature is described in the Results section and in Chapter III.

[b]The sequence composition of chimeras is described as fusions of GLUT1 (G1), GLUT2 (G2), GLUT3 (G3), and/or and GLUT4 (G4) sequence in which GLUT sequence numbering ignores the inserted c-myc epitope.

[c]Zero-trans uptake (ZT) of 100 μM 2-DG (fmol/μg protein/min) from medium containing 40 mM 3-MG was measured in transfected HEK cells depleted of intracellular sugar. Values are reported as mean ± SEM for a minimum of n = 3 assays unless noted, and are background-corrected for 2-DG uptake measured in non-transfected cells (41 ± 4 fmol/μg protein/min).

[d]Stimulation of 2-DG uptake observed under hetero-exchange conditions (extra- and intracellular [3-MG] = 40 mM) was determined as the ratio of hetero-exchange (HE) 2-DG uptake to ZT uptake (fmol/mg/min). Values are reported as mean ± SEM for a minimum of n = 3 assays.

ZT and HE uptakes were measured for GLUT1myc in every assay. This table reports the GLUT1myc data as a global mean ± SEM for a minimum of n=30 assays. The range observed in these assays for zero-trans uptake was 39.2 ± 5.36 to 185 ± 18.8 fmol/μg/min. The range observed for HE:ZT was 1.48 ± 0.11 to 2.3 ± 0.31

[e]Trans-acceleration is absent (N) when HE:ZT is not significantly greater than 1. Trans-acceleration is present (Y) when HE:ZT is significantly greater than 1. Significance was determined using an unpaired, 2-tailed student's t-test.

[f]Constructs were designed and made by Dr. K. Levine and Dr. J. DeZutter. Both inserts were put in the same vector (pcDNA 3.1 (+)) as the other chimeras listed, while using 5'HindIII and 3'XHOI sites. GLUT3+cG4 and 1311+cG4 represent a fusion of the C-terminal 13 amino acids of GLUT4 on the intact GLUT3 sequence or the chimera 1311 rather than a C-terminal substitution. Sequence range of TMs 4-6 substituted in 1311 differs slightly from TMs 4-6 of other chimeras reported in this study due to source of GLUT1 topology (for 1311, alignment reported in Joost and Thorens, 2001 was used; other chimeras use alignment reported in Blodgett et al., 2008).

*Both ZT and HE uptake were performed at 2 min instead of 5. The GLUT1myc-mediated ZT uptake at 2 min was 77.1 ± 10.3 fmol/μg/min in the same experiment. Each wtGLUT3myc experiment was performed n=1.

but was within a similar range of the GLUT4myc-3x mutant in both transport (86.2 ± 8.4 fmol/μg/min (Table 4.1) versus 77.4 ± 7.4 fmol/μg/min (Table 3.1)) and surface expression (Figure 4.4B). The surface expression of GLUT4myc-cG1 is still less than that of wtGLUT1myc. Upon characterization, we observe that this C-terminal substitution is without effect on trans-acceleration; GLUT4myc-cG1 does not display accelerated exchange (Figure 4.3 and Table 4.1). This is expected, as we have previously shown that the C-terminal half of the protein is not involved in trans-acceleration (288). However, when we substitute the sequence of GLUT3 ($_{189}$GFTIL$_{193}$/$_{199}$SAA$_{201}$ for GLUT4 $_{208}$GLTVL$_{212}$/$_{218}$LVL$_{220}$), which displays trans-acceleration, into the GLUT4myc-cG1 scaffold (GLUT4 (6, G3)), we observe a trans-acceleration gain-of-function (Figure 4.3).

Analysis of k_{cat}/K_m for Class I TM6 GLUT1 and GLUT4 mutants

In order to characterize whether the GLUT2 and GLUT3 sequence substitutions within TM6 cause changes to k_{cat}, it was necessary to measure relative surface expression of each transporter and scale the rates of uptake, as we have done previously (288). Biotinylated cell-surface transporters were pulled down and affinity-purified on streptavidin columns. Western blotting analysis with both α-myc and α-GLUT1 C-terminal antibodies (Figure 4.4A) shows that GLUT1myc exhibits the highest level of surface expression. Quantitation of the α-myc bands by densitometry (Figure 4.4B) reveals that the surface expression of the GLUT2 TM6 mutant of GLUT1 is 62 ± 5%

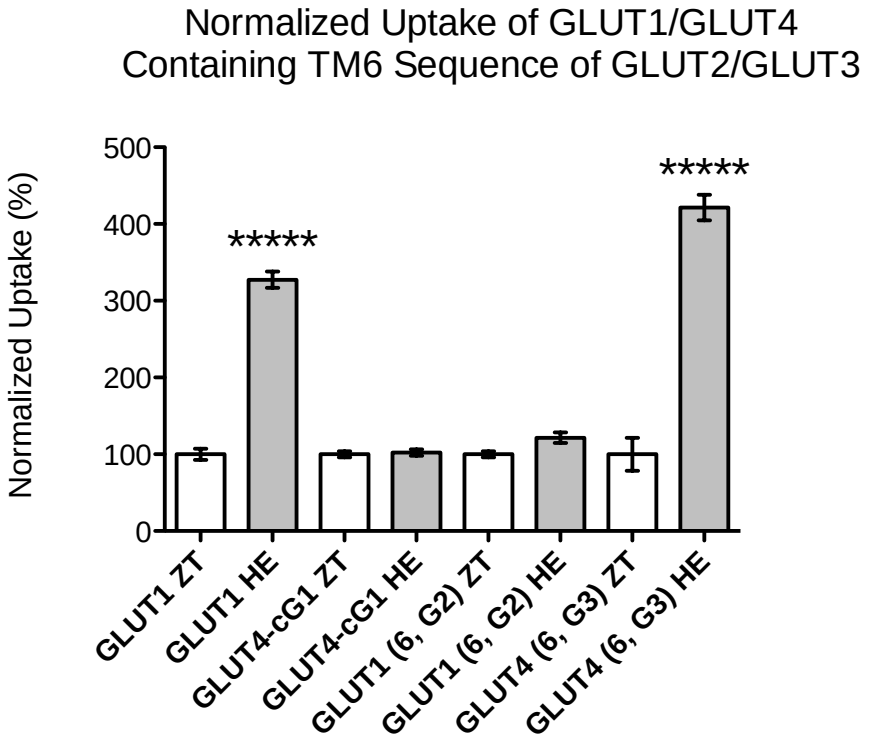

Figure 4.3 Comparison of transport by GLUTs 1 and 4 containing GLUTs 2-3 TM6 sequence substitutions

Normalized uptake of 100 μM 2-DG/40 mM 3-MG (*ordinate*) under zero-trans (ZT, 0 mM 3-MG_i; empty bars) or hetro-exchange (HE, 40 mM 3MG_i; shaded bars) conditions into HEK cells transfected with GLUT1myc, GLUT4myc containing the C-terminal 32 amino acids of GLUT1 (GLUT4-cG1), GLUT1myc containing the TM6 sequence of GLUT2 (GLUT1 (6, G2)), or GLUT4myc-cG1 containing the TM6 sequence of GLUT3 (GLUT4 (6, G3)) (*abscissa*). The value for normalized uptake was obtained by normalizing HE uptake to ZT for each transfected construct. Uptake was measured at 5 minutes at 37°C, and basal uptake by mock-transfected cells was subtracted from each data point. Data are plotted as mean ± SEM for four separate assays. An unpaired, 2-tailed Student's t-test yields the following P value: ***** $P \leq 0.00001$.

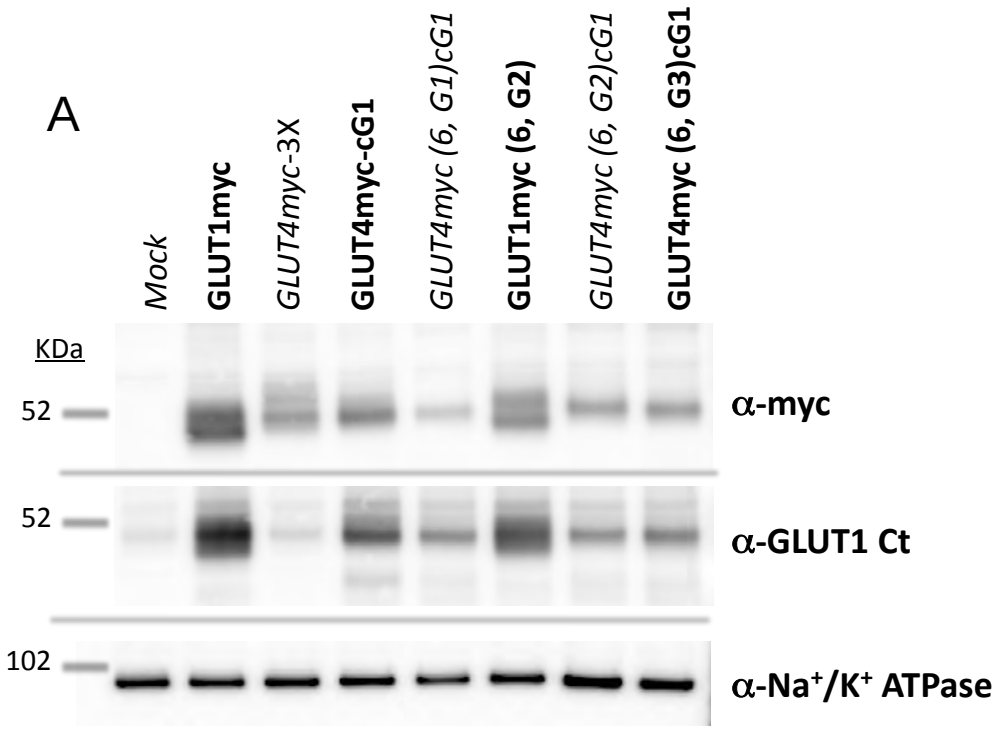
A
Mock
GLUT1myc
GLUT4myc-3X
GLUT4myc-cG1
GLUT4myc (6, G1)cG1
GLUT1myc (6, G2)
GLUT4myc (6, G2)cG1
GLUT4myc (6, G3)cG1
KDa
52
α-myc
52
α-GLUT1 Ct
102
α-Na+/K+ ATPase

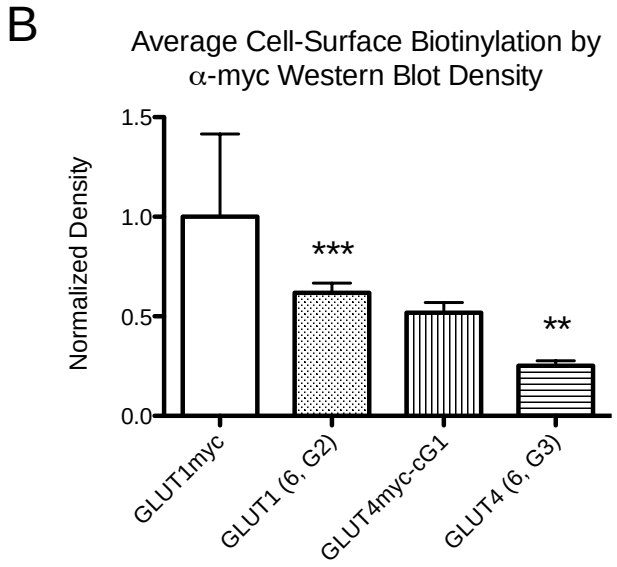
B
Average Cell-Surface Biotinylation by
α-myc Western Blot Density
Normalized Density
1.5
1.0
0.5
0.0
***
**
GLUT1myc
GLUT1 (6, G2)
GLUT4myc-cG1
GLUT4 (6, G3)

Figure 4.4 Cell-surface expression of GLUT1, GLUT4-cG1, and mutations to TM6

A, HEK cells were transfected with the construct indicated. Two days later, cell surface proteins were biotinylated, solubilized and affinity-purified on streptavidin beads. Transfected constructs were detected by α-myc and α-GLUT1 C-terminal antibodies. As a loading control, the α-subunit of the Na^+,K^+-ATPase was detected with α-Na^+,K^+-ATPase (α–subunit). The mobility of molecular weight standards is indicated. Transfected constructs that were investigated in additional experiments are shown in bold. *B*, Data obtained in the above experiment and two similar experiments were analyzed by densitometry, background corrected, normalized to loading controls, and averaged. The average density of α-myc bands normalized to GLUT1myc (*ordinate*) is plotted for the constructs of interest (*abscissa*). Data are plotted as mean ± SEM for three separate assays. The significance between the expression of each TM6 mutant relative to its scaffold was computed by an unpaired, 2-tailed Student's t-test yielding the following P values: ** $P \leq 0.01$; *** $P \leq 0.001$.

relative to GLUT1myc. While the GLUT1 C-terminal substitution in GLUT4myc was made to increase its expression, GLUT4myc-cG1 displayed only 52 ± 5% of GLUT1myc expression. The GLUT3 TM6 substitution in this GLUT4 scaffold showed even lower expression, at 25 ± 2% of GLUT1myc expression.

Using the relative surface expression to scale the zero-trans and hetero-exchange rates of transport (Table 4.1), we are able to uncover differences in the k_{cat} of transporters mutated in TM6. Upon examining differences in zero-trans rates of uptake (Figure 4.5A), we observe that the k_{cat} of GLUT1 (6, G2) shows a 2.3 ± 0.5-fold increase over that of wt GLUT1myc. In contrast, the k_{cat} of the gain-of-function mutant, GLUT4 (6, G3), is reduced 5.6 ± 3.1-fold from that of GLUT4myc-cG1. However, when the rates obtained from hetero-exchange uptake are scaled by the same relative surface expression values, no significant difference in k_{cat} is observed among the transporters (Figure 4.5B).

Analysis of GLUT1 domain 6 substitutions in GLUT2

Although our studies have not characterized the kinetics of transport by the other Class I GLUTs, we sought to examine whether TM6 is operant in the trans-acceleration profiles of GLUT2 and GLUT3. First, we had to establish whether we could observe the expected wild-type behavior of each transporter in the experimental system we established based on GLUTs 1 and 4. Due to concerns with the ability to express sufficient wtGLUT2 at the surface (289), we performed the same 32-amino acid exchange with GLUT1 C-terminal sequence that was used with GLUT4 above.

A

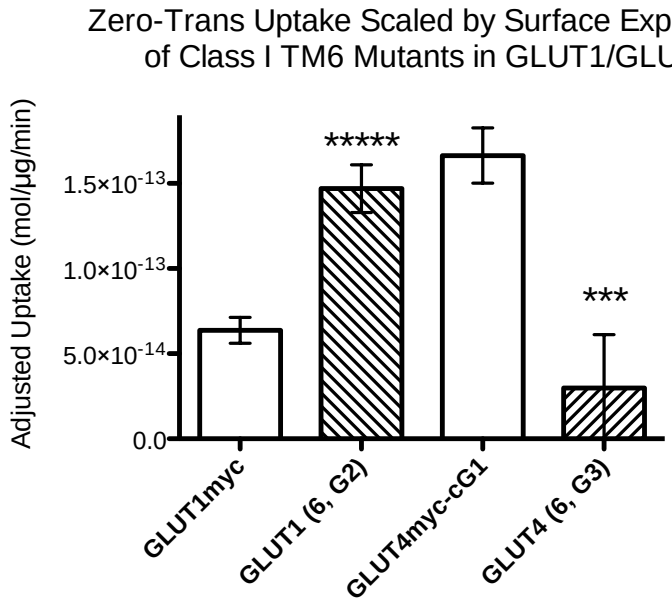
Zero-Trans Uptake Scaled by Surface Expression
of Class I TM6 Mutants in GLUT1/GLUT4
Adjusted Uptake (mol/µg/min)
1.5×10-13
1.0×10-13
5.0×10-14
0.0
*****
***
GLUT1myc
GLUT1 (6, G2)
GLUT4myc-cG1
GLUT4 (6, G3)

B

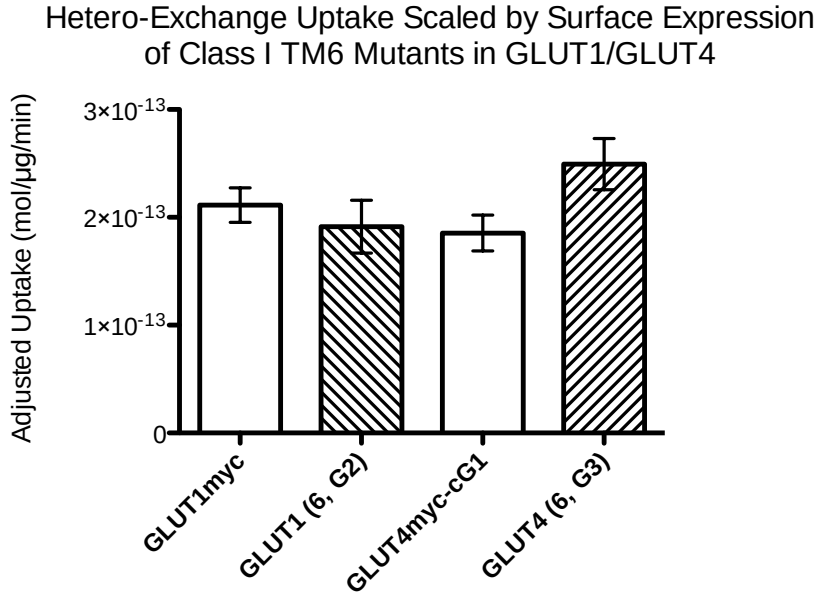
Hetero-Exchange Uptake Scaled by Surface Expression
of Class I TM6 Mutants in GLUT1/GLUT4
Adjusted Uptake (mol/µg/min)
3×10-13
2×10-13
1×10-13
0
GLUT1myc
GLUT1 (6, G2)
GLUT4myc-cG1
GLUT4 (6, G3)

Figure 4.5 Catalytic activity of cell surface GLUT1, GLUT4-cG1, and GLUTs 2-3 TM6 mutants

A, Adjusted zero-trans 100 μM 2DG/40 mM 3-MG uptake (*ordinate*) into HEK cells transfected with GLUT1myc, GLUT1 (6, G2), GLUT4myc-cG1 and GLUT4 (6, G3) (*abscissa*). *B*, Adjusted hetero-exchange uptake of 100 μM 2DG/40 mM 3-MG uptake (*ordinate*) into HEK cells transfected with GLUT1myc, GLUT1 (6, G2), GLUT4myc-cG1 and GLUT4 (6, G3) (*abscissa*). Adjusted rates were obtained by scaling the average zero-trans or hetero-exchange rate of each construct by its surface expression relative to GLUT1myc (Figure 4.4B). Data are plotted as mean ± SEM for n=3 assays. An unpaired, 2-tailed Student's t-test yields the following P values: *** $P \leq 0.001$; ***** $P \leq 0.00001$

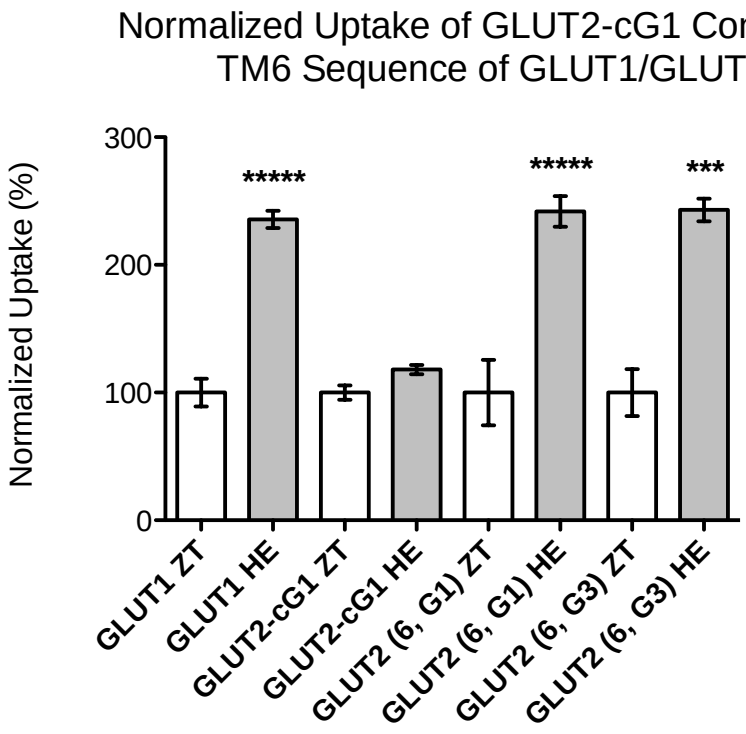

Figure 4.6 Comparison of transport by GLUT2-cG1 containing GLUT1 and GLUT3 TM6 sequence substitutions

Normalized uptake of 100 μM 2-DG/40 mM 3-MG (*ordinate*) under zero-trans (ZT, 0 mM 3-MG_i; empty bars) or hetro-exchange (HE, 40 mM 3-MG_i; shaded bars) conditions into HEK cells transfected with GLUT1myc, GLUT2myc containing the C-terminal 32 amino acids of GLUT1 (GLUT2-cG1), GLUT2-cG1 containing the TM6 sequence of GLUT1 (GLUT2 (6, G1)), or GLUT2-cG1 containing the TM6 sequence of GLUT3 (GLUT2 (6, G3)) (*abscissa*). The value for normalized uptake was obtained by normalizing HE uptake to ZT for each transfected construct. Uptake was measured at 5 minutes at 37°C, and basal uptake by mock-transfected cells was subtracted from each data point. Data are plotted as mean ± SEM for n=3 assays. An unpaired, 2-tailed Student's t-test yields the following P values: *** $P \leq 0.001$; ***** $P \leq 0.00001$.

When we tested GLUT2myc-cG1, as expected, we observed no trans-acceleration (Figure 4.6 and Table 4.1). Using the same chimeric strategies employed in earlier experiments, we substituted the TM6 sequence of GLUT1 $_{191}$SIIFI$_{195}$/$_{202}$CIV$_{204}$ or GLUT3 $_{189}$GFTIL$_{193}$/$_{199}$SAA$_{201}$ into GLUT2 sub-regions A and B sequence (GLUT2 $_{223}$GLSGV$_{227}$/$_{233}$SLL$_{235}$). Upon testing these chimeras, we observe that substitutions of TM6 sub-regions from both GLUT1 and GLUT3 cause a trans-acceleration gain-of-function in GLUT2myc-cG1 (Figure 4.6).

Analysis of trans-acceleration in GLUT3

In earlier studies aimed at elucidating regions of GLUT1 involved in trans-acceleration, we had tested two existing constructs in the laboratory containing substitutions of GLUT3 TMs 4-6 sequence in GLUT1 with an addition of the final C-terminal 13 amino acids of GLUT4 (1311+cG4), and complete GLUT3 sequence with an addition of the final C-terminal 13 amino acids of GLUT4, used as an epitope tag (GLUT3+cG4). Both of these constructs displayed trans-acceleration under standard HE versus ZT transport analysis (Figure 4.7 and Table 4.1). Based on the above results in GLUT2, we sought to test whether substitutions of GLUT2 and GLUT4 sequences into GLUT3 TM6 would result in a loss-of-function. However, when these constructs were engineered, they were based upon a new GLUT3 scaffold containing both the myc tag and a substitution of the C-terminal GLUT1 32 amino acids, for the sake of consistency with previous GLUT2- and GLUT4-based scaffolds. Unexpectedly, GLUT3myc-cG1

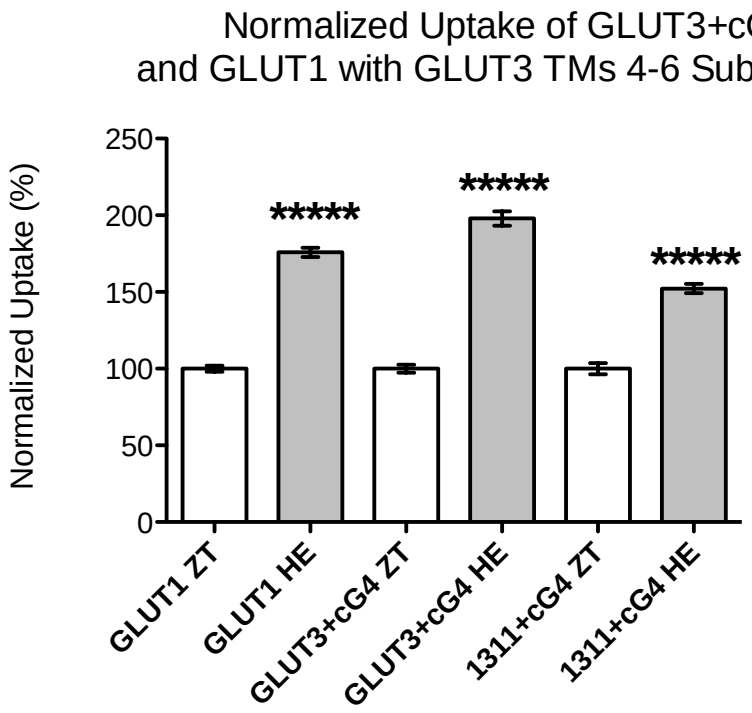

Figure 4.7 Comparison of transport by GLUT3+cG4 and GLUT1+cG4 containing GLUT3 TMs4-6 sequence substitution

Normalized uptake of 100 μM 2-DG/40 mM 3-MG (*ordinate*) under zero-trans (ZT, 0 mM 3-MG_i; empty bars) or hetro-exchange (HE, 40 mM 3-MG_i; shaded bars) conditions into HEK cells transfected with GLUT1myc, GLUT3 with the addition of the C-terminal 13 residues of GLUT4 (GLUT3+cG4), GLUT1myc containing the C-terminal addition of GLUT4 and TMs 4-6 sequence of GLUT3 (1311+cG4) (*abscissa*). The value for normalized uptake was obtained by normalizing HE uptake to ZT for each transfected construct. Uptake was measured at 5 minutes at 37°C, and basal uptake by mock-transfected cells was subtracted from each data point. Data are plotted as mean ± SEM for n=3 assays. An unpaired, 2-tailed Student's t-test yields the following P value: ***** $P \leq 0.00001$.

does not display trans-acceleration in the same conditions under which GLUT3+cG4 showed trans-acceleration (Figure 4.8A). We reasoned that the only major difference in these constructs was the C-terminal sequence, and that it would be best to proceed with a wt GLUT3 sequence in future experiments. However, the wt GLUT3myc construct still does not show trans-acceleration in our experimental system (Figure 4.8B). We tested this construct under normal assay conditions (5 min uptake) and also at a shorter time point (2 min). This implies that the experimental methods developed for measuring trans-acceleration in a GLUT1-based system are inadequate to measure the more rapid kinetics observed with GLUT3-mediated transport.

Discussion

Taken together, the similarities in Class I glucose transporter substrate specificity and differences in both affinities and sequence conservation raise several questions. First, although we have shown that TM6 sequence is critical for trans-acceleration in GLUTs 1 and 4, we have hypothesized that this is due to a modification in k_{cat} of the transporter during zero-trans sugar uptake. While this is supported by experimental data reporting values for k_{cat}/K_m , it assumes that modifications to TM6 do not affect the affinity of the transporter for substrate. Despite data from other studies reporting that residues within TM7 and nearby loops are involved in GLUT substrate specificity (199), (99), (100), clearly there exists a range of operational affinities for a single substrate among different

A

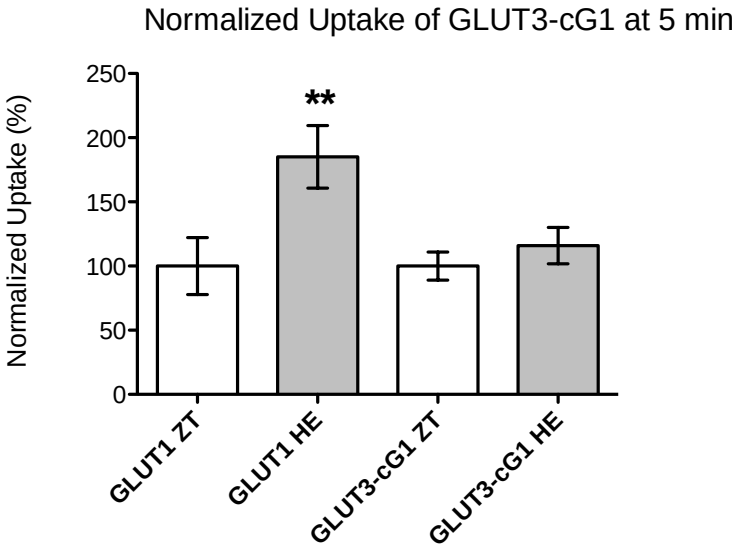
Normalized Uptake of GLUT3-cG1 at 5 min
Normalized Uptake (%)
250
200
150
100
50
0
**
GLUT1 ZT
GLUT1 HE
GLUT3-cG1 ZT
GLUT3-cG1 HE

B

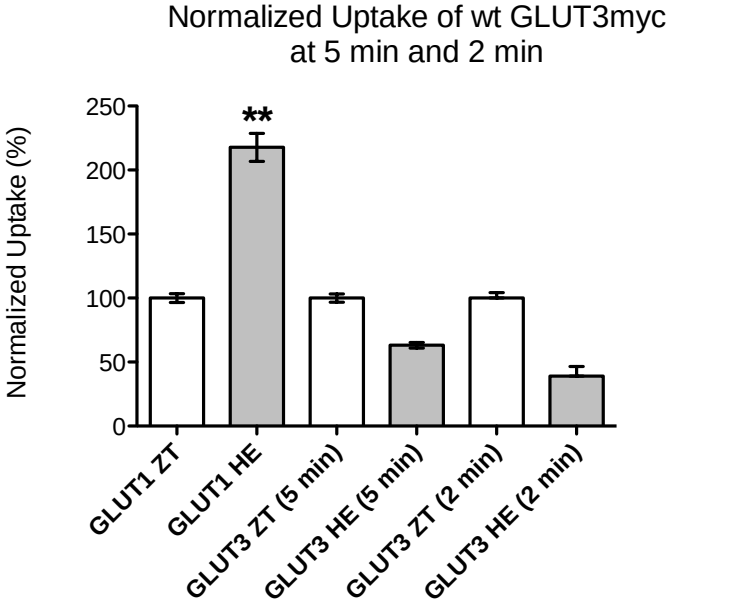
Normalized Uptake of wt GLUT3myc
at 5 min and 2 min
Normalized Uptake (%)
250
200
150
100
50
0
**
GLUT1 ZT
GLUT1 HE
GLUT3 ZT (5 min)
GLUT3 HE (5 min)
GLUT3 ZT (2 min)
GLUT3 HE (2 min)

Figure 4.8 Comparison of transport by GLUT3myc containing GLUT1 or wt C-terminal sequence

A, Normalized uptake of 100 mM 2-DG/40 mM 3-MG (*ordinate*) under zero-trans (ZT, 0 mM 3-MG_i; empty bars) or hetro-exchange (HE, 40 mM 3-MG_i; shaded bars) conditions into HEK cells transfected with GLUT1myc or GLUT3myc containing the C-terminal 32 amino acids of GLUT1 (GLUT3-cG1) (*abscissa*). Data are plotted as mean ± SEM for n=3 assays. An unpaired, 2-tailed Student's t-test yields the following P value: ** $P \leq 0.01$. *B*, Normalized uptake of 100 mM 2-DG/40 mM 3-MG (*ordinate*) under zero-trans (ZT, 0 mM 3-MG_i; empty bars) or hetro-exchange (HE, 40 mM 3-MG_i; shaded bars) conditions into HEK cells transfected with GLUT1myc or wt GLUT3myc (*abscissa*). Uptake was measured for the time indicated at 37°C, and basal uptake by mock-transfected cells was subtracted from each data point. The value for normalized uptake was obtained by normalizing HE uptake to ZT for each transfected construct.

transporters. In order to confirm that k_{cat} is changed by substitutions of TM6 sequence, it required investigation of whether the K_m remained unaffected by these changes.

Second, if the 8 disparate amino acids between GLUTs 1 and 4 represent the only major variation in TM6 sequence among the Class I GLUTs, can substitution of the sequences from GLUTs 2 and 3 cause associated trans-acceleration loss- and gain-of-function in GLUT1 and GLUT4, respectively? If so, is the same change in zero-trans k_{cat} observed for these substitutions? In addition, can the inverse substitutions of GLUTs 1 and 4 sequence into GLUTs 2 and 3 result in commensurate trans-acceleration gain- and loss-of-function?

In this study, we sought to further characterize mutations to TM6 within the Class I glucose transporters. First, we showed that the K_m for substrate (2-DG) of the GLUT1 TM6 mutant was similar to that of wt GLUT1. To complement these data, we confirmed that the $K_{i(app)}$ for inhibition of 2-DG uptake was also similar for the competing sugar (3-MG) used in our studies. Together, these results establish that the catalytic changes observed in previous studies (288) are indeed due to TM6-mediated alterations to k_{cat} of the transporter, and are not due to changes in carrier affinity for substrate.

However, analysis of the dose-response showed a greater V_{max} for wt GLUT1 than GLUT1 (6, G4), which is unexpected. Previous studies have indicated that the zero-trans V_{max} of GLUT1 (6, G4) is higher than wt GLUT1 (Table 3.1), which agrees with the faster zero-trans turnover observed with this mutant (Figure 3.8B). While it remains formally possible that the surface expression of GLUT1 (6, G4) was significantly lower

in the 2-DG dose-response experiment, the surface expression of this construct has been similar to that of wt GLUT1 in previous studies (Figure 3.8A). Thus the apparent differences in V_{max} could be further explored with additional experiments that test higher concentrations of substrate to ensure that the system saturates, and analysis of 3-MG uptake in order to obtain more accurate kinetic measurements.

We then extended this analysis of TM6 function in GLUT1 and GLUT4 trans-acceleration and k_{cat} properties by analyzing the substitution of TM6 sequence from the other two Class I GLUTs. A substitution of 8 residues from TM6 of GLUT2, which does not catalyze trans-acceleration, results in a loss-of-function in GLUT1. This is accompanied by an increase of the zero-trans k_{cat} in GLUT1 (6, G2). This same pattern is observed with the zero-trans k_{cat} changes in the GLUT4 TM6 mutant of GLUT1 (GLUT1 (6, G4); Figure 3.8B). However, a substitution of 8 amino acids from TM6 of GLUT3, which does catalyze trans-acceleration, results in a gain-of-function in GLUT4. With the GLUT4 (6, G3) mutant, we observe a similar decrease in k_{cat} to what we see with the GLUT1 TM6 mutant of GLUT4 (GLUT4 (6, G1); Figure 3.8B).

In our previous study, we explained the observed differences in zero-trans k_{cat} by hypothesizing that TM6 sequence is able to affect catalytic rate by slowing conformational changes (e.g. relaxation) in the empty carrier. This could be explained by TM6 interacting with residues in proximally arranged transmembrane domains, potentially TMs 1 and 3. The strength of interactions between TM6 and other TMs would be influenced by the sequence of these 8 amino acids within TM6, and inhibitory

sequence would slow the conformational change from e_1 to e_2. This would explain the basis for how trans-acceleration could occur. Binding of an intracellular sugar to e_1 could cause a structural rearrangement that would weaken the interaction(s) between TM6 and other TM(s), allowing e_1 to e_2 relaxation to progress at the same rate of translocation of substrate-bound e_2 to e_1, causing stimulation of uptake by intracellular sugar. If this were the case, one would expect the substitutions in TM6 sequence to be without effect on k_{cat} under hetero-exchange conditions, since intracellular sugar is present. This is indeed what we observe for all 4 mutations to TM6 in GLUT1 and GLUT4.

In seeking to extend the analysis of TM6 in trans-acceleration profiles of the other Class I transporters, we were able to show that substitution of the two sub-regions from GLUT1 or GLUT3 TM6 sequence into GLUT2 resulted in a trans-acceleration gain-of-function. This supports our hypothesis that TM6 plays a role in trans-acceleration outside of GLUTs 1 and 4. However, we did not test whether these modifications to GLUT2 TM6 sequence resulted in the same changes in k_{cat} pattern observed with the GLUT1 and GLUT4 TM6 mutants. Establishing whether the k_{cat} of GLUT2 is affected in the same way would further support a role for TM6 in carrier-associated conformational changes in the transport cycle.

In turn, further analysis of GLUT3 is required to determine whether TM6 plays a critical role in all Class I transporters. While we were not able to measure trans-acceleration in wt GLUT3 or GLUT3 containing the C-terminus of GLUT1, we did observe trans-acceleration by both full-length GLUT3 with the fusion of the 13 C-

terminal amino acids of GLUT4, and by GLUT1 containing the TMs 4-6 sequence of GLUT3. We hypothesize that the underlying problem may be one of catalytic rate versus ability to measure initial rates. Other studies have shown that GLUT3 has a higher turnover than any of the other Class I GLUTs, including GLUT1 (290). This is confirmed by our zero-trans uptake measurements; GLUT3 shows nearly a 2-fold faster rate of uptake than GLUT1 at 5 minutes. We reasoned that perhaps we were attempting to characterize kinetics at a time point beyond the window of initial rates. The trans-acceleration profile was unchanged at the faster time point of 2 minutes. However, the rate of basal uptake by GLUT3myc at 2 minutes (Table 4.1) was still ~1.7-fold faster than the average GLUT1myc-mediated rate of uptake at 5 minutes.

This supports our experimental observations that GLUT3-based kinetics appear to be more rapid and thus would require fine-tuning of experimental conditions. At the very least, time courses of 2-DG/3-MG uptake at 37°C and dose-responses would have to be performed in order to assess the best window for characterization of GLUT3-mediated trans-acceleration. The report which established GLUT3-mediated trans-acceleration in rat neurons (283) did so at a lower temperature, because transport was too rapid to measure accurately at 37°C. Although we employed an excess of 3-MG in our uptakes in order to slow uptake at 37°C through competitive inhibition, this may be insufficient for measurements of GLUT3-based transport.

Interestingly, the C-terminal substitutions in GLUT3 appeared to have an affect on the basal rate of zero-trans uptake at 5 minutes. While wt GLUT3myc showed nearly a

2-fold increase in V_{max} over GLUT1myc, we did not observe this increased rate in GLUT3-cG1, whose V_{max} was similar to that of wt GLUT1myc (Table 4.1). Indeed, we observed this lower V_{max} with GLUT3+cG4 as well. The C-termini of GLUTs 1-4 are highly variant in sequence and length (Figure 4.9); the C-terminus of GLUT3 is 6 residues longer than GLUT1. Our observations are supported by studies examining the effect of C-terminal sequence on the transport function of GLUT1. Deletion of the C-terminal 37 amino acids has shown that transport is ablated. With this deletion, the carrier is locked in the e_1 conformation, implying a role for the C-terminus in transport-associated conformational changes. (291). Truncations greater than the final 24 C-terminal residues (468-492) showed similar K_m but decreased V_{max} in GLUT1, as did point mutations at G466E and F467L. However, the point mutant R468L showed a lower K_m (107).

Additional studies have tested substitutions of other Class I GLUT C-terminal sequences. Analysis of GLUT1 containing the GLUT2 C-terminus showed a ~3.8-fold increase in K_m and a ~4.3-fold increase in V_{max} (289), which are more characteristic of GLUT2 than GLUT1 (292). Similarly, a chimera containing the C-terminus of GLUT4 in GLUT1 displayed both lower V_{max} and K_m under equilibrium exchange conditions, which are more characteristic of GLUT4-mediated transport (293). The inverse substitution (GLUT1 C-terminus in GLUT4) had the inverse effect; a 3- to 5-fold increase in K_m was observed (294). Both of these GLUT1/GLUT4 C-terminal chimeras showed increased turnover rates relative to the wild-type scaffold transporter (293). These results certainly

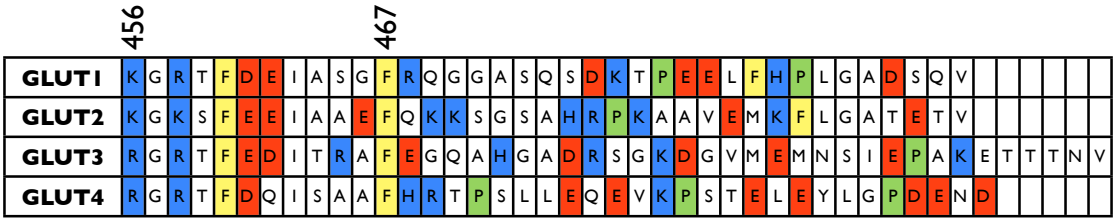

Figure 4.9 Alignment of C-terminal sequences of Class I GLUTs

The C-terminal sequence of GLUTs 1-4 is aligned, with the numbering corresponding to GLUT1 residues shown on top. The C-terminal sequence of GLUT3 is longer than the other Class I GLUTs. Residues which contain basic (blue) or acidic (red) side chains are colored accordingly. Phenylalanies (yellow) and prolines (green) are also indicated.

establish a role for the C-terminal sequence of GLUTs to affect both the turnover and affinity for substrate, which would in turn affect the ability to measure other kinetic parameters.

Previously, Dauterieve et al. showed that substituting the C-terminus of GLUT4 into the murine isoform of GLUT1 resulted in a loss of accelerated-exchange when the chimera was expressed in *Xenopus* oocytes (293). However, they did not observe a gain-of-function with the inverse substitution in mouse GLUT4. In direct contradiction of these results, we have shown that the C-terminus is not involved in trans-acceleration in human GLUTs 1, 2, and 4 ((288) and Figure 4.6). Although we were able to detect trans-acceleration in GLUT3+cG4, but not with GLUT3-cG1, we hypothesize that this difference is due to the experimental parameters not having been optimized for GLUT3. Regardless, until procedures are adjusted which allow detection of trans-acceleration in wt GLUT3, evaluating the GLUT3-based constructs containing TM6 substitutions of GLUTs 2 and 4 sequence is of limited value.

Despite the Class I mutagenesis resulting in trans-acceleration loss- and gain-of-function chimeras, no obvious ‘trans-acceleration motif’ is evident upon sequence comparison. While analysis of the Class I sequence conservation among mammals could provide some insight as to which residues of the disparate TM6 sequence could be the most critical in mediating trans-acceleration behavior, it is difficult to draw any conclusions without testing the trans-acceleration profile of each species variant. For example, the differences in ability to catalyze accelerated-exchange have been reported

for the rat isoform of GLUT2 and the rat and mouse isoforms of GLUT3 (208), (283), (182). Thus while we can deduce from our results that human GLUT2 also does not display trans-acceleration and sequence variation between rat and human GLUT2 is without effect, we cannot yet make the same claim for human GLUT3. Once more data in different species or heterologous expression systems is obtained, then perhaps such sequence comparisons can become more predictive rather than correlative. Although our understanding and characterization of trans-acceleration in the Class I glucose transporters remains incomplete, the results presented in this study expand the importance of TM6 in accelerated-exchange transport. The relation of specific GLUT sequence to distinct function is a key to identifying critical motifs in modes of substrate transport kinetics and conformational changes during the carrier cycle.

CHAPTER V

Conclusions and Future Directions

Despite over 50 years of kinetic characterization of the human basal glucose transporter GLUT1, the phenomenon of accelerated-exchange transport has remained unexplained. Possible explanations have included that the observation of trans-acceleration is an artifact of transport measurement methods, or that this behavior is contingent upon cell type and/or modulating cofactors. This thesis offers evidence that the ability to catalyze trans-acceleration is a sequence-based, intrinsic quality of glucose transporters.

In addition, the identification of GLUT1 TM6 as both necessary and sufficient for trans-acceleration provides insight into the mechanism of this kinetic phenomenon. We hypothesize that the sequence of TM6 affects trans-acceleration through interaction with other TM(s) within GLUT1 to alter the rate of relaxation of the carrier in the absence of intracellular sugar. When these potential interactions are strong, conformational relaxation of the empty carrier (e_1 to e_2) would be restrained, influencing the rate of zero-trans sugar entry. However, when intracellular sugar is bound, the conformation of $e.S_1$ might weaken these TM6-mediated interactions through rearrangement of the substrate-bound TMs. This would allow translocation to proceed at a faster rate than relaxation. Conversely, in transporters containing a TM6 sequence that does not display strong

interactions with other TMs, relaxation may proceed at an unimpeded rate equal to that of translocation. Thus intracellular sugar would have no effect on these interactions, and trans-acceleration would not be observed.

The TM6 region of the transporter is distinct from those domains implicated thus far in interactions with inhibitors, substrates, modulating factors, or other GLUT subunits. As a putative scaffolding domain coordinating the arrangement of the TMs forming the sugar translocation pore, TM6 is likely critical for conformational changes during the transport cycle. Studies examining the accessibility of TMs by proteolysis ((130), K. Lloyd and A. Carruthers, unpublished) and covalent modification (78) have shown that TM6 is one of the least exposed transmembrane segments of GLUT1, both in the presence and absence of substrate. This supports its hypothetical scaffolding role, as nearly all of TM6 appears to be buried in the membrane in more than one conformational state. This is in direct contrast to the other TMs which are thought to form the sugar translocation pore; TMs 1, 2, 4, 5, 7, and 8 are accessible to proteolytic cleavage by varying degrees. Transmembrane domains 1 and 8 readily dissociate from the membrane upon cleavage, while putative scaffolding domains 6, 3, 9, and 12 display no accessibility (with the exception of 1 site in TM3; (130)).

An extensive cysteine-scanning mutagenesis study of the residues within TM6 identifies several residues that appear to be crucial for proper transporter function (78). This is in contrast to the same analysis of putative scaffolding helix 12, where scanning Cys-mutagenesis produced no transport-deficient mutations (133). The cysteine

substitutions in TM6 that significantly perturbed or ablated transport function were those at positions Ile192, Pro196, Gln200, Gly201, Leu204, and Pro205. Interestingly, with the exception of Ile192, these residues are distinct from those we identified to be critical for trans-acceleration. Although the I192C mutation resulted in ~80% reduction of transport capability over the C-less GLUT1 scaffold transporter, mutation to another residue in the trans-acceleration region (S191C) caused a doubling of 2-DG uptake. It is interesting that single Cys mutations at each of these two sites appear to have a profound but opposite impact on transporter function, while our substitution of this entire sub-region (sub-region A: GLUT1 SIIFI 191-195) was insufficient to cause gain- or loss- of accelerated exchange (288). This is likely due to our use of conservative substitutions of actual TM6 sequence from other Class I transporters, as opposed to the strategy employed in the non-conservative Cys substitutions in a Cys-less transporter scaffold. This implies that the transport-deficient Cys-mutants tested by Makepeace and Mueckler have defective scaffolding interactions distinct from those we hypothesize to be important in trans-acceleration. All of the conservative substitutions we made in TM6 of the Class I GLUTs continued to transport sugar. This argues for interactions between residues of TM6 and those of other TMs to have different roles in stabilization, coordination, and conformational change of the carrier during the transport cycle.

In order to better understand the role of TM6 in such structural changes, it will be necessary to identify which TM(s) interact with different region(s) of TM6. Unfortunately, the current threaded model of GLUT1 on GlpT (116) did not report

pairings of TM6 residues with those of other proximally placed TMs, explicitly because no functional significance had been ascribed to the scaffolding TMs at the time the model was published. However, GLUT1 accelerated-exchange loss-of-function has been observed in GLUT1 mutants examined in other studies where TM6 has not been changed. When Liu et al. examined mutations to the nucleotide-binding motif in TM3, although this did not affect ATP interaction with GLUT1, the point mutant Gly111Ala failed to show trans-acceleration (235). While we have systematically ruled out a direct role for TM3 in trans-acceleration in GLUT1, this study implies the existence of critical contact(s) between TM6 and TM3. According to the current threaded model, TM3, along with TM1, are the domains located nearest to TM6 (116). We hypothesize that we did not observe changes in trans-acceleration capability with TM1 substitutions because of our strategy of exchanging GLUT1 and GLUT4 sequence. The conservation of TM1 sequence between GLUT1 and GLUT4 is high (81% across 31 amino acids). Thus, if critical contacts for TM6 exist within this domain, they were likely maintained in our chimeras and we were able to observe gain- and loss-of-function with only changes to TM6 sequence.

Although the sequence conservation between GLUT1 and GLUT4 is lower in TM3 (40% across 20 amino acids), it is possible that if critical contacts exist, they were either maintained in our chimeras by conserved residues, or that similar motifs (i.e. hydrophobic residues) are permitted in contact positions. According to the low-resolution TM arrangement model proposed by the extensive Cys-scanning mutagenesis of

Makepeace and Mueckler, TM5 may be positioned to make critical contacts with TM6 as well (134). Transmembrane domain 5 is also highly conserved between GLUT1 and GLUT4 (74% across 31 amino acids), so it is not surprising that our substitutions of TM5 sequence, alone or in combination with TM6 sequence, did not result in a change of accelerated exchange behavior in the scaffold protein.

One of the next steps toward expanding the role of TM6 in GLUT-mediated trans-acceleration would be to further characterize TM6 substitutions in GLUTs 2 and 3. While we have shown that GLUT1 or GLUT3 TM6 sequence causes a gain-of-function in a GLUT2 scaffold, we have not examined whether this elicits the same decrease in zero-trans k_{cat} we observed with the same sequence substitutions in GLUT4. While this could be examined experimentally in a similar manner, one caveat is the presence of the GLUT1 C-terminus in the GLUT2 chimera. While we have shown that the C-terminus has no direct role in trans-acceleration, several studies (293), (294), (289), (107), (291) conclude that changing C-terminal sequence can affect the affinity and turnover of the transporter. Unfortunately, modification to the C-terminus is one of the methods we began to utilize to increase surface expression of the chimeras.

One of the greatest challenges presented by these GLUT chimeras has been variation in surface expression and thus low levels of zero-trans sugar uptake, which complicates analysis of additional kinetic parameters. While some of the C-terminal substitutions aided expression, as in the case of GLUT2-cG1 and GLUT4-cG1 chimeras, we also observe that C-terminal GLUT1 substitutions have an effect on GLUT3- and

GLUT4-based turnover (Table 4.1). We have hypothesized that our inability to detect trans-acceleration in either wt GLUT3 or GLUT3-cG1 is due to a high turnover rate. This increase in turnover is inferred from the greater zero-trans V_{max} of uptake for both constructs, which we found was decreased in full-length GLUT3 fused with the C-terminus of GLUT4 (Table 4.1). In this construct, we are able to detect trans-acceleration.

When analyzing GLUT4-cG1, it is evident that the zero-trans k_{cat} (Figure 4.5) is ~3-fold greater than that of GLUT1. This is in contrast to the GLUT4 and GLUT4-3X constructs, which displayed a k_{cat} similar to GLUT1 (Figure 3.8). However, another study comparing C-terminal substitutions characterized GLUT1 as having a ~2-fold higher turnover than GLUT4, while a GLUT4-cG1 mutant was ~50% faster than GLUT1 (293). The disagreement in relative turnover between the studies may be due to differences in heterologous expression system (HEK cells versus *Xenopus* oocytes), substrate (2-DG versus 3-MG), or method for measuring surface expression (cell-surface biotinylation versus radiolabel incorporation and immunoprecipitation of membrane proteins). Such C-terminal substitutions add a layer of complexity in comparing turnover in the mutant transporters. Despite this, our analysis of changes in relative zero-trans k_{cat} shows the same pattern for TM6 substitutions, regardless of whether the chimera contains an altered C-terminus. However, future studies may aim to address improvement in chimera surface expression through some other means that is without effect on transporter turnover or affinity.

Because the accurate measurement of transporter at the plasma membrane is critical for determination of turnover, our studies would be strengthened by using an orthogonal approach for cell-surface quantitation. Several possibilities exist; while immunofluorescence (IF) microscopy proved to be merely qualitative (Appendix Figure A3.6), confocal microscopy may be able to provide better quantitative imaging. However, the same technical issues complicating traditional IF microscopy would likely extend to analysis by confocal microscopy.

The antibodies currently available for GLUT1 and GLUT4 utilize intracellular epitopes, requiring exofacial tags for antibody staining, which may increase the possibility of non-specific staining. Although the exclusive detection of surface-tagged proteins should be possible by avoiding detergent in treatment of the cells, fixation of cells by agents such as formaldehyde or methanol may result in some permeability. This increases the risk of signal from non-surface transporter present in vesicles or other intracellular compartments. In addition, these techniques are complicated by the relatively small size and high density of HEK cells, which grow in multiple adherent layers as they reach confluency. While seeding a lower population of cells yields better antibody staining and imaging, transfection efficiency declines precipitously when cells are below ~90% confluency. Thus the number of cells expressing transfected chimeras is very low (~10%) in cells at densities optimized for imaging, and does not accurately reflect the transfection efficiency or surface expression extant when transport determinations are made.

Another approach for transporter surface quantitation would be analysis by flow cytometry. While this technique has the same requirement for exofacially tagged proteins, the challenges of cell permeation and population density are overcome. Antibody staining can be performed on live cells without fixative, and confluent transfected cells may be dissociated from adherent layers by addition of non-proteolytic agents for single-cell analysis of a suspension. However, the effect of such treatment on long-term cell viability and transporter surface expression is not known. Another advantage of this technique is that calibration beads have been made with a determined number of IgG binding sites[1], which permit a direct correlation of fluorescence intensity and amount of bound secondary antibody. Thus a standard curve of bound antibody can be established and used to calculate number of cell-surface transporters. This may enable more quantitative rather than relative assessment of GLUT chimeras at the surface, which would either support or further refine our conclusions regarding TM6 sequence and changes in zero-trans turnover of the transporter.

Extension of this work to further investigate TM6 sequence in carrier turnover and interactions with other TMs would provide more information to evaluate the current models for transport, all of which are consistent with trans-acceleration. However, once we determined that substitutions in TM6 did not affect affinity for sugar uptake (Chapter IV), we were able to constrain parameters in a mathematical simulation of the transport cycle based on the simple carrier. In the case of trans-acceleration, this would extend to

---

[1] http://www.bangslabs.com/sites/default/files/bangs/docs/pdf/PDS%20814%20Web.pdf

the modified-fixed site carrier as well, as both models offer the same basis for an explanation of accelerated-exchange. We did not simulate fixed-site carrier-based geminate exchange because this would require, at minimum, additional measurements of substrate exit to approximate the affinity of the second binding site. These we could not perform with 2-DG, and we have not analyzed TM6 mutant transport of 3-MG alone. However, we are able to gain insights into the transport cycle based on evaluating predictions of the simple carrier.

Model Predictions and Implications

In using this mathematical model based on the simple carrier (Figure 5.1 and Table 5.1) to examine the transport cycle, arbitrary values were used as inputs, as some of these parameters cannot be measured or were not undertaken in the present study. This allows examination of the relationships between variables affecting different steps in the cycle. However, this model is constrained to reflect our experimentally observed affinity for zero-trans uptake of 2-DG ($K_{zt}^{21} \approx 0.5$-1 mM) and the consistently observed magnitude for trans-acceleration under exchange conditions (~1.8- to 2.5-fold).

In order to examine a scenario describing a transporter with characteristics like GLUT4, parameters must be adjusted to reflect the absence of trans-acceleration and the presence of symmetric transport (Table 5.2). This is accomplished by setting relaxation rates equal to translocation rates ($R_{oo} = R_{12} = R_{21} = R_{ee}$), and by requiring that uptake and efflux capacities are equal ($R_{21} = R_{12}$). When we set these parameters, we observe that the

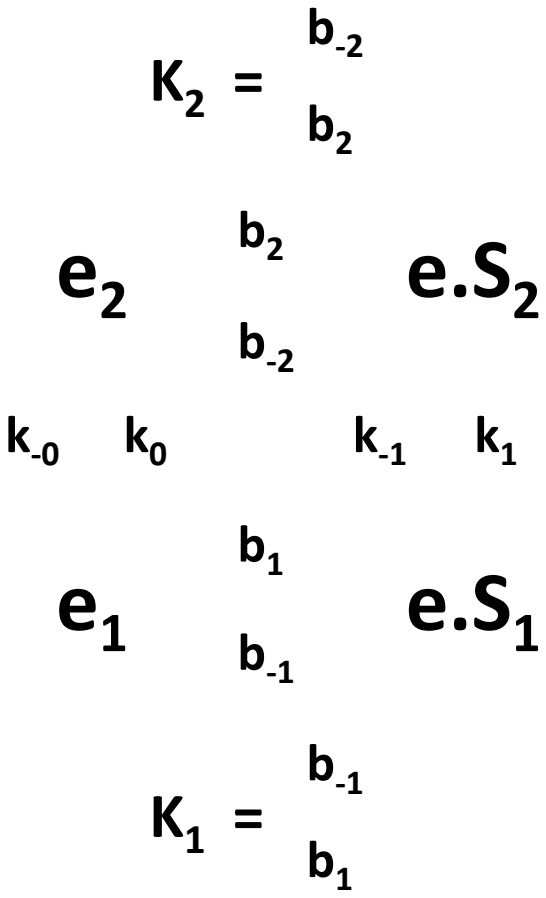

Figure 5.1 King-Altman diagram of the simple carrier transport cycle

The empty carrier in the exofacial conformation (e_2) becomes complexed with substrate S ($e.S_2$) in a way described by a dissociation constant (K_2) determined as the ratio of the rate of dissociation of a substrate from the eS_2 complex (b_{-2}) divided by the second order rate constant for S_2 and e_2 association (b_2). Once interstitial substrate is bound, translocation of substrate occurs and is described by the conformational change of $e.S_2$ to $e.S_1$. This is a reversible conformational change – the forward or reverse reactions are described by the first order rate constants (k_1 or k_{-1}, respectively). Substrate dissociation from $e.S_1$ into the cytoplasm yields the empty endofacial carrier (e_1), and is described by the dissociation constant K_1, which is the ratio of the rate of dissociation of substrate from the $e.S_1$ complex (b_{-1}) divided by the second order rate constant for substrate-e_1 association (b_1). In order for the carrier to import another extracellular substrate, e_1 must relax back to the e_2 state in a reaction described by the first-order rate constant, k_0. Relaxation is also reversible; e_2 can relax to the e_1 state via the rate constant, k_{-0}.

Table 5.1 Definition of Model Constants and Formulas

Parameter	Definition	Formula
R_{21}	Translocation during uptake (e.S_2 to e.S_1)	$\frac{k_0 + k_{-1}}{(k_0 \bullet k_{-1})}$
R_{12}	Translocation during efflux (e.S_1 to e.S_2)	$\frac{k_{-0} + k_1}{(k_{-0} \bullet k_1)}$
R_{ee}	Relaxation (e_2 to e_1)	$\frac{k_1 + k_{-1}}{(k_1 \bullet k_{-1})}$
R_{oo}	Relaxation (e_1 to e_2)	$\frac{k_0 + k_{-0}}{(k_0 \bullet k_{-0})}$
K	Michaelis constant	$K_1 \bullet \frac{k_0}{k_1}$
K_{zt}^{21}	Zero-trans uptake constant	$K \bullet \frac{R_{oo}}{R_{21}}$
K_{zt}^{12}	Zero-trans efflux constant	$K \bullet \frac{R_{oo}}{R_{12}}$
K_{ee}	Carrier isomerization constant	$K \bullet \frac{R_{oo}}{R_{ee}}$

If transport is symmetrical (GLUT4), $R_{21}=R_{12}$. If transport is asymmetrical (GLUT1), $R_{12}<R_{21}$.
If trans-acceleration occurs, $R_{oo}>R_{21}$ and $R_{21}>R_{12}>R_{ee}$.
In the absence of trans-acceleration, k_0, $k_{-0} > k_0$, k_{-0} when trans-acceleration is not observed.
Velocity constants are computed as

$\frac{1}{R}$; e.g . $V_{ZT}^{21} = \frac{1}{R_{21}}$

For a passive transporter, the relationship

$$\frac{V_{zt}^{21}}{K_{zt}^{21}} = \frac{V_{zt}^{12}}{K_{zt}^{12}} = \frac{V_{ee}}{K_{ee}}$$

must be satisfied because

$$R_{12} + R_{21} = R_{oo} + R_{ee}$$

The relative magnitude of the relaxation rates (k_0 and k_{-0}) are constrained through the following relationships:

$$b_{-1}k_{-1} > \frac{1}{R_{ee}}, \frac{1}{R_{21}}$$

$$b_{-2}k_{1} > \frac{1}{R_{ee}}, \frac{1}{R_{12}}$$

$$k_{0} > \frac{1}{R_{21}}, \frac{1}{R_{oo}}$$

$$k_{-0} > \frac{1}{R_{12}}, \frac{1}{R_{oo}}$$

$$k_{0} < \frac{1}{(R_{21} - R_{ee})}$$

$$k_{-0} < \frac{1}{(R_{12} - R_{ee})}$$

$$\frac{1}{R_{21}}, \frac{1}{R_{oo}} < k_{0} < \frac{1}{(R_{21} - R_{ee})}$$

Table 5.2 Parameters Illustrating a System without Trans-Acceleration or Asymmetry

Parameter	**Value**	**Parameter**	**Value**
k_0	20 min^{-1}	K_{zt}^{21}	0.67 mM
k_{-0}	20 min^{-1}	K_{zt}^{12}	0.67 mM
k_1	20 min^{-1}	K_{ee}	0.67 mM
k_{-1}	20 min^{-1}	V_{zt}^{21}	10 mM $L^{-1}min^{-1}$
b_1	30 $mM^{-1}min^{-1}$	V_{zt}^{12}	10 mM $L^{-1}min^{-1}$
b_{-1}	20 min^{-1}	V_{ee}	10 mM $L^{-1}min^{-1}$
b_2	30 $mM^{-1}min^{-1}$	**R_{21}**	**0.1 min $mM^{-1}L^{-1}$**
b_{-2}	20 min^{-1}	**R_{12}**	**0.1 min $mM^{-1}L^{-1}$**
K_1	**0.67 mM**	**R_{ee}**	**0.1 min $mM^{-1}L^{-1}$**
K_2	**0.67 mM**	**R_{oo}**	**0.1 min $mM^{-1}L^{-1}$**
Y	20	K	0.67 mM

Where Y is a constant of equality relating translocation, relaxation and binding rates defined as:

(Equation 5.1)

$$Y = \frac{k_{-1} b_{-1} k_0}{k_1 b_{-0}}$$

Rearrangement of the terms solves for the rate of relaxation (k_{-0}) as dependent on Y and the ratio of substrate binding rates inside and outside the cell:

(Equation 5.2)

$$b_2 k_{-1} b_{-1} k_0 = b_{-2} k_{-0} b_1 k_1$$
$$\rightarrow \frac{k_{-1} b_{-1} k_0}{b_{-2} k_1} = y = \frac{k_{-0} b_1}{b_2}$$
$$\therefore y b_2 = k_{-0} b_1$$
$$y \frac{b_2}{b_1} = k_{-0}$$

intracellular and extracellular dissociation constants (K_2 and K_1) must be equal in order for the rate constant for relaxation (k_{-0}) to be equal to the rates of the other transitions (k_0, k_1, k_{-1}). Even though the rates of substrate binding (b_1 and b_2) may be slower than the rates of dissociation (b_{-1} and b_{-2}), their ratios must remain the same in order to model a system without trans-acceleration or asymmetry.

In contrast, GLUT1 displays both trans-acceleration and asymmetry. In this scenario (Table 5.3), trans-acceleration is reflected as a slower rate of relaxation ($1/R_{oo}$) than either uptake or exit ($1/R_{21}$, $1/R_{12}$). In this case, we have modeled a 2.5-fold stimulation of uptake under exchange conditions versus zero-trans conditions ($V_{ee} = 2.5\ V_{zt}^{21}$), which is within the range of trans-acceleration we have observed experimentally. To accomplish trans-acceleration and asymmetry ($V_{zt}^{21} < V_{zt}^{12} < V_{ee}$), it is required that $R_{ee} < R_{12} < R_{21} < R_{oo}$ and $k_{-0} < k_0$, and K_1 must be greater than the extracellular binding constant, K_2. If the dissociation of bound substrate from $e.S_2$ and $e.S_1$ occurs at the same rate, this requires that the rate of substrate binding to e_1 is slower than binding to e_2 ($b_1 < b_2$). If the rate of substrate binding is equal at both surfaces, then the rate of dissociation must be faster on the inside ($b_{-1} > b_{-2}$). Adjusting the intracellular substrate dissociation constant K_1 to be two times greater than K_2 is the only way that forces the rate of relaxation to be slower, as defined in Equation 5.2.

The main conclusion of this model is the unexpected finding that the rates of binding and relaxation appear to be inter-dependent. When relaxation and translocation rates are equal, the asymmetry of binding is lost. This is particularly interesting in the

Table 5.3 Parameters Illustrating a System with Trans-Acceleration and Asymmetry

Parameter	**Value**	**Parameter**	**Value**
k_0	5 min^{-1}	K_{zt}^{21}	0.67 mM
k_{-0}	10 min^{-1}	K_{zt}^{12}	1 mM
k_1	20 min^{-1}	K_{ee}	1.5 mM
k_{-1}	20 min^{-1}	V_{zt}^{21}	4 mM $L^{-1}min^{-1}$
b_1	30 $mM^{-1}min^{-1}$	V_{zt}^{12}	6.67 mM $L^{-1}min^{-1}$
b_{-1}	60 min^{-1}	V_{ee}	10 mM $L^{-1}min^{-1}$
b_2	20 $mM^{-1}min^{-1}$	**R_{21}**	**0.25 min $mM^{-1}L^{-1}$**
b_{-2}	20 min^{-1}	**R_{12}**	**0.15 min $mM^{-1}L^{-1}$**
K_1	**2 mM**	**R_{ee}**	**0.1 min $mM^{-1}L^{-1}$**
K_2	**1 mM**	**R_{oo}**	**0.3 min $mM^{-1}L^{-1}$**
Y	15	K	0.5 mM

context of the role we have defined for TM6 in trans-acceleration. While we have presented our hypothesis that TM6 affects the relaxation rate of the empty carrier through interactions with other proximal transmembrane domains, TM6 must also affect substrate binding, presumably by altering the rate at which e_1 and e_2 become available for substrate. Although TM6 is a putative scaffolding domain and unlikely to bind substrate directly, the interactions of TM6 with other TMs may impact the exposed regions of the TMs forming the sugar translocation pore. This would in turn influence rates of substrate binding or dissociation, and could explain why changes to TM6 sequence that equalize isomerization rates of the inward- and outward-facing unliganded carrier also allow equal substrate binding rates on both sides of the membrane. In contrast, if transporters displaying trans-acceleration are more structurally constrained by the sequence of TM6, this would slow both relaxation of the empty carrier and affect the availability of substrate binding sites. According to our model, both of these conditions must occur in accelerated-exchange transport.

In order to test this hypothesis definitively, it will be necessary to obtain additional experimental transport measurements, particularly those for exit (R_{12}) and a comparison of the affinity constants under zero-trans (K_{zt}^{12} and K_{zt}^{21}) and exchange conditions (K_{ee}). This requires use of a sugar analog other than 2-DG, which is metabolically trapped inside the cell and thus precludes measurement of exit or exchange parameters. Ideally, 3-MG would be used to further test the predictions of this model in a system expressing GLUT1, GLUT4, and the TM6 substitution chimeras of each. These

experiments may prove more technically challenging, as transport of 3-MG is extremely rapid. Reliable measurements of initial transport rates must be performed at ice temperature, and may require cells with a larger equilibration volume than HEKs. In addition, variable surface expression of these chimeras would also complicate detailed kinetic analysis. This argues for the development of stably transfected cell lines for each construct, which would then require careful establishment of parameters for comparing 3-MG transport kinetics, such as time courses and dose-responses.

Many studies have focused on mutations of GLUT transmembrane domains in the sugar translocation pathway to examine their potential roles in substrate interaction, affinity and specificity. In contrast, the work present in this thesis examines a novel role for a scaffolding domain in affecting intrinsic rates of the transport cycle. Although the 8 TMs of the sugar translocation pore are coordinated by 4 scaffolding TMs, none of these scaffolding TMs has been previously assigned a role in transporter function. The importance of scaffolding domain sequence in modulating GLUT characteristics is supported by work from this laboratory showing that the scaffolding TM9 is critical for oligomerization of the transporter (Levine et al., in preparation). These studies clearly show that the range of operational activity among the GLUTs is determined by distinct regions of the protein, implying that different kinetic qualities of a transporter can be tuned separately from others.

Although the elucidation of such structure-function relationships is interesting to the characterization of glucose transporters, there are broader implications for the study

of other transport proteins as well. For example, the monocarboxylate transporters (MCTs) are critical for the symport of lactate and H+ in a multitude of tissues (4). While not all of the MCTs have been well-characterized, both MCT1 and MCT4 have shown trans-acceleration on the same orders of magnitude presented in this work (1.5- to 2.5-fold stimulation; (43), (295)). The accelerated-exchange observed by MCTs 1 and 4 can be stimulated by either substrate, lactate or H+. This is thought to occur through allosteric modulation of the affinity in the second catalytic site upon binding of the first substrate. While we do not argue a substrate-based allosteric modulation of binding site affinity in our above model, it is interesting that the current model for MCT accelerated-exchange also explains this phenomenon by both an impeded relaxation of the empty carrier and a change in substrate binding (4).

Although MCTs are also members of the Major Facilitator Superfamily of transporters, their sequence homology to other members is also quite divergent (i.e. MCT shows 10-15% sequence identity with GlpT and LacY). However, the same argument for assumption of similar transmembrane domain arrangement and topology in the MFS-based GLUT modeling studies can be extended to MCTs as well. In fact, like GLUTs 1 and 3, a putative structure for MCT1 has also been proposed by homology modeling on the GlpT crystal structure (296). Transmembrane domain 6, along with TM3, is also a putative scaffolding domain in MCT1 (297). These two scaffolding domains have been hypothesized to interact with the MCT1-associated cofactor basigin (CD147; (297)). Basigin acts as a chaperone to assist MCT1 localization to the plasma

membrane (298), but its continued interaction with MCT1 and MCT4 is also important for transport activity (299). It is tempting to speculate that this cofactor may affect MCT conformational changes by coordinating scaffolding domains of the transporter.

It would be interesting to determine which of the other MCTs display accelerated exchange transport, in addition to completing this analysis in the Class II and III GLUTs. While TM6 may not be operant in trans-acceleration among all these transporter isoforms, it is possible that a symmetric or homologous scaffolding domain is critical for this behavior. Further sequence comparisons among transporters that catalyze trans-acceleration may add to the understanding of interactions between TMs and their impact on the carrier transport cycle. Furthermore, extending this analysis to include comparing endogenous expression patterns of trans-accelerating carriers may yield additional insights. For example, MCTs also exhibit tissue-specific distribution. While both MCT1 and MCT4 display accelerated-exchange, MCT1, like GLUT1, is a basally expressed transporter with high levels detected in erythrocytes and oxidative muscle cells. MCT4, however, is expressed mostly in glycolytic cells of the heart and muscle (300). While not enough information is currently available, the continued characterization of differences in transporter kinetics and distribution will provide insight into the adaptive advantages of the distinct expression of transporter isoforms. While the variety of transporter substrate specificity, affinity, and catalytic efficiency are critical to the global homeostasis of metabolites, capacity for accelerated-exchange transport may be as well.

The physiological significance of trans-acceleration could be analyzed further through genetic manipulation of a model organism. For example, the loss-of-function GLUT1 (6, G4) mutant transporter could be expressed in transgenic mice, particularly in tissues where rapid equilibration is hypothesized to be critical (e.g. muscle cells, or endothelial barriers in the brain, retina, placenta, or lactating mammary gland). Possible phenotypes would include decreased function at these sites, such as impaired muscle contraction or endurance, seizures, loss of consciousness, impaired vision, retardation of fetal growth, or decreased milk production. Such *in vivo* studies would only serve to underscore both the importance of rapid equilibration in global glucose homeostasis, and the related expression and function of transporters which catalyze trans-acceleration.

BIBLIOGRAPHY

1. Marger, M. D. & Saier Jr, M. H. A major superfamily of transmembrane facilitators that catalyse uniport, symport and antiport. *Trends Biochem Sci* **18**, 13-20 (1993).
2. Pao, S. S., Paulsen, I. T. & Saier, M. H., Jr. Major facilitator superfamily. *Microbiol Mol Biol Rev* **62**, 1-34 (1998).
3. Henderson, P. J. & Maiden, M. C. Homologous sugar transport proteins in Escherichia coli and their relatives in both prokaryotes and eukaryotes. Review. *Philos Trans R Soc Lond B Biol Sci* **326**, 391-410 (1990).
4. Halestrap, A. P. & Price, N. T. The proton-linked monocarboxylate transporter (MCT) family: structure, function and regulation. *Biochem J* **343**, 281-299 (1999).
5. Wright, E. M. & Turk, E. The sodium/glucose cotransport family SLC5. *Pflugers Arch* **447**, 510-518 (2004).
6. Baldwin, S. A. Mammalian passive glucose transporters: members of an ubiquitous family of active and passive transport proteins. Review. *Biochim Biophys Acta* **1154**, 17-49 (1993).
7. Joost, H. G., Bell, G. I., Best, J. D., Birnbaum, M. J., Charron, M. J., Chen, Y. T., Doege, H., James, D. E., Lodish, H. F., Moley, K. H., Moley, J. F., Mueckler, M., Rogers, S., Schürmann, A., Seino, S. & Thorens, B. Nomenclature of the GLUT/ SLC2A family of sugar/polyol transport facilitators. *Am J Physiol Endocrinol Metab* **282**, E974-6 (2002).
8. Kasahara, M. & Hinkle, P. C. Reconstitution and purification of the D-glucose transporter from human erythrocytes. *J Biol Chem* **252**, 7384-7390 (1977).
9. Zoccoli, M. A., Baldwin, S. A. & Lienhard, G. E. The monosaccharide transport system of the human erythrocyte. Solubilization and characterization on the basis of cytochalasin B binding. *J Biol Chem* **253**, 6923-6930 (1978).
10. Zhao, F. Q. & Keating, A. F. Functional properties and genomics of glucose transporters. *Curr Genomics* **8**, 113-128 (2007).
11. Mueckler, M., Caruso, C., Baldwin, S. A., Panico, M., Blench, I., Morris, H. R., Allard, W. J., Lienhard, G. E. & Lodish, H. F. Sequence and structure of a human glucose transporter. *Science* **229**, 941-945 (1985).
12. Gorga, F. R. & Lienhard, G. E. Changes in the intrinsic fluorescence of the human erythrocyte monosaccharide transporter upon ligand binding. *Biochemistry* **21**, 1905-1908 (1982).
13. Pardridge, W. M., Boado, R. J. & Farrell, C. R. Brain-type glucose transporter (GLUT-1) is selectively localized to the blood-brain barrier. Studies with quantitative western blotting and in situ hybridization. *J Biol Chem* **265**, 18035-18040 (1990).

14. Takata, K., Kasahara, T., Kasahara, M., Ezaki, O. & Hirano, H. Localization of erythrocyte/HepG2-type glucose transporter (GLUT1) in human placental villi. *Cell Tissue Res* **267**, 407-412 (1992).
15. Vannucci, S. J., Reinhart, R., Maher, F., Bondy, C. A., Lee, W. H., Vannucci, R. C. & Simpson, I. A. Alterations in GLUT1 and GLUT3 glucose transporter gene expression following unilateral hypoxia-ischemia in the immature rat brain. *Brain Res Dev Brain Res* **107**, 255-264 (1998).
16. Thorens, B., Sarkar, H. K., Kaback, H. R. & Lodish, H. F. Cloning and functional expression in bacteria of a novel glucose transporter present in liver, intestine, kidney, and pancreatic islet cells. *Cell* **55**, 281-290 (1988).
17. Ibberson, M., Uldry, M. & Thorens, B. GLUTX1 (GLUT8), a Novel Mammalian Glucose Transporter Expressed in the Central Nervous System and Insulin-sensitive Tissues. *J Biol Chem* **275**, 4607-4612 (2000).
18. Burcelin, R. & Thorens, B. Evidence that extrapancreatic GLUT2-dependent glucose sensors control glucagon secretion. *Diabetes* **50**, 1282-1289 (2001).
19. Bady, I., Marty, N., Dallaporta, M., Emery, M., Gyger, J., Tarussio, D., Foretz, M. & Thorens, B. Evidence from glut2-null mice that glucose is a critical physiological regulator of feeding. *Diabetes* **55**, 988-995 (2006).
20. Kayano, T., Fukumoto, H., Eddy, R. L., Fan, Y. S., Byers, M. G., Shows, T.B. & Bell, G. I. Evidence for a family of human glucose transporter-like proteins. *J Biol Chem* **263**, 15245-15248 (1988).
21. Maher, F. & Simpson, I. A. The GLUT3 glucose transporter is the predominant isoform in primary cultured neurons: assessment by biosynthetic and photoaffinity labelling. *Biochem J* **301**, 379-384 (1994).
22. Wu, X. & Freeze, H. H. GLUT14, a duplicon of GLUT3, is specifically expressed in testis as alternative splice forms. *Genomics* **80**, 553-557 (2002).
23. Fukumoto, H., Kayano, T., Buse, J. B., Edwards, Y., Pilch, P. F., Bell, G.I. & Seino, S. Cloning and characterization of the major insulin-responsive glucose transporter expressed in human skeletal muscle and other insulin-responsive tissues. *J Biol Chem* **264**, 7776-7779 (1989).
24. Rumsey, S. C., Kwon, O., Xu, G. W., Burant, C. F., Simpson, I. & Levine, M. Glucose transporter isoforms GLUT1 and GLUT3 transport dehydroascorbic acid. *J Biol Chem* **272**, 18982-18989 (1997).
25. Vera, J. C., Rivas, C. I., Velásquez, F. V., Zhang, R. H., Concha, I. I. & Golde, D. W. Resolution of the facilitated transport of dehydroascorbic acid from its intracellular accumulation as ascorbic acid. *J Biol Chem* **270**, 23706-23712 (1995).
26. Rivas, C. I., Zúñiga, F. A., Salas-Burgos, A., Mardones, L., Ormazabal, V. & Vera, J. C. Vitamin C transporters. *J Physiol Biochem* **64**, 357-375 (2008).

27. Lachaal, M., Rampal, A. L., Ryu, J., Lee, W., Hah, J. & Jung, C. Y. Characterization and partial purification of liver glucose transporter GLUT2. *Biochim Biophys Acta* **1466**, 379-389 (2000).
28. Basketter, D. A. & Widdas, W. F. Asymmetry of the hexose transfer system in human erythrocytes. Comparison of the effects of cytochalasin B, phloretin and maltose as competitive inhibitors. *J Physiol* **278**, 389-401 (1978).
29. Baker, G. F., Basketter, D. A. & Widdas, W. F. Asymmetry of the hexose transfer system in human erythrocytes. Experiments with non-transportable inhibitors. *J Physiol* **278**, 377-388 (1978).
30. Burant, C. F., Takeda, J., Brot-Laroche, E., Bell, G. I. & Davidson, N. O. Fructose transporter in human spermatozoa and small intestine is GLUT5. *J Biol Chem* **267**, 14523-14526 (1992).
31. Rand, E. B., Depaoli, A. M., Davidson, N. O., Bell, G. I. & Burant, C. F. Sequence, tissue distribution, and functional characterization of the rat fructose transporter GLUT5. *Am J Physiol* **264**, G1169-1176 (1993).
32. Li, Q., Manolescu, A., Ritzel, M., Yao, S., Slugoski, M., Young, J. D., Chen, X. Z. & Cheeseman, C. I. Cloning and functional characterization of the human GLUT7 isoform SLC2A7 from the small intestine. *Am J Physiol Gastrointest Liver Physiol* **287**, G236-42 (2004).
33. Cheeseman, C. GLUT7: a new intestinal facilitated hexose transporter. *Am J Physiol Endocrinol Metab* **295**, E238-41 (2008).
34. Phay, J. E., Hussain, H. B. & Moley, J. F. Cloning and expression analysis of a novel member of the facilitative glucose transporter family, SLC2A9 (GLUT9). *Genomics* **66**, 217-220 (2000).
35. Doege, H., Bocianski, A., Scheepers, A., Axer, H., Eckel, J., Joost, H. G. & Schürmann, A. Characterization of human glucose transporter (GLUT) 11 (encoded by SLC2A11), a novel sugar-transport facilitator specifically expressed in heart and skeletal muscle. *Biochem J* **359**, 443-49 (2001).
36. Keembiyehetty, C., Augustin, R., Carayannopoulos, M. O., Steer, S., Manolescu, A., Cheeseman, C. I. & Moley, K. H. Mouse glucose transporter 9 splice variants are expressed in adult liver and kidney and are up-regulated in diabetes. *Mol Endocrinol* **20**, 686-697 (2006).
37. Augustin, R., Carayannopoulos, M. O., Dowd, L. O., Phay, J. E., Moley, J. F. & Moley, K. H. Identification and characterization of human glucose transporter-like protein-9 (GLUT9): alternative splicing alters trafficking. *J Biol Chem* **279**, 16229-16236 (2004).
38. Doblado, M. & Moley, K. H. Facilitative glucose transporter 9, a unique hexose and urate transporter. *Am J Physiol Endocrinol Metab* **297**, E831-835 (2009).
39. Caulfield, M. J., Munroe, P. B., O'Neill, D., Witkowska, K., Charchar, F. J., Doblado, M., Evans, S., Eyheramendy, S., Onipinla, A., Howard, P., Shaw-

Hawkins, S., Dobson, R. J., Wallace, C., Newhouse, S. J., Brown, M., Connell, J. M., Dominiczak, A., Farrall, M., Lathrop, G. M., Samani, N. J., Kumari, M., Marmot, M., Brunner, E., Chambers, J., Elliott, P., Kooner, J., Laan, M., Org, E.,Veldre, G., Viigimaa, M., Cappuccio, F. P., Ji, C., Iacone, R., Strazzullo, P., Moley, K. H. & Cheeseman, C. SLC2A9 Is a High-Capacity Urate Transporter in Humans. *PLoS Med* **5**, e197 (2008).

40. Wu, X., Li, W., Sharma, V., Godzik, A. & Freeze, H. H. Cloning and characterization of glucose transporter 11, a novel sugar transporter that is alternatively spliced in various tissues. *Mol Genet Metab* **76**, 37-45 (2002).
41. Scheepers, A., Schmidt, S., Manolescu, A., Cheeseman, C. I., Bell, A., Zahn, C., Joost, H. G. & Schürmann A. Characterization of the human SLC2A11 (GLUT11) gene: alternative promoter usage, function, expression, and subcellular distribution of three isoforms, and lack of mouse orthologue. *Mol Membr Biol* **22**, 339-351 (2005).
42. Sasaki, T., Minoshima, S., Shiohama, A., Shintani, A., Shimizu, A., Asakawa, S., Kawasaki, K. & Shimizu, N. Molecular cloning of a member of the facilitative glucose transporter gene family GLUT11 (SLC2A11) and identification of transcription variants. *Biochem Biophys Res Commun* **289**, 1218-1224 (2001).
43. DeBosch, B. J., Chi, M. & Moley, K. H. Glucose transporter 8 (GLUT8) regulates enterocyte fructose transport and global mammalian fructose utilization. *Endocrinology* **153**, 4181-4191 (2012).
44. Dawson, P. A., Mychaleckyj, J. C., Fossey, S. C., Mihic, S. J., Craddock, A. L. & Bowden, D. W. Sequence and functional analysis of glut10: a glucose transporter in the type 2 diabetes-linked region of chromosome 20q12-13.1. *Mol Genet Metab* **74**, 186-99 (2001).
45. Doege, H., Schurmann, A., Bahrenberg, G., Brauers, A. & Joost, H. G. GLUT8, a novel member of the sugar transport facilitator family with glucose transport activity. *J Biol Chem* **275**, 16275-16280 (2000).
46. Doege, H., Bocianski, A., Joost, H. G. & Schurmann, A. Activity and genomic organization of human glucose transporter 9 (GLUT9), a novel member of the family of sugar-transport facilitators predominantly expressed in brain and leucocytes. *Biochem J* **350 Pt 3**, 771-776 (2000).
47. Aerni-Flessner, L. B., Otu, M. C. & Moley, K. H. The amino acids upstream of NH(2)-terminal dileucine motif play a role in regulating the intracellular sorting of the Class III transporters GLUT8 and GLUT12. *Mol Membr Biol* **28**, 30-41 (2011).
48. Piroli, G. G., Grillo, C. A., Hoskin, E. K., Znamensky, V., Katz, E. B., Milner, T. A., McEwen, B. S., Charron, M. J. & Reagan, L. P. . Peripheral glucose administration stimulates the translocation of GLUT8 glucose transporter to the endoplasmic reticulum in the rat hippocampus. *J Comp Neurol* **452**, 103-114 (2002).

49. Lisinski, I., Schurmann, A., Joost, H. G., Cushman, S. W. & Al-Hasani, H. Targeting of GLUT6 (formerly GLUT9) and GLUT8 in rat adipose cells. *Biochem J* **358**, 517-22 (2001).
50. Rogers, S., Macheda, M. L., Docherty, S. E., Carty, M. D., Henderson, M. A., Soeller, W. C., Gibbs, E. M., James, D. E. & Best, J. D. Identification of a novel glucose transporter-like protein - GLUT-12. *Am J Physiol Endocrinol Metab* **282**, E733-738 (2002).
51. Uldry, M., Ibberson, M., Horisberger, J. D., Chatton, J. Y., Riederer, B. M. & Thorens, B. Identification of a mammalian H(+)-myo-inositol symporter expressed predominantly in the brain. *EMBO J* **20**, 4467-4477 (2001).
52. Schmidt, S., Joost, H. G. & Schurmann, A. GLUT8, the enigmatic intracellular hexose transporter. *Am J Physiol Endocrinol Metab* **296**, E614-8 (2009).
53. De Vivo, D. C., Trifiletti, R. R., Jacobson, R. I., Ronen, G. M., Behmand, R. A. & Harik, S. I. Defective glucose transport across the blood-brain barrier as a cause of persistent hypoglycorrhachia, seizures, and developmental delay. *New Engl J Med* **325**, 703-709 (1991).
54. Klepper, J. & Voit, T. Facilitated glucose transporter protein type 1 (GLUT1) deficiency syndrome: impaired glucose transport into brain-- a review. *Eur J Pediatr* **161**, 295-304 (2002).
55. Klepper, J., Willemsen, M., Verrips, A., Guertsen, E., Herrmann, R., Kutzick, C., Flörcken, A. & Voit, T. Autosomal dominant transmission of GLUT1 deficiency. *Hum Mol Genet* **10**, 63-68 (2001).
56. Brockmann, K. et al. Autosomal dominant glut-1 deficiency syndrome and familial epilepsy. *Ann Neurol* **50**, 476-485 (2001).
57. Wang, D., Pascual, J. M., Yang, H., Engelstad, K., Jhung, S., Sun, R. P. & De Vivo, D. C. Glut-1 deficiency syndrome: clinical, genetic, and therapeutic aspects. *Ann Neurol* **57**, 111-118 (2005).
58. Santer, R., Steinmann, B. & Schaub, J. Fanconi-Bickel syndrome--a congenital defect of facilitative glucose transport. *Curr Mol Med* **2**, 213-227 (2002).
59. Santer, R., Groth, S., Kinner, M., Dombrowski, A., Berry, G. T., Brodehl, J., Leonard, J. V., Moses, S., Norgren, S., Skovby, F., Schneppenheim, R., Steinmann, B. & Schaub, J. The mutation spectrum of the facilitative glucose transporter gene SLC2A2 (GLUT2) in patients with Fanconi-Bickel syndrome. *Hum Genet* **110**, 21-29 (2002).
60. Leturque, A., Brot-Laroche, E. & Le Gall, M. GLUT2 mutations, translocation, and receptor function in diet sugar managing. *Am J Physiol Endocrinol Metab* **296**, E985-92 (2009).
61. Yamamoto, T., Seino, Y., Fukumoto, H., Koh, G., Yano, H., Inagaki, N., Yamada, Y., Inoue, K., Manabe, T. & Imura, H. Over-expression of facilitative glucose

transporter genes in human cancer. *Biochem Biophys Res Commun* **170**, 223-230 (1990).
62. Hatanaka, M. Transport of sugars in tumor cell membranes. *Biochim Biophys Acta* **355**, 77-104 (1974).
63. Brown, R. S. & Wahl, R. L. Overexpression of Glut-1 glucose transporter in human breast cancer. An immunohistochemical study. *Cancer* **72**, 2979-2985 (1993).
64. Cantuaria, G., Fagotti, A., Ferrandina, G., Magalhaes, A., Nadji, M., Angioli, R., Penalver, M., Mancuso, S. & Scambia, G. GLUT-1 expression in ovarian carcinoma. *Cancer* **92**, 1144-1150 (2001).
65. Rudlowski, C., Moser, M., Becker, A. J., Rath,W., Buttner, R., Schroder, W. & Schurmann, A. GLUT1 mRNA and protein expression in ovarian borderline tumors and cancer. *Oncology* **66**, 404-410 (2004).
66. Nagase,Y., Takata, K., Moriyama, N., Aso, Y., Murakami, T. & Hirano, H. Immunohistochemical localization of glucose transporters in human renal cell carcinoma. *J Urol* **153**, 798-801 (1995).
67. Nishioka,T., Oda, Y., Seino, Y., Yamamoto, T., Inagaki, N., Yano, H., Imura, H., Shigemoto, R. & Kikuchi, H. Distribution of the glucose transporters in human brain tumors. *Cancer Res* **52**, 3972-3979 (1992).
68. Ogawa, J. I., Inoue, H. & Koide, S. Glucose-transporter-type-I-gene amplification correlates with Sialyl-Lewis-X synthesis and proliferation in lung cancer. *Int J Cancer* **74**, 189-192 (1997).
69. Haber, R. S., Rathan, A., Weiser, K. R., Pritsker, A., Itzkowitz, S. H., Bodian, C., Slater, G.,Weiss, A. & Burstein, D. E. GLUT1 glucose transporter expression in colorectal carcinoma. *Cancer* **83**, 34-40 (1998).
70. Baron-Delage, S., Mahraoui, L., Cadoret, A., Veissiere, D., Taillemite, J. L., Chastre, E., Gespach, C., Zweibaum, A., Capeau, J., Brot-Laroche, E. & Cherqui, G. Deregulation of hexose transporter expression in Caco-2 cells by ras and polyoma middle T oncogenes. *Am J Physiol* **270**, G314-23 (1996).
71. Day, R. E., Higgins, V. J., Rogers, P. J. & Dawes, I. W. Characterization of the putative maltose transporters encoded by YDL247w and YJR160c. *Yeast* **19**, 1015-1027 (2002).
72. Herman, M. A. & Kahn, B. B. Glucose transport and sensing in the maintenance of glucose homeostasis and metabolic harmony. *J Clin Invest* **116**, 1767-1775 (2006).
73. Macheda, M. L., Rogers, S. & Best, J. D. Molecular and cellular regulation of glucose transporter (GLUT) proteins in cancer. *J Cell Physiol* **202**, 654-662 (2005).
74. James, D. E., Burleigh, K. M. & Kraegen, E. W. Time dependence of insulin action in muscle and adipose tissue in the rat in vivo. An increasing response in adipose tissue with time. *Diabetes* **34**, 1049-1054 (1985).
75. Holman, G. D., Kozka, I. J., Clark, A. E., Flower, C. J., Saltis, J., Habberfield, A. D., Simpson, I. A. & Cushman, S. W. Cell surface labeling of glucose transporter

isoform GLUT4 by bis- mannose photolabel. Correlation with stimulation of glucose transport in rat adipose cells by insulin and phorbol ester. *J Biol Chem* **265**, 18172-18179 (1990).

76. Kraegen, E. W., Sowden, J. A., Halstead, M. B., Clark, P. W., Rodnick, K. J., Chisholm, D. J. & James, D. E. Glucose transporters and in vivo glucose uptake in skeletal and cardiac muscle: fasting, insulin stimulation and immunoisolation studies of GLUT1 and GLUT4. *Biochem J* **295**, 287-293 (1993).
77. Saltiel, A. R. & Kahn, C. R. Insulin signalling and the regulation of glucose and lipid metabolism. *Nature* **414**, 799-806 (2001).
78. Rossetti, L., Stenbit, A. E., Chen, W., Hu, M., Barzilai, N., Katz, E. B. & Charron, M. J. Peripheral but not hepatic insulin resistance in mice with one disrupted allele of the glucose transporter type 4 (GLUT4) gene. *J Clin Invest* **100**, 1831-1839 (1997).
79. Charron, M. J., Katz, E. B. & Olson, A. L. GLUT4 gene regulation and manipulation. *J Biol Chem* **274**, 3253-3256 (1999).
80. Zisman, A., Peroni, O. D., Abel, E. D., Michael, M. D., Mauvais-Jarvis, F., Lowell, B. B., Wojtaszewski, J. F., Hirshman, M. F., Virkamaki, A., Goodyear, L. J., Kahn, C. R. & Kahn, B. B. Targeted disruption of the glucose transporter 4 selectively in muscle causes insulin resistance and glucose intolerance. *Nat Med* **6**, 924-928 (2000).
81. Abel, E. D., Peroni, O., Kim, J. K., Kim, Y. B., Boss, O., Hadro, E., Minnemann, T., Shulman, G. I. & Kahn, B. B. Adipose-selective targeting of the GLUT4 gene impairs insulin action in muscle and liver. *Nature* **409**, 729-733 (2001).
82. Murata, H., Hruz, P. W. & Mueckler, M. The mechanism of insulin resistance caused by HIV protease inhibitor therapy. *J Biol Chem* **275**, 20251-20254 (2000).
83. Murata, H., Hruz, P. W. & Mueckler, M. Indinavir inhibits the glucose transporter isoform Glut4 at physiologic concentrations. *Aids* **16**, 859-863 (2002).
84. Behrens, G., Dejam, A., Schmidt, H., Balks, H. J., Brabant, G., Körner, T., Stoll, M. & Schmidt, R. E. Impaired glucose tolerance, beta cell function and lipid metabolism in HIV patients under treatment with protease inhibitors. *AIDS* **13**, F63-70 (1999).
85. Safrin, S. & Grunfeld, C. Fat distribution and metabolic changes in patients with HIV infection. *AIDS* **13**, 2493-2505 (1999).
86. Hruz, P. W., Murata, H. & Mueckler, M. Adverse metabolic consequences of HIV protease inhibitor therapy: the search for a central mechanism. *Am J Physiol Endocrinol Metab* **280**, E549-53 (2001).
87. Gan, S. K., Samaras, K., Carr, A. & Chisholm, D. Anti-retroviral therapy, insulin resistance and lipodystrophy. *Diabetes Obes Metab* **3**, 67-71 (2001).
88. Feig, D. I., Kang, D. H. & Johnson, R. J. Uric acid and cardiovascular risk. *N Engl J Med* **359**, 1811-1821 (2008).

89. Li, S., Sanna, S., Maschio, A., Busonero, F., Usala, G., Mulas, A., Lai, S., Dei, M., Orrù, M., Albai, G., Bandinelli, S., Schlessinger, D., Lakatta, E., Scuteri, A., Najjar, S. S., Guralnik, J., Naitza, S., Crisponi, L., Cao, A., Abecasis, G., Ferrucci, L., Uda, M., Chen, W. M. & Nagaraja, R. The GLUT9 gene is associated with serum uric acid levels in Sardinia and Chianti cohorts. *PLoS Genet* **3**, e194 (2007).
90. Witkowska, K., Smith, K. M., Yao, S. Y., Ng, A. M., O'Neill, D., Karpinski, E., Young, J. D. & Cheeseman, C. I. Human SLC2A9a and SLC2A9b isoforms mediate electrogenic transport of urate with different characteristics in the presence of hexoses. *Am J Physiol Renal Physiol* **303**, F527-39 (2012).
91. So, A. & Thorens, B. Uric acid transport and disease. *J Clin Invest* **120**, 1791-1799 (2010).
92. Chin, J. J., Jung, E. K. & Jung, C. Y. Structural basis of human erythrocyte glucose transporter function in reconstituted vesicles. *J Biol Chem* **261**, 7101-7104 (1986).
93. Hresko, R. C., Kruse, M., Strube, M. & Mueckler, M. Topology of the Glut 1 glucose transporter deduced from glycosylation scanning mutagenesis. *J Biol Chem* **269**, 20482-20488 (1994).
94. Alvarez, J., Lee, D. C., Baldwin, S. A. & Chapman, D. Fourier transform infrared spectroscopic study of the structure and conformational changes of the human erythrocyte glucose transporter. *J Biol Chem* **262**, 3502-3509 (1987).
95. Chin, J. J., Jung, E. K., Chen, V. & Jung, C. Y. Structural basis of human erythrocyte glucose transporter function in proteoliposome vesicles: circular dichroism measurements. *Proc Natl Acad Sci U S A* **84**, 4113-4116 (1987).
96. Maiden, M. C., Davis, E. O., Baldwin, S. A., Moore, D. C. & Henderson, P. J. Mammalian and bacterial sugar transport proteins are homologous. *Nature* **325**, 641-643 (1987).
97. Gorga, F., R., Baldwin, S., A. & Lienhard, G., E. The monosaccharide transporter from human erythrocytes is heterogeneously glycosylated. *Biochem Biophys Res Commun* **91**, 955-961 (1979).
98. Asano, T., Katagiri, H., Takata, K., Lin, J. L., Ishihara, H., Inukai, K., Tsukuda, K., Kikuchi, M., Hirano, H., Yazaki, Y. & Oka, Y. The role of N-glycosylation of GLUT1 for glucose transport activity. *J Biol Chem* **266**, 24632-24636 (1991).
99. Manolescu, A., Salas-Burgos, A. M., Fischbarg, J. & Cheeseman, C. I. Identification of a hydrophobic residue as a key determinant of fructose transport by the facilitative hexose transporter SLC2A7 (GLUT7). *J Biol Chem* **280**, 42978-42983 (2005).
100. Manolescu, A. R., Augustin, R., Moley, K. & Cheeseman, C. A highly conserved hydrophobic motif in the exofacial vestibule of fructose transporting SLC2A proteins acts as a critical determinant of their substrate selectivity. *Mol Membr Biol* **24**, 455-463 (2007).

101. Schürmann, A., Keller, K., Monden, I., Brown, F. M., Wandel, S., Shanahan, M. F. & Joost, H. G. Glucose transport activity and photolabelling with 3-[125I]iodo-4-azidophenethylamido-7-O-succinyldeacetyl (IAPS)-forskolin of two mutants at tryptophan-388 and -412 of the glucose transporter GLUT1: dissociation of the binding domains of forskolin and glucose. *Biochem J* **290**, 497-501 (1993).
102. Joost, H. G. & Thorens, B. The extended GLUT-family of sugar/polyol transport facilitators: nomenclature, sequence characteristics, and potential function of its novel members (review). *Mol Membr Biol* **18**, 247-256 (2001).
103. Garcia, J. C., Strube, M., Leingang, K., Keller, K. & Mueckler, M. M. Amino acid substitutions at tryptophan 388 and tryptophan 412 of the HepG2 (Glut1) glucose transporter inhibit transport activity and targeting to the plasma membrane in Xenopus oocytes. *J Biol Chem* **267**, 7770-7776 (1992).
104. Tamori, Y., Hashiramoto, M., Clark, A. E., Mori, H., Muraoka, A., Kadowaki, T., Holman, G. D. & Kasuga, M. Substitution at Pro385 of GLUT1 perturbs the glucose transport function by reducing conformational flexibility. *J Biol Chem* **269**, 2982-2986 (1994).
105. Mori, H., Hashiramoto, M., Clark, A. E., Yang, J., Muraoka, A., Tamori, Y., Kasuga, M. & Holman, G. D. Substitution of tyrosine 293 of GLUT1 locks the transporter into an outward facing conformation. *J Biol Chem* **269**, 11578-11583 (1994).
106. Schürmann, A., Doege, H., Ohnimus, H., Monser, V., Buchs, A. & Joost, HG. Role of conserved arginine and glutamate residues on the cytosolic surface of glucose transporters for transporter function. *Biochemistry* **36**, 12897-12902 (1997).
107. Muraoka, A., Hashiramoto, M., Clark, A. E., Edwards, L. C., Sakura, H., Kadowaki, T., Holman, G. D. & Kasuga, M. Analysis of the structural features of the C-terminus of GLUT1 that are required for transport catalytic activity. *Biochem J* **311**, 699-704 (1995).
108. Pellerin, L. & Magistretti, P. J. Glutamate uptake into astrocytes stimulates aerobic glycolysis: a mechanism coupling neuronal activity to glucose utilization. *Proc Natl Acad Sci USA* **91**, 10625-10629 (1994).
109. Belanger, M., Allaman, I. & Magistretti, P. J. Brain energy metabolism: focus on astrocyte-neuron metabolic cooperation. *Cell Metab* **14**, 724-738 (2011).
110. Marty, N., Dallaporta, M., Foretz, M., Emery, M., Tarussio, D., Bady, I., Binnert, C., Beermann, F. & Thorens, B. Regulation of glucagon secretion by glucose transporter type 2 (glut2) and astrocyte-dependent glucose sensors. *J Clin Invest* **115**, 3545-3553 (2005).
111. Marty, N., Dallaporta, M. & Thorens, B. Brain glucose sensing, counterregulation, and energy homeostasis. *Physiology* **22**, 241-251 (2007).
112. Hirai, T., Heymann, J. A., Shi, D., Sarker, R., Maloney, P. C. & Subramaniam, S. Three-dimensional structure of a bacterial oxalate transporter. *Nat Struct Biol* **9**, 597-600 (2002).

113. Abramson, J., Smirnova, I., Kasho, V., Verner, G., Kaback, H. R. & Iwata, S. Structure and mechanism of the lactose permease of Escherichia coli. *Science* **301**, 610-615 (2003).
114. Lemieux, M. J., Song, J., Kim, M. J., Huang, Y., Villa, A., Auer, M., Li, X. D. & Wang, D. N. Three-dimensional crystallization of the *Escherichia coli* glycerol-3-phosphate transporter: A member of the major facilitator superfamily. *Protein Sci* **12**, 2748-2756 (2003).
115. Holyoake, J., Caulfield, V., Baldwin, S. A. & Sansom, M. S. Modeling, docking, and simulation of the major facilitator superfamily. *Biophys J* **91**, L84-6 (2006).
116. Salas-Burgos, A., Iserovich, P., Zuniga, F., Vera, J. C. & Fischbarg, J. Predicting the three-dimensional structure of the human facilitative glucose transporter glut1 by a novel evolutionary homology strategy: insights on the molecular mechanism of substrate migration, and binding sites for glucose and inhibitory molecules. *Biophys J* **87**, 2990-2999 (2004).
117. Dwyer, D. S. Model of the 3-D structure of the GLUT3 glucose transporter and molecular dynamics simulation of glucose transport. *Proteins* **42**, 531-41 (2001).
118. Chang, G., Spencer, R. H., Lee, A. T., Barclay, M. T. & Rees, D. C. Structure of the MscL Homolog from Mycobacterium tuberculosis: A Gated Mechanosensitive Ion Channel. *Science* **282**, 2220-2226 (1998).
119. Walz, T., Hirai, T., Murata, K., Heymann, J. B., Mitsuoka, K., Fujiyoshi, Y., Smith, B. L., Agre, P. & Engel, A. The three-dimensional structure of aquaporin-1. *Nature* **387**, 624-627 (1997).
120. Mohan, S. S., Perry, J. J., Poulose, N., Nair, B. G. & Anilkumar, G. Homology modeling of GLUT4, an insulin regulated facilitated glucose transporter and docking studies with ATP and its inhibitors. *J Biomol Struct Dyn* **26**, 455-464 (2009).
121. Sheena, A., Mohan, S. S., Haridas, N. P. & Anilkumar, G. Elucidation of the glucose transport pathway in glucose transporter 4 via steered molecular dynamics simulations. *PLoS One* **6**, e25747 (2011).
122. Dang, S., Sun, L., Huang, Y., Lu, F., Liu, Y., Gong, H., Wang, J. & Yan, N. Structure of a fucose transporter in an outward-open conformation. *Nature* **467**, 734-738 (2010).
123. Yin, Y., He, X., Szewczyk, P., Nguyen, T. & Chang, G. Structure of the Multidrug Transporter EmrD from *Escherichia coli*. *Science* **312**, 741-744 (2006).
124. Wang, D., Kranz-Eble, P. & De Vivo, D. C. Mutational analysis of GLUT1 (SLC2A1) in Glut-1 Deficiency Syndrome. *Hum Mutat* **16**, 224-231 (2000).
125. Pascual, J. M., van Heertum, R. L., Wang, D., Engelstad, K. & De Vivo, D. C. Imaging the metabolic footprint of Glut1 deficiency on the brain. *Ann Neurol* **52**, 458-464 (2002).

126. Hruz, P. W. & Mueckler, M. M. Cysteine-scanning mutagenesis of transmembrane segment 7 of the GLUT1 glucose transporter. *J Biol Chem* **274**, 36176-36180 (1999).
127. Mueckler, M., Weng, W. & Kruse, M. Glutamine 161 of Glut1 glucose transporter is critical for transport activity and exofacial ligand binding. *J Biol Chem* **269**, 20533-20538 (1994).
128. Mueckler, M. & Makepeace, C. Identification of an amino acid residue that lies between the exofacial vestibule and exofacial substrate-binding site of the Glut1 sugar permeation pathway. *J Biol Chem* **272**, 30141-30146 (1997).
129. Mueckler, M. & Makepeace, C. Analysis of transmembrane segment 10 of the Glut1 glucose transporter by cysteine-scanning mutagenesis and substituted cysteine accessibility. *J Biol Chem* **277**, 3498-3503 (2002).
130. Blodgett, D. M., Graybill, C. & Carruthers, A. Analysis of glucose transporter topology and structural dynamics. *J Biol Chem* **283**, 36416-36424 (2008).
131. Mueckler, M., Roach, W. & Makepeace, C. Transmembrane segment 3 of the Glut1 glucose transporter is an outer helix. *J Biol Chem* **279**, 46876-46881 (2004).
132. Mueckler, M. & Makepeace, C. Transmembrane segment 6 of the Glut1 glucose transporter is an outer helix and contains amino acid side chains essential for transport activity. *J Biol Chem* **283**, 11550-11555 (2008).
133. Mueckler, M. & Makepeace, C. Transmembrane segment 12 of the Glut1 glucose transporter is an outer helix and is not directly involved in the transport mechanism. *J Biol Chem* **281**, 36993-36998 (2006).
134. Mueckler, M. & Makepeace, C. Model of the exofacial substrate-binding site and helical folding of the human Glut1 glucose transporter based on scanning mutagenesis. *Biochemistry* **48**, 5934-5942 (2009).
135. Mueckler, M. & Makepeace, C. Analysis of transmembrane segment 8 of the GLUT1 glucose transporter by cysteine-scanning mutagenesis and substituted cysteine accessibility. *J Biol Chem* **279**, 10494-10499 (2004).
136. Mueckler, M. & Makepeace, C. Cysteine-scanning mutagenesis and substituted cysteine accessibility analysis of transmembrane segment 4 of the Glut1 glucose transporter. *J Biol Chem* **280**, 39562-39568 (2005).
137. Lemieux, M. J. Eukaryotic major facilitator superfamily transporter modeling based on the prokaryotic GlpT crystal structure (Review). *Mol Membr Biol* **24**, 333-341 (2007).
138. Graybill, C., van Hoek, A. N., Desai, D., Carruthers, A. M. & Carruthers, A. Ultrastructure of Human Erythrocyte GLUT1. *Biochemistry* **45**, 8096-8107 (2006).
139. Hinkle, P. C., Sogin, D. C., Wheeler, T. J. & Teleford, J. N. in *Function and Molecular Aspect of Biomembrane Transport.* (ed Quagliariello, E.) 487−494 (Elsevier/North-Holland Biomedical Press, Amsterdam, 1979).

140. Hebert, D. N. & Carruthers, A. Cholate-solubilized erythrocyte glucose transporters exist as a mixture of homodimers and homotetramers. *Biochemistry* **30**, 4654-4658 (1991).
141. Hebert, D. N. & Carruthers, A. Glucose transporter oligomeric structure determines transporter function. Reversible redox-dependent interconversions of tetrameric and dimeric GLUT1. *J Biol Chem* **267**, 23829-23838 (1992).
142. Zottola, R. J., Cloherty, E. K., Coderre, P. E., Hansen, A., Hebert, D. N. & Carruthers, A. Glucose transporter function is controlled by transporter oligomeric structure. A single, intramolecular disulfide promotes GLUT1 tetramerization. *Biochemistry* **34**, 9734-9747 (1995).
143. Pessino, A., Hebert, D. N., Woon, C. W., Harrison, S. A., Clancy, B. M., Buxton, J. M., Carruthers, A. & Czech, M. P. Evidence that functional erythrocyte-type glucose transporters are oligomers. *J Biol Chem* **266**, 20213-20217 (1991).
144. Burant, C. F. & Bell, G. I. Mammalian facilitative glucose transporters: evidence for similar substrate recognition sites in functionally monomeric proteins. *Biochemistry* **31**, 10414-10420 (1992).
145. Gorga, F. R. & Lienhard, G. E. Equilibria and kinetics of ligand binding to the human erythrocyte glucose transporter. Evidence for an alternating conformation model for transport. *Biochemistry* **20**, 5108-5113 (1981).
146. Carruthers, A. ATP regulation of the human red cell sugar transporter. *J Biol Chem* **261**, 11028-11037 (1986).
147. Hebert, D. N. & Carruthers, A. Direct evidence for ATP modulation of sugar transport in human erythrocyte ghosts. *J Biol Chem* **261**, 10093-10099 (1986).
148. Cloherty, E. K., Diamond, D. L., Heard, K. S. & Carruthers, A. Regulation of GLUT1-mediated sugar transport by an antiport/uniport switch mechanism. *Biochemistry* **35**, 13231-13239 (1996).
149. Levine, K. B., Cloherty, E. K., Fidyk, N. J. & Carruthers, A. Structural and physiologic determinants of human erythrocyte sugar transport regulation by adenosine triphosphate. *Biochemistry* **37**, 12221-12232 (1998).
150. Cloherty, E. K., Levine, K. B., Graybill, C. & Carruthers, A. Cooperative nucleotide binding to the human erythrocyte sugar transporter. *Biochemistry* **41**, 12639-12651 (2002).
151. Carruthers, A. & Helgerson, A. L. The human erythrocyte sugar transporter is also a nucleotide binding protein. *Biochemistry* **28**, 8337-8346 (1989).
152. Blodgett, D. M., De Zutter, J. K., Levine, K. B., Karim, P. & Carruthers, A. Structural Basis of GLUT1 Inhibition by Cytoplasmic ATP. *J Gen Physiol* **130**, 157-168 (2007).
153. Levine, K. B., Hamill, S., Cloherty, E. K. & Carruthers, A. Alanine scanning mutagenesis of the human erythrocyte glucose transporter putative ATP binding domain. *Blood Cells Mol Dis* **27**, 139-142 (2001).

154. Chang, K. J. & Cuatrecasas, P. Adenosine triphosphate-dependent inhibition of insulin-stimulated glucose transport in fat cells. Possible role of membrane phosphorylation. *J Biol Chem* **249**, 3170-3180 (1974).
155. Bazuine, M., van den Broek, P. J. & Maassen, J. A. Genistein directly inhibits GLUT4-mediated glucose uptake in 3T3-L1 adipocytes. *Biochem Biophys Res Commun* **326**, 511-514 (2005).
156. Strobel, P., Allard, C., Perez-Acle, T., Calderon, R., Aldunate, R. & Leighton, F. Myricetin, quercetin and catechin-gallate inhibit glucose uptake in isolated rat adipocytes. *Biochem J* **386**, 471-478 (2005).
157. Vera, J. C., Reyes, A. M., Velásquez, F. V., Rivas, C. I., Zhang, R. H., Strobel, P., Slebe, J. C., Núñez-Alarcón, J. & Golde, D. W. Direct inhibition of the hexose transporter GLUT1 by tyrosine kinase inhibitors. *Biochemistry* **40**, 777-90 (2001).
158. Mohan, S., Sheena, A., Poulose, N. & Anilkumar, G. Molecular dynamics simulation studies of GLUT4: substrate-free and substrate-induced dynamics and ATP-mediated glucose transport inhibition. *PLoS One* **5**, e14217 (2010).
159. Goto, T., Horita, M., Nagai, H., Nagatomo, A., Nishida, N., Matsuura, Y. & Nagaoka, S. Tiliroside, a glycosidic flavonoid, inhibits carbohydrate digestion and glucose absorption in the gastrointestinal tract. *Mol Nutr Food Res* **56**, 435-445 (2012).
160. Heijnen, H. F., Oorschot, V., Sixma, J. J., Slot, J. W. & James, D. E. Thrombin stimulates glucose transport in human platelets via the translocation of the glucose transporter GLUT-3 from alpha-granules to the cell surface. *J Cell Biol* **138**, 323-330 (1997).
161. Daneman, D., Zinman, B., Elliott, M. E., Bilan, P. J. & Klip, A. Insulin-stimulated glucose transport in circulating mononuclear cells from nondiabetic and IDDM subjects. *Diabetes* **41**, 227-234 (1992).
162. Fu, Y., Maianu, L., Melbert, B. R. & Garvey, W. T. Facilitative glucose transporter gene expression in human lymphocytes, monocytes, and macrophages: a role for GLUT isoforms 1, 3, and 5 in the immune response and foam cell formation. *Blood Cells Mol Dis* **32**, 182-190 (2004).
163. Maratou, E., Dimitriadis, G., Kollias, A., Boutati, E., Lambadiari, V., Mitrou, P. & Raptis, S. A. Glucose transporter expression on the plasma membrane of resting and activated white blood cells. *Eur J Clin Invest* **37**, 282-290 (2007).
164. Harrison, S. A., Buxton, J. M., Helgerson, A. L., MacDonald, R. G., Chlapowski, F. J., Carruthers, A. & Czech, M. P. Insulin action on activity and cell surface disposition of human HepG2 glucose transporters expressed in Chinese hamster ovary cells. *J Biol Chem* **265**, 5793-5801 (1990).
165. Egert, S., Nguyen, N. & Schwaiger, M. Myocardial Glucose Transporter GLUT1: Translocation Induced by Insulin and Ischemia. *J Mol Cell Cardiol* **31**, 1337-1344 (1999).

166. Marette, A. Richardson, J. M., Ramlal, T., Balon, T. W., Vranic, M., Pessin, J. E. & Klip, A. Abundance, localization, and insulin-induced translocation of glucose transporters in red and white muscle. *Am J Physiol* **263**, C443-52 (1992).
167. Piper, R. C., Tai, C., Kulesza, P., Pang, S., Warnock, D., Baenziger, J., Slot, J. W., Geuze, H. J., Puri, C. & James, D. E. GLUT-4 NH2 terminus contains a phenylalanine-based targeting motif that regulates intracellular sequestration. *J Cell Biol* **121**, 1221-1232 (1993).
168. Corvera, S., Chawla, A., Chakrabarti, R., Joly, M., Buxton, J. & Czech, M. P. A double leucine within the GLUT4 glucose transporter COOH-terminal domain functions as an endocytosis signal. *J Cell Biol* **126**, 979-989 (1994).
169. Verhey, K. J. & Birnbaum, M. J. A Leu-Leu sequence is essential for COOH-terminal targeting signal of GLUT4 glucose transporter in fibroblasts. *J Biol Chem* **269**, 2353-2356 (1994).
170. Araki, S., Yang, J., Hashiramoto, M., Tamori, Y., Kasuga, M. & Holman, G. D. Subcellular trafficking kinetics of GLU4 mutated at the N- and C-terminal. *Biochem J* **315**, 153-159 (1996).
171. Al-Hasani, H., Kunamneni, R. K., Dawson, K., Hinck, C. S., Müller-Wieland, D. & Cushman, S. W. Roles of the N- and C-termini of GLUT4 in endocytosis. *J Cell Sci* **115**, 131-140 (2002).
172. Shewan, A. M., Marsh, B. J., Melvin, D. R., Martin, S., Gould, G. W. & James, D. E. The cytosolic C-terminus of the glucose transporter GLUT4 contains an acidic cluster endosomal targeting motif distal to the dileucine signal. *Biochem J* **350**, 99-107 (2000).
173. Bryant, N. J., Govers, R. & James, D. E. Regulated transport of the glucose transporter GLUT4. *Nat Rev Mol Cell Biol* **3**, 267-277 (2002).
174. Gonzalez, E. & McGraw, T. E. Insulin signaling diverges into Akt-dependent and -independent signals to regulate the recruitment/docking and the fusion of GLUT4 vesicles to the plasma membrane. *Mol Biol Cell* **17**, 4484-4493 (2006).
175. Martin, O. J., Lee, A. & McGraw, T. E. GLUT4 distribution between the plasma membrane and the intracellular compartments is maintained by an insulin-modulated bipartite dynamic mechanism. *J Biol Chem* **281**, 484-490 (2006).
176. Wilson, C. M. & Cushman, S. W. Insulin stimulation of glucose transport activity in rat skeletal muscle: increase in cell surface GLUT4 as assessed by photolabelling. *Biochem J* 755-759 (1994).
177. Toyoda, N., Flanagan, J. E. & Kono, T. Reassessment of insulin effects on the Vmax and Km values of hexose transport in isolated rat epididymal adipocytes. *J Biol Chem* **262**, 2737-2745 (1987).
178. Sone, H., Deo, B. K. & Kumagai, A. K. Enhancement of glucose transport by vascular endothelial growth factor in retinal endothelial cells. *Invest Ophthalmol Vis Sci* **41**, 1876-1884 (2000).

179. Heo, J. S. & Han, H. J. PKC and MAPKs pathways mediate EGF-induced stimulation of 2-deoxyglucose uptake in mouse embryonic stem cells. *Cell Physiol Biochem* **17**, 145-158 (2006).
180. Kurth-Kraczek, E. J., Hirshman, M. F., Goodyear, L. J. & Winder, W. W. 5' AMP-activated protein kinase activation causes GLUT4 translocation in skeletal muscle. *Diabetes* **48**, 1667-171. (1999).
181. Fujii, N., Hayashi, T., Hirshman, M. F., Smith, J. T., Habinowski, S. A., Kaijser, L., Mu, J., Ljungqvist, O., Birnbaum, M. J., Witters, L. A., Thorell, A. & Goodyear, L. J. Exercise induces isoform-specific increase in 5'AMP-activated protein kinase activity in human skeletal muscle. *Biochem Biophys Res Commun* **273**, 1150-1155 (2000).
182. Cura, A. J. & Carruthers, A. Acute modulation of sugar transport in brain capillary endothelial cell cultures during activation of the metabolic stress pathway. *J Biol Chem* **285**, 15430-15439 (2010).
183. Cura, A. J. & Carruthers, A. AMP kinase regulation of sugar transport in brain capillary endothelial cells during acute metabolic stress. *Am J Physiol Cell Physiol* **303**, C806-14 (2012).
184. Cura, A. J. & Carruthers, A. The role of Monosaccharide Transport Proteins in carbohydrate assimilation, distribution, metabolism and homeostasis. *Compr Physiol* **2**, 863-914 (2012).
185. Naftalin, R. J. & Holman, G. D. in *Membrane transport in red cells* (eds Ellory, J. C. & Lew, V. L.) 257-300 (Academic Press, New York, 1977).
186. Stein, W. D. *Transport and diffusion across cell membranes* (Academic Press, New York, 1986).
187. Widdas, W. F. The asymmetry of the hexose transfer system in the human red cell membrane. *Curr. Top. Memb. Transp.* **14**, 165-223 (1980).
188. Miller, D. M. The kinetics of selective biological transport. III. Erythrocyte-monosaccharide transport data. *Biophys J* **8**, 1329-1338 (1968).
189. Miller, D. M. The kinetics of selective biological transport. IV. Assessment of three carrier systems using the erythrocyte-monosaccharide transport data. *Biophys J* **8**, 1339-1352 (1968).
190. Miller, D. M. The kinetics of selective biological transport. V. Further data on the erythrocyte–monosaccharide transport system. *Biophys J* **11**, 915–923 (1971).
191. Gould, G. W. & Lienhard, G. E. Expression of a functional glucose transporter in Xenopus oocytes. *Biochemistry* **28**, 9447-9452 (1989).
192. Keller, K. & Mueckler, M. Different mammalian facilitative glucose transporters expressed in Xenopus oocytes. *Biomed Biochim Acta* **49**, 1201-1203 (1990).
193. Levine, K. B., Cloherty, E. K., Hamill, S. & Carruthers, A. Molecular determinants of sugar transport regulation by ATP. *Biochemistry* **41**, 12629-12638 (2002).

194. Alisio, A. & Mueckler, M. Purification and characterization of mammalian glucose transporters expressed in Pichia pastoris. *Protein Expr Purif* **70**, 81-87 (2010).
195. Bachelard, H. S. Deoxyglucose and brain glycolysis. *Biochem J* **127**, 83P (1972).
196. Jay, T. M., Dienel, G. A., Cruz, N. F., Mori, K., Nelson, T. & Sokoloff, L. Metabolic stability of 3-O-methyl-D-glucose in brain and other tissues. *J Neurochem* **55**, 989-1000 (1990).
197. Vera, J. C. & Rosen, O. M. Functional expression of mammalian glucose transporters in Xenopus laevis oocytes: evidence for cell-dependent insulin sensitivity. *Mol Cell Biol* **9**, 4187-4195 (1989).
198. Janicot, M. & Lane, M. D. Activation of glucose uptake by insulin and insulin-like growth factor I in Xenopus oocytes. *Proc Natl Acad Sci USA* **86**, 2642-2646 (1989).
199. Uldry, M., Ibberson, M., Hosokawa, M. & Thorens, B. GLUT2 is a high affinity glucosamine transporter. *FEBS Lett* **524**, 199-203 (2002).
200. Hansen, P., Gulve, E., Gao, J., Schluter, J., Mueckler, M. & Holloszy, J. Kinetics of 2-deoxyglucose transport in skeletal muscle: effects of insulin and contractions. *Am J Physiol* **268**, C30-5 (1995).
201. Keller, K., Strube, M. & Mueckler, M. Functional expression of the human HepG2 and rat adipocyte glucose transporters in Xenopus oocytes. Comparison of kinetic parameters. *J Biol Chem* **264**, 18884-18889 (1989).
202. Nishimura, H., Pallardo, F. V., Seidner, G. A., Vannucci, S., Simpson, I. A. & Birnbaum, M. J. Kinetics of GLUT1 and GLUT4 glucose transporters expressed in Xenopus oocytes. *J Biol Chem* **268**, 8514-8520 (1993).
203. Taylor, L. P. & Holman, G. D. Symmetrical kinetic parameters for 3-O-methyl-D-glucose transport in adipocytes in the presence and in the absence of insulin. *Biochim Biophys Acta* **642**, 325-335 (1981).
204. Barnett, J. E., Holman, G. D. & Munday, K. A. An explanation of the asymmetric binding of sugars to the human erythrocyte sugar-transport systems. *Biochem J* **135**, 539-541 (1973).
205. Holman, G. D., Busza, A. L., Pierce, E. J. & Rees, W. D. Evidence for negative cooperativity in human erythrocyte sugar transport. *Biochim Biophys Acta* **649**, 503-514 (1981).
206. Baker, G. F. & Naftalin, R. J. Evidence of multiple operational affinities for D-glucose inside the human erythrocyte membrane. *Biochim Biophys Acta* **550**, 474-484 (1979).
207. Lowe, A. G. & Walmsley, A. R. The kinetics of glucose transport in human red blood cells. *Biochim Biophys Acta* **857**, 146-154 (1986).
208. Craik, J. D. & Elliott, K. R. Kinetics of 3-O-methyl-D-glucose transport in isolated rat hepatocytes. *Biochem J* **182**, 503-508 (1979).

209. Taylor, L. P. & Holman, G. D. Symmetrical kinetic parameters for 3-O-methyl-D-glucose transport in adipocytes in the presence and in the absence of insulin. *Biochim Biophys Acta* **642**, 325-335 (1981).
210. Blodgett, D. M. & Carruthers, A. Conventional transport assays underestimate sugar transport rates in human red cells. *Blood Cells Mol Dis* **32**, 401-407 (2004).
211. Widdas, W. F. Inability of diffusion to account for placental glucose transfer in the sheep and consideration of the kinetics of a possible carrier transfer. *J Physiol* **118**, 23–39 (1952).
212. Jardetzky, O. Simple allosteric model for membrane pumps. *Nature* **211**, 969-970 (1966).
213. Krupka, R. M. & Devés, R. An experimental test for cyclic versus linear transport models. The mechanism of glucose and choline transport in erythrocytes. *J Biol Chem* **256**, 5410-5416 (1981).
214. Lieb, W. R. & Stein, W. D. Testing and characterizing the simple carrier. *Biochim Biophys Acta* **373**, 178-196 (1974).
215. Carruthers, A. & Helgerson, A. L. Inhibitions of sugar transport produced by ligands binding at opposite sides of the membrane. Evidence for simultaneous occupation of the carrier by maltose and cytochalasin B. *Biochemistry* **30**, 3907-3915 (1991).
216. Carruthers, A. & Melchior, D. L. Asymmetric or symmetric? Cytosolic modulation of human erythrocyte hexose transfer. *Biochim Biophys Acta* **728**, 254-266 (1983).
217. Carruthers, A. & Melchior, D. L. Transport of α- and β-D-glucose by the intact human red cell. *Biochemistry* **24**, 4244-4250 (1985).
218. Naftalin, R. J. & Rist, R. J. Re-examination of hexose exchanges using rat erythrocytes: evidence inconsistent with a one-site sequential exchange model, but consistent with a two-site simultaneous exchange model. *Biochim Biophys Acta* **1191**, 65-78 (1994).
219. Barnett, J. E., Holman, G. D. & Munday, K. A. Structural requirements for binding to the sugar-transport system of the human erythrocyte. *Biochem J* **131**, 211-221 (1973).
220. Colville, C. A., Seatter, M. J. & Gould, G. W. Analysis of the structural requirements of sugar binding to the liver, brain and insulin-responsive glucose transporters expressed in oocytes. *Biochem J* **294**, 753-760 (1993).
221. Kane, S., Seatter, M. J. & Gould, G. W. Functional studies of human GLUT5: effect of pH on substrate selection and an analysis of substrate interactions. *Biochem Biophys Res Commun* **238**, 503-505 (1997).
222. Barnett, J. E., Holman, G. D., Chalkley, R. A. & Munday, K. A. Evidence for two asymmetric conformational states in the human erythrocyte sugar-transport system. *Biochem J* **145**, 417-429 (1975).

223. Manolescu, A. R., Witkowska, K., Kinnaird, A., Cessford, T. & Cheeseman, C. Facilitated hexose transporters: new perspectives on form and function. *Physiology* **22**, 234-240 (2007).
224. Blodgett, D. M. & Carruthers, A. Quench-Flow Analysis Reveals Multiple Phases of GluT1-Mediated Sugar Transport. *Biochemistry* **44**, 2650-2660 (2005).
225. Carruthers, A. Mechanisms for the facilitated diffusion of substrates across cell membranes. *Biochemistry* **30**, 3898-3906 (1991).
226. Cloherty, E. K., Heard, K. S. & Carruthers, A. Human erythrocyte sugar transport is incompatible with available carrier models. *Biochemistry* **35**, 10411-10421 (1996).
227. Helgerson, A. L. & Carruthers, A. Equilibrium ligand binding to the human erythrocyte sugar transporter. Evidence for two sugar-binding sites per carrier. *J Biol Chem* **262**, 5464-5475 (1987).
228. Hamill, S., Cloherty, E. K. & Carruthers, A. The human erythrocyte sugar transporter presents two sugar import sites. *Biochemistry* **38**, 16974-16983 (1999).
229. Cloherty, E. K., Levine, K. B. & Carruthers, A. The red blood cell glucose transporter presents multiple, nucleotide-sensitive sugar exit sites. *Biochemistry* **40**, 15549-15561 (2001).
230. Helgerson, A. L., Hebert, D. N., Naderi, S. & Carruthers, A. Characterization of two independent modes of action of ATP on human erythrocyte sugar transport. *Biochemistry* **28**, 6410-6417 (1989).
231. Lacko, L., Wittke, B. & Kromphardt, H. *Eur J Biochem* **25**, 447-454 (1972).
232. Craik, J. D., Young, J. D. & Cheeseman, C. I. GLUT-1 mediation of rapid glucose transport in dolphin (Tursiops truncatus) red blood cells. *Am J Physiol* **274**, R112-9 (1998).
233. Helgerson, A. L. & Carruthers, A. Analysis of protein-mediated 3-O-methylglucose transport in rat erythrocytes: rejection of the alternating conformation carrier model for sugar transport. *Biochemistry* **28**, 4580-4594 (1989).
234. Levine, K. B., Robichaud, T. K., Hamill, S., Sultzman, L. A. & Carruthers, A. Properties of the human erythrocyte glucose transport protein are determined by cellular context. *Biochemistry* **44**, 5606-5616 (2005).
235. Liu, Q., Vera, J. C., Peng, H. & Golde, D. W. The predicted atp-binding domains in the hexose transporter glut1 critically affect transporter activity. *Biochemistry* **40**, 7874-781 (2001).
236. Leitch, J. M. & Carruthers, A. ATP-dependent sugar transport complexity in human erythrocytes. *Am J Physiol* **292**, C974-86 (2007).
237. Gould, G. W., Thomas, H. M., Jess, T. J. & Bell, G. I. Expression of human glucose transporters in Xenopus oocytes: kinetic characterization and substrate specificities of the erythrocyte, liver, and brain isoforms. *Biochemistry* **30**, 5139-5145 (1991).

238. Appleman, J. R. & Lienhard, G. E. Kinetics of the purified glucose transporter. Direct measurement of the rates of interconversion of transporter conformers. *Biochemistry* **28**, 8221-8227 (1989).
239. Naftalin, R. J. Alternating Carrier Models of Asymmetric Glucose Transport Violate the Energy Conservation Laws. *Biophys J* **95**, 4300-4314 (2008).
240. Carruthers, A., Dezutter, J., Ganguly, A. & Devaskar, S. U. "Will the Original Glucose Transporter Isoform Please Stand Up!" *Am J Physiol Endocrinol Metab* **297**, E836-848. (2009).
241. Uchida, Y., Ohtsuki, S., Katsukura, Y., Ikeda, C., Suzuki, T., Kamiie, J. & Terasaki, T. Quantitative targeted absolute proteomics of human blood-brain barrier transporters and receptors. *J Neurochem* **117**, 333-45 (2011).
242. Takata, K., Kasahara, T., Kasahara, M., Ezaki, O. & Hirano, H. Erythrocyte/HepG2-type glucose transporter is concentrated in cells of blood-tissue barriers. *Biochem Biophys Res Commun* **173**, 67-73 (1990).
243. Knott R. M., Grant G., Bardocz S., Pusztai A., de Carvalho A. F., & Hesketh J. E. Alterations in the level of insulin receptor and GLUT-4 mRNA in skeletal muscle from rats fed a kidney bean (Phaseolus vulgaris) diet. *Intl J Biochem* **24**, 897-902 (1992).
244. Zhao, F. Q., Glimm, D. R. & Kennelly, J. J. Distribution of mammalian facilitative glucose transporter messenger RNA in bovine tissues. *Int J Biochem* **25**, 1897-1903 (1993).
245. Shepherd, P. R., Gould, G. W., Colville, C. A., McCoid, S. C., Gibbs, E. M. & Kahn, B. B. Distribution of GLUT3 glucose transporter protein in human tissues. *Biochem Biophys Res Commun* **188**, 149-154 (1992).
246. Haber, R. S., Weinstein, S. P., O'Boyle, E. & Morgello, S. Tissue distribution of the human GLUT3 glucose transporter. *Endocrinology* **132**, 2538-2543 (1993).
247. Huang, S. & Czech, M. P. The GLUT4 glucose transporter. *Cell Metab* **5**, 237-252 (2007).
248. Haney, P. M., Slot, J. W., Piper, R. C., James, D. E. & Mueckler, M. Intracellular targeting of the insulin-regulatable glucose transporter (GLUT4) is isoform specific and independent of cell type. *J Cell Biol* **114**, 689-699 (1991).
249. Slot, J. W., Geuze, H. J., Gigengack, S., James, D. E. & Lienhard, G. E. Translocation of the glucose transporter GLUT4 in cardiac myocytes of the rat. *Proc Natl Acad Sci USA* **88**, 7815-7819 (1991).
250. Miller, C. Pretty structures, but what about the data? *Science* **315**, 459 (2007).
251. Miller, G. Scientific publishing. A scientist's nightmare: software problem leads to five retractions. *Science* **314**, 1856-1857 (2006).
252. Mueckler, M., Caruso, C., Baldwin, S. A., Panico, M., Blench, I., Morris, H. R., Allard, W. J., Lienhard, G. E. & Lodish, H. F. Sequence and structure of a human glucose transporter. *Science* **229**, 941-945 (1985).

253. Ploug, T., van Deurs, B., Ai, H., Cushman, S. W. & Ralston, E. Analysis of GLUT4 distribution in whole skeletal muscle fibers: identification of distinct storage compartments that are recruited by insulin and muscle contractions. *J Cell Biol* **142**, 1429-1446 (1998).
254. Robinson, L. J., Pang, S., Harris, D. S., Heuser, J. & James, D. E. Translocation of the glucose transporter (GLUT4) to the cell surface in permeabilized 3T3-L1 adipocytes: effects of ATP insulin, and GTP gamma S and localization of GLUT4 to clathrin lattices. *J Cell Biol* **117**, 1181-1196 (1992).
255. Sargeant, R. J. & Paquet, M. R. Effect of insulin on the rates of synthesis and degradation of GLUT1 and GLUT4 glucose transporters in 3T3-L1 adipocytes. *Biochem J* (1993).
256. Kohn, A. D., Summers, S. A., Birnbaum, M. J. & Roth, R. A. Expression of a constitutively active Akt Ser/Thr kinase in 3T3-L1 adipocytes stimulates glucose uptake and glucose transporter 4 translocation. *J Biol Chem* **271**, 31372-31378 (1996).
257. Emoto, M., Langille, S. E. & Czech, M. P. A role for kinesin in insulin-stimulated GLUT4 glucose transporter translocation in 3T3-L1 adipocytes. *J Biol Chem* **276**, 10677-10682 (2001).
258. Harrison, S. A., Buxton, J. M., Clancy, B. M. & Czech, M. P. Insulin regulation of hexose transport in mouse 3T3-L1 cells expressing the human HepG2 glucose transporter. *J Biol Chem* **265**, 20106-20116 (1990).
259. Livak, K. J. & Schmittgen, T. D. Analysis of relative gene expression data using real-time quantitative PCR and the 2(-Delta Delta C(T)) Method. *Methods* **25**, 402-408 (2001).
260. Green, H. & Meuth, M. An established pre-adipose cell line and its differentiation in culture. *Cell* **3**, 127-133 (1974).
261. Green, H. & Kehinde, O. An established preadipose cell line and its differentiation in culture. II. Factors affecting the adipose conversion. *Cell* **5**, 19-27 (1975).
262. Baker, G. F. & Widdas, W. F. The asymmetry of the facilitated transfer system for hexoses in human red cells and the simple kinetics of a two component model. *J Physiol* **231**, 143-165 (1973).
263. Calderhead, D. M., Kitagawa, K., Tanner, L. I., Holman, G. D. & Lienhard, G. E. Insulin regulation of the two glucose transporters in 3T3-L1 adipocytes. *J Biol Chem* **265**, 13801-13808 (1990).
264. Asano, T., Shibasaki, Y., Ohno, S., Taira, H., Lin, J. L., Kasuga, M., Kanazawa, Y., Akanuma, Y., Takaku, F. & Oka, Y. Rabbit brain glucose transporter responds to insulin when expressed in insulin-sensitive Chinese hamster ovary cells. *J Biol Chem* **264**, 3416-3420 (1988).

265. Tordjman, K. M., Leingang, K. A. & Mueckler, M. Differential regulation of the HepG2 and adipocyte/muscle glucose transporters in 3T3L1 adipocytes. Effect of chronic glucose deprivation. *Biochem J* **271**, 201-207 (1990).
266. Harrison, S. A., Buxton, J. M. & Czech, M. P. Suppressed intrinsic catalytic activity of GLUT1 glucose transporters in insulin-sensitive 3T3-L1 adipocytes. *Proc Natl Acad Sci USA* **88**, 7839-7843 (1991).
267. Mann, G. E., Yudilevich, D. L. & Sobrevia, L. Regulation of amino acid and glucose transporters in endothelial and smooth muscle cells. *Physiol Rev S* **83**, 183-252 (2003).
268. Harik, S. I., Kalaria, R. N., Andersson, L., Lundahl, P. & Perry, G. Immunocytochemical localization of the erythroid glucose transporter: abundance in tissues with barrier functions. *J Neurosci* **10**, 3862-3872 (1990).
269. Thorens, B. & Mueckler, M. Glucose transporters in the 21st Century. *Am J Physiol Endocrinol Metab* **298**, E141-5 (2010).
270. Cushman, S. W. & Wardzala, L. J. Potential mechanism of insulin action on glucose transport in the isolated rat adipose cell. *J Biol Chem* **255**, 4755-4762 (1980).
271. Boado, R. J. Brain-derived peptides regulate the steady state levels and increase stability of the blood-brain barrier GLUT1 glucose transporter mRNA. *Neurosci Lett* **197**, 179-182 (1995).
272. Hellwig, B. & Joost, H. G. Differentiation of erythrocyte-(GLUT1), liver-(GLUT2), and adipocyte-type (GLUT4) glucose transporters by binding of the inhibitory ligands cytochalasin B, forskolin, dipyridamole, and isobutylmethylxanthine. *Mol Pharmacol* **40**, 383-389 (1991).
273. Lieb, W. R. & Stein, W. D. Testing and characterizing the simpler pore. *Biochim Biophys Acta* **373**, 165-177 (1974).
274. Huang, Y., Lemieux, M. J., Song, J., Auer, M. & Wang, D. N. Structure and mechanism of the glycerol-3-phosphate transporter from Escherichia coli. *Science* **301**, 616-620 (2003).
275. Seatter, M. J., De la Rue, S. A., Porter, L. M. & Gould, G. W. QLS motif in transmembrane helix VII of the glucose transporter family interacts with the C-1 position of D-glucose and is involved in substrate selection at the exofacial binding site. *Biochemistry* **37**, 1322-1326 (1998).
276. Baldwin, S. A., Baldwin, J. M., Gorga, F. R. & Lienhard, G. E. Purification of the cytochalasin B binding component of the human erythrocyte monosaccharide transport system. *Biochim Biophys Acta* **552**, 183-188 (1979).
277. Sogin, D. C. & Hinkle, P. C. Binding of cytochalasin B to human erythrocyte glucose transport. *Biochemistry* **19**, 5417–5420 (1980).
278. Bissonnette, P., Gagne, H., Blais, A. & Berteloot, A. 2-Deoxyglucose transport and metabolism in Caco-2 cells. *Am J Physiol* **270**, G153-62 (1996).

279. Naftalin, R. J. & Rist, R. J. 3-O-methyl-D-glucose transport in rat red cells: effects of heavy water. *Biochim Biophys Acta* **1064**, 37-48 (1991).
280. Lieb, W. R. & Stein, W. D. Testing and characterizing the simple carrier. *Biochim Biophys Acta* **373**, 178–196 (1974).
281. Baker, P. F. & Carruthers, A. 3-O-methylglucose transport in internally dialysed giant axons of Loligo. *J Physiol* **316**, 503-525 (1981).
282. Naftalin, R. J. Pre-steady-state uptake of D-glucose is inconsistent with a circulating carrier mechanism. *Biochim Biophys Acta* **946**, 431-438 (1988).
283. Maher, F., Davies-Hill, T. M. & Simpson, I. A. Substrate specificity and kinetic parameters of GLUT3 in rat cerebellar granule neurons. *Biochem J* **315**, 827-831 (1996).
284. Takata, K., Kasahara, T., Kasahara, M., Ezaki, O. & Hirano, H. Ultracytochemical localization of the erythrocyte/HepG2-type glucose transporter (GLUT1) in cells of the blood-retinal barrier in the rat. *Invest Ophth Vis Sci* **33**, 377-383 (1992).
285. Colville, C. A., Seatter, M. J., Jess, T. J., Gould, G. W. & Thomas, H. M. Kinetic analysis of the liver-type (GLUT2) and brain-type (GLUT3) glucose transporters in Xenopus oocytes: substrate specificities and effects of transport inhibitors. *Biochem J* 701-706 (1993).
286. Marette, A., Burdett, E., Douen, A., Vranic, M. & Klip, A. Insulin induces the translocation of GLUT4 from a unique intracellular organelle to transverse tubules in rat skeletal muscle. *Diabetes* **41**, 1562-1569 (1992).
287. Palfreyman, R. W., Clark, A. E., Denton, R. M., Holman, G. D. & Kozka, I. J. Kinetic resolution of the separate GLUT1 and GLUT4 glucose transport activities in 3T3-L1 cells. *Biochem J* (1992).
288. Vollers, S. S. & Carruthers, A. Sequence Determinants of GLUT1-mediated Accelerated-Exchange Transport - Analysis by Homology-Scanning Mutagenesis. *J Biol Chem* (2012).
289. Katagiri, H., Asano, T., Ishihara, H., Tsukuda, K., Lin, J. L., Inukai, K., Kikuchi, M., Yazaki, Y. & Oka, Y. Replacement of intracellular C-terminal domain of GLUT1 glucose transporter with that of GLUT2 increases Vmax and Km of transport activity. *J Biol Chem* **267**, 22550-22555 (1992).
290. Simpson, I. A., Dwyer, D., Malide, D., Moley, K. H., Travis, A. & Vannucci, S. J. The facilitative glucose transporter GLUT3: 20 years of distinction. *Am J Physiol Endocrinol Metab* **295**, E242-253 (2008).
291. Oka, Y., Asano, T., Shibasaki, Y., Lin, J. L., Tsukuda, K., Katagiri, H., Akanuma, Y. & Takaku F. C-terminal truncated glucose transporter is locked into an inward-facing form without transport activity. *Nature* **345**, 550-553 (1990).
292. Johnson, J. H., Newgard, C. B., Milburn, J. L., Lodish, H. F. & Thorens, B. The high Km glucose transporter of islets of Langerhans is functionally similar to the

low affinity transporter of liver and has an identical primary sequence. *J Biol Chem* **265**, 6548-6551 (1990).
293. Dauterive, R., Laroux, S., Bunn, R. C., Chaisson, A., Sanson,T. & Reed, B. C. C-terminal mutations that alter the turnover number for 3-O-methylglucose transport by GLUT1 and GLUT4. *J Biol Chem* **271**, 11414-11421 (1996).
294. Due, A. D., Qu, Z. C., Thomas, J. M., Buchs, A., Powers, A. C. & May, J. M. Role of the C-terminal tail of the GLUT1 glucose transporter in its expression and function in Xenopus laevis oocytes. *Biochemistry* **34**, 5462-71 (1995).
295. Dimmer, K. S., Friedrich, B., Lang, F., Deitmer, J. W. & Broer, S. The low-affinity monocarboxylate transporter MCT4 is adapted to the export of lactate in highly glycolytic cells. *Biochem J* **350 Pt 1**, 219-227 (2000).
296. Manoharan, C., Wilson, M. C., Sessions, R. B. & Halestrap, A. P. The role of charged residues in the transmembrane helices of monocarboxylate transporter 1 and its ancillary protein basigin in determining plasma membrane expression and catalytic activity. *Mol Membr Biol* **23**, 486-498 (2006).
297. Wilson, M. C., Meredith, D., Bunnun, C., Sessions, R. B. & Halestrap, A. P. Studies on the DIDS-binding site of monocarboxylate transporter 1 suggest a homology model of the open conformation and a plausible translocation cycle. *J Biol Chem* **284**, 20011-20021 (2009).
298. Kirk, P., Wilson, M. C., Heddle, C., Brown, M. H., Barclay, A. N. & Halestrap, A. P. CD147 is tightly associated with lactate transporters MCT1 and MCT4 and facilitates their cell surface expression. *EMBO J* **19**, 3896-3904 (2000).
299. Wilson, M. C., Meredith, D. & Halestrap, A. P. Fluorescence resonance energy transfer studies on the interaction between the lactate transporter MCT1 and CD147 provide information on the topology and stoichiometry of the complex in situ. *J Biol Chem* **277**, 3666-3672 (2002).
300. Halestrap, A. P. The monocarboxylate transporter family--Structure and functional characterization. *IUBMB Life* **64**, 1-9 (2012).

APPENDIX

Table A1 Primers Used in Molecular Cloning and Mutant Construct Creation

Construct	Primer(s)
WT GLUT1 5'FWD EcoRV	CGATATCATGGAGCCCAGCAGCAAG
WT GLUT1 3'REV Not1	AGCGGCCGCTCATCACACTTGGGAATC
GLUT1 myc 5'FWD	GAGCAAAAGCTTATTTCTGAAGAGGACTTGCTGCCCACCACGCTCACC
GLUT1 myc 3'REV	CAAGTCCTCTTCAGAAATAAGCTTTTGCTCGATGCTCTCCCCATAGCG
WT GLUT4 5'FWD EcoRV	CGATATCATGCCGTCGGGCTTC
WT GLUT4 3'REV Not1	AGCGGCCGCTCATCAGTCGTTCTCATC
GLUT4 myc 5'FWD	GAGCAAAAGCTTATTTCTGAAGAGGACTTGCCTCCAGGCACCCTCACC
GLUT4 myc 3'REV	CAAGTCCTCTTCAGAAATAAGCTTTTGCTCGATGGAGCTGGGTCCCTC
GLUT4 F5A Quick Change 5'FWD	GCAGATATGCCGTCGGGCGCCCAACAGATAGGCTCCGAAGATGGG
GLUT4 LL489/490AA Quick Change 5'FWD	CCTTCCACCGGACACCCTCTGCTGCAGAGCAGGAGGTGAAACCC
GLUT4 F5A 5'FWD EcoRV	CGATATCATGCCGTCGGGCGCC
11(1)44 5'FWD	CTGGAGCTGTTCCGCTCCCCCACCCA WT GLUT1 5'FWD EcoRV
11(1)44 3'REV	GATCAGGGGCTGCCGGTGGGTGGGG WT GLUT4 3'REV Not1
11(4)44 5'FWD	TGCATCGTGCTGCCCTTCTGCCCCGA WT GLUT1 5'FWD EcoRV
11(4)44 3'REV	GAGGTAGCGGGGGCTCTCGGGGCAG WT GLUT4 3'REV Not1
44(1)11 5'FWD	CTGGTCCTGCTGCCCTTCTGTCCCGA GLUT4 F5A 5'FWD EcoRV
44(1)11 3'REV	CAGGAAGCGGGGACTCTCGGGACAG WT GLUT1 3'REV Not1
44(6)11 5'FWD	CTCCAGCTCCTGGGCAGCCGTGCCT GLUT4 F5A 5'FWD EcoRV
44(6)11 3'REV	GAGGATGGGCTGGCGGTAGGCACGG WT GLUT1 3'REV Not1
1444 5'FWD	TCGAAACTGGGCAAGTCCTTTGAAAT WT GLUT1 5'FWD EcoRV
1444 3'REV	TCGTCCAAGGATGAGCATTTCAAAGG WT GLUT4 3'REV Not1
4111 5'FWD	GCCAATGCTGCTGCCTCCTATGAGAT GLUT4 F5A 5'FWD EcoRV

4111 3’REV	GCGGCCCAGGATCAGCATCTCATAG WT GLUT1 3’REV Not1
1411 5’FWD	WT GLUT1 5’FWD EcoRV 1444 5’FWD 44(1)11 5’FWD
1411 3’REV	1444 3’REV 44(1)11 3’REV WT GLUT1 3’REV Not1
4144 5’FWD	GLUT4 F5A 5’FWD EcoRV 4111 5’FWD 11(4)44 5’FWD
4144 3’REV	4111 3’REV 11(4)44 3’REV WT GLUT4 3’REV Not1
G4 (4/5) 5’FWD	GLUT4 F5A 5’FWD EcoRV 4111 5’FWD ATGGGCAACAAGGACCTGTGGCCAC
G4 (4/5) 3’REV	4111 3’REV TGTGAGGCCCAGGAGCAGTGGCCAC WT GLUT4 3’REV Not1
G4 (5/6) 5’FWD	GLUT4 F5A 5’FWD EcoRV GTGGGGGAGATTGCTCCCACTGCCC 11(4)44 5’FWD
G4 (5/6) 3’REV	GCCCAGGGCCCCACGAAGGGCAGTG 11(4)44 3’REV WT GLUT4 3’REV Not1
G4 (5) 5’FWD	GLUT4 F5A 5’FWD EcoRV G4 (5/6) 5’FWD G4 (4/5) 5’FWD
G4 (5) 3’REV	G4 (5/6) 3’REV G4 (4/5) 3’REV WT GLUT4 3’REV Not1
G4 (6) 5’FWD	GLUT4 F5A 5’FWD EcoRV CTGGGCACTGCCAGCCTGTGGCCCC 11(4)44 5’FWD
G4 (6) 3’REV	GATGATGCTCAGCAGCAGGGGCCAC 11(4)44 3’REV WT GLUT4 3’REV Not1
G1 (6) 5’FWD	WT GLUT1 5’FWD EcoRV G4 (4/5) FWD 44(1)11 5’FWD
G1 (6) 3’REV	G4 (4/5) 3’REV 44(1)11 3’REV WT GLUT1 3’REV Not1
GLUT1 SIIFI 191-195 GLTVL Quick Change 5’FWD	TGGCCCCTGCTGCTGGGCCTCACAGTGCTACCGGCCCTGCTG
GLUT1 CIV 202-204 LVL Quick Change 5’FWD	CCGGCCCTGCTGCAGCTGGTCCTGCTGCCCTTCTGTCCC
GLUT4 GLTVL 208-212 SIIFI Quick Change 5’FWD	TGGCCACTGCTCCTGAGCATCATCTTCATCCCTGCCCTCCTGCAGC
GLUT4 LVL 218-220 CIV Quick Change 5’FWD	CCTGCCCTCCTGCAGTGCATCGTGCTGCCCTTCTGTCCC
GLUT2 5’FWD EcoRV	CGATATCATGACAGAAGATAAGGTC

GLUT2 3‘REV Not1	AGCGGCCGCTCATTACACAGTCTCTGT
GLUT2 myc 3’REV	CAAGTCCTCTTCAGAAATAAGCTTTTGCTCATGTCTATAGTGAGA
GLUT2 myc 5’FWD	GAGCAAAAGCTTATTTCTGAAGAGGACTTGGTTTTGGGTGTTCC ACTG
GLUT2 cG1 5’FWD	ACCAAAGGAAAGTCTTTTGAGGAGATCGCTTCCGGCTT
GLUT2 cG1 3‘REV Not1	AAGCCGGAAGCGATCTCCTCAAAAGACTTTCCTTTGGT
WT GLUT3 5’FWD BamH1	CGGATCCATGGGGACACAGAAGGTC
WT GLUT3 3‘REV Not1	AGCGGCCGCTCATTAGACATTGGTGGT
GLUT3 myc 3‘REV	CAAGTCCTCTTCAGAAATAAGCTTTTGCTCCTTGTCCGTCAAAGT
GLUT3 myc 5’FWD	GAGCAAAAGCTTATTTCTGAAGAGGACTTGGGAAATGCCCCACC CTCT
GLUT3 cG1 5’FWD	ACCCGTGGCAGGACTTTTGAGGAGATCGCTTCCGGCTT
GLUT3 cG1 3‘REV Not1	AAGCCGGAAGCGATCTCCTCAAAAGTCCTGCCACGGGT
GLUT2 GLSGV 223-227 SIIFI/SLL 233-235 CIV 5‘FWD EcoRV	AGCATCATCTTCATCAGGGCTATTCTACAATGCATCGTGCTCTTTT TCTGTCCAGAA
GLUT2 GLSGV 223-227 SIIFI/SLL 233-235 CIV 3‘REV Not1	CACGATGCATTGTAGAATAGCCCTGATGAAGATGATGCTAAGCAG GATGTGCCA
GLUT2 GLSGV 223-227 GFTIL/SLL 233-235 SAA 5‘FWD EcoRV	GGTTTTACCATCCTTAGGGCTATTCTACAAAGTGCAGCCCTCTTTT TCTGTCCAGAA
GLUT2 GLSGV 223-227 GFTIL/SLL 233-235 SAA 3‘REV Not1	GGCTGCACTTTGTAGAATAGCCCTAAGGATGGTAAAACCAAGCA GGATGTGCCA
GLUT3 GFTIL 189-193 GLSGV/SAA 199-201 SLL 5‘FWD BamHI	GGCCTGTCTGGTGTGCCAGCAATTTTGCAGTCTCTGCTACTTCCA TTTTGCCCTGAA
GLUT3 GFTIL 189-193 GLSGV/SAA 199-201 SLL 3‘REV Not1	TAGCAGAGACTGCAAAATTGCTGGCACACCAGACAGGCCCAGTA GCAGCGGCCA
GLUT3 GFTIL 189-193 GLTVL/SAA 199-201 LVL 5‘FWD BamHI	GGCCTCACAGTGCTACCAGCAATTTTGCAGCTGGTCCTGCTTCCA TTTTGCCCTGAA
GLUT3 GFTIL 189-193 GLTVL/SAA 199-201 LVL 3‘REV Not1	CAGGACCAGCTGCAAAATTGCTGGTAGCACTGTGAGGCCCAGTA GCAGCGGCCA

Table A2 Primers Used in Genomic/RT-PCR and Q-PCR GLUT Screens

Mouse GLUT1 RT 5'FWD	GAACCTGTTGGCCTTTGTGGC
Mouse GLUT1 RT 3'REV	GCTGGCGGTAGGCGGGTGAGCG
Mouse GLUT4 RT 5'FWD	TGCAACGTGGCTGGGTAGGC
Mouse GLUT4 RT 3'REV	AGGGAGTACTGTGAGAGCCAG
Mouse GLUT1 Q 5'FWD	AGCCCTGCTACAGTGTAT
Mouse GLUT1 Q 3'REV	AGGTCTCGGGTCACATC
Mouse EIF1α	CAACATCGTCGTAATCGGACA
Mouse EIF1α	GCTTAAGACCCAGGCGTACTT
Human GLUT Genomic/RT- and Q-PCR Primers	
GLUT1 RT 5'FWD	GCGGAATTCAATGCTGATGA
GLUT1 RT 3'REV	TCTTGGCCCGGTTCTCCTCG
GLUT2 RT 5'FWD	TACCTTTACATCAAGTTAGA
GLUT2 RT 3'REV	TAGAATAGGCTGTCGGTAGC
GLUT3 RT 5'FWD	CTGCGGACTCTGCACAGGTT
GLUT3 RT 3'REV	TTTCTGTTAATGAGCAAAAA
GLUT4 RT 5'FWD	CCCCGCCCGGCAGCCATGGC
GLUT4 RT 3'REV	AGAGAGGGTGTCCGGTGGAA
GLUT5 RT 5'FWD	AGGCTGACGCTTGTGCTTGC
GLUT5 RT 3'REV	TGCCAAATTTATTCACCAAG
GLUT6 RT 5'FWD	AGGGGCGGAGCCTGGCCGGT
GLUT6 RT 3'REV	AGACCAGGGCATACCCAAAG
GLUT7 RT 5'FWD	AAAGGGGACCCTGCTGATCA
GLUT7 RT 3'REV	CCGGGTTGCCCAAGATGGCC
GLUT8 RT 5'FWD	CGCGCCCCGCGGCCGCCGCG
GLUT8 RT 3'REV	AGGCTCAGCTTGCGCCCGGC
GLUT9 RT 5'FWD	GGTTTGGTCATTGAGCACCT
GLUT9 RT 3'REV	CTGGCCCACTGCAGAAAGAG
GLUT10 RT 5'FWD	CTGGAGACTCTGGCCTGCTG
GLUT10 RT 3'REV	CCAGTTGAAGCTGTTGCAGA
GLUT11 RT 5'FWD	GTGTGAGCATGAACATCCAG

GLUT11 RT 3’REV	GGGAGGCGAGCTGGAGCGCC
GLUT12 RT 5’FWD	TAACTTCTAGCATGAACTGG
GLUT12 RT 3’REV	TATAAACATAACAACAAAAA
GLUT13 RT 5’FWD	CAGGTGTGAAAATGAAACCA
GLUT13 RT 3’REV	ATACTCTGCTGTGTGTAAAA
GLUT1 Q 5’FWD	ATCGTGGCCATCTTTGGCTTTGTG
GLUT1 Q 3’REV	CTGGAAGCACATGCCCACAATGAA
GLUT3 Q 5’FWD	AGCTCTCTGGGATCAATGCTGTGT
GLUT3 Q 3’REV	ATGGTGGCATAGATGGGCTCTTGA
GLUT4 Q 5’FWD	AAGAATCCCTGCAGCCTGGTAGAA
GLUT4 Q 3’REV	CCACGGCCAAACCACAACACATAA
GLUT6 Q 5’FWD	GCTCGGCAATTTCAGCTTTGGGTA
GLUT6 Q 3’REV	TGGGATTTGGTCAGATGCAGGTCA
GLUT8 Q 5’FWD	AGGGTTTATTCCCATCACTGCCCA
GLUT8 Q 3’REV	TGAGCCCAAGGAAGTAGCCAGAAA
GLUT9 Q 5’FWD	TTCTGGCCATCATCGCCTCTTTCT
GLUT9 Q 3’REV	GTTGACGGTGCCTGCAATGATGAA
GLUT10 Q 5’FWD	AAGAGACGGTTCACCCTGAGCTTT
GLUT10 Q 3’REV	TCCAGAATTTCCAGGCAGACGGAT
GAPDH Q 5’FWD	GAAGGTGAAGGTCGGAGTC
GAPDH Q 3’REV	GAAGATGGTGATGGGATTTC
GLUT1MYC 114 Q 5’FWD	GGTGATCGAGGAGTTCTACAACCAGA
GLUT1MYC 278 Q 3’REV	ACAGAGAAGGAGCCAATCATGC
GLUT4MYC 158 Q 5’FWD	AACAGAGCTACAATGAGACGTGGCTG
GLUT4MYC 355 Q 3’REV	TCCTTCCAAGCCACTGAGAGATGA

Table A3 Calculated Product Size of Human GLUT-Specific Genomic Primers in PCR Screening of Genomic DNA and RT-PCR Screening of RNA

GLUT	Genomic DNA Product Size (bp)	RT-PCR Product Size (bp)	mRNA Detection
1	990	400	Y
2	652	184	
3	862/850	242	Y
4	657	223	Y
5	802	259	
6	817	267	?
7	1107	275	
8	609/998	248	Y
9	3145	422	
10	882	343	Y
11	758	210	
12	4824	142	?
13	4379/386	265	
14	1130	173	?

All product sizes indicated are based on primers reported in Appendix Table A2. For transporters with extremely faint product bands (Appendix Figure A3.1) or inability to verify primers via genomic DNA PCR screening, specific qPCR primers were designed (Table A2) and these transporters were included in qPCR analysis of HEK endogenous transporter expression (Figure 3.2).

Table A4 Calculated Molecular Weight and Isoelectric Point of Chimeras

Construct	Calculated MW (Da)	Calculated PI
GLUT1	54084	8.93
GLUT1myc	54787	6.47
GLUT4	55269	8.43
GLUT4myc	55973	5.75
GLUT4myc-3x	55812	5.75
44(1)11	56114	5.94
11(1)44	55204	7.65
44(4)11	55877	6.05
11(4)44	54968	8.19
1444	54728	8.33
4111	56353	5.94
1411	55030	8.55
4144	56052	5.75
GLUT4 (4,5 G1)	55972	5.75
GLUT4 (5,6 G1)	55957	5.75
GLUT4 (5, G1)	55877	5.75
GLUT4 (6, G1)	55892	5.75
GLUT1 (6, G4)	55189	8.48

Molecular weight and isoelectric point were calculated for each chimera sequence using the Bioinformatics Resource Portal ExPASy calculator (http://web.expasy.org/compute_pi/).

A

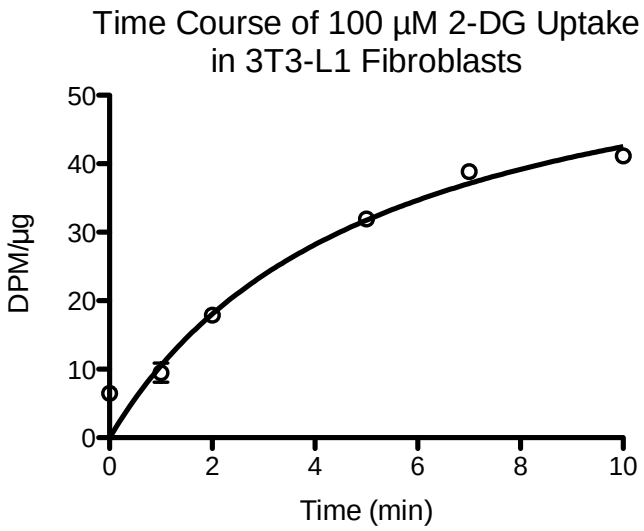
Time Course of 100 µM 2-DG Uptake
in 3T3-L1 Fibroblasts
DPM/µg
50
40
30
20
10
0
0
2
4
6
8
10
Time (min)

B

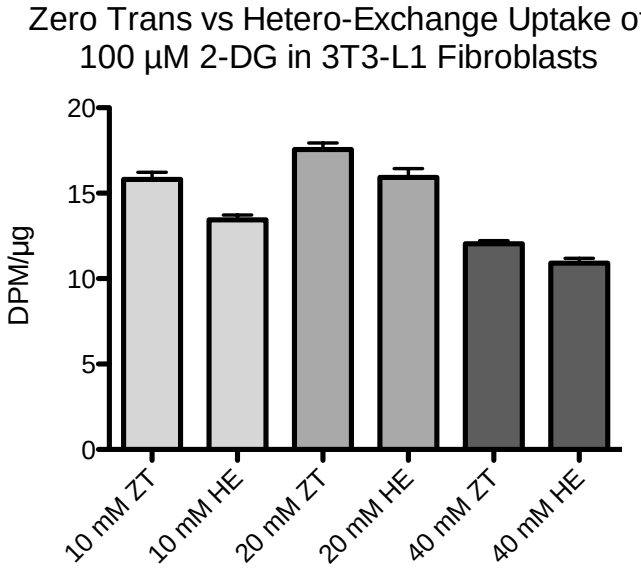
Zero Trans vs Hetero-Exchange Uptake of
100 µM 2-DG in 3T3-L1 Fibroblasts
DPM/µg
20
15
10
5
0
10 mM ZT
10 mM HE
20 mM ZT
20 mM HE
40 mM ZT
40 mM HE

Figure A3.1 Analysis of hetero-exchange uptake in 3T3-L1 Fibroblasts

A, Time course of 100 μM 2-DG uptake in 3T3-L1 fibroblasts at 37ºC. Amount of uptake of ^{3}[H]-2-DG was corrected for background, normalized to total protein concentration (*ordinate*) and plotted for the length of time of uptake (*abscissa*). Data are plotted as mean ± SEM for n=2 assays. Curves drawn through the data were computed by nonlinear regression assuming that uptake is described by Equation 2.1, with $R^2 = 0.9577$. *B*, Comparison of zero-trans and hetero-exchange uptake of 100 μM 2-DG from medium containing 10-40 mM 3-MG, normalized to total protein concentration (*ordinate*) in fibroblasts pre-loaded with 10-40 mM 3-MG (*abscissa*). Data are plotted as mean ± SEM for n=2 assays. Uptake was performed at 3 minutes at 37ºC.

A

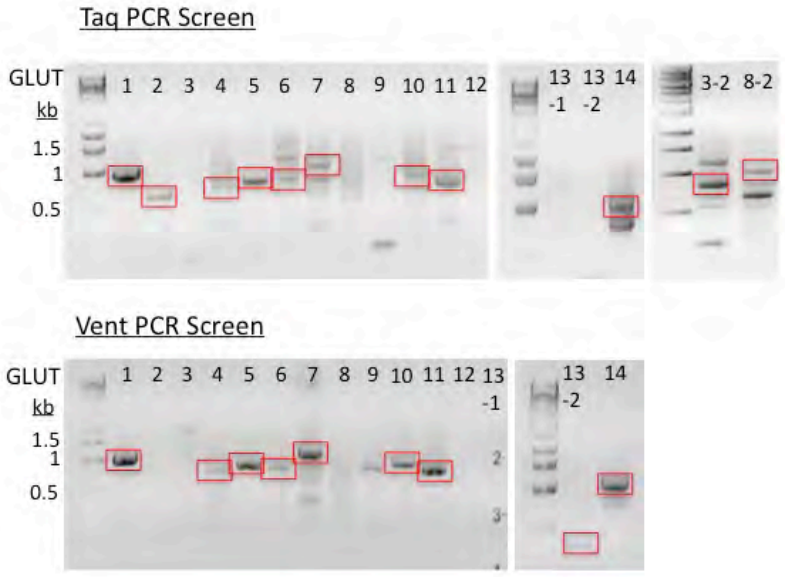
Taq PCR Screen
GLUT
kb
1.5
1
0.5
1 2 3 4 5 6 7 8 9 10 11 12
13 13 14
-1 -2
3-2 8-2
Vent PCR Screen
GLUT
kb
1.5
1
0.5
1 2 3 4 5 6 7 8 9 10 11 12 13
-1
2
3
13 14
-2

B

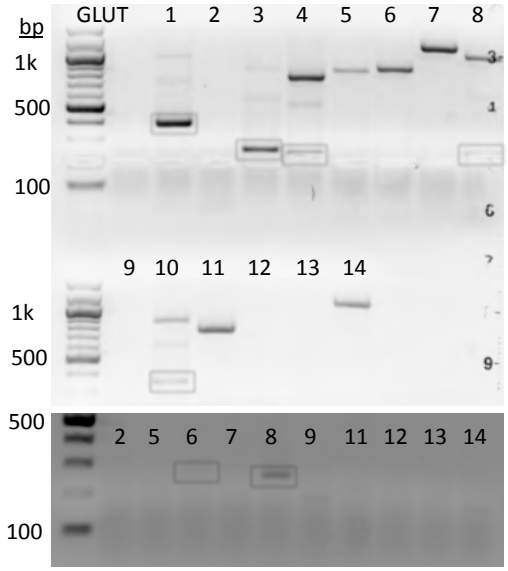
bp
1k
500
100
GLUT 1 2 3 4 5 6 7 8
9 10 11 12 13 14
1k
500
500
100
2 5 6 7 8 9 11 12 13 14

Figure A3.2 Primer verification and RT-PCR screen of GLUTs expressed in HEK cells

A, Genomic primers against all 14 GLUTs were designed such that a PCR screen of HEK genomic DNA would yield products of a large size for verification (Appendix Table A2). Genomic DNA was prepared according to the Qiagen Genomic DNA Purification kit and 1 μg DNA per reaction was analyzed by PCR using both Taq (top panel) and Vent (bottom panel) polymerases. Products were resolved on a 1.5% ethidium bromide gel and visualized by UV light. Target product size bands are boxed in red. *B*, The same primers verified in *A* were used to analyze HEK mRNA in an RT-PCR screen for smaller size products indicative of message (Table A2). HEK mRNA was isolated and prepared according to the Qiagen RNeasy kit. RT-PCR was performed according to the Qiagen One-Step RT-PCR kit using 1 μg RNA per reaction. Products were resolved on a 1.5% ethidium bromide gel and visualized by UV light. Target product size bands are boxed in red. In cases where large intron-exon spacing complicated the design of genomic primers, multiple primers were tested (i.e. GLUT13). Any RT-PCR products detected in *B* were then screened by qPCR (Figure 3.2). In the case where a genomic primer could not be verified or detected in RT-PCR screens (i.e. GLUT12), this transporter was included in the qPCR analysis.

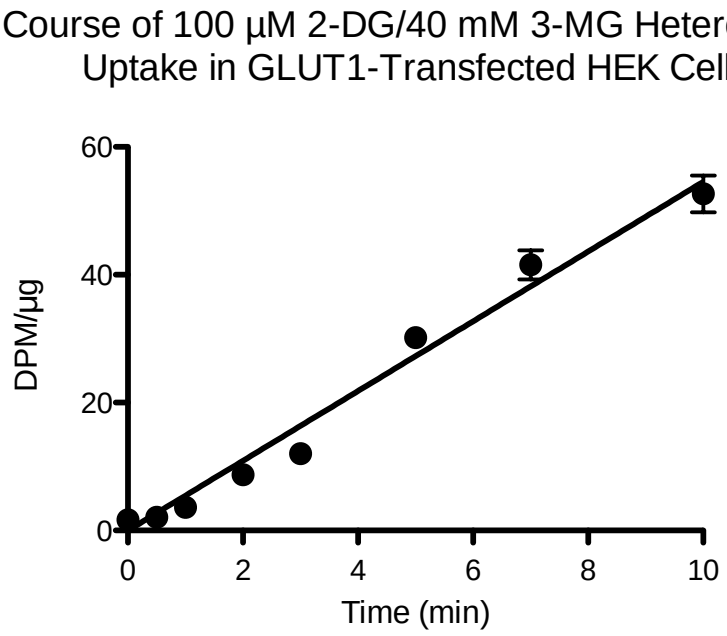

Figure A3.3 Time course of 2-DG/3-MG uptake under hetero-exchange conditions

Uptake of 100 µM 2-DG from medium containing 40 mM 3-MG in GLUT1-transfected HEK cells pre-loaded with 40 mM 3-MG. Uptake was corrected for background, mock-subtracted and normalized to total protein concentration (*ordinate*), and plotted for the length of time of uptake (*abscissa*). Lines drawn through the data were computed by linear regression. Data are plotted as mean ± SEM for n=3 assays.

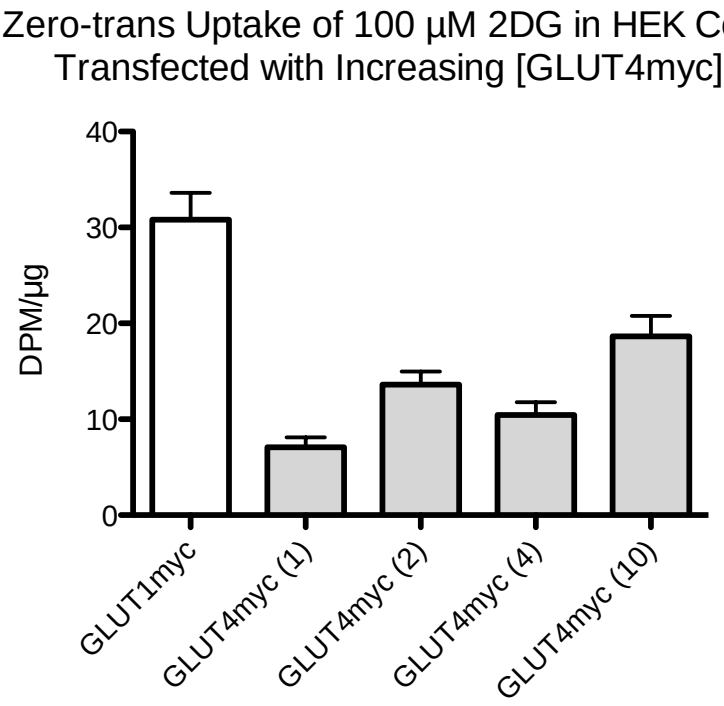

Figure A3.4 Sugar uptake in HEK cells transfected with increasing [GLUT4]

Zero-trans uptake of 100 µM 2-DG was corrected for background, mock-subtracted, normalized to total protein concentration (*ordinate*) and plotted for HEK cells transfected with 1, 2, 4, or 10 µg [GLUT4myc] DNA (*abscissa*). For reference, the standard amount of [GLUT1myc] transfected in all assays (2 µg) was included. Data are plotted as mean ± SEM for n=2 assays.

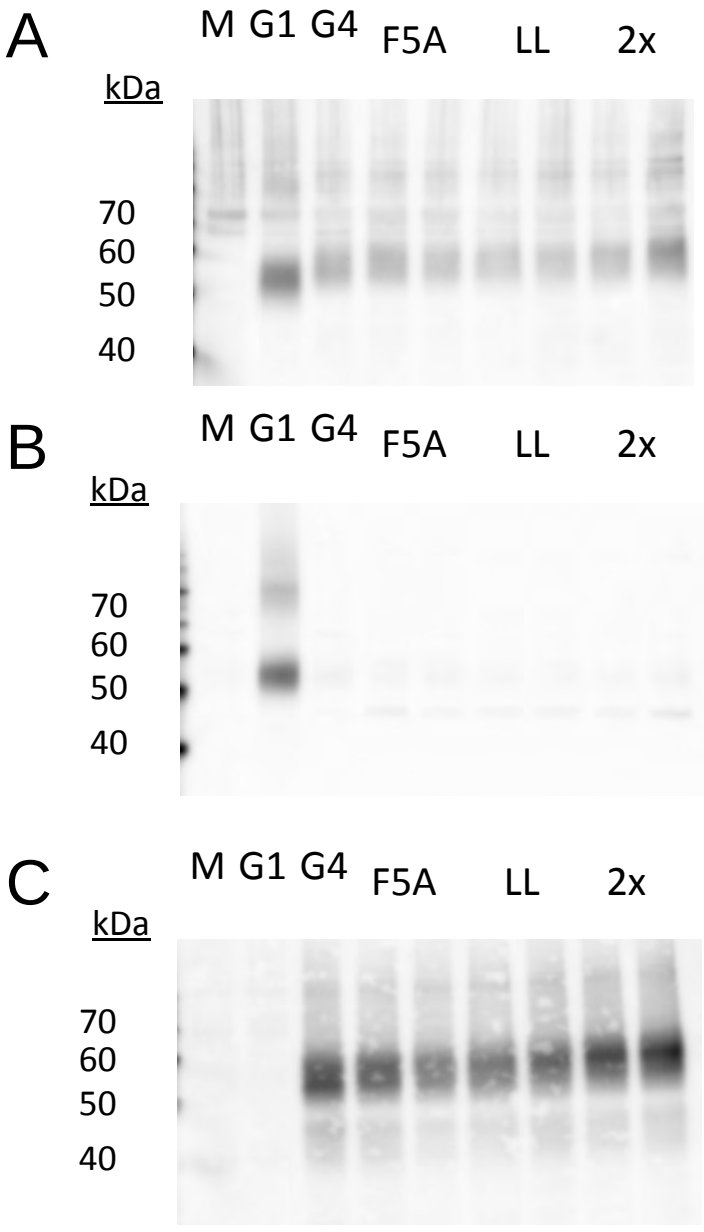
A
M G1 G4 F5A LL 2x
kDa
70
60
50
40
B
M G1 G4 F5A LL 2x
kDa
70
60
50
40
C
M G1 G4 F5A LL 2x
kDa
70
60
50
40

Figure A3.5 Verification of cell-surface expression of transporters with 3 mutations to GLUT4 localization motifs

HEK cells were either mock-transfected (M) or transfected with GLUT1myc (G1), GLUT4myc (G4), or 3 of the surface expression mutants of GLUT4myc (F5A, LL489-490AA (LL), or both mutations (2x)). Cells were biotinylated at 4ºC, and surface-labeled proteins were affinity-purified on streptavidin beads. Lysates were resolved by SDS-PAGE and blotted with anti-myc antibody (*A*). Both anti-GLUT1 C-terminal antibody (*B*) and anti-GLUT4 C-terminal antibody (*C*) were used to verify identity of the construct. Mobility of molecular weight standards is indicated.

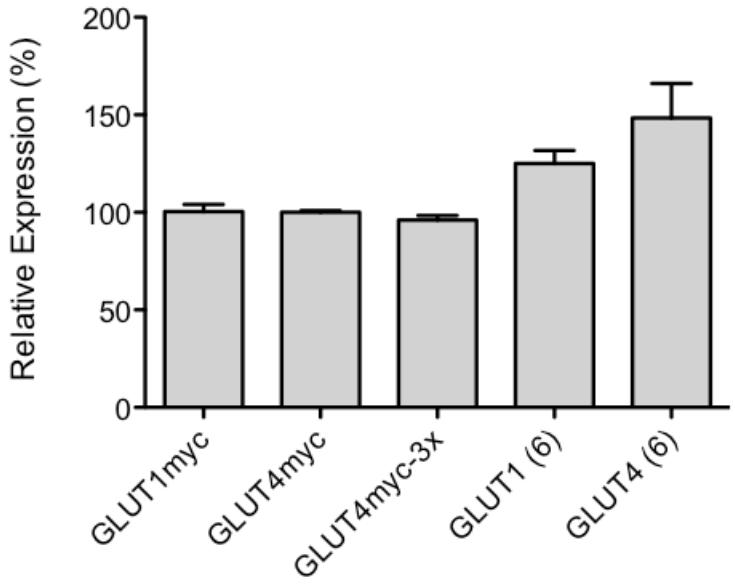

Figure A3.6 Relative expression of myc-tagged transfected construct mRNA by qPCR

Primers designed against both GLUT transporter sequence and the incorporated myc tag (Appendix Table A2) were used to analyze the relative amount of transfected message in RNA isolated from HEK cells transfected with 2 μg of DNA. RNA was prepared according to the Qiagen RNeasy kit and qPCR was performed according to the BioRad SYBRgreen qPCR kit. Relative expression normalized to GLUT1 (*ordinate*) is plotted for each of the main constructs used for TM6 comparisons (*abscissa*). Results are plotted as mean ± SEM for n=3 assays.

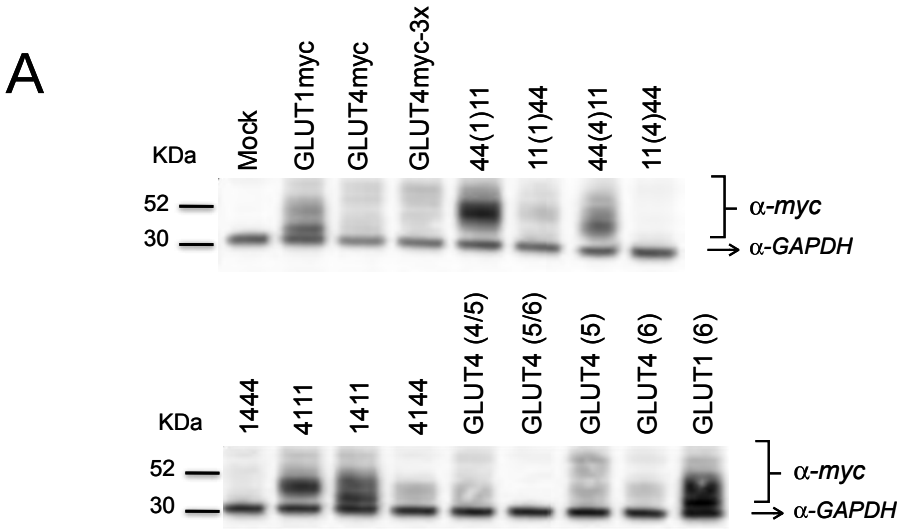
A
KDa
Mock
GLUT1myc
GLUT4myc
GLUT4myc-3x
44(1)11
11(1)44
44(4)11
11(4)44
52
30
α-myc
α-GAPDH
KDa
1444
4111
1411
4144
GLUT4 (4/5)
GLUT4 (5/6)
GLUT4 (5)
GLUT4 (6)
GLUT1 (6)
52
30
α-myc
α-GAPDH

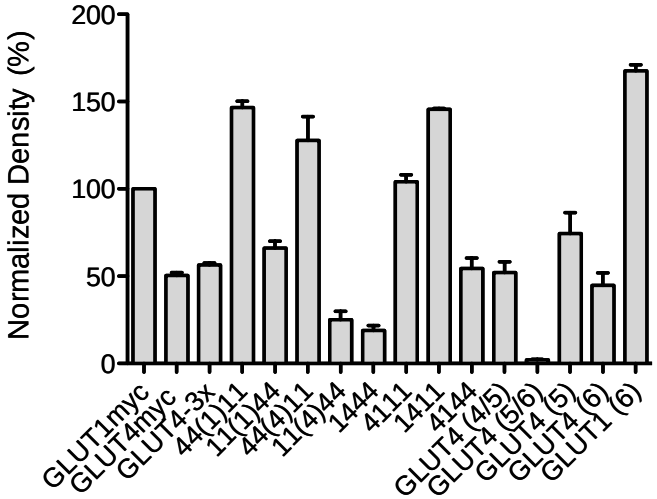
B
Normalized Density (%)
200
150
100
50
0
GLUT1myc
GLUT4myc
GLUT4-3x
44(1)11
11(1)44
44(4)11
11(4)44
1444
4111
1411
4144
GLUT4 (4/5)
GLUT4 (5/6)
GLUT4 (5)
GLUT4 (6)
GLUT1 (6)

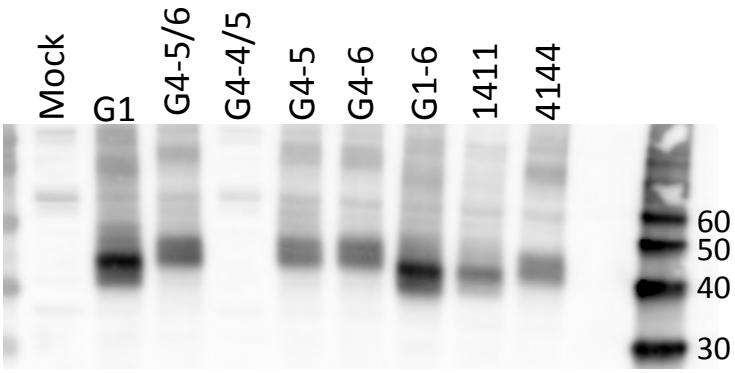
C
Mock
G1
G4-5/6
G4-4/5
G4-5
G4-6
G1-6
1411
4144
60
50
40
30

Figure A3.7 Variations in chimera protein expression detected by Western blot

HEK cells were transfected with the constructs indicated and whole cell lysates were extracted and resolved by SDS-PAGE. Western blots were dually probed with anti-myc antibody (*A*) and GAPDH antibody as a loading control. The identity of all chimeras was also verified by blotting with anti-C-terminal antibodies for GLUT1 and GLUT4. Mobility of molecular weight markers is indicated. *B*, Bands from *A* were quantitated by densitometry. *C*, HEK cells transfected with the constructs indicated were biotinylated at 4ºC. Cell-surface proteins were pulled down on streptavidin columns and resolved by SDS-PAGE. Cell surface expression of chimeras was detected by blotting with anti-myc antibody. Variations in apparent molecular weight of each construct correlate with variations in calculated molecular weight and isoelectric point, as determined by sequence-based calculations (Appendix Table A4).

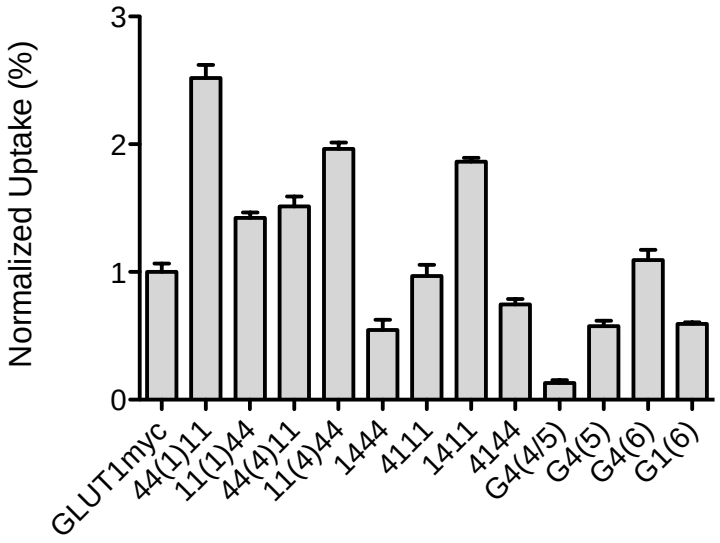

Figure A3.8 Variations in chimera expression detected by sugar transport

Zero-trans uptake of 100 μM 2-DG was performed at 5 minutes at 37ºC in HEK cells transfected with the constructs indicated (*abscissa*). Amount of uptake was mock-subtracted, corrected for background, normalized to total protein content, and normalized to uptake by GLUT1myc (*ordinate*).

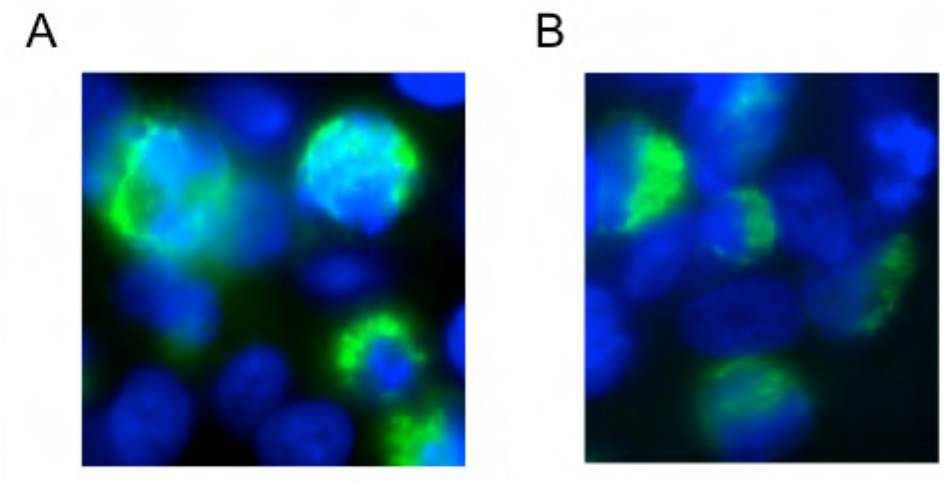

Figure A3.9 Immunofluorescence microscopy of permeabilized HEK cells expressing myc-tagged GLUT1

Two fields of view at 100x (*A*, *B*) representative of areas which showed positive staining for GLUT1myc in transfected HEK cells. Cells were fixed with 4% formaldehyde at 4ºC, permeabilized with 0.5% Triton X-100 with 1%FBS, and incubated overnight with anti-myc antibody (9E10 at 1:1000). An alexa 488-conjugated secondary antibody was used to detect anti-myc signal (green). Cells were mounted with Vetcashield containing DAPI staining (blue) for nuclear localization. Mock-transfected cells showed no alexa 488-associated signal. Non-permeabilizing modifications to detect only surface myc-tagged transporters showed either no staining or diffuse non-specific staining.